POLITECHNIKA GDAŃSKA

Preparation and characterization of hydrophobic membranes based on PVDF and graphene and evaluation of their applicability in the membrane distillation process

DOCTORAL DISSERTATION

Emilia Gontarek-Castro

Gdańsk 2022

GDAŃSK UNIVERSITY OF TECHNOLOGY
FACULTY OF CHEMISTRY

Author of the PhD dissertation: **Emilia Gontarek-Castro, BEng, MSc**
Scientific discipline: **Chemical Sciences**

DOCTORAL DISSERTATION

Title of PhD dissertation: **Preparation and characterization of hydrophobic membranes based on PVDF and graphene and evaluation of their applicability in the membrane distillation process**

Title of PhD dissertation (in Polish): **Otrzymywanie i charakterystyka hydrofobowych membran na bazie PVDF i grafenu oraz ocena możliwości zastosowanie ich w procesie destylacji membranowej**

Supervisor *signature*
Marek Lieder, BEng, DSc, Assoc. Prof.

Gdańsk, 2022

GDAŃSK UNIVERSITY OF TECHNOLOGY
FACULTY OF CHEMISTRY

STATEMENT

The author of the PhD dissertation: Emilia Gontarek-Castro, BEng, MSc

I, the undersigned, agree/~~do not agree~~* that my PhD dissertation entitled:
Preparation and characterization of hydrophobic membranes based on PVDF and graphene and evaluation of their applicability in the membrane distillation process
may be used for scientific or didactic purposes.[1]

Gdańsk, …….

signature of the PhD student

Aware of criminal liability for violations of the Act of 4th February 1994 on Copyright and Related Rights (Journal of Laws 2006, No. 90, item 631) and disciplinary actions set out in the Law on Higher Education (Journal of Laws 2012, item 572 with later amendments),[2] as well as civil liability, I declare, that the submitted PhD dissertation is my own work.

I declare, that the submitted PhD dissertation is my own work performed under and in cooperation with the supervision of Marek Lieder, BEng, DSc, Assoc. Prof.

This submitted PhD dissertation has never before been the basis of an official procedure associated with the awarding of a PhD degree.

All the information contained in the above thesis which is derived from written and electronic sources is documented in a list of relevant literature in accordance with art. 34 of the Copyright and Related Rights Act.

I confirm that this PhD dissertation is identical to the attached electronic version.

Gdańsk, ……

signature of the PhD student

I, the undersigned, agree/~~do not agree~~* to include an electronic version of the above PhD dissertation in the open, institutional, digital repository of Gdańsk University of Technology, Pomeranian Digital Library, and for it to be submitted to the processes of verification and protection against misappropriation of authorship.

Gdańsk,…….

signature of the PhD student

[1] Decree of Rector of Gdansk University of Technology No. 34/2009 of 9th November 2009, TUG archive instruction addendum No. 8.

[2] Act of 27th July 2005, Law on Higher Education: Chapter 7, Criminal responsibility of PhD students, Article 226.

DESCRIPTION OF DOCTORAL DISSERTATION

Author of the PhD dissertation: Emilia Gontarek-Castro, BEng, MSc

Title of PhD dissertation: Preparation and characterization of hydrophobic membranes based on PVDF and graphene and evaluation of their applicability in the membrane distillation process

Title of PhD dissertation in Polish: Otrzymywanie i charakterystyka hydrofobowych membran na bazie PVDF i grafenu oraz ocena możliwości zastosowanie ich w procesie destylacji membranowej

Language of PhD dissertation: English

Supervision: Marek Lieder, BEng, DSc, Assoc. Prof.

Date of doctoral defense:

Keywords of PhD dissertation in Polish: destylacja membranowa, grafen, transport pary wodnej, odsalanie

Keywords of PhD dissertation in English: membrane distillation, graphene, water vapor transport, desalination

Summary of PhD dissertation in Polish: Destylacja membranowa (ang. membrane distillation, MD) to obiecująca technologia odsalania wody morskiej ze względu na zdolność przetwarzania wód o wysokim zasoleniu i możliwość wykorzystania ciepła odpadowego lub alternatywnych źródeł energii. Zastosowanie dostępnych membran do MD jest ograniczone z powodu niskiego współczynnika przepływu pary wodnej oraz problemy z porastaniem membran. Coraz bardziej popularne staje się zastosowanie nanomateriałów w celu otrzymania nowych materiałów membranowych. Część teoretyczna pracy przedstawia przegląd aktualnych danych literaturowych opisujących otrzymywanie superhydrofobowych membran, z wykorzystaniem nieorganicznych nanomateriałów. Omówiony został również wpływ nieorganicznych dodatków na porastanie membrany, jej stabilność i wydajność w procesie odsalania. Część doświadczalna to opis badań własnych. Stosując dwa różne podejścia przygotowano hydrofobowe membrany na bazie PVDF i grafenu. W pierwszym z nich wymieszano grafen w matrycę polimerową, natomiast w drugim osadzono grafen na powierzchni membrany polimerowej. Zbadano wpływ płytek grafenowych w hydrofobowych mikroporowatych membranach polimerowych na morfologię, strukturę i wydajność odsalania membran. W wyniku modyfikacji osiągnięto znaczną poprawę produktywności i efektywności odsalania podczas procesu destylacji membranowej oraz powstanie wieloskalowej szorstkiej struktury, która wzmocniła odporność na zwilżanie i porastanie. W obu przypadkach osiągnięto lepszy przepływ i pełne odrzucenie soli w porównaniu z niemodyfikowanymi membranami PVDF.

Summary of PhD dissertation in English: Membrane distillation (MD) is a promising alternative to conventional seawater desalination. It requires the use of a hydrophobic microporous membrane, which separates the feed and the permeate. Numerous hydrophobic membranes have been developed and tested in the laboratory on model brine solutions, proving the efficiency of MD in water desalination. Nevertheless, membrane fouling and wetting remain open issues, especially for real seawater processing. The theoretical part of this thesis presents an overview of the current literature data describing the preparation of superhydrophobic membranes using inorganic nanomaterials. The influence of inorganic additives on

membrane fouling, stability, and efficiency in the desalination process is also discussed. The experimental part is a description of my own research. Using two different approaches, hydrophobic membranes based on PVDF and graphene were prepared. In the first one, graphene was mixed into a polymer matrix, while in the second one, graphene was deposited on the surface of the polymer membrane. The effects of graphene nanoplatelets (GNPs) in hydrophobic microporous polymeric membranes on the morphology, structure, and desalination performance was examined. As a result of modification, a significant improvement in productivity and efficiency was achieved along with the creation of a multiscale rough structure that amplified the wetting and fouling resistance. For both approaches, a superior flux compared to pristine PVDF and complete salt rejection were achieved.

Contents

Chapter 1

1.1. Introduction

Over the past century, the population of the world has increased, as has the demand for water. This global challenge of water supply will become even more serious due to further expansion in population and economic growth, followed by a continuing increase in demands on water resources. The World Water Council evaluated that by 2030 a few billion people will suffer from water scarcity or poor water quality [1]. Thus, it is not surprising that governments and industry have tried to develop alternative water sources, water recycling, water imports, and desalination in order to resolve the problem of the world's growing demand for clean water. Desalination of water is a process that removes excess salts and other dissolved substances, which leads to the production of drinking water with a reduced salt concentration, at or below the World Health Organization's limit of 500 ppm [2]. Although desalination has been known for centuries, it has gained particular attention in the last few decades, along with the development of membrane technology in the mid-1900s.

In general, desalination techniques can be divided into two groups: thermal-based and membrane-based. Basically, thermal technologies require the supply of thermal energy in order to induce the evaporation of water molecules from seawater; the vapor is subsequently condensed to give drinking water. The most commonly used thermal processes include multi-stage flash, multi-effect distillation, and vapor compression distillation [3]. Despite its versatility and ease of operation, thermal desalination has one significant disadvantage. Due to its high energy consumption, it is an expensive and environmentally unfriendly method. For this reason, alternative methods to thermal desalination are sought, mainly in order to reduce the costs of the process. Currently, one of the most dynamically developing desalination technique is membrane-based technology. Membrane technologies are becoming more popular due to their lower energy consumption, compact modular construction, lower environmental footprint, and the possibility of regenerating spent media [4]. Among membrane-based technologies, the dominant one used for desalination (in terms of the amount of treated water) is reverse osmosis (RO), which, according to the literature, produces up to 60% of the world's desalted water (Figure 1) [5].

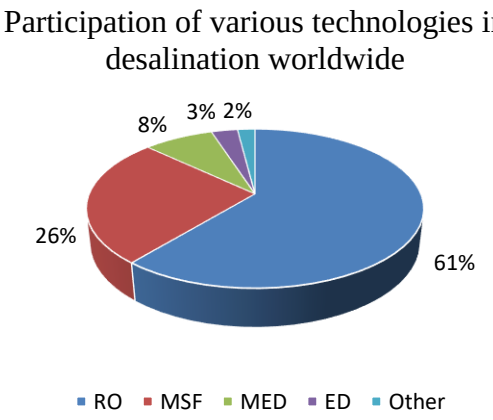

Figure 1. Participation of various technologies in desalination worldwide [6].

In contrast, thermal techniques such as multi-stage flash (MSF) and multi-effect distillation (MED) comprise 26% and 8% of the global share, respectively. One of the major challenges in using RO in seawater desalination is the energy cost of a RO plant, which is generated by the high feed pressure required for the process. Membrane distillation (MD), which can operate using low-grade or waste heat, is a potentially promising technique for seawater desalination. The driving force of the process is based on a vapor pressure gradient across the membrane. This gradient is induced by the temperature difference between the feed and permeate solutions. The solutions are separated by a hydrophobic microporous membrane that allows the diffusion of vapor and prevents the permeation of the aqueous phase. Water evaporates at the solid/liquid interface on the heated feed side of the membrane, then diffuses through the air trapped in the membrane pores, and finally condenses at the cooler permeate side. Simultaneously, non-volatile substances remain in the aqueous feed solution. Although RO is more energy efficient, MD gives the capacity to utilize low-grade thermal energy and to treat high-salinity brines. Thus, the application of MD is highly advantageous in cases where low-grade or renewable heat sources, including waste heat from industrial processes or solar thermal collectors, can be used [7].

1.2. MD – process fundamentals and principles

MD was first described by Bodell [8] in 1963, who patented the devices and method for converting non-potable aqueous solutions to potable water. The basis of the operation of this apparatus was that the vapor, but not the liquid, was permeable through a silicone rubber membrane. In 1967, Weyl [9] patented the use of a porous hydrophobic membrane for improving the efficiency of desalination. In the late 1960s, Findley published a study on vaporization through a porous membrane using various membrane materialsand also a basic theoretical study on direct contact MD (DCMD) [10,11]. The author noted the potential of MD as an economical method of evaporation; however, he pointed out that first low-cost and long-life membranes with appropriate properties needed to be developed. At that time, the interest in MD process decreased rapidly; however, the advent of new membrane manufacturing techniques in the early 1980s renewed interest in this process, as membranes with a high porosity value and low thickness became available.

1.2.1. Heat and mass transfer

Water vapor diffusing through the membrane generates the transfer of both mass and heat. There are two main mechanisms of heat transfer. The first is conductive heat transfer, which occurs together with vapor diffusion along the membrane pores and leads to temperature changes at the feed and permeate membrane boundary layers. This generates a temperature gradient between the bulk and boundary layer in both the feed and permeate solutions and induces convective heat transfer. A schematic illustration of heat transfer with the direct contact configuration of MD is shown in Figure 2.

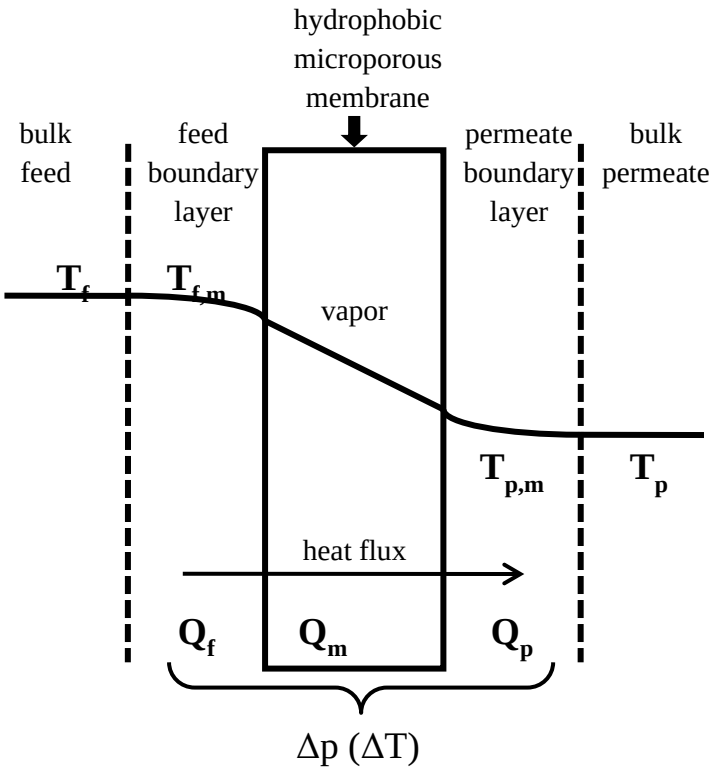

Figure 2. Schematic illustration of heat transfer with the direct contact configuration of MD [12].

The conductive heat transfer that occurs together with the vapor diffusion across the membranes is defined by Eq. (1):

$$Q_m = h_m(T_{f,m} - T_{p,m}) + J\Delta H_v \quad (1)$$

According to Figure 2, convective heat transfer at the feed side Q_f can be defined by Eq. (2):

$$Q_f = h_f(T_f - T_{f,m}) \quad (2)$$

while convective heat transfer at the permeate side Q_p is described by Eq. (3):

$$Q_p = h_p(T_{p,m} - T_p) \quad (3)$$

where h_m, h_f, and h_p are the heat transfer coefficients of the membrane, feed, and permeate, respectively, and $T_{f,m}$, $T_{p,m}$, T_f, and T_p stand for the temperature of the feed in the boundary layer, the temperature of the permeate in the boundary layer, the temperature of the feed, and the temperature of the permeate, respectively [13]. The temperature differences between the boundary layers and the bulk phases at both membrane sides reduce the driving force for vapor diffusion. This phenomenon is called temperature polarization (ψ) and is defined as follows:

$$\psi = \frac{T_{f,m} - T_{p,m}}{T_f - T_p} \quad (4)$$

According to Eq. (4), when the temperature polarization value is equal to 1, the feed and permeate temperatures are constant regardless of the distance from the membrane. However, this is the ideal situation and could only happen if the membrane did not conduct heat at all. Otherwise, when the value reaches 0, the temperature at the feed boundary layer is similar to the temperature at the permeate boundary layer, making the negative effect of temperature polarization very significant. The average value of the temperature polarization for the direct contact configuration of MD lies between 0.4 and 0.7 [14].

Mass transfer in the MD process occurs due to the vapor transport that is induced by the driving force of the process. In the case of MD, mass transfer can be generalized by a molecular diffusion or Knudsen diffusion model. The applicable type of model depends on the membrane pore size [14]. Molecular diffusion applies to membranes with a relatively large pore size. It states that collisions between diffusing molecules predominate, as described by Eq. (5).

$$N' = \frac{\varepsilon}{\tau\delta}\frac{PD_{ij}}{RT}\frac{(p_1-p_2)}{|p_a|_{ln}} \quad (5)$$

where ε, P, D, p_1, p_2, τ, δ, and p_a are the porosity, the total pressure in the pore, Fick's diffusion coefficient, the partial vapor pressure at the feed membrane surface, the partial vapor pressure at the permeate membrane surface, the tortuosity, the membrane thickness, and the air pressure in the pore, respectively.

The Knudsen model applies to systems where the collisions between diffusing molecules and the pore walls determine the mass transfer, as denoted by Eq. (6).

$$N' = \frac{1}{RT}\frac{2}{3\tau}\varepsilon r\left(\frac{8RT}{\pi M_i}\right)^{1/2}\frac{(p_1-p_2)}{\delta} \quad (6)$$

where r and M_i are the pore radius and molecular weight of water vapor, respectively.

While the MD process operates, the concentration of solutes in the feed solution increases at the liquid/gas interface and is higher than the concentration in the bulk feed. This phenomenon is called concentration polarization and its coefficient (CPC) is given by equation (7):

$$CPC = \frac{c_{f,m}}{c_f} \quad (7)$$

where $c_{f,m}$ is the concentration of the solute close to the membrane surface (liquid/gas interface) and c_f is the concentration of the solute in the bulk feed.

1.2.2. MD configurations

There are different configurations of the MD process, such as direct contact MD (DCMD), air gap MD (AGMD), sweeping gas MD (SGMD) and vacuum MD (VMD). In general, the main difference between them is the method used for vapor condensation on the permeate side (Figure 3).

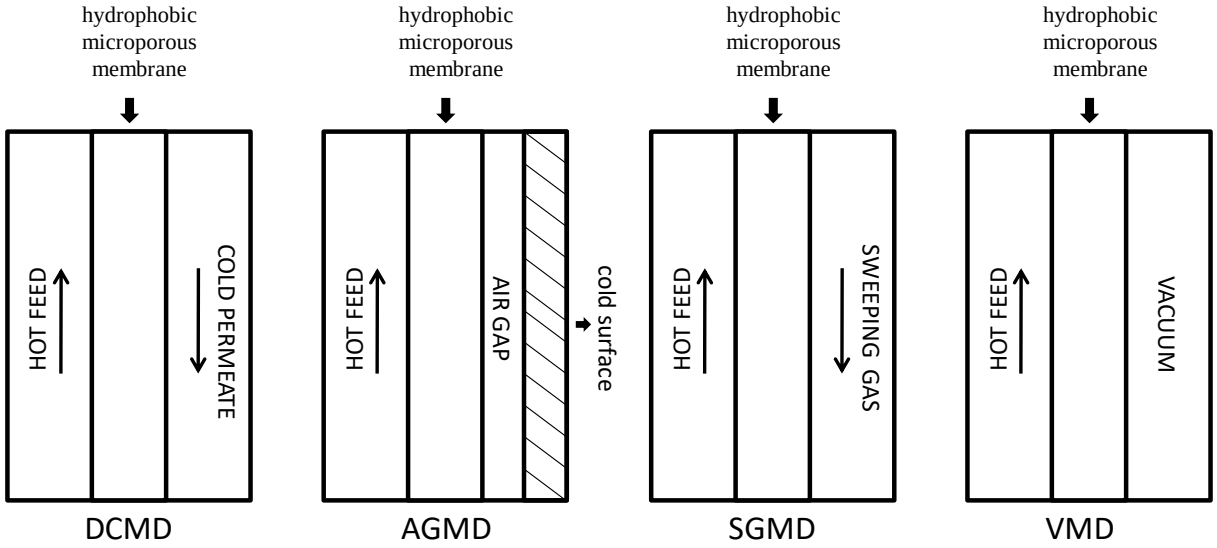

Figure 3. Schemes of MD configurations [12].

In the case of DCMD, both the feed and permeate solutions are in direct contact with the surface of the membrane. As the permeate is cooler than the feed it takes on the role of a condensing fluid. The DCMD setup is known to be the simplest among the various configurations, and thus it is the one most often used in laboratories. However, the main disadvantage of this configuration is the significant heat loss across the membrane, due to the direct contact of liquids with the membrane. In the AGMD configuration, diffusing vapor condenses on the cold surface on the distillate side. Between the membrane and cold surface there is an air gap, which is meant to effectively reduce the heat loss generated by the vapor transport. In the SGMD configuration, vapor diffusing through the membrane is swept away by a cold inert gas and carried outside the membrane module where it condenses. Although this configuration causes low heat loss, its higher operational cost makes it relatively rarely used. VMD is characterized by a vacuum applied on the permeate side, which acts as the driving force of the process. Due to the low pressure on the permeate side, vapor diffusion through the membrane is facilitated. One of the major advantages of VMD is the negligible conductive heat loss through the membrane. On the other hand, the degradation of the hydrophobic properties of the membrane can lead to membrane wetting and direct permeation of the feed liquid.

1.3. The theory of surface wettability

Water droplets that rest on the solid surface generate three interfacial tensions γ_{LV}, γ_{SL}, and γ_{SV}, which relate to the existence of interfaces between the liquid and vapor, solid and liquid, and solid and vapor, respectively. The balance between them determines whether a droplet spreads on the surface or takes a spherical-like shape (Figure 4) [15]. The balance of forces at the contact line between these three interfaces can be represented by Young's equation (8):

$$cos\theta_e = \frac{\gamma_{SV}-\gamma_{SL}}{\gamma_{LV}} \quad (8)$$

where θ_e is the instantaneous (dynamic) contact angle and γ_{SV}, γ_{SV}, and γ_{LV} are the solid–vapor, solid–liquid, and liquid-vapor interfacial tensions. This approach works well with smooth and homogenous surfaces.

1.3.1. Contact angle

The contact angle (CA) is usually used to determine the wettability of a surface with specific liquids. On a completely hydrophilic surface, a water droplet spreads and creates a CA with the surface of 0º; however, the surface is considered as hydrophilic for all cases when $\gamma_{SV}<\gamma_{SL}$, with the contact angle being lower than 90°. On the contrary, on a completely hydrophobic surface a water droplet doesn't have any contact with the surface, which corresponds to contact angle equal to 180º; however, a surface is conventionally described as hydrophobic when $\gamma_{SV}>\gamma_{SL}$, with the contact angle being greater than 90°.

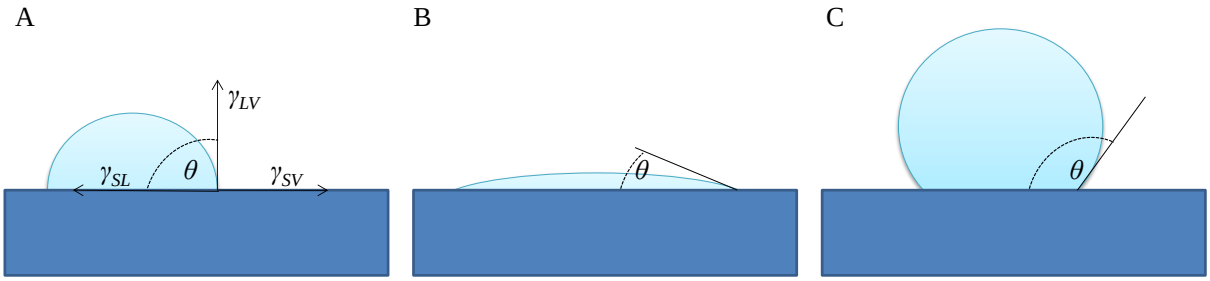

Figure 4. A) the contact angle of a droplet resting on a solid surface and the three interfacial tensions; B) a droplet resting on a hydrophilic surface and its contact angle; C) a droplet resting on a hydrophobic surface and its contact angle.

Those surfaces with highly wetting-resistant properties and a water contact angle of more than 150° are known as superhydrophobic surfaces. There has been a great interest in their use in membrane development for various separation processes. Some plants and animal furs are examples of surfaces with strongly water-repellent properties that can be found in nature. The microstructure of these surfaces reveals their specific topography. For instance, the surface of lotus leaves, which are the most popular biological example of superhydrophobic surfaces, consists of an epicuticular wax and a combination of two-scale roughness, existing on a microscale and nanoscale [16]. Such surfaces are also referred to as hierarchical. The water CA of a lotus leaf reaches 161 ± 2.7º [17]. Due to its properties and structure, a phenomenon called the "lotus effect" is observed, which refers to the self-cleaning properties of the lotus leaf. As droplets roll away on its surface, they gather and transport dust, which results in the cleaning of the plant surfaces [16] [18]. Properties similar to those of lotus leaves can be achieved by creating a rough, hydrophobic surface. The roughness further enhances the contact angle of hydrophobic surfaces [19]. It can be accurately described by the Wenzel equation (9) [20]:

$$cos\theta_r = r cos\theta_e \quad (9)$$

where r is the roughness factor, θ_r is the CA on a rough surface, and θ_e is Young's equilibrium CA.

According to equation (9), the roughness amplifies the effect of the surface chemistry. As a result, small changes in Young's equilibrium CA become larger changes in the CA of a rough surface. It is worth pointing out the importance of the point when the θe value equals 90°, where there is a changeover in the sign of the cosine term. It means that for hydrophilic surfaces with θ<90°, the roughness factor's enhancement will cause a further reduction in the Wenzel contact angle toward 0°, whereas for hydrophobic surfaces with θ>90°, it will lead to a further increase in the Wenzel contact angle toward 180°. However, the Wenzel equation is limited only to homogeneous surfaces and was extended by Cassie and Baxter in 1944 [21]. The Cassie-Baxter equation applies to porous heterogeneous surface. The presence of air in the pores prevents the

pores from being filled with water, and the water only bridges between parts of the solid surface. Although the Cassie–Baxter equation (10) refers to topographically structured surface, the roughness factor does not enter directly into the equation:

$$cos\theta_{CB} = f_1 cos\theta_e - (1 - f_1) \quad (10)$$

where θ_{CB} is the heterogeneous CA, f_1 is the fraction of the contact line of the liquid with the solid, and thus $(1 - f_1)$ is the area bridged between solid surface features.

According to equation (10), θ_{CB} will increase as f_1 decreases, meaning that to improve the surface hydrophobicity, the area of contact between the liquid and solid must be kept to a minimum. Therefore, the surface roughness does matter in this case, but only indirectly, since it defines the fraction of the solid surface in contact with the droplet.

Figure 5 shows a droplet of water on a hydrophobic surface according to the A) Wenzel and B) Cassie-Baxter state. In the case of the Wenzel state, the droplet is in contact with the whole rough surface, while in the case of the Cassie-Baxter state, the droplet remains suspended on top of the surface protrusions. For hydrophobic surfaces, both states lead to an increase in the CA; however, only the Cassie-Baxter state provides low CA hysteresis.

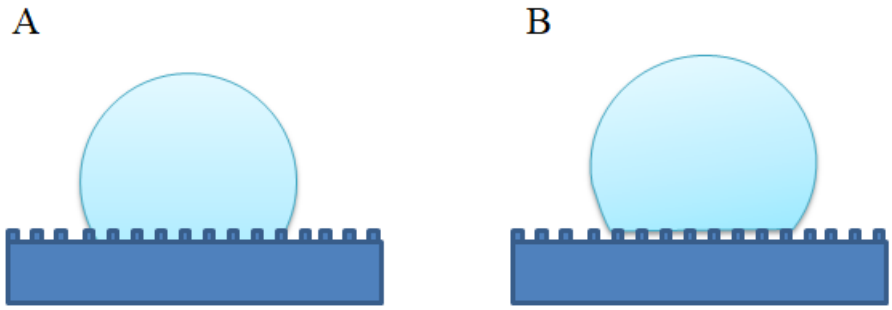

Figure 5. A droplet on a rough hydrophobic surface according to the A) Wenzel state, B) Cassie-Baxter state.

1.3.2. Surface roughness and morphology

All the irregularities on the surface of the material represent surface roughness. The roughness factor is defined as the ratio between the area of the actual surface and geometric surface [22]. Quantitative roughness statistics can be obtained from instrumental analyses such as atomic force microscopy (AFM). Membrane surface roughness is usually represented by two parameters, R_{RMS} (*Rq*) and $R_{average}$ (*Ra*). *Rq* is defined as the average of the measured height deviations taken within the evaluation area and measured from the mean linear surface, while *Ra* is the arithmetical mean deviation of the roughness profile. Both are functions of height deviations from mean surface levels [23]. Not only surface roughness, but also membrane morphology, affects surface wettability. According to Tuteja et al. [24], a so-called re-entrant geometry of the surface is one of the critical factors in the design of materials with superior antiwetting properties. A re-entrant structure refers to a concave topography in which the cross-sectional solid area decreases from the top to the bottom [25]. Re-entrant morphology together with a low surface tension can easily achieve a Cassie-Baxter state for the liquid-solid-vapor interfaces with most liquids.

1.3.3. Superhydrophobicity of MD membranes

Although the MD process has many advantages, there are still some open issues, such as fouling and wetting, that need to be solved [26]. MD fouling takes different forms, depending on the chemical composition of the feed solution, namely inorganic, organic, and biological fouling. For instance, the desalination of brine often results in scale formation [27] or the growth a crystal layer at the membrane surface while desalination proceeds. On the other hand, during the treatment of protein-type solutions, it is common to observe their adsorption at the membrane surface [28]. Biofouling occurs through the growth of bacteria, fungi, and algae. Fouling phenomena reduce the vapor transport through the membrane in two possible ways. Firstly, a homogeneous layer of foulant leads to pore clogging, generating additional mass transfer resistance. Secondly, a porous fouling layer can increase heat transfer and simultaneously increase susceptibility to the temperature polarization effect, which consequently reduces the driving force of the process. The molecules of foulants are attached to the membrane surface through physical interactions or chemical bonds [29]. The formation of any deposit carries a risk that the pores may be filled with the feed liquid, resulting in a wetting phenomenon [30]. The use of an appropriate membrane material may hinder fouling and wetting phenomena.

For efficient desalination via the MD process, the membrane should exhibit strongly hydrophobic properties. This feature is highly desired since it may effectively repel the water molecules in the liquid state and promote vapor transport. Therefore, superhydrophobic membranes with a CA value over 150^{o} have gained great attention in the MD process. It was observed that superhydrophobic membrane surfaces have a positive effect on the elimination of undesirable phenomena such as pore fouling and wetting, due to the creation of micro- and nanostructured surfaces [24,25]. For instance, the complex topography of a membrane creating a Cassie-Baxter state inhibits or reduces the penetration of liquid into the surface. Therefore, a strongly water repellent membrane can be created through the formation of a micro- and nanostructured surface, as shown in Figure 6.

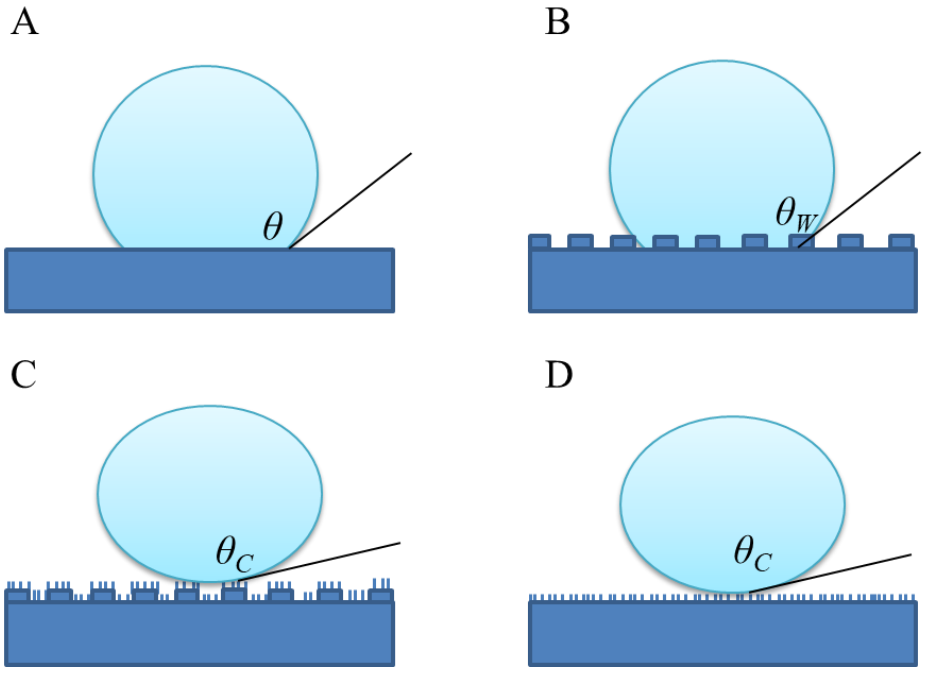

Figure 6. Schematic illustrations of water drop on different membrane surfaces. (a) Flat surface, (b) Microstructured surface, (c) Hierarchical surface, and (d) Nanostructured surface.

In our study, I conducted a literature review aimed at selecting the newest methods of fabricating superhydrophobic membranes for desalination using MD. I paid special attention to methods using nanomaterials, as it turned out that they can have a positive impact on many aspects of the operation of the MD process. I provided an overview of the typical nanomaterials used for the modification of MD membranes as well as the underlying mechanism leading to an improvement in MD performance. Subsequently, I tried to obtain superhydrophobic membranes for desalination through MD. As the availability of membranes designed for efficient MD is limited, nanocomposite membranes represent an interesting field to be explored, since they offer novel functionalities generally not achievable in pristine materials. Two approaches have been used to prepare MD membranes. The first was to mix a nanomaterial into the polymeric structure. I planned to use multilayer graphene nanoplatelets (GNPs), with a thickness of around five graphene layers, as a nanofiller for spherulitic-like PVDF membranes. Such membranes showed assisted transport mechanisms when tested in DCMD. As a result, potable water was produced from salt solutions. My results show the absence of thermal polarization, outstanding anti-wetting properties, enhanced breaking resistance, and antifungal activity. This study presents evidence about the role of interactions activated at the water/graphene interface that result in assisted vapor transport. In the second approach, a nanostructured coating of GNPs was created on the surface of a pristine PVDF membrane. The complex surface topography formed after graphene coating gave rise to much improved antiwetting and antifouling properties. The effectiveness of GNP-coated membranes was tested during desalination via the DCMD process using mixtures of NaCl and humic acid (HA) as a feed solution, and the results showed that these new functional membranes are promising materials for application in high-performing MD operations.

Chapter 2

Research goals

The scientific purpose of this PhD work was to obtain graphene-modified hydrophobic membranes for desalination using MD with enhanced transport properties and stability.

To achieve the intended goal, the following steps were carried out:

- An up-to-date and critical literature review in order to identify the need for the undertaken research and to place it within the context of the existing literature. The main topics covered in the review concerned the role of nanomaterials in the formation of hydrophobic surfaces and the effect of increased hydrophobicity on the performance of membranes in the MD process.

- The preparation of polymeric PVDF membranes and their modification with graphene using two different approaches: the creation of mixed matrix membranes (MMMs) and coated membranes.

- Understanding the effect of graphene introduction to the membrane structure on membrane surface and transport properties.

- Correlation of the morphological and structural properties of the membranes with their operation during the MD process. An explanation of graphene's role in the desalination mechanism.

Chapter 3

Research description

The research topics and results related to this PhD dissertation are discussed in detail in the following four publications:

P1. Gontarek-Castro, E.; Castro-Muñoz, R.; Lieder, M. New insights of nanomaterials usage toward superhydrophobic membranes for water desalination via membrane distillation: A review. *Critical Reviews in Environmental Science and Technology* **2022**, *52*, 2104-2149, https://doi.org/10.1080/10643389.2021.1877032, **IF: 12.561, Q1, 200 points.**

P2. Gontarek-Castro, E.; Macedonio, F.; Militano, F.; Giorno, L.; Lieder, M.; Politano, A.; Drioli, E.; Gugliuzza, A. Adsorption-assisted transport of water vapour in super-hydrophobic membranes filled with multilayer graphene platelets. *Nanoscale* **2019**, *11*, 11521-11529, https://doi.org/10.1039/C9NR02581B, **IF: 7.790, Q1, 140 points.**

P3. Gontarek-Castro, E.; Rybarczyk, M. K.; Castro-Muñoz, R.; Morales-Jiménez, M.; Barragán-Huerta, B.; Lieder, M. Characterization of PVDF/Graphene Nanocomposite Membranes for Water Desalination with Enhanced Antifungal Activity, *Water* **2021**, *13*, 1279-1290, https://doi.org/10.3390/w13091279, **IF: 3.103, Q2, 100 points.**

P4. Gontarek-Castro, E.; Luca, G.D.; Lieder, M.; Gugliuzza, A. Graphene-Coated PVDF Membranes: Effects of Multi-Scale Rough Structure on Membrane Distillation Performance. *Membranes* **2022**, *12*, 511. https://doi.org/10.3390/membranes12050511, **IF: 4.11, Q2, 100 points.**

The above-mentioned scientific publications are attached in accordance with the numbering in the **Attachments**. Briefly, the most important achievements of each paper are discussed below.

3.1. The role of inorganic materials in hydrophobicity enhancement for MD membranes

Various studies have proven that the incorporation of nanomaterials in polymeric membranes can tune their structural and physicochemical properties, such as hydrophobicity, porosity, surface charge density, and their chemical, thermal, and mechanical stability [33]. Recently, a new trend in hydrophobic MD membrane preparation has been to incorporate inorganic materials into the membrane structure. The most popular are nanomaterials such as carbon nanotubes, graphene, and nanoparticles of silica and titanium dioxide. The detailed characteristics of these additives are summarized in the manuscript **P1**. Although modification with nanomaterials brings many benefits, there are some issues that make the preparation of such membranes challenging.

For instance, during nanocomposite fabrication one of the most commonly occurring phenomena is nanoparticle aggregation. The susceptibility to aggregation increases with the concentration of nanomaterial in the polymer matrix. On the other hand, the concentration of nanomaterial is often a critical parameter in the optimization of membrane performance and durability. Aggregation causes porosity and reductions in mechanical strength and vapor flux [34]. According to the literature, mechanical dispersion, ultrasonication, stirring, and chemical modification proved to be effective strategies for improved dispersion of nanomaterials [35][36][37]. The addition of inorganic nanoparticles to MD polymeric membranes has beneficial effects visible during the desalination process (Figure 7). Firstly, the influence of nanomaterials on the surface properties of the membrane often leads to strong water repellency, a hierarchical and rough structure, and a large effective surface area. These features may contribute to increased membrane flux and prevent salt deposition. Additionally, for MMMs, superhydrophobic nanofillers may accelerate diffusion in the membrane pores. Three positive changes took place in the MD process after the modification of membranes with nanomaterials:

1) stable performance,
2) flux enhancement,
3) improved permeate quality.

Table 1 summarizes the most important studies on preparing superhydrophobic MD membranes using different nanomaterials, together with their performance details. [P1]

3.1.1. Performance stability

Various processes and phenomena such as fouling, concentration polarization, and heat transfer may hamper flux stability during the MD process. For instance, the deposition of foulants on membrane surfaces can lead to a reduction in the vapor diffusion rate through the pores in two possible ways. Firstly, the creation of a homogeneous fouling layer on the membrane surface causes pore clogging and flow rate reduction due to the increased mass transfer resistance. On the other hand, a porous layer created on the membrane surface by the foulants increases susceptibility to temperature polarization effects. Thus, the small contact area between solid and liquid that is offered by superhydrophobic surfaces may effectively reduce the contact between inorganic foulants and membrane surfaces, preventing their deposition [38]. Modification of the membranes using nanoparticles was found to be an effective method in fouling control and wetting mitigation. For example, surface-modified PVDF membranes using silver nanoparticles exhibited a stable performance during DCMD, in contrast to unmodified PVDF, even though both membranes were characterized by a similar pore size distribution [39].

Table 1. Relevant papers on preparing superhydrophobic membranes for desalination using MD.

MD configuration and process parameters:	Nanomaterial used:	Contact angle:	LEP:	Operating time:	Flux (kg/m^2 h):	Rejection:	References:
DCMD 3.5 wt.% NaCl Tf: 70 °C Tp: 25 °C	TiO_2	163 ° ± 3 °	190 kPa	8 h	~ 30	-	[31]
DCMD 3.5 wt.% NaCl Tf: 60 °C Tp: 20 °C	SiO_2	>150 °	150 kPa	25 h	24.6 ± 1.2	>99.99%	[40]
DCMD 3.5 wt% NaCl Tf: 60 °C Tp: 20 °C	Ag	153° ± 4°	146 ± 12 kPa	8 h	31.6	-	[39]
VMD 200 g/L NaCl Tf: 60 °C ΔP: 80 kPa	ZnO	152 °	277 ± 8 kPa	8h	4.5	~99.99%	[41]
DCMD 3.5 wt.% NaCl Tf: 70 °C Tp: 20 °C	SiO_2	156 °	275 kPa	15 h	~8	99.99%	[42]
VMD 15 wt% NaCl + 6 wt% $MgCl_2$ Tf: 80 °C ΔP: 0.096 MPa	SiO_2	150°	-	12 h	~4.5	-	[43]
DCMD 70 g/L NaCl Tf: 60 ± 1 °C	CNT	158.5 ° ± 1.5 °	99 kPa	5 h	29.5	>99.99%	[44]

Tp: 20 ± 1 °C							
DCMD 35 g/L NaCl Tf: 60 °C Tp: 20 °C	CNT	150.4 ° ± 0.8 °	40.5 ± 2.8 kPa	6 h	48.1	>99.98%	[36]
DCMD 3.5 wt% NaCl Tf: 60 °C Tp: 20 °C	SiO_2	153.9 °	179 kPa	50 h	18.9	-	[45]
DCMD 3.5 wt% NaCl Tf: 60 °C Tp: 20 °C	SiO_2	155.6 °	230 kPa	24 h	41.1	>99.99%	[37]
DCMD 30×10^3 mgL^{-1} NaCl Tf: 60 °C Tp: 20 °C	SiO_2	>150°	84.2± 2.8 kPa	50 h	34.2	>99.9%	[46]
DCMD 3.5 wt% NaCl Tf: 70 °C Tp: 25 °C	TiO_2	157.1 °	158 kPa	10 h	73.4	99.99%	[47]

In both cases, the stability enhancement was wholly attributed to the better surface water repellency of the modified membranes. The water contact angle was 153º and 154º for silver- and silica-modified membranes, respectively. Other authors prepared superhydrophobic MD membranes by modifying poly (vinylidene fluoride-co-hexafluoropropylene) (PcH) membranes with TiO_2 [48]. It turned out to be an effective method for membrane regeneration during real seawater desalination. After a 5-day test, the water CA of the nanoparticle-modified membrane was still recoverable up to values of 150.2 º. In another study, TiO_2 coating and fluorination resulted in an increase in the water CA from 125º for pristine PVDF up to 163º after modification [31]. Moreover, the modified membrane exhibited a significantly higher flux recovery compared to the unmodified one.

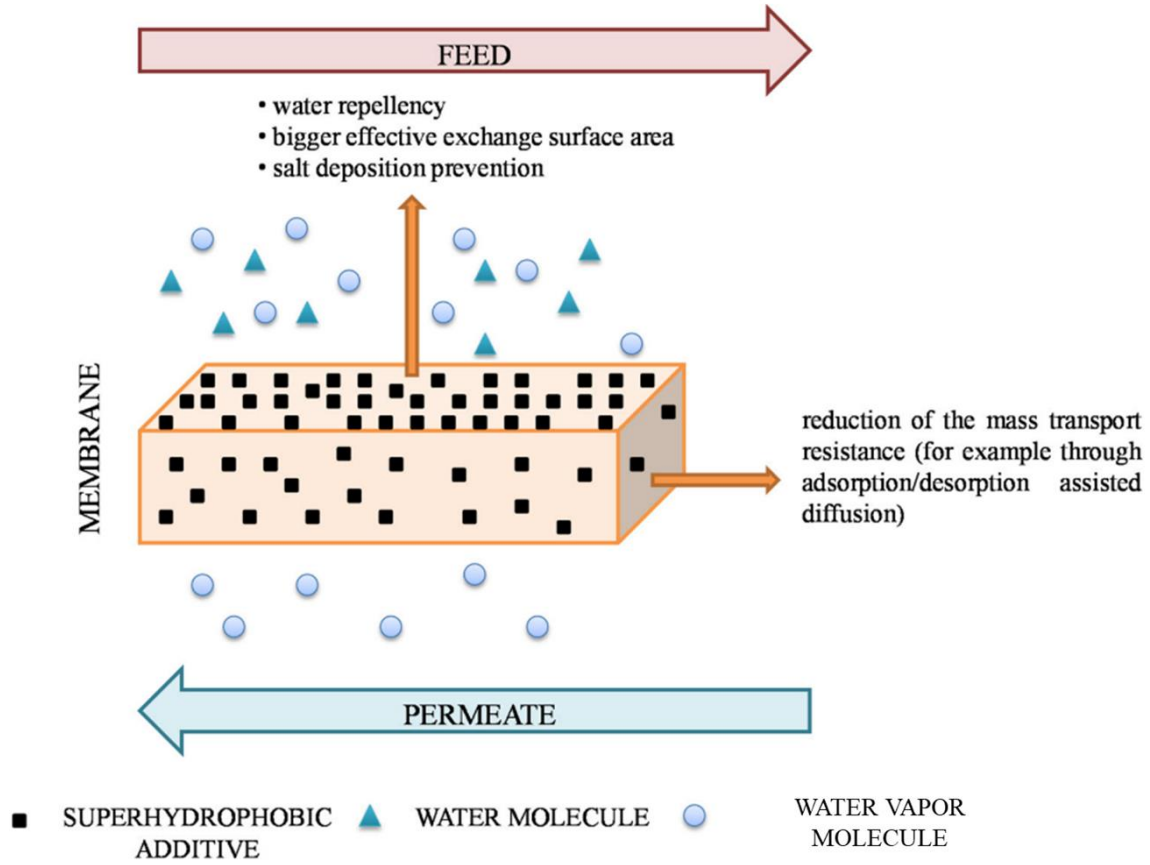

Figure 7. Schematic illustration of the nanoparticles' effect on the MD membrane's characteristics and performance.

3.1.2. Flux enhancement

In general, there are two strategies to increase the vapor flux through the membrane. The first one includes various approaches to increasing the driving force through the membrane, and the second is to reduce the resistance to mass transport. The driving force of the MD process is the difference in vapor pressure between the different sides of the membrane. Therefore, an increase in the temperature gradient between the feed and permeate, or an increase in the effective evaporation area on the feed side, will both lead to driving force enhancement. It was observed that an increase in hydrophobicity can generate higher vapor fluxes thanks to

the effective evaporation area increasing. As the hydrophobic surface prevents the water from penetrating the membrane pores, the susceptibility of pores to flooding is minimized, and consequently the available surface area for vapor exchange increases. Silica nanoparticles were used by several authors to prepare superhydrophobic membranes [37][45][40]. These modified membranes, besides stable performance, were also characterized by increased flux when compared to unmodified ones. Surface characterization revealed the strong water repellency of these membranes, which was achieved by incorporating silica nanoparticles, resulting in superhydrophobic nanocomposite PVDF membranes. They offered a higher effective liquid evaporation area than pristine PVDF nanofiber membranes. The multiscale rough surface provided numerous holes and slots, which reduced the membrane/liquid contact area and simultaneously increased the membrane/vapor contact area. For instance, the vapor flux increased from 12.3 kg/m^{2}h for PVDF nanofiber membranes, up to 18.9 kg/m^{2}h for silica/PVDF nanocomposite membranes. Moreover, this value of vapor flux made this membrane a competitive alternative to commercial flat-sheet PVDF membranes (vapor flux around 10 kg/m^{2}h).

Mass transfer resistance through the membranes comes from collisions between vapor molecules and the pore walls (Knudsen diffusion model) as well as from collisions between diffusing vapor and air molecules inside the membrane pores (molecular diffusion). The hydrophobic properties of the membrane can promote mass transfer through reducing the friction between the membrane pore walls and diffusing vapor molecules. Thus, mass transfer through a hydrophobic membrane is a method facilitating vapor flux through the membrane. Recently, the term adsorption-assisted transport has appeared in the literature, which mainly concerns membranes modified with carbon nanomaterials [36][44]. These membranes also show improved vapor flux, which results from the reduction in the collisions between the pore walls and vapor molecules. The scheme of assisted transport is shown in Figure 8. Chaotic unassisted transport results in many collisions that prolong the path of vapor molecules from one side of the membrane to the other. On the other hand, assisted diffusion, due to the adsorption/desorption assistance, facilitates the transport of vapor molecules.

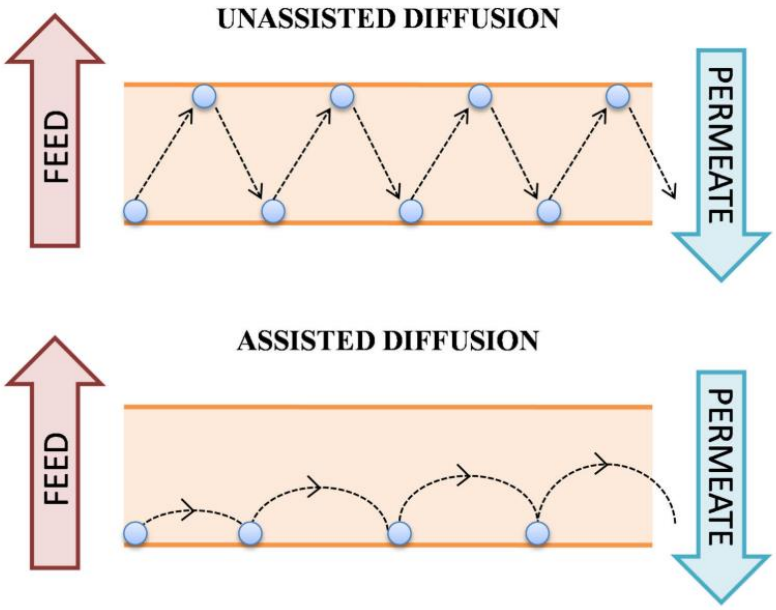

Figure 8. Schematic illustrations of unassisted and assisted diffusion through the membrane during MD.

A positive effect of assisted transport was observed for electrospun nanofiber membranes with anchored functionalized carbon nanotubes [36]. Homogeneous dispersion of this nanomaterial resulted in the membrane acquiring superhydrophobic properties, which facilitated transport by Knudsen and molecular diffusion. These authors observed a 35% higher vapor flux for the modified membrane, which reached 48.1 L/m^2h. In another study, using a similar modification, the authors observed increased surface roughness, which led to a CA increase up to 158°. The incorporation of carbon nanotubes into nanofiber membranes contributed to 33% and 59% higher vapor fluxes, for 35 and 70 g/L NaCl feed solutions, respectively.

3.1.3. Permeate quality

Desalination by MD often leads to salt crystallization on the membrane surface. Salt deposition generates partial wetting, as the pores can be filled with the saline feed solution, and consequently increases the salt concentration on the permeate side [30]. A highly hydrophobic membrane effectively reduces the salt deposition, decreases the susceptibility of the membrane to wetting, and thus increases the permeate quality [49]. For instance, a superhydrophobic surface incorporating TiO_2 coated with perfluoroalkylsilyl groups resulted in the water CA increasing from 134° to 160° [29]. After modification, the membrane exhibited a higher resistance to concentrated salt solutions than non-modified membranes. The as-prepared membrane surface was characterized by a reduced contact area with the feed solution as a result of its strongly water repellent properties. Other studies stated that rougher surfaces reduced the susceptibility to partial membrane wetting and increased the capability for salt rejection. A novel ZnO-modified PVDF membrane with a micro/nanoscale rough structure and a superhydrophobic surface with a CA of 152° was used in an 8 h VMD run [41]. Although, the modification did not affect the vapor flux, a much higher quality of permeate was observed for the modified membrane compared to a pristine one. The ionic conductivities of the permeate reached 190.88 lS/cm and 10.19 lS/cm for the pristine PVDF membrane and ZnO-modified membrane, respectively. Finally, a graphene modified PcH membrane showed complete salt rejection (100%) during long-term MD, while the commercial membrane tested over the same conditions displayed only 99.2% [50]. Such promising results were explained by the formation of multilevel roughness and the following suitable morphological properties: LEP (>186 kPa), CA (>162°), and porosity (>88%).

Graphene gains increasing attention as a unique nanofiller material that can provide interesting functionalities to the nanocomposite material for various research fields [51]. Graphene is two-dimensional material composed of sp^2 carbon atoms in hexagonal honeycomb lattices. This nanomaterial possess characteristic particularly attractive for MD application, such as hydrophobicity, high mechanical stiffness, and anti-fouling properties [52]. Moreover, literature refers about the ability of graphene to promote a partial and reversible dissociation of water molecules [53], which may result in promoted water vapor transport. Thus, I exploited the desired properties of graphene to enhance the overall properties of a PVDF membrane towards the production of a hydrophobic membrane for effective membrane distillation. Since excellent properties of graphene makes it competitive with other nanomaterials, it was worth to investigate how graphene modification can affect process stability, flux and permeate quality during desalination using DCMD. Moreover, it was crucial to describe the mechanisms of vapor permeation through graphene-modified membranes.

3.2. The preparation of PVDF membranes and their modification with graphene

The preparation procedures for the graphene-modified polymeric PVDF membranes included two different approaches. The first was to produce a MMM. GNPs were dispersed in 1-Methyl-2-pyrrolidinone (NMP) using an ultrasonic bath alternated with mechanical stirring for 2 hours at 30 °C. Dispersions with various graphene loadings were prepared (0.33%, 0.5%, 5%, 10%, and 20%). PVDF was added to the dispersions at a concentration of 12 wt%, and the mixtures were left under mechanical stirring at 30 °C for 24 h. For the preparation of pristine PVDF membranes, 12 wt% of PVDF powder was dissolved in NMP under mechanical stirring for 24 h at 30 °C. After the stirring, the solution was left for 3–4 hours without stirring for the removal of bubbles. The membranes were deposited onto glass with a micrometric film applicator using a gap size of 250 μm, immersed sequentially for 10 min in 2-propanol for coagulation, and cleaned several times with deionized water. The membrane was then dried at room temperature overnight. Five different mixed membranes were prepared in this step, named as GNP0.33%, GNP0.5%, GNP5%, GNP10%, and GNP20%, referring to the content of the nanofiller. A schematic diagram of the mixed matrix PVDF/GNP membrane fabrication is shown in Figure 9.

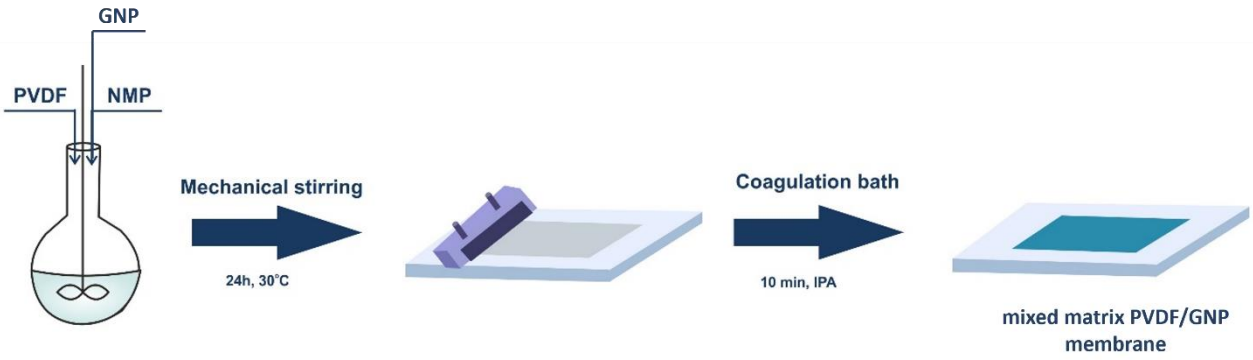

Figure 9. Schematic illustration of mixed matrix PVDF/GNP membrane fabrication.

The second approach was to prepare graphene-coated PVDF membranes. These membranes were fabricated through a combined phase inversion and wet-filtration approach, starting with the preparation of a dispersion of GNPs. The GNPs were added to a water/2-propanol mixture (volume ratio 7/3) at concentrations of 0.05 $mgmL^{-1}$ and 0.005 $mgmL^{-1}$. Each suspension then underwent approximately 20 stirring/sonication cycles to create fine dispersions. A dead-end filtration cell was applied for graphene deposition onto the surface of pristine PVDF membranes. 20 ml of dispersion was poured into the cell and left to distribute uniformly on the membrane surface. After 10 minutes, pressure was applied (~1 bar) for 10 min. The permeate was clean and did not contain any graphene contamination. The membrane was then dried in air for 24 h. The flat sheet phase-inversed PVDF membrane was denoted as pristine PVDF and used for comparison. Two different graphene-coated membranes were prepared in this step, named as 0.05G/PVDF and 0.005G/PVDF, which referred to the concentration of the dispersion used for coating. A schematic diagram of the graphene-coated membrane fabrication is shown in Figure 10.

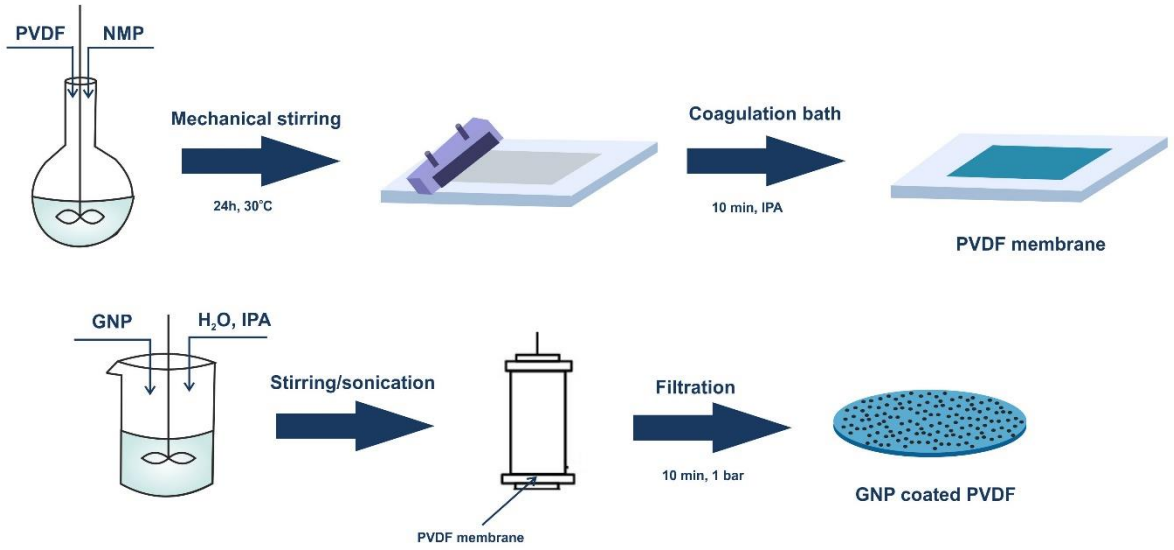

Figure 10. Schematic illustration of graphene-coated membrane fabrication.

Mixed matrix PVDF/GNP membranes and graphene-coated membranes were successfully fabricated. FTIR spectroscopy and X-ray diffractometry were performed on all the samples to gain insight into the structure of the obtained membranes and confirm the presence of graphene. PVDF is a semi-crystalline material, and XRD analysis revealed that its structure was dominated by both the α and γ crystalline phases. The coexistence of these forms was further confirmed by FTIR analysis. Importantly, the addition of graphene did not generate any change in the membrane characteristics in terms of their crystalline phase. Furthermore, XRD spectra collected on graphene-modified membranes showed additional peaks at 26.5 (002) and 54.6° (004), which represented the perpendicular direction (c-axis) to the graphite hexagonal planes [54]. In the case of graphene-coated membranes, additional broad IR adsorptions in the regions 1500-2000 cm^{-1} and 2500-3720 cm^{-1} were detected, especially in the case of the membranes coated with the highly concentrated graphene dispersion (0.05G/PVDF). Pore size and porosity measurements, as well as SEM analysis, were carried out for all the samples, in order to investigate the changes in the structure of the modified membranes.

As an effect of wet-phase inversion, a method for the preparation of flat sheet porous membranes with a mean pore size of 0.2–0.5 μm and an overall porosity (ε) ranging from 60 to 80% was obtained **[P2-P4]**. In the case of MMMs, GNPs were found to be clearly discernable inside the polymeric matrix. The high overall porosity values indicated that the free volume fraction of the membranes was preserved. A slight decrease in the value was observed due to cluster formation, but only for the membrane with the highest graphene loading. The topography of these membranes was complex, considering the presence of the graphene platelets, which were randomly dispersed in the polymeric structure. Detailed structural and morphological characteristic can be found in **P3**. SEM analysis confirmed the presence of GNP in the PVDF matrix. The pristine PVDF showed a sponge-like structure and a relatively smooth surface, which became more compact with the graphene addition. The structural changes were indicated by a significant reduction in pore size, especially for GNP5% and GNP10% (from 0.5 μm down to 0.27 and 0.24 μm, respectively). A uniform and well-dispersed distribution of GNPs was found for GNP0.33% and GNP0.5% (Figure 11). In the case of graphene-coated membranes, 0.005G/PVDF showed values for the mean and largest pore size comparable to pristine PVDF, while a reduction was observed for 0.05G/PVDF. On the other hand, the overall porosity and

the thickness were similar for all samples. This may suggest that the structure of each membrane was preserved, and GNPs were confined to the membrane surface. SEM images of the membrane cross section showed the formation of a thin graphene layer on the top of the PVDF surface, especially visible at higher concentrations of graphene. These micrographs confirmed that there were no nanoplatelets inside the membrane structure (Figure 12). The polymeric membrane was characterized by a sponge-like morphology, which was particularly pronounced for the PVDF pristine membrane. The deposition of a larger amount of graphene flakes caused the formation of a cracked graphene layer on the top of the membrane, which reduced the size of, or entirely clogged, the pores on the top surface. In the case of the graphene dispersion with a lower concentration, it did not form a uniform graphene layer on the top, but rather a random distribution of GNPs throughout the surface was obtained, and thus the pores were not covered [**P4**].

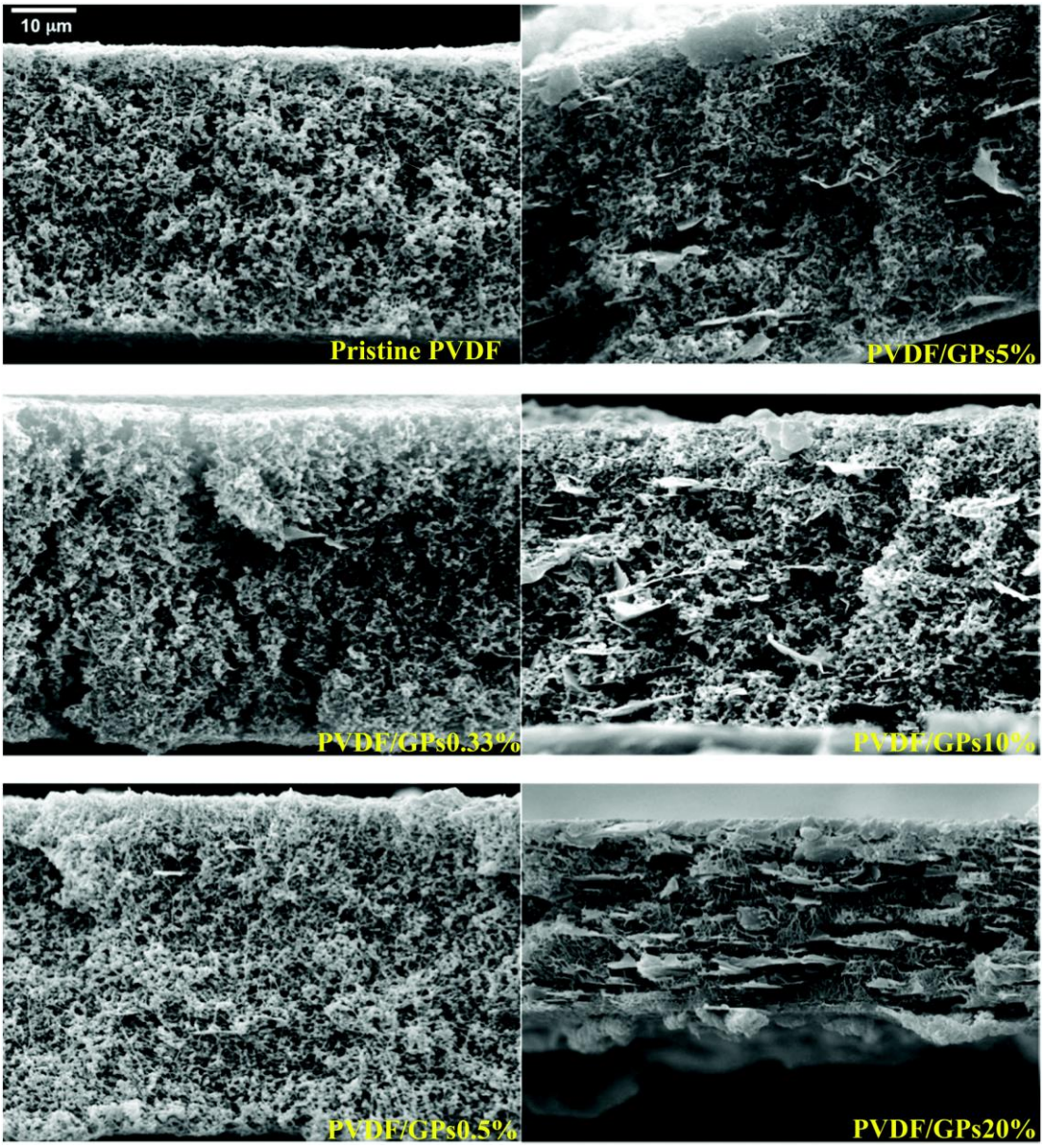

Figure 11. SEM images of the cross-section of mixed-matrix graphene/PVDF membranes.

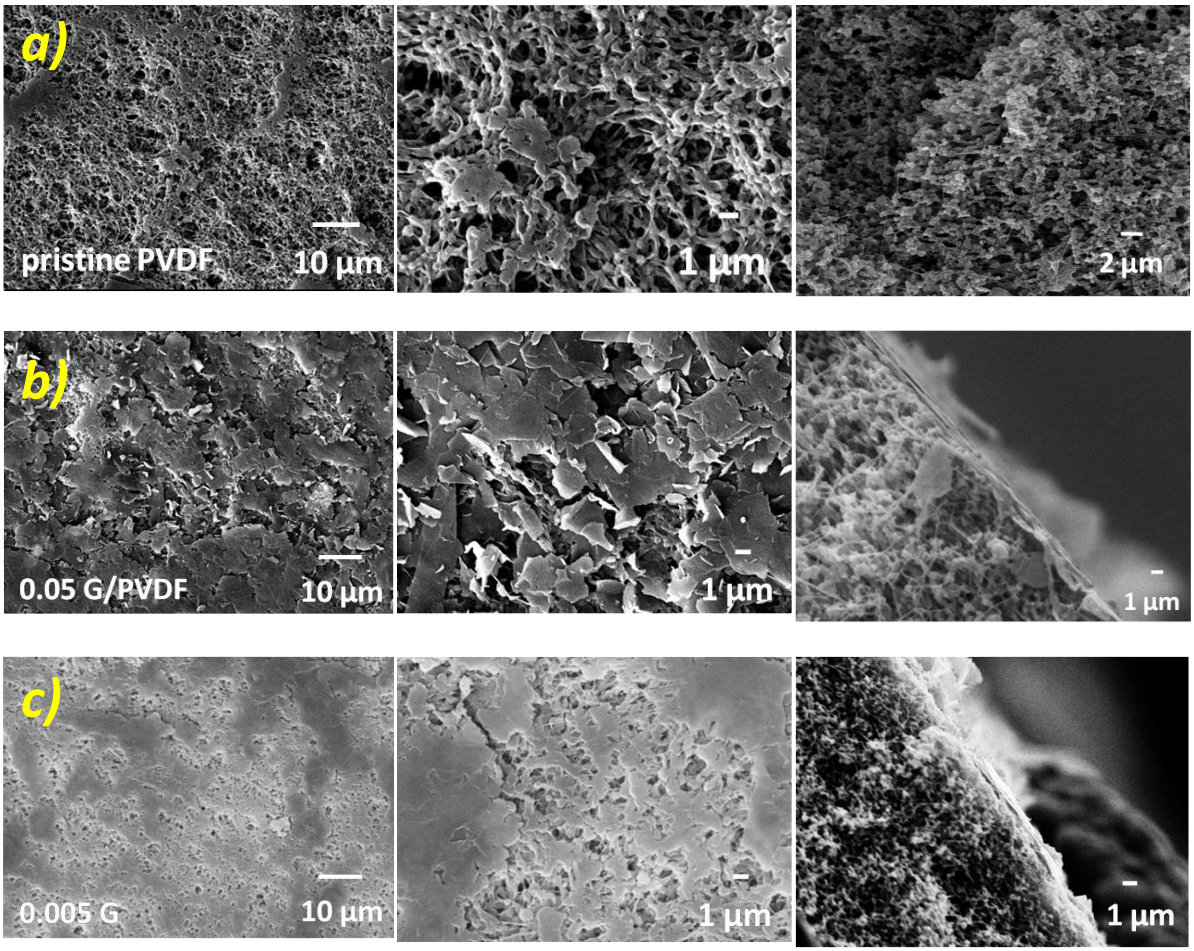

Figure 12. SEM images of the top surface (first and second column) and cross-section (third column) of graphene-coated PVDF membranes.

3.3. Physicochemical properties of graphene-modified membranes

The membranes were further tested in order to evaluate the feasibility of applying them in the MD desalination process. CA measurements were crucial to evaluating the hydrophobicity of the membranes, which ensured the diffusion of only the gas phase in the pores, which is a basic condition of MD. The incorporation of nanofiller inside the polymeric matrix caused a general increase in hydrophobicity. Importantly, a significant increase in the CA value was noted for the graphene fraction of 0.5%, yielding 151±3 ° when in contact with saline water (0.6 M NaCl solution). The results of the enhanced water resistance were further supported by the values of the resistance to liquid entry pressure (LEP), which reached around 1 bar for each MMM. These parameters were found to be suitable for the use of such membranes in the MD process.

Importantly, nanofiller addition gave the further advantage of making the membrane more durable. After strength testing, an increase in the Young's modulus up to 1400 N mm^{-2} was obtained for GNP0.5%. Moreover, at lower GNP loadings, an increase in the resistance to stretching was also observed, with values up to 85 ± 10%. Nevertheless, a further addition of nanofiller to the membrane matrix made the membrane

particularly brittle and unmanageable, especially for GNP20%. Due to its poor mechanical properties, the GNP20% membrane was not approved for further tests and measurements.

According to the AFM images, the non-modified PVDF membrane possessed a smooth microporous surface, with an Rq value of around 289 nm. After the incorporation of nanofiller, this roughness parameter increased up to 524 and 375 nm for GNP0.33% and GNP0.5%, respectively. On the other hand, graphene aggregation led to an Rq reduction down to 292 and 183 nm for GNP5% and GNP10%, respectively. Thus, the roughness enhancement only occurred for well-dispersed GNPs in the membrane matrix with lower nanofiller loading [55]. It is believed that complex surface topography forms an air gap between the surface protrusions and creates a gas–liquid interface that separates the feed liquid and membrane surface. These features are beneficial while dealing with wetting and fouling issues in MD [**P3**].

The membrane material used for sea water desalination should possess antifungal activity to produce potable water free from microbial pathogens and to mitigate biofouling, which significantly reduces the productivity and efficiency of the process. *Curvularia* sp. is one of the common fungi that have been detected in drinking water distribution systems [56], so this hyphomycete fungus was chosen for the antifungal test. To the best of our knowledge, the antifungal activity of PVDF/GNP MMMs hasn't been evaluated so far, thus in study **P3**, we carried out this tests for the first time. The results were presented as an inhibition percentage against a *Curvularia* sp. fungal strain after 72 h. The most promising antifungal properties were achieved for the GNP0.33% and GNP0.5% membranes, with an inhibition percentage of 74.9% and 75.7%, respectively. A slightly lower inhibition percentage was observed for GNP5% (61.7%), while pristine PVDF and GNP10% showed very weak antifungal activity. A clear antimicrobial effect of graphene-modified membranes can be observed in photographs taken after 72 h of fungal growth on the membranes (Figure 13).

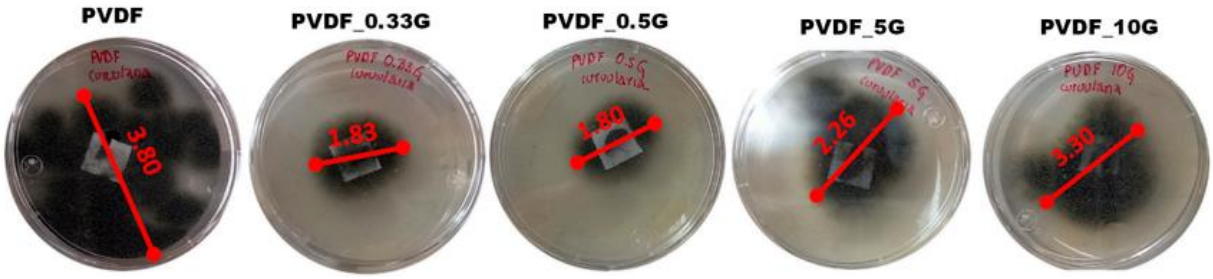

Figure 13. Photographs taken after 72 h of fungal growth on the membranes.

In the case of graphene-coated membranes, chemical and morphological changes brought variations in the wetting behavior. The deposition of a low content of graphene dispersion on the PVDF surface gave rise to improved hydrophobicity with CA values of 136 ± 4° and 124 ± 4° for 0.005G/PVDF and pristine PVDF, respectively. On the other hand, the deposition of more highly concentrated graphene dispersions generated a reduction in hydrophobicity down to 97 ± 2°. The fluctuations in these values result from the fact that the degree of graphene hydrophobicity depends on numerous features, such as the degree of oxidation, the number of sheets, the presence of defects in the structure, the supporting substrate, and the presence of impurities [57][58]. The high hydrophobicity values for the 0.005G/PVDF membranes may be a consequence of the fact that the deposition formed a non-uniform graphene layer on the membrane surface. Therefore, the effects of both the liquid-graphene and liquid-substrate interactions, as well as the chemical affinity, surface heterogeneities, and surface roughness, could be responsible for the CA enhancement. In study **P4**, it was also relevant to observe how the water droplet spread within the first 30 min on the surface of pristine PVDF, 0.005G/PVDF, and 0.05G/PVDF. A reduction in the CA by 10 and 12% was calculated for pristine PVDF and

0.05G/PVDF compared to the initial values. Importantly, the 0.005G/PVDF exhibited stable wetting resistance over time with a just slight decrease of 4% in the CA value. AFM images proved that graphene introduces additional nanoscale structures on the membrane surfaces. The presence of micro- and nanoscale roughness was observed for graphene-coated membranes obtained from 0.005 $mgmL^{-1}$ graphene liquid dispersions, exhibiting $Ra = 272 \pm 10$ nm. A larger deposition of GNPs led to the creation of a more flattened surface with values of $Ra = 97 \pm 7$ nm, which was the lowest surface roughness among the coated samples. Thus, the 0.05G/PVDF membrane was expected to produce a lower resistance to liquid spreading. In contrast, the pristine PVDF surface showed surface roughness values of $Ra = 214 \pm 19$ nm, due to the presence of pores and other surface deformities that resulted from its spherulitic-like polymer structure.

3.4. The effect of graphene on membrane transport properties

The structural and chemical features of MMMs fit well with MD criteria, so the membranes were further tested in order to assess the involvement of GNPs in water vapor diffusion [**P2**]. Compared to pristine PVDF membranes, higher values of the MD coefficient (defined as the ratio between the flux and partial pressure gradient) were detected for membranes with a lower graphene loading, namely GNP0.33% and GNP0.5%. A further increase in the graphene loading resulted in a reduced diffusion of water vapor. The MD coefficient calculated for MMMs showed a fluctuating trend as the driving force of the process increased. FTIR spectra were collected on membrane samples after water vapor had passed through. Additional absorption bands were observed around 3850 and 3750 cm^{-1} for MMMs. These bands were previously noted in pressurized water vapor [59], and their presence can be regarded as a proof of water decomposition at GNP defects and edges. Importantly, more intense absorptions shifted to higher wavenumbers were detected for the GNP0.33% and GNP0.5% membranes. For GNP10%, a shift toward lower wavenumbers was observed, which may indicate stronger interactions established with water vapor resulting in a lower mass transfer. The diffusion of water vapor through the MMMs seemed to be assisted by intermolecular interactions between the defect sites of the filler and water vapor molecules. A low graphene concentration in the polymer matrix activated adhesive interactions resulting in enhanced vapor transport. On the other hand, a significant increase in the concentration of the graphene could cause massive water absorption, generating potential competition between adhesive and cohesive forces, which could prolong the presence of water vapor molecules inside the membrane matrix. This hypothesis was confirmed by the observation of the onset of the permeation of water vapor through the membrane. When the concentration of nanofiller increased, a longer time was required for collecting water at the permeate side, suggesting a longer residence of the water vapor inside the matrix. Based on the experimental results, the GNP0.5% membrane was found to be the one exhibiting a well-balanced sorption–desorption mechanism of the water vapor on graphene edges and vacancies, thus resulting in the highest flux value. Therefore, this sample was chosen for a long-term test. Figure 14 confirms the stability of the membrane over 18 h of the MD desalination process, together with a high permeate quality of around 99.86% for the final rejection factor.

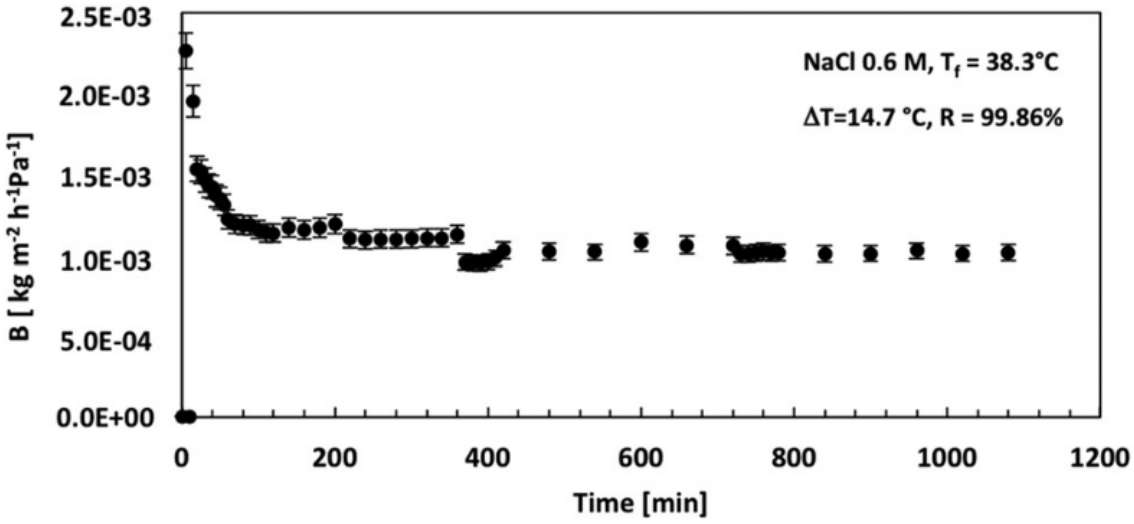

Figure 14. The changes in MD coefficient during desalination using DCMD.

In the case of the graphene-coated membranes, 6 h DCMD tests were carried out in order to evaluate their desalination ability [**P4**]. A better performance in terms of higher fluxes was observed for the graphene-coated membranes. For instance, increases of 106% and 77% in flux were detected for 0.005G/PVDF and 41% and 31% for 0.05G/PVDF compared to the pristine membrane, when working with pure water and 0.6 M NaCl solution, respectively. Importantly, a total salt rejection (100%) was obtained during desalination using 0.005G/PVDF, and a value of 99.84 % was noted for 0.05G/PVDF. In general, the worse performance of 0.05G/PVDF was attributed to its smaller pore size, which resulted in additional mass transfer resistance. Moreover, this membrane presented less MD-suitable morphological features, such as a lower resistance to wetting and a smoother surface. Thus, further tests were applied to pristine PVDF and 0.005G/PVDF membranes only.

A mixture of humic acid (HA) and NaCl was used as a feed solution in order to investigate the antifouling properties and reliability of uncoated and coated membranes. Although a reduction in the flux was detected for both tested membranes, 0.005G/PVDF continued to exhibit a better performance in this experiment. Higher fluxes, total salt rejection, and antifouling properties resulted from the presence of multiscale roughness on 0.005G/PVDF. The created holes and slots throughout the graphene-coated surface reduced the contact area between the membrane and liquid feed, thus enhancing the effective surface area. Moreover, considering the increased flow through the membrane, the role of graphene in providing effective sorption sites that are available for water vapor molecules cannot be neglected. Figure 15 schematically shows the proposed mechanism of the improved 0.005G/PVDF membrane operation.

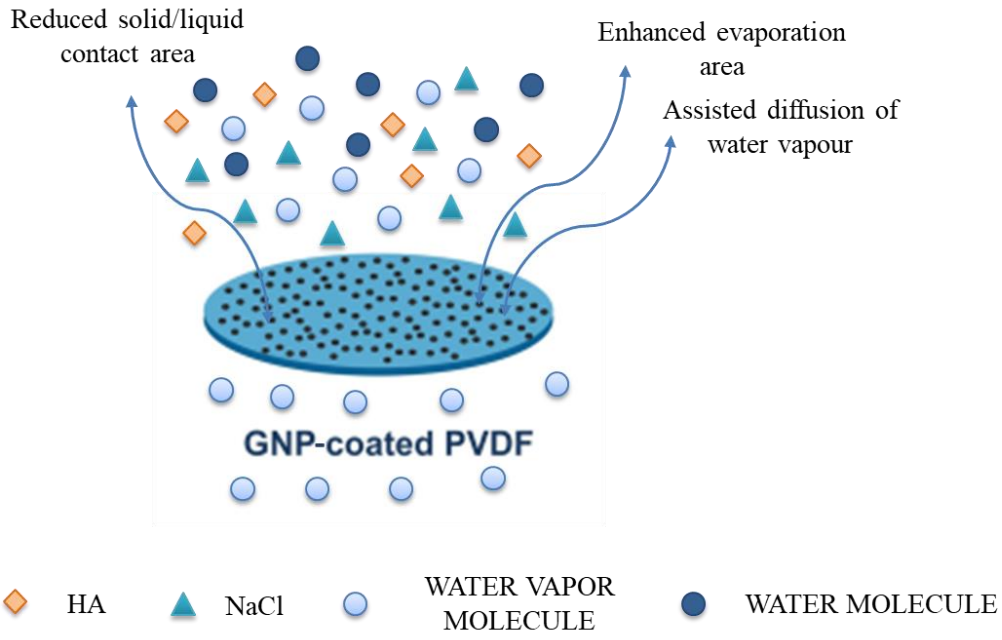

Figure 15. The mechanism of the improved 0.005G/PVDF membrane operation.

We compared our results with other studies on the modification of MD membranes using graphene-based materials. It turned out that the random distribution of GNPs deposited on the surface led to the best performance in terms of productivity, selectivity, and economics [**P4**]. The membrane produced in our study (0.005G/PVDF) was considered competitive due to the following reasons:

(a) We obtained a relatively high flux with respect to employing a low feed temperature and using small temperature differences across the membranes, compared to other studies;

(b) We proved that the simpler and less expensive DCMD configuration can be used to achieve better productivity and selectivity compared to the VMD configuration;

(c) Other literature studies reported the modification of PVDF membranes using graphene oxide or graphene quantum dots, while GNPs have not been employed to date as additives for PVDF surface modification by the wet-filtration approach.

Chapter 4

Conclusions

The results discussed in this dissertation were obtained from the research conducted within the scope of the PhD toward understanding the research aims and achieving the research goals presented in Chapter 2. I provided an overview of superhydrophobic membranes used in the MD process, together with the mechanisms leading to effective MD performance. I demonstrated that nanomaterial-modified membranes may improve the membrane stability in long-term MD processes, increase the vapor flux, and enhance the permeate quality. Subsequently, we examined the effects of graphene incorporation inside the PVDF matrix and on its surface. When applied in MD processes, there was a possibility of assisted or hindered transport of water vapor in both cases, depending on the graphene content. Importantly, this study presents the feasibility of PVDF membrane modification using GNPs. Complex topography due to the incorporation of an additional nanoscale structure was detected on the graphene-coated membranes. The multiscale surface roughness is considered to be responsible for the improved antiwetting and antifouling behavior and an increase in the effective evaporation area of the modified membrane. After six hours of desalination tests, membranes exhibited good stability and total recovery of the initial water. My findings suggest a great potential for graphene-modified membranes in high-performance MD processes.

The novelty of the presented work is summarized in the following statements:

a) The use of GNPs in MD led to the fabrication of membranes that could be used for adsorption-assisted transport through the exploitation of water vapor interactions at the vacancy and edge sites of the nanofiller;

b) PVDF membranes with well-dispersed graphene in the matrix can be potentially used in real seawater desalination using the MD process due to their anti-wetting and antifungal activity;

c) Graphene-coated membranes led to a high vapor flux at a lower feed temperature, using the simpler and less expensive configuration of DCMD, compared to other graphene-based membranes, resulting in a cheaper process.

Literature references:

1. Pendergast, M.M.; Hoek, E.M.V. A Review of Water Treatment Membrane Nanotechnologies. *Energy Environ. Sci.* **2011**, *4*, 1946, doi:10.1039/c0ee00541j.

2. Esfahani, I.J.; Rashidi, J.; Ifaei, P.; Yoo, C. Efficient Thermal Desalination Technologies with Renewable Energy Systems: A State-of-the-Art Review. *Korean J. Chem. Eng.* **2016**, *33*, 351–387, doi:10.1007/s11814-015-0296-3.

3. Harandi, H.B.; Rahnama, M.; Jahanshahi Javaran, E.; Asadi, A. Performance Optimization of a Multi Stage Flash Desalination Unit with Thermal Vapor Compression Using Genetic Algorithm. *Appl. Therm. Eng.* **2017**, *123*, 1106–1119, doi:10.1016/j.applthermaleng.2017.05.170.

4. Lee, A.; Elam, J.W.; Darling, S.B. Membrane Materials for Water Purification: Design, Development, and Application. *Environ. Sci. Water Res. Technol.* **2016**, *2*, 17–42, doi:10.1039/C5EW00159E.

5. Darre, N.C.; Toor, G.S. Desalination of Water: A Review. *Curr. Pollut. Reports* **2018**, *4*, 104–111, doi:10.1007/s40726-018-0085-9.

6. Nair, M.; Kumar, D. Water Desalination and Challenges: The Middle East Perspective: A Review. *Desalin. Water Treat.* **2013**, *51*, 2030–2040, doi:10.1080/19443994.2013.734483.

7. Deshmukh, A.; Boo, C.; Karanikola, V.; Lin, S.; Straub, A.P.; Tong, T.; Warsinger, D.M.; Elimelech, M. Membrane Distillation at the Water-Energy Nexus: Limits, Opportunities, and Challenges. *Energy Environ. Sci.* **2018**, *11*, 1177–1196, doi:10.1039/c8ee00291f.

8. B.R. Bodell Silicone Rubber Vapor Diffusion in Saline Water Distillation 1963.

9. Weyl P. K. Recovery Demineralised Water from Saline Water 1967.

10. Findley, M.E. Vaporization through Porous Membranes. *Ind. Eng. Chem. Process Des. Dev.* **1967**, *6*, 226–230, doi:10.1021/i260022a013.

11. Findley, M.E.; Tanna, V. V.; Rao, Y.B.; Yeh, C.L. Mass and Heat Transfer Relations in Evaporation through Porous Membranes. *AIChE J.* **1969**, *15*, 483–489, doi:10.1002/aic.690150404.

12. Gontarek-Castro, E.; Lieder, M. Food Bioactive Ingredients Processing Using Membrane Distillation. In *Membrane Separation of Food Bioactive Ingredients.*; 2021; pp.103–130 ISBN 978-3-030-84642-8.

13. Srisurichan, S.; Jiraratananon, R.; Fane, A.G. Mass Transfer Mechanisms and Transport Resistances in Direct Contact Membrane Distillation Process. *J. Memb. Sci.* **2006**, *277*, 186–194, doi:10.1016/j.memsci.2005.10.028.

14. Curcio, E.; Drioli, E. Membrane Distillation and Related Operations - A Review. *Sep. Purif. Rev.* **2005**, *34*, 35–86, doi:10.1081/SPM-200054951.

15. Shirtcliffe, N.J.; McHale, G.; Atherton, S.; Newton, M.I. An Introduction to Superhydrophobicity. *Adv. Colloid Interface Sci.* **2010**, *161*, 124–138, doi:10.1016/j.cis.2009.11.001.

16. Barthlott, W.; Neinhuis, C. Purity of the Sacred Lotus, or Escape from Contamination in Biological Surfaces. *Planta* **1997**, *202*, 1–8, doi:10.1007/s004250050096.

17. Sun, T.; Feng, L.; Gao, X.; Jiang, L. Bioinspired Surfaces with Special Wettability. *Acc. Chem. Res.* **2005**, *38*, 644–652, doi:10.1557/mrs.2013.100.

18. Neinhuis, C.; Barthlott, W. Characterization and Distribution of Water-Repellent, Self-Cleaning Plant Surfaces. *Ann. Bot.* **1997**, *79*, 667–677, doi:10.1006/anbo.1997.0400.

19. McHale, G.; Shirtcliffe, N.J.; Newton, M.I. Super-Hydrophobic and Super-Wetting Surfaces: Analytical Potential? *Analyst* **2004**, *129*, 284–287.

20. Wenzel, R.N. Resistance of Solid Surfaces to Wetting by Water. *Ind. Eng. Chem.* **1936**, *28*, 988–994, doi:10.1021/ie50320a024.

21. Cassie, A.B.D.; Baxter, S. Wettability of Porous Surfaces. *Trans. Faraday Soc.* **1944**, *40*, 546, doi:10.1039/tf9444000546.

22. Wenzel, R.N. Surface Roughness and Contact Angle. *J. Phys. Colloid Chem.* **1949**, *53*, 1466–1467, doi:10.1021/j150474a015.

23. Yao, M.; Tijing, L.D.; Naidu, G.; Kim, S.H.; Matsuyama, H.; Fane, A.G.; Shon, H.K. A Review of Membrane Wettability for the Treatment of Saline Water Deploying Membrane Distillation. *Desalination* **2020**, *479*, 114312, doi:10.1016/j.desal.2020.114312.

24. Tuteja, A.; Choi, W.; Ma, M.; Mabry, J.M.; Mazzella, S.A.; Rutledge, G.C.; McKinley, G.H.; Cohen, R.E. Designing Superoleophobic Surfaces. *Science (80-.).* **2007**, *318*, 1618–1622, doi:10.1126/science.1148326.

25. Lu, K.J.; Chen, Y.; Chung, T.S. Design of Omniphobic Interfaces for Membrane Distillation – A Review. *Water Res.* **2019**, *162*, 64–77, doi:10.1016/j.watres.2019.06.056.

26. Tijing, L.D.; Woo, Y.C.; Choi, J.S.; Lee, S.; Kim, S.H.; Shon, H.K. Fouling and Its Control in Membrane Distillation-A Review. *J. Memb. Sci.* **2015**, *475*, 215–244, doi:10.1016/j.memsci.2014.09.042.

27. Kullab, A.; Martin, A. Membrane Distillation and Applications for Water Purification in Thermal Cogeneration Plants. *Sep. Purif. Technol.* **2011**, *76*, 231–237, doi:10.1016/j.seppur.2010.09.028.

28. Hausmann, A.; Sanciolo, P.; Vasiljevic, T.; Weeks, M.; Schroën, K.; Gray, S.; Duke, M. Fouling Mechanisms of Dairy Streams during Membrane Distillation. *J. Memb. Sci.* **2013**, *441*, 102–111, doi:10.1016/j.memsci.2013.03.043.

29. Meng, S.; Ye, Y.; Mansouri, J.; Chen, V. Fouling and Crystallisation Behaviour of Superhydrophobic Nano-Composite PVDF Membranes in Direct Contact Membrane Distillation. *J. Memb. Sci.* **2014**, *463*, 102–112, doi:10.1016/j.memsci.2014.03.027.

30. Gryta, M. Influence of Polypropylene Membrane Surface Porosity on the Performance of Membrane Distillation Process. *J. Memb. Sci.* **2007**, *287*, 67–78, doi:10.1016/j.memsci.2006.10.011.

31. Razmjou, A.; Arifin, E.; Dong, G.; Mansouri, J.; Chen, V. Superhydrophobic Modification of TiO2 Nanocomposite PVDF Membranes for Applications in Membrane Distillation. *J. Memb. Sci.* **2012**, *415–416*, 850–863, doi:10.1016/j.memsci.2012.06.004.

32. Woo, Y.C.; Tijing, L.D.; Shim, W.G.; Choi, J.S.; Kim, S.H.; He, T.; Drioli, E.; Shon, H.K. Water Desalination Using Graphene-Enhanced Electrospun Nanofiber Membrane via Air Gap Membrane Distillation. *J. Memb. Sci.* **2016**, *520*, 99–110, doi:10.1016/j.memsci.2016.07.049.

33. Yin, J.; Deng, B. Polymer-Matrix Nanocomposite Membranes for Water Treatment. *J. Memb. Sci.* **2015**, *479*, 256–275, doi:10.1016/j.memsci.2014.11.019.

34. Kumar, R.; Ahmed, M.; Bhadrachari, G.; Al-Mesri, A.; Thomas, J.P. A Facile Approach of Thin Film Coating Consisted of Hydrophobic Titanium Dioxide over Polypropylene Membrane for Membrane Distillation. *J. Membr. Sci. Res.* **2020**, *6*, 196–202, doi:10.22079/JMSR.2019.110904.1273.

35. Ma, P.C.; Siddiqui, N.A.; Marom, G.; Kim, J.K. Dispersion and Functionalization of Carbon Nanotubes for Polymer-Based Nanocomposites: A Review. *Compos. Part A Appl. Sci. Manuf.* **2010**, *41*, 1345–1367, doi:10.1016/j.compositesa.2010.07.003.

36. An, A.K.; Lee, E.J.; Guo, J.; Jeong, S.; Lee, J.G.; Ghaffour, N. Enhanced Vapor Transport in Membrane Distillation via Functionalized Carbon Nanotubes Anchored into Electrospun Nanofibres. *Sci. Rep.* **2017**, *7*, 1–11, doi:10.1038/srep41562.

37. Li, X.; Yu, X.; Cheng, C.; Deng, L.; Wang, M.; Wang, X. Electrospun Superhydrophobic Organic/Inorganic Composite Nanofibrous Membranes for Membrane Distillation. *ACS Appl. Mater. Interfaces* **2015**, *7*, 21919–21930, doi:10.1021/acsami.5b06509.

38. Horseman, T.; Yin, Y.; Christie, K.S.; Wang, Z.; Tong, T.; Lin, S. Wetting, Scaling, and Fouling in Membrane Distillation: State-of-the-Art Insights on Fundamental Mechanisms and Mitigation Strategies. *ACS ES&T Eng.* **2020**, doi:10.1021/acsestengg.0c00025.

39. Liao, Y.; Wang, R.; Fane, A.G. Engineering Superhydrophobic Surface on Poly(Vinylidene Fluoride) Nanofiber Membranes for Direct Contact Membrane Distillation. *J. Memb. Sci.* **2013**, *440*, 77–87, doi:10.1016/j.memsci.2013.04.006.

40. Liao, Y.; Loh, C.H.; Wang, R.; Fane, A.G. Electrospun Superhydrophobic Membranes with Unique Structures for Membrane Distillation. *ACS Appl. Mater. Interfaces* **2014**, *6*, 16035–16048, doi:10.1021/am503968n.

41. Wang, M.; Liu, G.; Yu, H.; Lee, S.H.; Wang, L.; Zheng, J.; Wang, T.; Yun, Y.; Lee, J.K. ZnO Nanorod Array Modified PVDF Membrane with Superhydrophobic Surface for Vacuum Membrane Distillation Application. *ACS Appl. Mater. Interfaces* **2018**, *10*, 13452–13461, doi:10.1021/acsami.8b00271.

42. Zhang, J.; Song, Z.; Li, B.; Wang, Q.; Wang, S. Fabrication and Characterization of Superhydrophobic Poly (Vinylidene Fluoride) Membrane for Direct Contact Membrane Distillation. *Desalination* **2013**, *324*, 1–9, doi:10.1016/j.desal.2013.05.018.

43. Shao, Y.; Han, M.; Wang, Y.; Li, G.; Xiao, W.; Li, X.; Wu, X.; Ruan, X.; Yan, X.; He, G.; et al. Superhydrophobic Polypropylene Membrane with Fabricated Antifouling Interface for Vacuum Membrane Distillation Treating High Concentration Sodium/Magnesium Saline Water. *J. Memb. Sci.* **2019**, *579*, 240–252, doi:10.1016/j.memsci.2019.03.007.

44. Tijing, L.D.; Woo, Y.C.; Shim, W.G.; He, T.; Choi, J.S.; Kim, S.H.; Shon, H.K. Superhydrophobic Nanofiber Membrane Containing Carbon Nanotubes for High-Performance Direct Contact Membrane Distillation. *J. Memb. Sci.* **2016**, *502*, 158–170, doi:10.1016/j.memsci.2015.12.014.

45. Liao, Y.; Wang, R.; Fane, A.G. Fabrication of Bioinspired Composite Nanofiber Membranes with Robust Superhydrophobicity for Direct Contact Membrane Distillation. *Environ. Sci. Technol.* **2014**, *48*, 6335–6341, doi:10.1021/es405795s.

46. Nthunya, L.N.; Gutierrez, L.; Verliefde, A.R.; Mhlanga, S.D. Enhanced Flux in Direct Contact Membrane Distillation Using Superhydrophobic PVDF Nanofibre Membranes Embedded with Organically Modified SiO2 Nanoparticles. *J. Chem. Technol. Biotechnol.* **2019**, *94*, 2826–2837, doi:10.1002/jctb.6104.

47. Ren, L.F.; Xia, F.; Chen, V.; Shao, J.; Chen, R.; He, Y. TiO2-FTCS Modified Superhydrophobic PVDF Electrospun Nanofibrous Membrane for Desalination by Direct Contact Membrane Distillation. *Desalination* **2017**, *423*, 1–11, doi:10.1016/j.desal.2017.09.004.

48. Guo, J.; Deka, B.J.; Kim, K.J.; An, A.K. Regeneration of Superhydrophobic TiO2 Electrospun Membranes in Seawater Desalination by Water Flushing in Membrane Distillation. *Desalination* **2019**, *468*, 114054, doi:10.1016/j.desal.2019.06.020.

49. Wei, X.; Zhao, B.; Li, X.M.; Wang, Z.; He, B.Q.; He, T.; Jiang, B. CF 4 Plasma Surface Modification of Asymmetric Hydrophilic Polyethersulfone Membranes for Direct Contact Membrane Distillation. *J. Memb. Sci.* **2012**, *407–408*, 164–175, doi:10.1016/j.memsci.2012.03.031.

50. Woo, Y.C.; Kim, Y.; Shim, W.G.; Tijing, L.D.; Yao, M.; Nghiem, L.D.; Choi, J.S.; Kim, S.H.; Shon, H.K. Graphene/PVDF Flat-Sheet Membrane for the Treatment of RO Brine from Coal Seam Gas Produced Water by Air Gap Membrane Distillation. *J. Memb. Sci.* **2016**, *513*, 74–84, doi:10.1016/j.memsci.2016.04.014.

51. Guan, L.Z.; Zhao, L.; Wan, Y.J.; Tang, L.C. Three-Dimensional Graphene-Based Polymer Nanocomposites: Preparation, Properties and Applications. *Nanoscale* **2018**, *10*, 14788–14811, doi:10.1039/c8nr03044h.

52. Surwade, S.P.; Smirnov, S.N.; Vlassiouk, I. V.; Unocic, R.R.; Veith, G.M.; Dai, S.; Mahurin, S.M. Water Desalination Using Nanoporous Single-Layer Graphene. *Nat. Nanotechnol.* **2015**, *10*, 459–464, doi:10.1038/nnano.2015.37.

53. Politano, A.; Cattelan, M.; Boukhvalov, D.W.; Campi, D.; Cupolillo, A.; Agnoli, S.; Apostol, N.G.; Lacovig, P.; Lizzit, S.; Farías, D.; et al. Unveiling the Mechanisms Leading to H 2 Production Promoted by Water Decomposition on Epitaxial Graphene at Room Temperature. *ACS Nano* **2016**, *10*, 4543–4549, doi:10.1021/acsnano.6b00554.

54. Sun, G.; Li, X.; Qu, Y.; Wang, X.; Yan, H.; Zhang, Y. Preparation and Characterization of Graphite Nanosheets from Detonation Technique. *Mater. Lett.* **2008**, *62*, 703–706, doi:10.1016/j.matlet.2007.06.035.

55. Papageorgiou, D.G.; Kinloch, I.A.; Young, R.J. Mechanical Properties of Graphene and Graphene-Based Nanocomposites. *Prog. Mater. Sci.* **2017**, *90*, 75–127, doi:10.1016/j.pmatsci.2017.07.004.

56. Aguas, Y.; Hincapie, M.; Fernández-Ibáñez, P.; Polo-López, M.I. Solar Photocatalytic Disinfection of Agricultural Pathogenic Fungi (Curvularia Sp.) in Real Urban Wastewater. *Sci. Total Environ.* **2017**, *607–608*, 1213–1224, doi:10.1016/j.scitotenv.2017.07.085.

57. Bello, R.H.; Coelho, L.A.; Becker, D. Role of Chemical Funcionalization of Carbon Nanoparticles in Epoxy Matrices. *J. Compos. Mater.* **2018**, *52*, 449–464, doi:10.1177/0021998317709082.

58. Hong, G.; Han, Y.; Schutzius, T.M.; Wang, Y.; Pan, Y.; Hu, M.; Jie, J.; Sharma, C.S.; Müller, U.; Poulikakos, D. On the Mechanism of Hydrophilicity of Graphene. *Nano Lett.* **2016**, *16*, 4447–4453, doi:10.1021/acs.nanolett.6b01594.

59. Vigasin, A.A.; Jin, Y.; Ikawa, S. On the Water Dimer Contribution to the OH Stretching Absorption Band Profile in Pressurized Water Vapour. *Mol. Phys.* **2008**, *106*, 1155–1159, doi:10.1080/00268970802021353.

List of academic achievements

JCR-listed publications

1. Rybarczyk, M. K.; Gontarek-Castro, E.; Lieder, M.; Titirici, M. M. Salt melt synthesis of curved nitrogen-doped carbon nanostructures: ORR kinetics boost. *Applied Surface Science*, **2018**, *435*, 543-551, https://doi.org/10.1016/j.apsusc.2017.11.064, **IF: 6.182, Q1, 140 points.**

2. Gontarek-Castro, E.; Macedonio, F.; Militano, F.; Giorno, L.; Lieder, M.; Politano, A.; Drioli, E.; Gugliuzza, A. Adsorption-assisted transport of water vapour in super-hydrophobic membranes filled with multilayer graphene platelets. *Nanoscale.* **2019**, *11*, 11521-11529, https://doi.org/10.1039/C9NR02581B, **IF: 7.790, Q1, 140 points.**

3. Castro-Munoz, R.; Boczkaj, G.; Gontarek-Castro, E.; Cassano, A.; Fila, V. Membrane technologies assisting plant-based and agro-food by-products processing: A comprehensive review. *Trends in Food Science & Technology*, **2020**, *95*, 219-232, https://doi.org/10.1016/j.tifs.2019.12.003, **IF: 12.563, Q1, 200 points.**

4. Castro-Munoz, R.; Diaz-Montes, E.; Cassano, A.; Gontarek-Castro, E. Membrane separation processes for the extraction and purification of steviol glycosides: an overview. *Critical Reviews in Food Science and Nutrition*, **2021**, *61*, 2152-2174, https://doi.org/10.1080/10408398.2020.1772717, **IF: 11.176, Q1, 200 points.**

5. Rybarczyk. M. K.; Gontarek-Castro. E.; Ollik, K., Lieder, M. Biomass-Derived Nitrogen Functionalized Carbon Nanodots and Their Anti-Biofouling Properties. *Processes.* **2021**, *9*, 61-74, https://doi.org/10.3390/pr9010061, **IF: 2.847, Q3, 70 points.**

6. Gontarek-Castro, E.; Castro-Muñoz, R.; Lieder, M. New insights of nanomaterials usage toward superhydrophobic membranes for water desalination via membrane distillation: A review. *Critical Reviews in Environmental Science and Technology*. **2022**, *52*, 2104-2149, https://doi.org/10.1080/10643389.2021.1877032, **IF: 12.561, Q1, 200 points.**

7. Gontarek-Castro, E.; Rybarczyk, M. K.; Castro-Muñoz, R.; Morales-Jiménez, M.; Barragán-Huerta, B.; Lieder, M. Characterization of PVDF/Graphene Nanocomposite Membranes for Water Desalination with Enhanced Antifungal Activity, *Water*. **2021**, *13*, 1279-1290, https://doi.org/10.3390/w13091279, **IF: 3.103, Q2, 100 points.**

8. Castro-Muñoz, R.; Cruz-Cruz, A.; Alfaro-Sommers, Y.; Aranda-Jarillo, L. X.; Gontarek-Castro, E. Reviewing the recent developments of using graphene-based nanosized materials in membrane separations. *Critical Reviews in Environmental Science and Technology*. **2021**, -, -, https://doi.org/10.1080/10643389.2021.1918509, **IF: 12.561, Q1, 200 points.**

9. Castro-Munoz, R.; Diaz-Montes, E.; Gontarek-Castro, E.; Boczkaj, G.; Galanakis, C. M. A comprehensive review on current and emerging technologies toward the valorization of bio-based wastes and by products from foods, *Comprehensive Reviews in Food Science and Food Safety*, **2022**, *21*, 46-105, https://doi.org/10.1111/1541-4337.12894, **IF: 12.811, Q1, 200 points.**

10. Castro-Munoz, R.; Correa-Delgado, M.; Córdova-Almeida, R.; Lara-Nava, D.; Chávez-Muñoz, M.; Velásquez-Chávez, V. F.; Hernández-Torres, C. E.; Gontarek-Castro, E.; Ahmad, M. Z. Natural sweeteners:

Sources, extraction and current uses in foods and food industries, *Food Chemistry*, **2022**, *370*, 130991, https://doi.org/10.1016/j.foodchem.2021.130991, **IF: 7.514, Q1, 200 points.**

11. Castro-Munoz, R.; Gontarek-Castro, E.; Jafari, S. M. Up-to-date strategies and future trends towards the extraction and purification of Capsaicin: A comprehensive review, *Trends in Food Science & Technology*, **2022**, *123*, 161-171, https://doi.org/10.1016/j.tifs.2022.03.014, **IF:12.563, Q1, 200 points.**

12. Gontarek-Castro, E.; Luca, G.D.; Lieder, M.; Gugliuzza, A. Graphene-Coated PVDF Membranes: Effects of Multi-Scale Rough Structure on Membrane Distillation Performance. Membranes **2022**, 12, 511. https://doi.org/10.3390/membranes12050511 **IF: 4,11, Q2, 100 points.**

13. Castro-Munoz, R.; Gontarek-Castro, E.; Karczewski, J.; Cabezas, R.; Venturelli, G. M.; Araya Lopez, C. C.; Boczkaj, G. Hybrid cross-linked chitosan/protonated-proline:glucose DES membranes with superior pervaporation performance for ethanol dehydration, *Journal of Molecular Liquids*, **2022**, 119499, 10.1016/j.molliq.2022.119499, **IF: 6,165, Q1, 100 points.**

Citations (SCOPUS): 183

h-index (SCOPUS): 7

Book chapters

1. Castro-Munoz, R.; Gontarek-Castro, E.; Figoli, A. Membranes for toxic- and heavy-metal removal. In book Current Trends and Future Developments on (Bio-) Membranes, *Elsevier*, 2020, 125-149, ISBN 9780128167786, https://doi.org/10.1016/B978-0-12-816778-6.00007-2.

2. Castro-Munoz, R.; Gontarek-Castro, E. Nanofiltration in the food industry. In book Handbook of Food Nanotechnology, *Academic Press* 2020, 73-106, ISBN 9780128158661, https://doi.org/10.1016/B978-0-12-815866-1.00003-0.

3. Gontarek-Castro, E., Lieder, M. Food Bioactive Ingredients Processing Using Membrane Distillation. In book Membrane Separation of Food Bioactive Ingredients. Food Bioactive Ingredients, *Springer*, 2021, 103-130, ISBN 978-3-030-84643-5, https://doi.org/10.1007/978-3-030-84643-5_4.

Conferences

1. Gontarek-Castro, E.; Lieder, M. *Doctoral Symposium of Nanotechnology NanoMat*, **19-20 June 2017**, Łódź, Poland, „Otrzymywanie kompozytowych membran na bazie chitozanu i tlenku grafenu oraz badanie ich właściwości" (oral speech).

2. Gontarek-Castro, E.; Lieder, M. *XII Summer School for Postgraduate Students and Young Researchers „Interfacial Phenomena in Theory and Practice"*, **25-30 June 2017**, Rybaki near Koscierzyna, Poland, „Preparation and properties of chitosan/graphene oxide nanocomposite membranes" (oral speech).

3. Gontarek-Castro, E.; Lieder, M. *XIII Summer School for Postgraduate Students and Young Researchers „Interfacial Phenomena in Theory and Practice"*, **24-29 June 2018**, Rybaki near Koscierzyna, Poland, „Nanocomposite membranes for membrane distillation process" (oral speech).

4. Gontarek-Castro, E.; Lieder, M. *IX Kongres Technologii Chemicznej*, **03–07 September 2018**, Gdansk, Poland, „Membrany na bazie PVDF i grafenu w procesie destylacji membranowej" (poster).

5. Gontarek-Castro, E.; Lieder, M. *NANOSMAT 2018*, **11-14 September 2018**, Gdansk, Poland, „Effect of graphene addition on membrane performance in membrane distillation process" (poster).

6. Gontarek-Castro, E.; Lieder, M. *IV Interdyscyplinarna Akademicka Konferencja Ochrony Środowiska IAKOŚ 2019*, **05-07 April 2019**, Gdansk, Poland, „Wspomagany transport pary wodnej w superhydrofobowych membranach podczas odsalania wody w procesie destylacji membranowej" (poster).

7. Gontarek-Castro, E.; Macedonio, F.; Giorno, L.; Lieder, M.; Drioli, E.; Gugliuzza, A. *6th International Scientific Conference on Pervaporation, Vapor Permeation, Gas Separation, and Membrane Distillation*, **14-17 May 2019**, Toruń, Poland, „Adsorption-assisted transport of water vapour in hydrophobic PVDF/graphene composite membranes" (oral speech).

8. Gontarek-Castro, E.; Lieder, M. *XIV Summer School for Postgraduate Students and Young Researchers „Interfacial Phenomena in Theory and Practice"*, **24-28 June 2019**, Rybaki near Koscierzyna, Poland, „Assisted Transport of water vapour during desalination using hydrophobic PVDF/graphene membranes" (oral speech).

9. Gontarek-Castro, E.; Lieder, M. *InterNanoPoland 2019*, **16-17 October 2019**, Katowice, Poland, „The effect of graphene deposition on polymer PVDF membranes for water desalination" (poster).

10. Gontarek-Castro, E.; Luca, G. D.; Lieder, M,; Gugliuzza, A. *37th European Membrane Society Summer School 2022*, **29 May – 3 June 2022**, Aldeia da Serra, Portugal, „Graphene-coated PVDF membranes: effects of multi-scale rough structure on membrane distillation performance" (poster).

Internships

1. **30.06.2017-29.12.2017**, Institute on Membrane Technology – National Research Council of Italy, **Rende, Italy,** *Development of composite membranes*, under the supervision of Annarosa Gugliuzza, funded by the Erasmus+ program.

2. **01.10.2018-31.03.2019**, Institute on Membrane Technology – National Research Council of Italy, **Rende, Italy,** *Nanocomposite membranes for membrane distillation process*, under the supervision of Annarosa Gugliuzza, funded by the POW ER program.

3. **15.08.2020 – 13.09.2020**, Escuela Nacional de Ciencias Biológicas at Instituto Politécnico Nacional, **Mexico City, Mexico,** *Bioactivity of graphene modified membranes*, under the supervision of Blanca Barragan, funded by the PROM program.

Projects

1. **April 2021 – May 2021,** "Jednorazowe pieluchy dziecięce: monitorowanie wybranych związków toksycznych poprzez zastosowanie nowych metod analitycznych", National Science Centre, OPUS, UMO-2020/37/B/ST4/02886, PhD student.

Scholarships

1. **October 2018 – September 2022**, scholarship in a frame of *"Development of interdisciplinary doctoral program with international dimension"* (POWR.03.02.00-00-I002/16-002 program)

2. **April 2021 – March 2022**, scholarship for PhD students in a frame of the Integrated Development Program of the Gdańsk University of Technology (POWR.03.05.00-00-Z044/17 program)

Organizational activity

1. Member of the organizing committee of *XIII Summer School for Postgraduate Students and Young Researchers „Interfacial Phenomena in Theory and Practice"*, **24-29 June 2018**, Rybaki near Koscierzyna, Poland

2. Organization of popular science workshops during the Baltic and Pomeranian Science Festival from 2017, Gdańsk , Poland.

Co-authors statements of contribution

GDAŃSK UNIVERSITY OF TECHNOLOGY
FACULTY OF CHEMISTRY

May 21, 2022

Emilia Gontarek-Castro
Department of Process Engineering and Chemical Technology
Faculty of Chemistry
Gdansk University of Technology
Gabriela Narutowicza 11/12
80-233 Gdansk, Poland

Statement of contribution

As a co-author of the articles:

- Gontarek-Castro, E.; Macedonio, F.; Militano, F.; Giorno, L.; Lieder, M.; Politano, A.; Drioli, E.; Gugliuzza, A. Adsorption-assisted transport of water vapour in super-hydrophobic membranes filled with multilayer graphene platelets. *Nanoscale*. **2019**, *11*, 11521-11529, https://doi.org/10.1039/C9NR02581B.

- Gontarek-Castro, E.; Rybarczyk, M. K.; Castro-Muñoz, R.; Morales-Jiménez, M.; Barragán-Huerta, B.; Lieder, M. Characterization of PVDF/Graphene Nanocomposite Membranes for Water Desalination with Enhanced Antifungal Activity, *Water*. **2021**, *13*, 1279-1290, https://doi.org/10.3390/w13091279.

- Gontarek-Castro, E.; Luca, G.D.; Lieder, M.; Gugliuzza, A. Graphene-Coated PVDF Membranes: Effects of Multi-Scale Rough Structure on Membrane Distillation Performance. *Membranes* **2022**, *12*, 511. https://doi.org/10.3390/membranes12050511.

I certify that my contribution consisted of development of the synthesis method, membrane preparation, characterization of the membranes using FTIR, XRD and contact angle measurements, evaluation of membranes porosity, pore size and thickness, investigation of vapor transport performance through the membranes using DCMD process, data analysis, development and preparation of manuscript content, original draft writing, editorial proofreading.

- Gontarek-Castro, E.; Castro-Muñoz, R.; Lieder, M. New insights of nanomaterials usage toward superhydrophobic membranes for water desalination via membrane distillation: A review. *Critical Reviews in Environmental Science and Technology*. **2021**, *52*, 2104-2149, https://doi.org/10.1080/10643389.2021.1877032.

In the above article I conducted a literature review, initiated a research topic (idea), and drafted the manuscript, prepared answers for reviewers, prepared the published versions of manuscript.

Gontarek - Castro

……..
Emilia Gontarek-Castro

GDAŃSK UNIVERSITY OF TECHNOLOGY
FACULTY OF CHEMISTRY

May 21, 2022

Marek Lieder, Professor
Department of Process Engineering and Chemical Technology
Faculty of Chemistry
Gdansk University of Technology
Gabriela Narutowicza 11/12
80-233 Gdansk, Poland

Statement of contribution

As a co-author of the articles:

- Gontarek-Castro, E.; Macedonio, F.; Militano, F.; Giorno, L.; Lieder, M.; Politano, A.; Drioli, E.; Gugliuzza, A. Adsorption-assisted transport of water vapour in super-hydrophobic membranes filled with multilayer graphene platelets. Nanoscale. 2019, 11, 11521-11529, https://doi.org/10.1039/C9NR02581B.
- Gontarek-Castro, E.; Rybarczyk, M. K.; Castro-Muñoz, R.; Morales-Jiménez, M.; Barragán-Huerta, B.; Lieder, M. Characterization of PVDF/Graphene Nanocomposite Membranes for Water Desalination with Enhanced Antifungal Activity, Water. 2021, 13, 1279-1290, https://doi.org/10.3390/w13091279.
- Gontarek-Castro, E.; Luca, G.D.; Lieder, M.; Gugliuzza, A. Graphene-Coated PVDF Membranes: Effects of Multi-Scale Rough Structure on Membrane Distillation Performance. Membranes 2022, 12, 511, https://doi.org/10.3390/membranes12050511.
- Gontarek-Castro, E.; Castro-Muñoz, R.; Lieder, M. New insights of nanomaterials usage toward superhydrophobic membranes for water desalination via membrane distillation: A review. *Critical Reviews in Environmental Science and Technology*. **2021**, *52*, 2104-2149, https://doi.org/10.1080/10643389.2021.1877032.

I certify that my contribution was to supervise the progress of work, discuss the results, reviewing and editing the original draft and editorial proofreading.

……

Marek Lieder, Professor

GDAŃSK UNIVERSITY OF TECHNOLOGY
FACULTY OF CHEMISTRY

May 21, 2022

Annarosa Gugliuzza, PhD
Institute on Membrane Technology
(CNR-ITM)
c/o University of Calabria
Via P. Bucci cubo 17/C
87030 Rende CS
Italy

Statement of contribution

As a co-author of the articles:

- Gontarek-Castro, E.; Macedonio, F.; Militano, F.; Giorno, L.; Lieder, M.; Politano, A.; Drioli, E.; **Gugliuzza, A**. Adsorption-assisted transport of water vapour in super-hydrophobic membranes filled with multilayer graphene platelets. *Nanoscale* **2019**, *11*, 11521-11529, https://doi.org/10.1039/C9NR02581B.

- Gontarek-Castro, E.; Luca, G.D.; Lieder, M.; **Gugliuzza, A**. Graphene-Coated PVDF Membranes: Effects of Multi-Scale Rough Structure on Membrane Distillation Performance. *Membranes* **2022**, *12*, 511. https://doi.org/10.3390/membranes12050511.

I certify that my contribution was consisted of conceptualization of the work, coordination and supervision of the experimental part, development and preparation of manuscript content, reviewing and editing the original draft and editorial proofreading.

Annarosa Gugliuzza, PhD

GDAŃSK UNIVERSITY OF TECHNOLOGY
FACULTY OF CHEMISTRY

May 21, 2022

Francesca Macedonio, PhD
Institute on Membrane Technology
(CNR-ITM)
c/o University of Calabria
Via P. Bucci cubo 17/C
87030 Rende CS
Italy

Statement of contribution

As a co-author of the article:

- Gontarek-Castro, E.; **Macedonio, F**.; Militano, F.; Giorno, L.; Lieder, M.; Politano, A.; Drioli, E.; Gugliuzza, A. Adsorption-assisted transport of water vapour in super-hydrophobic membranes filled with multilayer graphene platelets. *Nanoscale* **2019**, *11*, 11521-11529, https://doi.org/10.1039/C9NR02581B.

I certify that my contribution was consisted of conceptualization and supervision of membrane distillation experiments.

Francesca Macedonio

Francesca Macedonio, PhD

GDAŃSK UNIVERSITY OF TECHNOLOGY
FACULTY OF CHEMISTRY

May 21, 2022

Francesca Militano, PhD
Institute on Membrane Technology
(CNR-ITM)
c/o University of Calabria
Via P. Bucci cubo 17/C
87030 Rende CS
Italy

Statement of contribution

As a co-author of the article:

- Gontarek-Castro, E.; Macedonio, F.; Militano, F.; Giorno, L.; Lieder, M.; Politano, A.; Drioli, E.; Gugliuzza, A. Adsorption-assisted transport of water vapour in super-hydrophobic membranes filled with multilayer graphene platelets. *Nanoscale* **2019**, *11*, 11521-11529, https://doi.org/10.1039/C9NR02581B.

I certify that my contribution was to prepare membranes and to conduct SEM analysis.

Francesca Militano, PhD

GDAŃSK UNIVERSITY OF TECHNOLOGY
FACULTY OF CHEMISTRY

May 21, 2022

Lidietta Giorno, PhD
Institute on Membrane Technology
(CNR-ITM)
c/o University of Calabria
Via P. Bucci cubo 17/C
87030 Rende CS
Italy

Statement of contribution

As a co-author of the article:

- Gontarek-Castro, E.; Macedonio, F.; Militano, F.; Giorno, L.; Lieder, M.; Politano, A.; Drioli, E.; Gugliuzza, A. Adsorption-assisted transport of water vapour in super-hydrophobic membranes filled with multilayer graphene platelets. *Nanoscale* **2019**, *11*, 11521-11529, https://doi.org/10.1039/C9NR02581B.

I certify that my contribution was consisted of conceptualization and supervision of the work.

Lidietta Giorno, PhD

GDAŃSK UNIVERSITY OF TECHNOLOGY
FACULTY OF CHEMISTRY

May 21, 2022

Antonio Politano, Professor
Department of Physical and Chemical Sciences
University of L'Aquila
Via Vetoio
67100 L'Aquila
Italy

Statement of contribution

As a co-author of the article:

- Gontarek-Castro, E.; Macedonio, F.; Militano, F.; Giorno, L.; Lieder, M.; **Politano, A.**; Drioli, E.; Gugliuzza, A. Adsorption-assisted transport of water vapour in super-hydrophobic membranes filled with multilayer graphene platelets. *Nanoscale* **2019**, *11*, 11521-11529, https://doi.org/10.1039/C9NR02581B.

I certify that my contribution consisted of coordination and supervision of the HREELS experiments, development and preparation of manuscript content and reviewing and editing the original draft.

Firmato digitalmente da: Antonio Politano
Organizzazione: UNIVERSITA' DEGLI STUDI DELL'AQUILA/01021630668
Limitazioni d'uso: Explicit Text: Il titolare fa uso del presente certificato solo per le finalità di lavoro per le quali esso è rilasciato. The certificate holder must use the certificate only for the purposes for which it is issued.
Luogo: L'Aquila
Data: 14/06/2022 11:58:35

Antonio Politano

GDAŃSK UNIVERSITY OF TECHNOLOGY
FACULTY OF CHEMISTRY

May 21, 2022

Enrico Drioli, Professor
Institute on Membrane Technology
(CNR-ITM)
c/o University of Calabria
Via P. Bucci cubo 17/C
87030 Rende CS
Italy

Statement of contribution

As a co-author of the article:

- Gontarek-Castro, E.; Macedonio, F.; Militano, F.; Giorno, L.; Lieder, M.; Politano, A.; **Drioli, E.**; Gugliuzza, A. Adsorption-assisted transport of water vapour in super-hydrophobic membranes filled with multilayer graphene platelets. *Nanoscale* **2019**, *11*, 11521-11529, https://doi.org/10.1039/C9NR02581B.

I certify that my contribution was consisted of conceptualization and supervision of the work.

.....
Enrico Drioli, Professor

GDAŃSK UNIVERSITY OF TECHNOLOGY
FACULTY OF CHEMISTRY

May 21, 2022

Maria Rybarczyk, PhD
Chemical Faculty
Warsaw University of Technology
Noakowskiego 3
00-664 Warsaw
Poland

Statement of contribution

As a co-author of the article:

- Gontarek-Castro, E.; **Rybarczyk, M. K.**; Castro-Muñoz, R.; Morales-Jiménez, M.; Barragán-Huerta, B.; Lieder, M. Characterization of PVDF/Graphene Nanocomposite Membranes for Water Desalination with Enhanced Antifungal Activity, *Water* **2021**, *13*, 1279-1290, https://doi.org/10.3390/w13091279.

I certify that my contribution was consisted of fund acquisition for the AFM measurements and editorial proofreading.

Maria Rybarczyk

Maria Rybarczyk, PhD

GDAŃSK UNIVERSITY OF TECHNOLOGY
FACULTY OF CHEMISTRY

May 21, 2022

Roberto Castro-Muñoz, PhD
Tecnologico de Monterrey
Campus Toluca
Avenida Eduardo Monroy Cardenas 2000
San Antonio Buenavista
Toluca de Lerdo
Mexico

Statement of contribution

As a co-author of the articles:

- Gontarek-Castro, E.; **Castro-Muñoz, R.**; Lieder, M. New insights of nanomaterials usage toward superhydrophobic membranes for water desalination via membrane distillation: A review. *Critical Reviews in Environmental Science and Technology* **2021**, *52*, 2104-2149, https://doi.org/10.1080/10643389.2021.1877032.

- Gontarek-Castro, E.; Rybarczyk, M. K.; **Castro-Muñoz, R.**; Morales-Jiménez, M.; Barragán-Huerta, B.; Lieder, M. Characterization of PVDF/Graphene Nanocomposite Membranes for Water Desalination with Enhanced Antifungal Activity, *Water* **2021**, *13*, 1279-1290, https://doi.org/10.3390/w13091279.

I certify that my contribution was consisted of reviewing and editing the original draft and editorial proofreading.

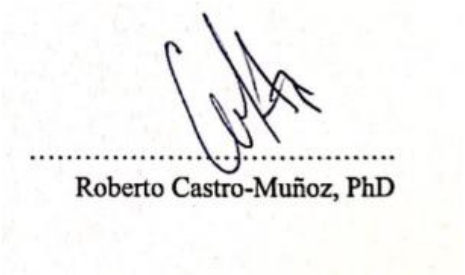

GDAŃSK UNIVERSITY OF TECHNOLOGY
FACULTY OF CHEMISTRY

May 21, 2022

Giuseppe di Luca
Institute on Membrane Technology
(CNR-ITM)
c/o University of Calabria
Via P. Bucci cubo 17/C
87030 Rende CS
Italy

Statement of contribution

As a co-author of the article:

- Gontarek-Castro, E.; **Luca, G.D.**; Lieder, M.; Gugliuzza, A. Graphene-Coated PVDF Membranes: Effects of Multi-Scale Rough Structure on Membrane Distillation Performance. *Membranes* **2022**, *12*, 511. https://doi.org/10.3390/membranes12050511.

I certify that my contribution was consisted of membrane preparation and membrane testing in DCMD process.

Giuseppe di Luca

GDAŃSK UNIVERSITY OF TECHNOLOGY
FACULTY OF CHEMISTRY

May 21, 2022

Monica Morales-Jiménez, PhD
Escuela Nacional de Ciencias Biológicas
Instituto Politécnico Nacional
Avenida Wilfrido Massieu s/n
Unidad Profesional Adolfo López Mateos
Mexico City 07738
Mexico

Statement of contribution

As a co-author of the article:

- Gontarek-Castro, E.; Rybarczyk, M. K.; Castro-Muñoz, R.; **Morales-Jiménez, M.**; Barragán-Huerta, B.; Lieder, M. Characterization of PVDF/Graphene Nanocomposite Membranes for Water Desalination with Enhanced Antifungal Activity, *Water* **2021**, *13*, 1279-1290, https://doi.org/10.3390/w13091279.

I certify that my contribution was consisted of evaluation of the antifungal properties of the membrane.

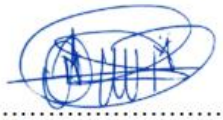

.....
Monica Morales-Jiménez, PhD

GDAŃSK UNIVERSITY OF TECHNOLOGY
FACULTY OF CHEMISTRY

May 21, 2022

Blanca Barragán-Huerta, Professor
Escuela Nacional de Ciencias Biológicas
Instituto Politécnico Nacional
Avenida Wilfrido Massieu s/n
Unidad Profesional Adolfo López Mateos
Mexico City 07738
Mexico

Statement of contribution

As a co-author of the article:

- Gontarek-Castro, E.; Rybarczyk, M. K.; Castro-Muñoz, R.; Morales-Jiménez, M.; **Barragán-Huerta, B.**; Lieder, M. Characterization of PVDF/Graphene Nanocomposite Membranes for Water Desalination with Enhanced Antifungal Activity, *Water* **2021**, *13*, 1279-1290, https://doi.org/10.3390/w13091279.

I certify that my contribution was consisted of conceptualization and supervision of the antifungal activity measurements.

Blanca Barragán-Huerta, Professor

CRITICAL REVIEWS IN ENVIRONMENTAL SCIENCE AND TECHNOLOGY
https://doi.org/10.1080/10643389.2021.1877032

Taylor & Francis
Taylor & Francis Group

Check for updates

New insights of nanomaterials usage toward superhydrophobic membranes for water desalination via membrane distillation: A review

Emilia Gontarek-Castro[a], Roberto Castro-Muñoz[b], and Marek Lieder[a]

[a]Faculty of Chemistry, Department of Process Engineering and Chemical Technology, Gdansk University of Technology, Gdansk, Poland; [b]Tecnologico de Monterrey, Campus Toluca, Avenida Eduardo Monroy Cárdenas 2000 San Antonio Buenavista, Toluca de Lerdo, Mexico

ABSTRACT

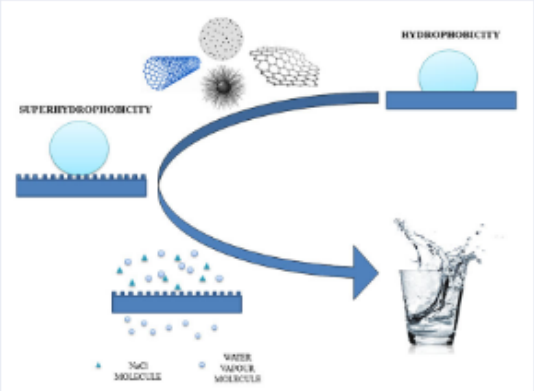

Membrane distillation (MD) is a promising technology for seawater desalination due to the ability to process high-salinity waters and the ability to be driven by low-grade or waste heat. However, practical applications of MD membranes are limited by the low vapor flux and fouling problem. Recently, there is a growing interest in developing novel MD membrane materials with enhanced hydrophobicity to improve the efficiency of desalination performance. Interestingly, the incorporation of nanomaterials for tailoring superhydrophobic properties of MD membranes has attracted enormous attention in MD. Herein, according to the new insights of the available literature data, the current trend for achieving superhydrophobic MD membranes by embedding inorganic nanomaterials is provided. The influence of the inorganic additives on membrane fouling, stability, separation performance, is also discussed. Finally, theoretical principles of MD, the milestones of the evolution of developing superhydrophobic membrane surfaces, and future trends are also given for the new readers in the field.

KEYWORDS Desalination; membrane distillation; nanomaterials; superhydrophobic membranes; vapor transport; water treatment

1. Introduction

Membrane distillation is a thermally-driven process, which is known for its high potential for water treatment. Briefly, the real possibility of application, especially in seawater desalination processes, regards to its high water

CONTACT Emilia Gontarek-Castro emilia.gontarek@pg.edu.pl Faculty of Chemistry, Department of Process Engineering and Chemical Technology, Gdansk University of Technology, Gdansk, Poland; Roberto Castro-Muñoz food.biotechnology88@gmail.com, castromr@tec.mx Tecnologico de Monterrey, Campus Toluca, Avenida Eduardo Monroy Cárdenas 2000 San Antonio Buenavista, Toluca de Lerdo, Mexico.

Nomenclature

AGMD	air gap membrane distillation	PTFE	polytetrafluoroethylene
B	geometric factor determined by pore structure	PVDF	poly (vinylidene fluoride)
		RO	reverse osmosis
CNT	carbon nanotube	SDS	sodium dodecyl sulfate
FAS	fluoroalkylsilane	VMD	vacuum membrane distillation
GO	graphene oxide	γ	surface tension
LEP	liquid entry pressure	d	pore diameter
M	molecular weight	ε	porosity
MD	membrane distillation	λ	heat of vaporization
MMM	mixed matrix membranes	τ	tortuosity
PcH	Polyvinylidene fluoride-co-hexafluoropropylene	δ	membrane thickness
PP	polypropylene		

recovery and ability to treat high-salinity waters. Although, reverse osmosis is the most energy efficient desalination technology, membrane distillation has the potential to become less energy intensive by incorporating low grade energy or waste heat (Deshmukh et al., 2018). In particular, MD process requires the use of hydrophobic micro-porous membrane, which separates two different aqueous solutions but allows only vapor permeation. The driving force of the process is the vapor pressure difference across the membrane, which is induced by the temperature difference between feed and permeate. In principle, due to membrane hydrophobicity, vapor is the only one able to pass through the membrane pores, making MD a good candidate for the separation of nonvolatile compounds from water solution. When dealing with seawater desalination, the most typical configuration is direct contact membrane distillation (DCMD), in which hydrophobic micro-porous membrane is directly exposed to both streams (i.e. heated feed and cold permeate), as illustrated in Figure 1. Typically, both streams are operated in a counterflow configuration. It is worth to mention that DCMD configuration owes its popularity to the easy construction, while in fact its performance is less efficient than other configurations e.g. air gap membrane distillation (AGMD) and vacuum membrane distillation (VMD). For instance, Eykens, Hitsov, et al. (2017) stated that AGMD configuration modules showed a higher flux and lower energy consumption compared to direct contact membrane distillation (DCMD) in a pilot scale experiments, while Cerneaux et al. (2009) observed much higher fluxes of VMD than DCMD during desalination using ceramic membranes.

For an efficient operation of a MD process, the perm-selective barrier should present a highly hydrophobic surface, which is preferred since it may concurrently repel the water molecules in liquid state and favor the vapor transport. For this reason, superhydrophobic membranes gained special attention in MD process. Such a term implies to those membranes that

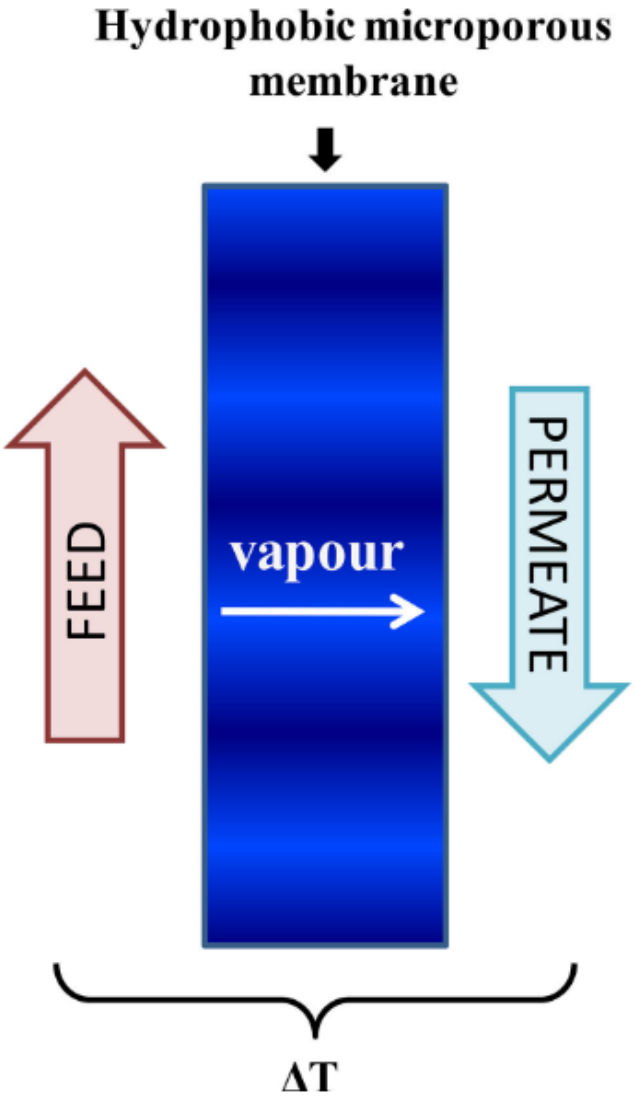

Figure 1. The scheme of direct contact membrane distillation (DCMD).

may display a high water contact angle (over 150°). However, most of the membrane materials do not display such a high contact angle, as shown in Table 1.

For this reason, there is a growing trend in developing new strategies for improving the existing materials, as well as tailoring new materials, to obtain superhydrophobic membranes. For instance, Figure 2 depicts the growing interest of researchers in exploring superhydrophobic membranes over the last 10 years.

Furthermore, few review papers dedicated to membranes for MD application have been published within the last years. Eykens, De Sitter, et al. (2017) provided a literature review on the different methods for MD

Table 1. Some examples of hydrophobic membrane materials and their water contact angles.

Membrane	Chemical structure	Water contact angle	References
PVDF (GE Osmonics)	$(CH_2CF_2)_n$	113°	Zhang et al. (2010)
Nanofibrous PVDF	$(CH_2CF_2)_n$	>135°	Liao, Wang, Tian, et al. (2013)
PTFE (Membrane Solutions)	$(CF_2CF_2)_n$	126°	Zhang et al. (2010)
PP (Membrana GmbH)	$[CH_2CH(CH_3)]_n$	98°	Gryta (2018)
Matrimid 5218	3,3′-4, 4′-benzophenone tetracarboxylic-dianhydride diaminophenylindane	85°	Francis et al. (2013)
Nanofibrous Matrimid	3,3′-4, 4′-benzophenone tetracarboxylic-dianhydride diaminophenylindane	130°	Francis et al. (2013)
Nanofibrous polystyrene	$[CH_2CH(C_6H_5)]_n$	114°	Ke et al. (2016)
Polysulfone	$[C_6H_4\text{-}4\text{-}C(CH_3)_2C_6H_4\text{-}4\text{-}OC_6H_4\text{-}4\text{-}SO_2C_6H_4\text{-}4\text{-}O]_n$	106°	Peng et al. (2013)
Hyflon AD	$(C_4F_6O_3)n(C_2F_4)_m$	130–150°	Gugliuzza et al. (2006)

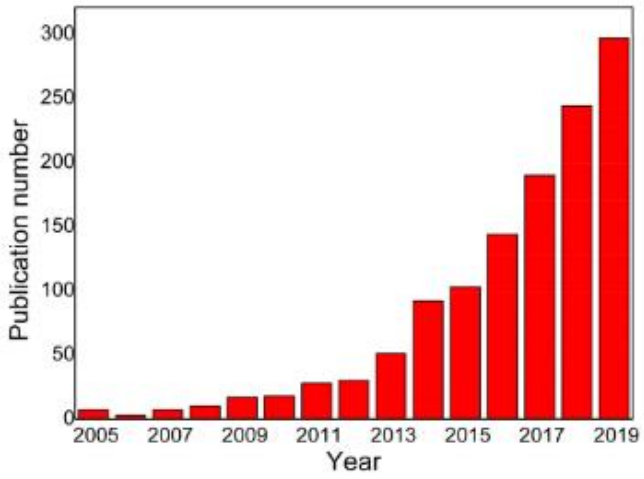

Figure 2. Publication trend on developing superhydrophobic membranes over the last 10 years (source Web of Science, Keywords: superhydrophobic membrane).

membranes synthesis including basic process principle, parameters evaluation and module types used for MD. Himma et al. (2019) focused on the preparation methods of only superhydrophobic membrane, including direct processing method and surface modification. Nthunya, Gutierrez, Derese, et al. (2019) provided a comprehensive review regarding MD process, additionally, some examples of membrane modification by incorporation of nanoparticles were discussed. Pan et al. (2019) reviewed electrospun nanofibrous membranes for MD applications, emphasized on the research developments in recent 3 ~ 4 years. An analysis on the relationship between the membrane structures and the MD performance has been provided. Yao et al. (2020) focused on various types of surface special wettability, and their fabrication methods for MD. Nevertheless, most of the above mentioned works were mainly devoted to methods of membrane preparation

and synthesis. Considering the recent updates in MD regarding the role of nanomaterials in tailoring membrane morphology and water vapor transport during desalination, we believe that it is necessary to organize a new review paper that will emphasize the effect of these materials on membrane performance through the state-of-the-art research development discussion. Therefore, this paper brings and elucidates the recent literature review on strategies adopted by the research community in fabricating superhydrophobic MD membranes for desalination, giving special attention to polymeric membranes containing different nanomaterials. An overview of the typical and emerging nanomaterials used for MD membranes modification as well as the underlying mechanism leading to improvement of MD performance has been introduced. In addition to this, we provide the theoretical principles and requirements for MD membranes.

2. Theoretical principles of MD process

2.1. Mass transfer

Within membrane distillation process, the mass transfer takes place due to the vapor pressure gradient between feed and permeate. First, volatile species are transported from the bulk feed to the membrane surface, subsequently such compounds diffuse through the membrane pores in gaseous phase; finally, the gaseous volatiles are transported from the permeate membrane surface to the bulk permeate. To date, the mass transfer during MD has been described by four possible mechanisms: Knudsen diffusion, viscous flow, surface diffusion and molecular diffusion (Orfi et al., 2016). In general, for DCMD process, viscous flow and surface diffusion can be omitted (Lawson & Lloyd, 1997), while for some specific cases the models can be further simplified depending on the pore size, as described below (Khayet et al., 2004).

1. Knudsen diffusion model: systems where collisions between molecule and pore wall are dominant, as denoted by Eq. (1):

$$N' = \frac{1}{RT}\frac{2}{3}\frac{\varepsilon r}{\tau}\left(\frac{8RT}{\pi M_i}\right)^{1/2}\frac{(p_1 - p_2)}{\delta} \quad (1)$$

where ε, r, τ, M_i and δ are porosity, pore radius, tortuosity, molecular weight of water vapor and membrane thickness, respectively.

2. Molecular diffusion model: systems, where the membrane pore size is relatively large, the mass transfer is mainly determined by the collisions between the molecules:

$$N' = \frac{\varepsilon}{\tau\delta}\frac{PD_{ij}}{RT}\frac{(p_1 - p_2)}{|p_a|_{ln}} \tag{2}$$

where D, P and p_a are the Fick's diffusion coefficient, total pressure in the pore and air pressure in the pore, respectively.

During MD operation the concentration of solutes in feed solution becomes higher at the liquid/gas interface than in the bulk feed. This phenomenon is called concentration polarization. Concentration polarization coefficient (*CPC*) is given by Eq. (3):

$$CPC = \frac{c_{f,m}}{c_f} \tag{3}$$

where $c_{f,m}$ is a concentration of the solute at the membrane surface and c_f is a concentration of the solute in the bulk feed.

2.2. Heat transfer

Along with the mass, the heat transfer also occurs. Heat transfer represents an important aspect in all MD configurations. For instance, the heat transfer in DCMD is usually considered in two important mechanisms (Alkhudhiri et al., 2012). The conductive heat transfer along the membrane pores that occurs together with the vapor diffusion causes temperature change at the both membrane boundary layers. This leads to a temperature gradient in the feed and permeate (between the bulk and boundary layer) and results in the convective heat transfer (Srisurichan et al., 2006).

Convective heat transfer at the feed boundary layer can be given by Eq. (4):

$$Q_f = h_f\left(T_f - T_{f,s}\right) \tag{4}$$

while for permeate at the boundary layer:

$$Q_p = h_p\left(T_{p,s} - T_p\right) \tag{5}$$

In the case of the heat transfer across the membrane, it can be denoted by Eq. (6):

$$Q_m = h_m\left(T_{f,s} - T_{p,s}\right) + J\Delta H_v \tag{6}$$

where h_f, h_p and h_m represent the heat transfer coefficients of the feed, permeate and membrane, respectively, T_f and T_p are the temperature of the feed and permeate, respectively. $T_{f,s}$ and $T_{p,s}$ are the surface temperatures on the feed and permeate side, respectively.

With the increasing difference between the bulk feed and permeate temperatures, as well as the surface temperature at the corresponding side of the membrane, the effect of temperature polarization also raises

(Termpiyakul et al., 2005). Temperature polarization (ψ) is defined as follows:

$$\psi = \frac{T_{f,s} - T_{p,s}}{T_f - T_p} \tag{7}$$

Such equation relates to the effect of heat transfer at the boundary layer and the total heat transfer resistance for a given system. When the ψ value reaches 1, the resistances of thermal boundary layer are reduced, while when the value is equal to 0, the system is controlled by large thermal boundary layer resistance. Typically, for DCMD temperature polarization value lies between 0.4 and 0.7 (Curcio & Drioli, 2005).

2.3. Fouling phenomena

The fouling is defined as the deposition of any material on the membrane surface or in the membrane pores, that leads to a meaningful change in the membrane separation performance (Smolders & Franken, 1989). The fouling in MD can occur in various forms depending on the chemical composition of the feed bulk solution including organic, inorganic, and biological fouling. In MD processes, mineral scaling is usually referred to inorganic fouling. For example, during desalination of concentrated salt solutions, it is common to observe scale formation at the membrane surface (Kullab & Martin, 2011). There are different ions in hypersaline wastewaters that may form sparingly soluble minerals, such as sulfates, carbonates, and silicates. During MD process, the feed solution get concentrated as water evaporates, leading in some cases to the growth of a layer of mineral crystals on the membrane surface (He et al., 2008). Organic fouling rises from treatment of solutions containing protein-type macromolecules, humic acids, or emulsified oil droplets, that leads to their adsorption at the membrane surface (Hausmann et al., 2013). Biological fouling (biofouling) is caused by the growth of bacteria, fungi, and algae, also called as a biofilm formation on the membrane surface. In general, fouling increases the resistance to heat and mass transfer, and leads to the rapid flux decline and membrane wetting (Goh et al., 2013). To improve the MD stability against different fouling types, membranes with special surface wettability, such as Janus, omniphobic and superhydrophobic have been developed (Yao et al., 2020).

3. Membrane requirements for MD process

It has been documented that MD process operates with lower temperatures and pressures compared to other membrane processes for water desalination (e.g. reverse osmosis). In addition to this, MD is characterized by a high salt

rejection rates, and lower tendency to concentration polarization phenomena (Macedonio & Drioli, 2008). The limiting factor for the development of a more efficient MD process is the lack of suitable membrane materials. This efficiency will be ensured when the membrane will be free from pore blocking and wetting. However, the feed solution during MD sea water desalination may contain substances, such as organic matter and oil particles, that promote fouling and wetting of conventional hydrophobic membranes. Moreover, the treatment of hypersaline brine results in mineral scaling on the membrane surface that leads to significant flux reduction, while the presence of low surface tension liquids in the feed reduces the overall surface tension of the feed and results in pore wetting. For this reason, the technology of MD membrane preparation faces few challenges including pore wetting, mineral scaling, and membrane fouling (Horseman et al., 2021). Several studies have been devoted to the preparation of synthetic membranes that would meet all of the requirements of MD process. So far, the most popular membrane materials for MD process are stretched or phase inverted polymers, such as polypropylene (PP) (Tang et al., 2010), polytetrafluoroethylene (PTFE) (Zhu et al., 2013) and poly (vinylidene fluoride) (PVDF) (Devi et al., 2014). Ceramic materials are less used since they display high thermal conductivity, leading to heat loss through the membrane (Wang et al., 2016). Furthermore, ceramic-based materials are usually more expensive than polymeric ones. According to these disadvantages, few development works using ceramic membranes have been reported (Cerneaux et al., 2009; Fang et al., 2012; Larbot et al., 2004). Therefore, special emphasis has been paid over the last years at improving polymeric membranes. Nevertheless, several works have addressed unreliability of the polymeric membranes in long-term operations (Jeong et al., 2016; Khayet et al., 2005). For this reason, there is a need to improve some physical and chemical properties, including pore size, contact angle, porosity, and thermal conductivity. These properties directly affect membrane separation performance in terms of energy efficiency (heat loss through the membrane), stability, retention and flux (Eykens, De Sitter, et al., 2017). Therefore, to fill this gap on the membrane market, there is a need to develop MD membranes with high mass transfer, excellent anti-wetting and anti-fouling properties, chemical inertness, and low cost.

As the MD membranes are contactors between two phases, they must possess a hydrophobic layer, which prevents the wetting provoked by the feed solution and concurrently provide retention of nonvolatile solutes. The use of a superhydrophobic membrane can significantly improve MD efficiency, this phenomenon is described in detail in next sections. To evaluate the membrane susceptibility to wetting, the liquid entry pressure (LEP) parameter must be determined. LEP is defined as the pressure value that is required for the liquid to pass through the membrane. According to the

literature, for a proper operation of MD plant, LEP of the feed solution should be above 2.5 bar (Schneider et al., 1988). LEP is described based on Laplace equation:

$$LEP_w = \frac{B\gamma_L \cos\theta}{r_{max}} \tag{8}$$

where B is a geometric factor of pore structure (equal to 1 for cylindrical pores), γ_L is the surface tension of the liquid, θ is the liquid/membrane contact angle and r_{max} is the maximum pore size (Franken et al., 1987). As a result, to achieve high LEP, membrane material should have small pore size, high surface tension and low interface energy between membrane and liquid.

Another important parameter for the optimal membrane performance is its thickness. Membrane thickness significantly affects the vapor flux through the membrane. Thicker membrane increases the mass transfer resistance, and thus reduces the vapor flux. On the other hand, thicker membrane reduces the heat loss. To date, several studies indicate that the optimal membrane thickness for a MD membrane should be in the range of 30–60 µm (Laganà et al., 2000). However, it is important to point out that this value may vary depending on the feed concentration, process conditions and membrane properties. In addition to this, the membrane porosity determines the process efficiency. Porosity is defined as the relationship of the volume of the pores and the total volume of the membrane. Membrane porosity is proportional to the evaporation surface area, and consequently, higher porosity membranes have higher vapor flux. According to the literature, the suggested membrane porosity value for an efficient MD should range from 30 to 85% (El-Bourawi et al., 2006). Knowing the densities of membrane and membrane material, the porosity can be calculated with the method proposed by Smolders and Franken (Smolders & Franken, 1989):

$$\varepsilon = 1 - \frac{\rho_m}{\rho_{mat}} \tag{9}$$

Furthermore, it has been also reported that higher porosity reduces conductive heat loss, this is due to the fact that the gases filling the pores of the membrane are less heat conductive than polymeric membrane materials (El-Bourawi et al., 2006). The pore features also influence the MD process, e.g. one of these parameters concerns the deviation of the pore shape from the cylindrical structure, which is called membrane tortuosity (τ). In theory, for a higher vapor flux, lower tortuosity is desired (Srisurichan et al., 2006). There is a direct correlation between porosity and tortuosity value, that can be calculated with the following equation proposed by Mackie and Meares (Mackie & Meares, 1955):

$$\tau = \frac{(2-\varepsilon)^2}{\varepsilon} \tag{10}$$

As mentioned previously, microporous membranes are usually needed for MD application. However, a slight variance regarding an optimal pore size can be found in the literature. For instance, Schneider et al. (1988) have reported that for pore flooding prevention, a maximum pore diameter should be in the range 0.5–0.6 µm, while El-Bourawi et al. (2006) noted that this range can be extended to 0.1–1 µm. Although for bigger pores higher fluxes are expected, it has been also reported that too large pore dimensions cause membrane wettability. Nevertheless, to estimate the optimal pore size, the surface tension of the feed solution must be taken into account.

As the driving force of the process is temperature difference, an important aspect during membrane designing is the conductivity of the membrane material. Less heat loss during the process leads to higher energy efficiency and less susceptibility to temperature polarization phenomena, thus improved flux through the membrane can be obtained. Thermal conductivities of most often used polymers for MD membranes, such as PP, PTFE, PVDF, are similar to each other, ranging from 0.11 for PP up to 0.27 $Wm^{-1}K^{-1}$ for PTFE at 23 °C (Alkhudhiri et al., 2012).

4. Toward the enhancement of hydrophobicity

The history of superhydrophobic surfaces studies dates back to the early 20th century when Ollivier (1907) observed the contact angles of nearly 180°, long before membrane distillation has been patented (Bodell, 1963) (see Figure 3). Nevertheless, first artificial superhydrophobic surfaces have been reported and demonstrated by Onda et al. (1996) and it was the beginning of the development of various methods for superhydrophobic surfaces preparation. In 2009, materials with a contact angle above 150° started to be implemented for MD membranes (Zeyu et al., 2009).

The phenomena of surface wetting by a liquid and its physicochemical principle have been already well studied. A droplet resting on a solid surface can take a form of equilibrated shape and remain on the surface as a droplet or spread into a thin layer on the material surface. The behavior of the droplet depends on three thermodynamically balanced interfacial tensions that relate to the existence of an interface between liquid and vapor, solid and liquid and solid and vapor (Shirtcliffe et al., 2010). The wettability of the solid surface is mainly dominated by its chemical composition and structure.

The design of superhydrophobic surface has been inspired by the structure of lotus leaves with a contact angle in excess of 150° and self-cleaning

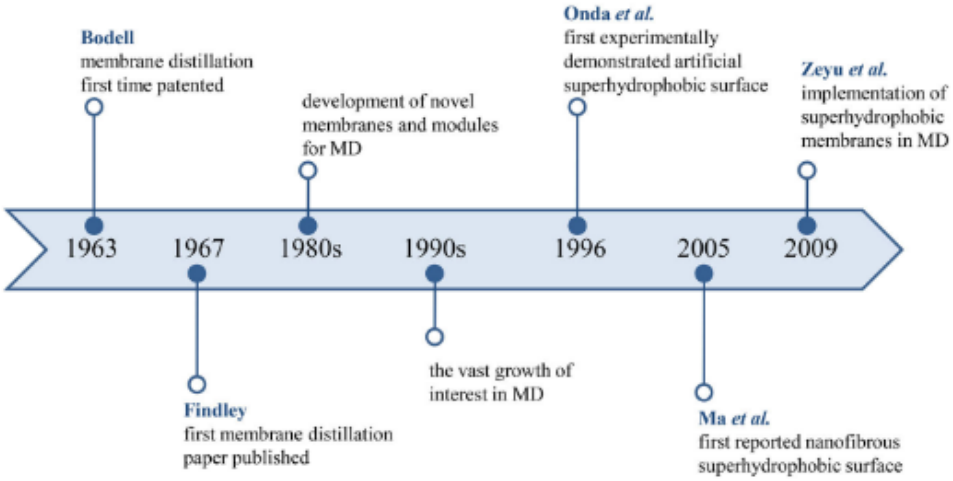

Figure 3. Timeline of MD and superhydrophobic surface developments (Findley, 1967; Ma et al., 2005).

properties. This effect can be achieved by creating a rough and hydrophobic surface. The roughness enhances the contact angle of hydrophobic surfaces well beyond that possible to achieve by chemistry itself (McHale et al., 2004). This was well described by Wenzel equation (11) (Wenzel, 1936):

$$\cos\theta_r = r\cos\theta_e \tag{11}$$

where r is a roughness factor, θ_r is a contact angle on a rough surface, and θ_e is Young's equilibrium contact angle. According to the Wenzel's equation, the surface roughness amplifies the effect of the surface chemistry which in this equation is determined as $\cos\theta_e$. The equation shows that for hydrophilic surfaces with $\theta < 90°$, the roughness factor enhancement will cause further reduction of the Wenzel contact angle toward 0°, whereas for hydrophobic surfaces with $\theta > 90°$, it will lead to further increase of the Wenzel contact angle toward 180°. Nevertheless, the Wenzel equation is limited to the homogeneous rough surface, and it was extended by Cassie and Baxter in 1944 (Cassie & Baxter, 1944). Cassie-Baxter equation applies for the porous membrane with a heterogeneous surface. In this case, the presence of the air in the pores of the material prevents the pores from being filled with liquid and liquid only bridges between the solid surface. Although the surface is topographically structured, the roughness factor does not directly enter into the Cassie–Baxter equation (12):

$$\cos\theta_{CB} = f_1\cos\theta_e - (1 - f_1) \tag{12}$$

where θ_{CB} is heterogeneous contact angle, f_1 is a fraction of the contact line of liquid with the solid, thus $(1 - f_1)$ is the area bridged between solid surface features. According to Cassie-Baxter equation, θ_{CB} will increase with

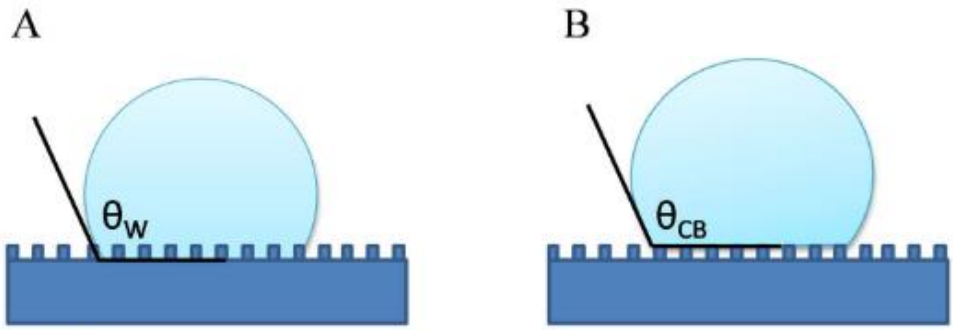

Figure 4. Scheme of the A) Wenzel and B) Cassie – Baxter state for a droplet.

the decrease of f_1. It means that to enhance the hydrophobicity of the surface the contact line of liquid with the solid has to be minimized. Thus, the roughness indirectly matters because it determines the solid surface fraction. Thus, a Cassie – Baxter state is one in which the liquid does not penetrate into the hollows of the rough surface but remains suspended on top of the surface protrusions (see Figure 4B), while in Wenzel state the liquid is in contact with the entire exposed surface of the solid (Figure 4A) (Giacomello et al., 2012).

4.1. Different approaches for hydrophobicity enhancement

There are different ways for wettability diminishment that are usually based on the combination of surface patterning and surface modification technologies starting from the chemical modification (Ogawa et al., 2007), electrospinning (Liao, Wang, Tian, et al., 2013), nanocomposite preparation (Tijing et al., 2016), sol-gel approach (Zhang & Wang, 2013) through nanoparticles coating (Chen et al., 2018; Razmjou et al., 2012; Shao et al., 2019), surface silanization (Boo et al., 2016) and plasma fluorination (Yang et al., 2014, 2015). A summary of various approaches used for hydrophobicity enhancement is given in Table 2.

The hydrophobicity of the uniform polymeric structures is usually not sufficient for MD process. In practice, the enhancement of the observed surface hydrophobicity is based on increasing the surface roughness and lowering solid/liquid interface energy. According to the literature (Takashi et al., 1999), an effective way for lowering solid/liquid interface energy is its functionalization by fluorinated alkyl units, however, there is a certain limitation in hydrophobicity improvement of smooth surfaces. For example, in the case of smooth PVDF, a surface that is saturated by fluorinated methyl groups, it is possible to reach a maximum 120° contact angle (Yue et al., 2013). Therefore, the enhancement of the surface hydrophobicity is based on increasing the surface roughness (Li et al., 2007). Thus, to achieve

Table 2. Different approaches for hydrophobicity enhancement.

Strategy used	Polymer type	Initial contact angle (°)	Final contact angle (°)	LEP	References
CF_4 plasma treatment	PVDF	137	162.5	–	Yang et al. (2015)
Spray deposition of PDMS/SiO_2 nanoparticles mixture	PVDF	107	156	275 kPa	Zhang et al. (2013)
Modification with fluorinated silica layer	PEI	66.7	124.8	–	Zhang and Wang (2013)
Dispersion of detonation nanodiamonds	PVDF	110	119	–	Bhadra et al. (2014)
Clay nanocomposite formation	PVDF	128	154.2	200 kPa	Prince et al. (2012)
SiO_2 coating and fluorination	PP	120	150	–	Shao et al. (2019)
Electrospinning of PVDF-silica layer	PVDF	135	>150	150 kPa	Liao, Wang, et al. (2014)
Chemical modification with perfluoropolyether	PVDF	88	115	390 kPa	Yang et al. (2011)
Coagulation bath with N-methylpyrrolidone	PSf	105	144	260 kPa	Tian et al. (2015)

a strong water repellent rough membrane, a proper modification has to be adopted focusing on the creation of micro- and nanostructured surface, as shown in the Figure 5. In such approach, the authors obtained complex topography via depositing TiO_2 nanoparticles on microporous PVDF membranes (Razmjou et al., 2012). Due to the Cassie-Baxter model (Cassie & Baxter, 1944), capillary forces may inhibit or reduce the penetration of the liquid into the rough and complex surface. As a result, water droplets sit upon the top of surface protrusions and air gaps rather than follow the surface contours. In the case of multilevel roughness, there is an unusually strong water-repellency on the surfaces due to the increase in the number of sharp and narrow protrusion that are in contact with water droplet. In other words, the increase of surface roughness reduces the contact area between liquid and solid and as a consequence reduces the adhesion of a droplet to the solid surface.

A facile way to fabricate membranes with rough surfaces is electrospinning technique. Electrospinning of polymers allows fabricating nanofiber membranes. During electrospinning process, polymeric solution is exposed to the electric field. When the applied electrostatic force overcome the surface tension, a so called fiber jet is ejected, followed by the rapid evaporation of the solvents and the fiber deposition on the collector (Reneker & Yarin, 2008). Thanks to the presence of microscale and nanoscale fibers in the structure, the electrospun membranes are highly porous and have high surface-to-volume ratio and three-dimensional interconnected structure. Such particular structure and ease of preparation made electrospun membranes to promote their applications in various fields, such as filtration (Wang et al., 2012), fuel cell technology (Tamura & Kawakami, 2010) and tissue engineering (Bhattarai et al., 2004). One of the advantages of electrospinning is the diversity of the polymers that can be used for fabrication MD membranes in contrary to commercial MD

membrane synthesis that is limited to the polymers such as PVDF, PP, PTFE (as mentioned in previous section). As an example, styrene–butadienestyrene (SBS) has been recently electrospun into nanofibrous MD membrane (Duong et al., 2018). Results showed that SBS electrospun membrane exhibited higher hydrophobicity compared to the commercial PTFE membrane. A common method for further roughness enhancement and hierarchical structure creation is an addition of hydrophobic nanomaterials, such as graphene, CNTs or silica nanoparticles into electrospinning dope solutions (Liao, Wang, et al., 2014; Tijing et al., 2016; Woo, Tijing, et al., 2016). For instance, Tijing et al. (2016) added different concentrations (1–5 wt%) of carbon nanotubes (CNTs) into the PcH dope solution for electrospinning. With CNTs concentration of 5 wt%, the nanofiber membranes obtained a very high contact angle of 158.5° and high LEP of 99 kPa due to presence of CNTs in/on the nanofibers which produced beads on the surface of the membrane leading to increased roughness. An effective method to functionalize electrospun membranes is electrospraying in order to cover the nanofibrous membrane with inorganic/organic micro/nano particles. The combination of electrospinning and electrospraying was used to fabricate PcH nanofibrous membrane functionalized with TiO_2 nanoparticles (Seyed Shahabadi et al., 2017). The contact angle increased from 142° up to 162° after electrospraying.

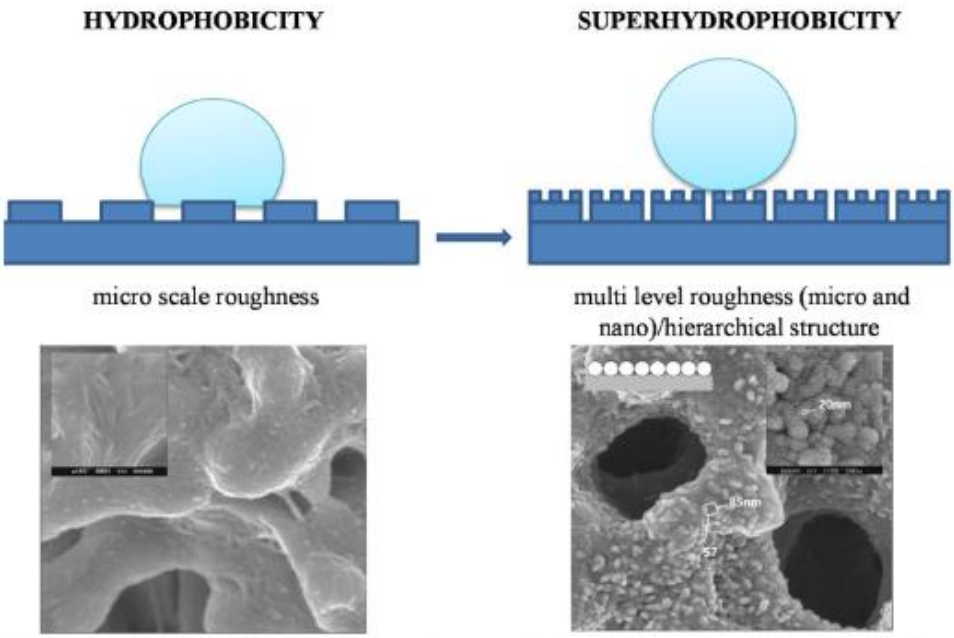

Figure 5. The effect of multilevel roughness on hydrophobicity (SEM images taken from Razmjou et al. (2012)). Copyright permission (License number 4903670873694).

4.2. Incorporation of inorganic nanomaterials

Different studies have shown that the incorporation of nanofillers into polymers could tune the structure and physicochemical properties of membranes, such as hydrophobicity but also porosity, surface charge density, chemical, thermal and mechanical stability (Castro-Muñoz, Ahmad & Fila, 2019; Yin & Deng, 2015). Recently, the use of several inorganic materials, such as carbon nanotubes, graphene, clay, silica and titanium dioxide, has become a new trend for superhydrophobic MD membranes preparation.

4.2.1. Graphene-based materials

It is likely that graphene-based materials are currently among the most deeply explored additives. Graphene has attracted considerable attention for water treatment and purification processes, especially for pressure-driven membrane processes, and the advantages of its use have been proven both by molecular simulations (Cohen-Tanugi & Grossman, 2012) and experimental studies (Han et al., 2013). To the date, different mechanisms of selective permeation of graphene and graphene oxide have been proposed, e.g. Nair et al. (2012) suggested a network of parallel channels between stacked graphene oxide layers (see Figure 6). Such channels are arranged perpendicularly to a mass transport vector. The bottom and ceiling of these channels are usually permeable to water or ions due to presence of holes in them. It has been documented that, even when the mixture of water and other compounds (e.g. gases and liquids) was fed, the water permeation rate could be at least five orders of magnitude higher than that of the other component (Castro-Muñoz, Buera-González, et al., 2019). The presence of nanochannels in membrane structure together with different chemical interactions, that occurs between the transported ions and oxygen functional groups, are responsible for the selective permeation of GO membranes (Sun et al., 2013). According to Joshi et al. (2014), nanochannels in graphene oxide structure can open up only in the hydrated state, and the sieving properties of GO may depend on the humidity of the surroundings as this parameter defines the interlayer spacing. The water molecules intercalation between single GO sheets causes the swelling of the layer. It is mentioned that the interlayer spacing can reach the value of 13.5 Å, and concurrently makes the membrane permeable to most of the hydrated ions (as the diameter of most of the hydrated ions is smaller than 13.5 Å) (Abraham et al., 2017). After chemical or thermal reduction, this interlayer spacing decreases to only 3.6 Å due to nanochannels collapse (Su et al., 2014). This space is not enough for water and also other molecules to permeate between graphene sheets. Thus, the only permeation path is through the structural defects. Nevertheless, the addition of

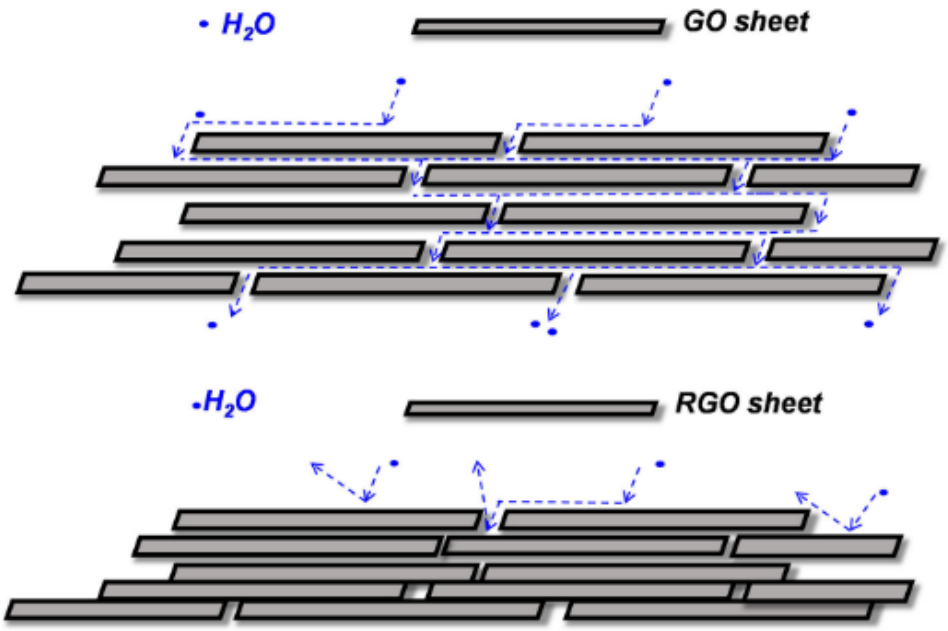

Figure 6. Scheme of the possible permeation route of water molecules through GO and rGO layers.

graphene into materials can bring desired benefits of a different mechanism. Graphene in the membrane matrix reduces the mass transfer resistance caused by collisions between vapor molecules and pore walls due to its vapor adsorption/desorption capacity (Gontarek et al., 2019; Woo, Tijing, et al., 2016).

The use of graphene for polymeric membrane modification has been proposed by different researchers. Leaper et al. (2018) prepared mixed-matrix PVDF membranes incorporating GO for AGMD and observed the enhancement of the permeate flux by 52% compared to pure PVDF. Bhadra et al. (2016) prepared GO immobilized PTFE membrane with the enhanced water vapor transport during DCMD. They suggested that multiple factors, such as selective sorption, nanocapillary effect, and reduced temperature polarization affect the improved membrane performance. Nevertheless, the results showed the water droplet on pristine PTFE membrane had a contact angle 110°, while the modification of the polymer with GO resulted in a drop of the angle to 90.6° ± 2.1. This means that GO may reduce the efficiency of MD membranes and is not recommended as an additive for modification of superhydrophobic surfaces. Non-oxidized forms of graphene are a better way to obtain superhydrophobic membrane surfaces. Woo, Kim, et al. (2016) proved the robustness graphene-modified PVDF membrane with improved wetting resistance in long-term air gap membrane distillation. Jafari et al. (2018) prepared a nanofibrous

membrane modified with graphene quantum dots (GQD). The results showed an increase in liquid entry pressure of water with a slight decrease in water contact angle. Furthermore, compared to neat PVDF nanofibrous membrane, the GQD-modified membranes revealed higher water flux and salt rejection for air gap MD experiments.

4.2.2. Carbon nanotubes

Other emerging inorganic material, like carbon nanotubes (CNTs), have proved the ability to improve the vapor flux in polymeric matrixes compared to conventional MD membranes (Jamed et al., 2019; Lee et al., 2017). CNTs have a nanocylindrical shape of a rolled-up graphene sheet. Besides strong mechanical properties, CNTs are also chemically and thermally resistant. It is especially important for MD application that CNTs based membranes are characterized by excellent hydrophobicity and porosity. CNTs are able to affect the water-membrane interaction and reduce the permeation of liquid water while favoring the transport of water vapor molecules (Dumée et al., 2011; Gethard et al., 2011). These interactions play an important role in membrane performance, especially in permeability and selectivity. CNT-modified membranes have been applied in solvent extraction (Sae-Khow & Mitra, 2010b), pervaporation (Sae-Khow & Mitra, 2010a) and desalination (Gethard et al., 2011), providing superior performance. It is supposed that water molecules can diffuse through polymer/CNTs mixed matrix membranes (MMMs) following three possible mechanisms; 1) direct diffusion through continuous polymer matrix, 2) diffusion inside the CNTs through the inner wall, and 3) surface diffusion through the outer wall of CNTs (Lee et al., 2014). Additionally, molecular simulations proved that there exist ordered hydrogen bonds between water molecules during molecular flow through inner part of CNTs (Hinds et al., 2004). These bonds together with the weak interactions between water and hydrophobic walls of CNTs might lead to almost frictionless, thus accelerated flow. In addition, deposited layer of CNTs on a hydrophobic support increases conductive heat transfer from the bulk to the membrane surface, thus reduces thermal polarization and increase membrane performance (Tang et al., 2017). However, high cost of CNTs limits their wide commercial applications. Moreover, in the perspective of water treatment, the point of concern should be focused on the health risks due to the liberation of CNTs into the treated water stream and CNTs stability within the matrix that still remain unknown (Roy et al., 2020).

4.2.3. Metal-oxide nanoparticles

Recently, sphere-like nanoparticles, such as TiO_2, SiO_2 and ZnO, have been reported for MD to create nano-roughness on membrane surfaces. This

bioinspired surface is supposed to mimic the lotus effect and create water super-repellency (Chen, Guo, et al., 2016). Usually, this super-hydrophobization method includes first nanoparticles coating onto the membrane and then the fluorosilanization with low solid/liquid interface energy material (Boo et al., 2016; Ren et al., 2017; Wang et al., 2018). Such modification not only generates the hierarchical morphology but also decreases diameter of membrane pore providing effective solution to alleviate the issue of membrane pore wetting. Recent studies indicated that coating fluorinated TiO_2 or SiO_2 nanoparticles onto the membrane surface could impart the additional local reentrant structure, which resist wetting by both water and low surface tension liquids (Abd Aziz et al., 2020; Lee et al., 2016).

Among sphere-like nanoparticles, TiO_2 offers some advantages. In principle, it is widely known as an abundant, nontoxic and stable semiconductor and its annual world consumption reaches 4.4 million tones. TiO_2 nanoparticles with various morphologies, such as nanoflowers, nanorods and etc., can be prepared through fast and low-cost hydrothermal synthesis (Chen, Guo, et al., 2016; Mali et al., 2011). Several works confirmed a successful TiO_2 implementation to achieve rough and hierarchical surface for applications in membrane distillation (Abd Aziz et al., 2020; Razmjou et al., 2012). Nevertheless, this modification requires an additional step in order to reduce the surface energy. In general, fluorosilanization is the most typical modification applied for conversion of hydrophilic TiO_2 nanoparticles to hydrophobic, however, phosphonic acid modification of TiO_2 has been also reported (Kumar et al., 2020).

Similar to TiO_2 silica is hydrophilic material, however, it is possible to prepare superhydrophobic silica nanoparticles via direct synthesis using hexamethyldisiloxane precursor (Yue et al., 2013), or via postmodification using hydrophobic binders, such as tetraethoxysilane or alkoxysilane (Petcu et al., 2017). These methods provide rough nanoparticles with low interfacial energy. Nevertheless, for MD membrane preparation more popular is a two-step modification strategy including creation of hierarchically micro/nano-scaled roughness using silica nanoparticles (SiNPs) followed by surface energy reduction by fluorination (Shao et al., 2019). To avoid the usage of hazardous fluorinated chemical, Liao et al. (2020) proposed one-step colloid electrospinning/electrospraying to construct hierarchical superhydrophobic surfaces by incorporating silica fumes in the dope solutions. The deposition of modified SiNPs can tune the morphology of various surfaces into superhydrophobic through the formation of a dual-scale roughness layer (Jia et al., 2013). Moreover, modification of silica nanoparticles using hydrophobic molecules enhances their dispersity in polymeric matrixes and organic solvents (Li et al., 2006). On the other hand, it was observed that the incorporation of SiNPs as nanofillers into the membrane

weakens the mechanical strength, therefore, they are usually used together with reinforcement additives such as MWCNTs. Zhou et al. (2019) studied the effect of integrated MWCNTs and SiO_2 on the morphology and performance of the PVDF membrane. When the amount of SiO_2 was relatively low, the vapor flux increased as a result of the synergistic effects between the two filling materials. One of these effects provided by MWCNTs is the increase of overall porosity, while SiO_2 causes the growth of the macrovoids. However, the effect brought by MWCNTs was more dominant. On the other hand, increasing the amount of SiO_2 led to the disappearance of asymmetric structure and low mechanical strength.

Useful properties and rich variety of nanostructures made ZnO well-known for several practical applications, such as optoelectronics, sensors, transducers and biomedical sciences (Wang, 2004). It can be synthesized from readily available raw materials, using low-cost and scalable chemical (Kołodziejczak-Radzimska & Jesionowski, 2014). ZnO nanoparticles are considered to be a promising nanofiller due to their desirable shape, high surface-to-volume ratio, stability under high temperatures and harsh operational conditions and stronger antibacterial property than SiO_2 and TiO_2 (Adams et al., 2006; Anitha et al., 2013; Suresh et al., 2018). Membrane functionalized with ZnO nanoparticles exhibit a rough hierarchical morphology, high contact angle values and low solid/liquid interface energy (Deka et al., 2019). Additionally, ZnO nanoparticles were found to be more economical than other nanoparticles such as TiO_2, and Al_2O_3 (Liang et al., 2012). In the case of alumina, it already gained a huge interest for modification of MF and UF membranes (Gu et al., 2020; Yan et al., 2006; Zhu, Liu, Guan, et al., 2019), however, there are only a few works describing the effect of Al_2O_3 nanoparticles on polymeric membranes for desalination through MD. Although, it was shown recently that it is possible to achieve superhydrophobic surfaces and enhanced PVDF nanofibrous membrane performance using alumina nanoparticles (Attia et al., 2017), the addition of Al_2O_3 has been mainly explored for ceramic MD membranes (Fang et al., 2012; García-Fernández et al., 2017; Subramanian et al., 2019).

4.2.4. Clays

Less popular are clay-based nanocomposites. Although the clay nanocomposites have already found an application in gas separation process (Villaluenga et al., 2007; Xu et al., 2006), there are only a few papers in which clay was used to modify MD membranes. Clays are minerals consist of anionic layered silicates and metal cations, such as Na^+, K^+, Ca^{2+}. The presence of hydrated ions makes them hydrophilic, however, using surfactants through organic cations exchange process, their surface can be easily transformed into hydrophobic (Naderi-Samani et al., 2017). Generally, the

addition of clay nanofiller enhances the thermal and surface properties of nanocomposites. The researchers have found out that PVDF-clay hollow fiber membranes showed an increased hydrophobicity and membrane performance during MD testing (Bonyadi & Chung, 2007) than pristine membranes. In another work, nanocomposite nanofiber membranes based on PVDF and clay showed an improved performance in DCMD process and better membrane wetting prevention with the increasing concentration of clay particles (Prince et al., 2012).

4.2.5. Zeolitic imidazolate frameworks

Zeolitic imidazolate frameworks (ZIFs) represent a new class of porous nanostructures. They are a special subclass of metal-organic frameworks (MOFs) with a 3 D tetrahedral framework in which metal cations are linked with imidazolate anions. The zeolites framework consists of many cavities and channels (Chen et al., 2014; Lai, 2018) that make it a potential sorbent material. Due to the physical and chemical properties such as high adsorption capacity, ion exchange property and high thermal and chemical stability, ZIFs can be useful for membrane modification. Kebria et al. (2019) prepared a membrane with ultrathin ZIF/chitosan layer on the PVDF surface for AGMD process. Although no significant change in water contact angle was observed, the LEP value increased significantly from 2.2 up to 3.1 bar and the permeate water flux increased about 350% for modified membrane. Li et al. (2020) formed porous hydrophobic ZIF/PVDF layer on the outer surface of PVDF hollow fiber support membrane in order to further improve the hydrophobicity of the membrane and thus provide special adsorption capacity to the coating layer. In the work conducted by Salehi et al. (2018), the ZIF nanoparticles have been modified in order to increase their hydrophobicity. They have used modified ZnO nanoparticles and silane coupling agent to make the core-shell structure of MZnO@ZIF-8. They observed that the presence of ZIF in membrane increased its porosity, hydrophobicity, permeate flux and rejection.

4.2.6. Dispersion, agglomeration and toxicity of nanomaterials

During the fabrication of nanocomposite membranes, one of the commonly occurring phenomena is nanoparticle aggregation and agglomeration. The nanomaterial concentration can be critical to optimize the performance and durability of nanocomposite membranes. The susceptibility of nanomaterials to aggregate increases when their concentration increases in polymer matrix. This phenomenon often led to a drop-in porosity value and vapor flux reduction (Kumar et al., 2020). For instance, Woo, Tijing, et al. (2016) stated that the increase in graphene concentrations in dope solution caused aggregation issues. They observed a decrease in porosity from 94.7% for

neat PcH to 82.3% for electrospun membrane with 10 wt% graphene loading. Moreover, it has been proved that the agglomerates result in diminished mechanical strength of nanocomposite. Few strategies have been proposed for improved dispersion of nanofillers including mechanical dispersion, ultrasonication, stirring, chemical modification and physical method (Ma et al., 2010). An et al. (2017) proposed chemical functionalization of CNTs. Non-modified CNTs showed strong agglomeration in entangled bundles. Surface fluorosilanization using FTES led to the significant reduction of agglomeration, improved stability of CNTs and to the fabrication of a well-dispersed membrane. Li et al. (2015) performed the hydrophobization of SiO_2 NPs using OTS in order to improve their dispersion in the PVDF matrix and avoid the nanoparticles agglomeration. Liao, Wang, et al. (2014) grafted perfluoropolyether (Fluorolink S10) onto the silica surface to assure the homogeneity of dope solution during electrospinning. Unfortunately, most of fluorine compounds exhibit poor degradability in the environment, moreover, they are easily accumulating in living organisms, what may lead to long-term harm. Thus, the evaluation of the potential use of chemicals with lower toxicity should be considered.

Nanomaterials are being increasingly applied in many fields of science. Thus, some of them are inevitably released to the environment, which may bring some harmful effects. For instance, the increase of the concentration of TiO_2 NPs, affects plant growth parameters (Movafeghi et al., 2018), high concentrations of ZnO NPs may reduce the seedlings growth, (Singh et al., 2018) and CNTs affect the oxidation behavior of enzymes in water molecules, which produce toxicity to microorganisms (Chen, Qin, et al., 2016). In the case of unmodified graphene, GO and rGO, the majority of current literature agree that they are cytotoxic and genotoxic. Surface modified graphene materials are often less toxic, however, the dose is one of the most important toxicity factor (Guo & Mei, 2014). On the other hand, the presence of nanomaterials can bring a positive effect on environment remediation, such as organic pollutants and heavy metal absorption (Zhu, Liu, Hu, et al., 2019).

As a preliminary conclusion of this section, we can notice that specific emerging nano-sized materials are releasing interesting properties to the pristine polymer membranes to reach featured morphological properties for MD separations. The next section addresses the relevant advances in tailoring superhydrophobic membranes and their performance for water desalination.

5. Advances in superhydrophobic membranes improving MD performance

In general, the addition of nanoparticles for polymeric MD membrane preparation can bring excellent water repellency together with a

hierarchical and rough structure, and large effective surface area, thereby enhancing the membrane's anti-wetting properties. This can prevent salt deposition, as depicted in the Figure 7. Additionally, in case of MMMs, superhydrophobic inorganic additives can reduce the boundary-layer effect, thus accelerate diffusion in the membrane pores (for example, through an adsorption/desorption assisted diffusion). Such a phenomenon may bring different effects on membrane performance. Herein, the following subsections describe in detail the influence of these superhydrophobic pore walls and surface on membrane performance and have been divided into: *i)* stable performance, *ii)* flux enhancement and *iii)* permeate quality. For instance, Table 3 enlists the most relevant development works in preparing superhydrophobic membranes, and their performance in desalination applications.

5.1. Performance stability

The durability of the MD system can be hampered by various processes and phenomena, including fouling, heat transfer and concentration polarization. The deposition of foulants can cause the reduction of the flow rate through the membrane in two possible ways, depending on the fouling

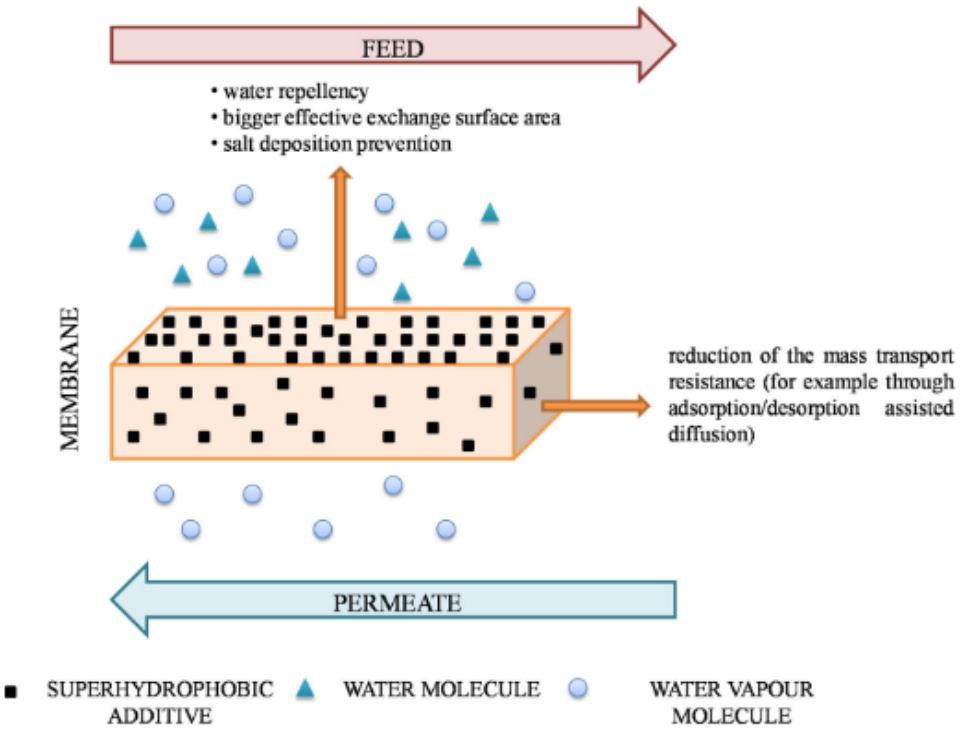

Figure 7. The effect of superhydrophobic additives on MD membrane.

Table 3. Relevant development works in preparing superhydrophobic membranes for desalination.

MD configuration and process parameters	Membrane type	Nanomaterial concentration/ nanomaterial layer thickness	Contact angle	LEP	Operating time	Flux/ rejection	References
DCMD 3.5 wt.% NaCl Tf: 70 °C Tp: 25 °C	TiO_2 coated PVDF followed by fluorosilanization	no data	163° ± 3°	190 kPa	8 h	~ 30 kg/m^2 h	Razmjou et al. (2012)
DCMD 3.5 wt.% NaCl Tf: 60 °C Tp:20 °C	PVDF-SiO_2 on PVDF nanofibrous support PVDF-SiO_2 on nonwoven support	6 – 10 wt%/– 8 – 10 wt%/–	>150°	150 kPa 50 kPa	25 h	24.6 ± 1.2 kg/m^2 h >99.99% 20.8 ± 2.8 kg/m^2 h >99.99%	Liao, Loh, et al. (2014)
DCMD 3.5 wt% NaCl Tf: 60 °C Tp: 20 °C	PVDF-PDA-Ag-thiol nanofiber integrally-modified PVDF-PDA-Ag-thiol nanofiber surface-modified	1 wt%/–	153° ± 4° 158° ± 3°	146 ± 12 kPa 86 ± 22 kPa	8 h	31.6 kg/m^2 h 5.4 kg/m^2 h	Liao, Wang and Fane (2013)
VMD 200 g/L NaCl Tf: 60 °C ΔP: 80 kPa	ZnO nanorods modified PVDF	–/~2 μm	152°	277 ± 8 kPa	8h	4.5 kg/m^{2}h ~99.99%	Wang et al. (2018)
DCMD 3.5 wt.% NaCl Tf: 70 °C Tp: 20 °C DCMD 25 wt.% NaCl Tf: 70 °C Tp: 20 °C	SiO_2 nanoparticles spray-deposited on PVDF	0.2 – 1.5 wt%/–	156°	275 kPa	15 h 180 h	~8 kg/m^2 h 99.99% ~5.5 – 4.5 kg/m^2 h 99.99%	Zhang et al. (2013)
VMD 15 wt% NaCl + 6 wt% $MgCl_2$ Tf: 80 °C ΔP: 0.096 MPa	SiO_2 coated PP followed by fluorination	0 – 2.4 wt%/–	150°	–	12 h	~4.5 kg/m^2 h	Shao et al. (2019)
DCMD 3.5 wt.% NaCl Tf: 80 °C Tp: 17 ± 2 °C	electrospun PVDF-clay nanocomposite	0 – 8 wt%/–	154.2° ± 3.0°	200 ± 6 kPa	8 h	~5.75 kg/m^2 h >99.9%	Prince et al. (2012)
DCMD 0.6 M NaCl Tf: 38–56 °C Tp: 15 °C	PVDF/graphene composite	0–10 wt%/–	151° ± 3°	100 kPa	18 h	~9 kg/m^2 h 99.97 – 99.99%	Gontarek et al. (2019)
DCMD 70 g/L NaCl Tf: 60 ± 1 °C Tp: 20 ± 1 °C	CNT-incorporated PcH	1–5 wt%/–	158.5° ± 1.5°	99 kPa	5 h	29.5 kg/m^2 h >99.99%	Tijing et al. (2016)

(*continued*)

Table 3. Continued.

MD configuration and process parameters	Membrane type	Nanomaterial concentration/ nanomaterial layer thickness	Contact angle	LEP	Operating time	Flux/ rejection	References
DCMD 35 g/L NaCl Tf: 60 °C Tp: 20 °C	CNT-PVDF-HFP	0–2 wt%/–	150.4° ± 0.8°	40.5 ± 2.8 kPa	6 h	48.1 kg/m^2 h >99.98%	An et al. (2017)
DCMD 3.5 wt% NaCl Tf: 60 °C Tp: 20 °C	PVDF-SiO_2	10 wt%/–	153.9°	179 kPa	50 h	18.9 kg/m^2 h	Liao, Wang, et al. (2014)
DCMD 3.5 wt% NaCl Tf: 60 °C Tp: 20 °C	PVDF/SiO_2 composite	~6.5 wt%/–	155.6°	230 kPa	24 h	41.1 kg/m^2 h >99.99%	Li et al. (2015)
AGMD 3.5 wt% NaCl Tf: 60 °C Tp: 20 °C	PcH/graphene	0.1–2 wt%/–	>162°	>186 kPa	60 h	22.9 kg/m^2 h 100%	Woo, Tijing, et al. (2016)
DCMD 30 × 10^3 mgL^{-1} NaCl Tf: 60 °C Tp: 20 °C	SiO_2 embedded PVDF	1 wt%/–	>150°	84.2 ± 2.8 kPa	50 h	34.2 kg/m^2 h >99.9%	Nthunya, Gutierrez, Verliefde, et al. (2019)
DCMD 3.5 wt% NaCl Tf: 70 °C Tp: 25 °C DCMD RO brine Tf: 70 °C Tp: 25 °C	TiO_2 coated PVDF followed by fluorination	–/3 μm	157.1°	158 kPa	10 h 21 h	73.4 kg/m^2 h 99.99% 40.5 kg/m^2 h 99.98%	Ren et al. (2017)
VMD 3.5 wt% NaCl Tf: 50 °C ΔP: 31.3 kPa	ZIFs-incorporated PVDF	0–2 wt%/–	136.5°	215 kPa	60 h	27.1 kg/m^2 h 99.9%	Li et al. (2020)
DCMD 5 g/L NaCl + 0.4 mM SDS ΔT: 53 °C	FAS grafted PVDF withCNTintermediate layer	0.2 wt%/ca.15 μm	180°	–	8 h	28.46 kg/m^2 h –	Wang et al. (2020)

Note. AGMD: air gap membrane distillation, CNT: carbon nanotube, GO: graphene oxide, HFP: hexafluoropropylene, LEP: liquid entry, pressure, LMH: (l/m^{2}h), PcH: Polyvinylidene fluoride-co-hexafluoropropylene, PDA: poly-dopamine, PP: polypropylene, PTFE: polytetrafluoroethylene, PVDF: poly (vinylidene fluoride), Tf: feed temperature, Tp: permeate temperature, VMD: vacuum membrane distillation, ZIF: zeolitic imidazolate framework.

layer structure, e.g. a homogeneous fouling layer causes pore clogging and reduces the flow rate due to mass transfer resistance, while a porous fouling layer increases susceptibility to temperature polarization effect. Small liquid – solid contact area of a superhydrophobic membrane may effectively reduce the available area for inorganic fouling deposition on the membrane surface (Horseman et al., 2021). Successes in fouling control and wetting mitigation during MD have been observed after membrane coating or modification with nanoparticles. Chen et al. (2018) deposited ZnO nanoparticles on a hydrophilic glass fiber membrane via chemical bath deposition method followed by the surface fluorination and the addition of a polymer coating. The SEM images showed that the ZnO nanoparticles created hierarchical structures on the glass fiber membrane, resulting in water contact angle increase up to 152.8°.The stable water flux was maintained up to 8 h for the low surface tension feed solution. Liao, Wang and Fane (2013) have prepared integrally-modified and surface-modified PVDF membranes via electrospinning and surface modification. Such membrane preparation protocols involved three steps: the coating nanofiber membrane with poly-dopamine (membrane activation), the coating of the activated surface with silver nanoparticles (morphology and roughness modification), and finally the modification of the surface chemistry with 1-dodecanethiol. Compared with the surface-modified PVDF membranes, integrally-modified PVDF membranes have been firstly wetted ensuring the introduction of the reagents inside the membrane structure and modification throughout the membrane pores. Interestingly, the proposed method was found to be a simple and effective way to fabricate superhydrophobic nanofiber polymeric membranes. The authors also compared the membrane performance in DCMD process with the unmodified membrane. As both were characterized by a similar pore size distribution, the reason of stable performance in DCMD process for integrally-modified PVDF was its surface properties. Afterwards, the same authors prepared a nature-inspired membrane with a lotus leaf structure. The membrane consisted of scaffold-like PVDF support and a silica-PVDF composite superhydrophobic selective layer made by electrospinning. The membrane exhibited great durability in a continuous DCMD test. Stable performance was observed over 50 h of tests, with the flux of 18.9 kg/m^2 h, while the PVDF nanofiber membrane without a superhydrophobic selective layer displayed only 12.3 kg/m^2 h, the enhanced stability was totally attributed to better surface water repellency.

Zhang et al. (2013) fabricated a superhydrophobic surface by spray-deposition of SiO_2 nanoparticles and PDMS mixture on PVDF membrane. They observed an irregular adhesion of SiO_2 nanoparticles on PVDF surface which contributed to roughness increase. As prepared membranes were characterized with a water contact angle of 156°, and higher LEP

value compared to the nonmodified PVDF membranes, which increased from 210 up to 275 kPa. In the case of this modification, the flux decreased as a function of the silica content in deposited layer, in other words, the additional layer on the membrane surface caused an increase in its resistance to mass transfer. However, the permeate conductivity of spray-deposited membrane during MD test was constant in the range of 30–50 μS, while in the case of the nonmodified membrane a sharp increase of conductivity can be observed, proving partial wetting of the membrane. It is worth to point out that the modified membrane exhibited better durability and stability during 180 h of operation for high salinity solution with the final NaCl rejection above 99.99%.

Similar to Zhang's study, Li et al. (2015) also used silica nanoparticles to prepare PVDF organic/inorganic composite nanofibrous membranes, which have been found to display an excellent superhydrophobic property together with high LEP of water, resulting in good waterproofness. According to SEM images, the morphology of the membrane contained microwrinkles and nanoprotrusions creating a hierarchical roughness. The modification brought an important improvement to the stability during long-term MD process (over 24 h operating time). Using electrospun PVDF/silica, authors achieved the vapor flux of 41.1 kg/m^2 h, and low permeate conductivity (~2.45 μS/cm). Furthermore, no membrane wetting was detected.

Similar results have been found for superhydrophobic membrane obtained by electrospinning of PVDF-clay nanocomposites, which were able to demonstrate a water contact angle up to 154.2°. It has been noted that the contact angle value increased with the clay concentration increase in the membrane. In case of the superhydrophobic membrane with the highest clay concentration of 8 wt.%, no flux decline was observed up to 8 h of operating time. However, the flux of electrospun PVDF–clay presented during DCMD was quite low (~5.5 kg/m^{2}h) compared to other membranes used for this application (Prince et al., 2012).

Razmjou et al. (2012) prepared superhydrophobic membranes through the modification of PVDF membranes with TiO_2 coating, which was followed by the surface fluorosilanization. The enhancement of surface hydrophobicity was correlated with the increase of surface roughness together with the reduction in liquid/surface interfacial energy. As a result, the water contact angle ranged from 125° ± 1° for non-modified PVDF up to 163° ± 3° for TiO_2 coated and fluorosilanizated membranes. Moreover, the resulting membranes were characterized with good mechanical and thermal stability. Although no significant enhancement in vapor flux and antifouling properties was observed, there was an important improvement in LEP value for the modified membrane from 120 to 190 kPa. The effect of the LEP

value on the membrane properties was investigated during MD process using 3.5 wt.% sodium chloride solution, where a significant increase in permeate conductivity was observed for the pristine PVDF membrane in comparison with the modified PVDF due to the partial pores wetting.

Incorporation of nanomaterials can also bring a simple way for membrane regeneration during real seawater desalination by membrane distillation. For instance, Guo et al. (2019) fabricated nanofiber PcH membranes coated with TiO_2 nanoparticles and assessed their performance in 5-day long-term test. Coupled with a ferrate pretreatment followed by dissolved air floatation, MD achieved an improved fouling control. After 5–10 days of MD operation, the water contact angle of the TiO_2 modified membrane was still recoverable up to 150.2° after 30 mins of simple water flushing.

Recently, slippery surface attracts more attention in mitigating the scaling and fouling phenomena in MD (Su et al., 2019). According to Xiao et al. (2019) "slippery surface" refers to the membrane with surface ability to prevent scaling. They introduced the definition of a "stick" or "slippery" surface based on its sliding angle. A "sticky" surface with high sliding angle above 90° might cause non-slip of the liquid phase at the surface. In contrary, the "slippery" surface with low sliding angle exhibits anti-scaling behavior because the liquid remains floating above the polymer phase which arises from very limited interaction of the liquid and the membrane surface. Wang et al. (2020) performed a robust superhydrophobization process by incorporating CNT intermediate layer over commercial PVDF membrane followed with grafting the FAS. As a result, they achieved a superhydrophobic surface with water contact angle of 180° and the water sliding angle of $1-5°$ indicating slippery surface property. Interestingly, a constant flux of 28.46 ± 0.37 kg/m^{2}h and a superior wetting resistance against 0.4 mM SDS were obtained in DCMD tests as the benefit of constructing the CNT intermediate layer. Superhydrophobic membranes with slippery property were found to reduce the extent of 8 water vapor flux decline caused by gypsum scaling. Yin et al. (2020) formed the superhydrophobic surface through the incorporation of materials with ultra-low surface energy (17-FAS) and a hierarchical texture through grafting of two layers of SiNPs on the PVDF membrane surface. Authors noticed that the incorporation of two different sizes of nanoparticles (120 nm and 30 nm) enhanced the movement of water droplet on the membrane surface, resulting in a slippery property. The superhydrophobic PVDF-Si-FAS membrane with a slippery surface postponed the induction of water flux decline due to gypsum scaling by ~100 min compared to pristine PVDF membrane. Similar mitigating effect of membrane with an engineered "slippery" surface on gypsum scaling was reported by Karanikola et al. (2018).

The stability of the coating nanomaterial layers plays an important role in maintaining the membrane performance. However, during MD applications (especially DCMD), membranes are often exposed to high temperatures and cross-flow streams of feed and permeate which could cause the lost of attached nanoparticles. Although not all authors discuss the stability of the nanomaterials in the polymer matrix, performance stability during MD operation may be its determinant. For instance, we can observe a stable vapor flux, for superhydrophobic membranes with hierarchical surface prepared through nanoparticles deposition. As long as we observe a constant vapor flux, we can conclude that the nanomaterials remain on the membrane, simultaneously maintaining its surface properties and structure. Abd Aziz et al. (2020) tested stability of TiO_2 micro/nanoparticles on the membranes surface. They did not observed any significant changes of contact angle after immersing membranes in NaCl solution over 10 days, which indicates high chemical stability of the coating. Razmjou et al. (2012) analyzed the thermal stability of the TiO_2 coated PVDF membranes by immersing the membrane in hot water (90 °C) for 15 min. They observed a marginal decrease of the contact angle of membrane after the exposure, however, it still remained in the superhydrophobic range. For mixed matrix membranes, physical entrapment can maintain stability of the nanomaterial in the polymer matrix. Tijing et al. (2016) assured that CNTs will not wear off from the membrane structure as a portion of the CNTs is well encapsulated in the polymeric nanofibers. Very recently, Gontarek et al. (2019) collected a vibrational spectra of filtered residues from feed and permeate streams at the end of MD operation using graphene entrapped membrane. The results indicated no graphene leaking from membranes. Even though these results appear to be promising, most researchers cannot guarantee the stability of the membranes in long-term MD operation as their tests last for a very short duration.

5.2. Flux enhancement

The enhancement of the vapor flux due to the increase in membrane hydrophobicity has been already observed in MD (Dumée et al., 2011; Martînez et al., 2003). There are two possibilities to increase the vapor flux through the membrane, *i)* to increase its driving force, or *ii)* to reduce resistance to mass transport. The increase of the driving force consists of increasing the difference in vapor pressure between both membrane sides, which can be achieved by increasing the temperature difference between feed and permeate, or increasing the effective evaporation area on the feed side. As mentioned previously, an increase in hydrophobicity can prevent the water from penetrating the membrane pores. While the tendency of the

pores flooding is minimized, the available vapor exchange surface increases, thus leading to higher vapor flux.

Liao, Loh, et al. (2014) have proposed two different methods for superhydrophobic membrane preparation via electrospinning. In the first approach, a 3 D superhydrophobic PVDF-silica ultrathin skin was electrospun on nanofibrous PVDF support. Second approach comprised the electrospinning of the thicker layer of 3 D superhydrophobic PVDF-silica onto commercial nonwoven support. The superhydrophobic nature of the membrane was confirmed using contact angle measurements, revealing value greater than 150°. The authors proved that the prepared membranes with larger pore size can be potentially used in MD process due to the surface high hydrophobicity. As it turns out, both types of modifications bring valuable improvements to the membrane performance. In the case of nanofiber supported membrane, the enhanced flux can be attributed to the higher porosity, while nonwoven supported membrane was characterized by better mechanical durability for continuous MD operations due to its thicker 3 D structure. Silica nanoparticles were used by Li et al. (2015) and Liao, Wang, et al. (2014) to prepare superhydrophobic organic/inorganic nanofibrous membranes. These membranes, besides stable performance, were also characterized by increased flux when compared to commercial unmodified membranes. Liao, Wang, et al. (2014) also noticed strong water repellency of the surface, which was achieved using silica nanoparticles that prevented the membrane from water droplets. The superhydrophobic composite PVDF membrane offered higher effective liquid evaporation area than PVDF nanofiber membrane (see Figure 8). Hierarchical rough structures provided numerous holes and slots, which reduce the contact area between solid and liquid, and at the same time increase liquid/vapor contact area. This type of structure promotes water vapor evaporation, and thus increases the permeation flux. In consequence, they have observed flux enhancement from 12.3 kg/m^{2}h for PVDF nanofiber membrane, up to 18.9 kg/m^{2}h for silica/PVDF composite membranes. Importantly, such permeation rates make these membranes highly competitive when compared to commercial flat-sheet PVDF membranes (vapor flux around 10 kg/m^{2}h). Li et al. (2020) observed an increased vapor flux through ZIFs-PVDF hollow fiber composite membrane up to 27.1 kg/m^{2}h. They found that their results could be attributed to four positive effects that emerged with the modification of the membranes. First of all, the formation of ZIF/PVDF layer contributed to the enhancement of membrane roughness and surface water contact angle from 94.5 to 136.5°. Moreover, low thermal conductivity and strong vapor adsorption characteristics of ZIFs effectively accelerate the mass transfer through the membrane, additionally weaken the temperature polarization.

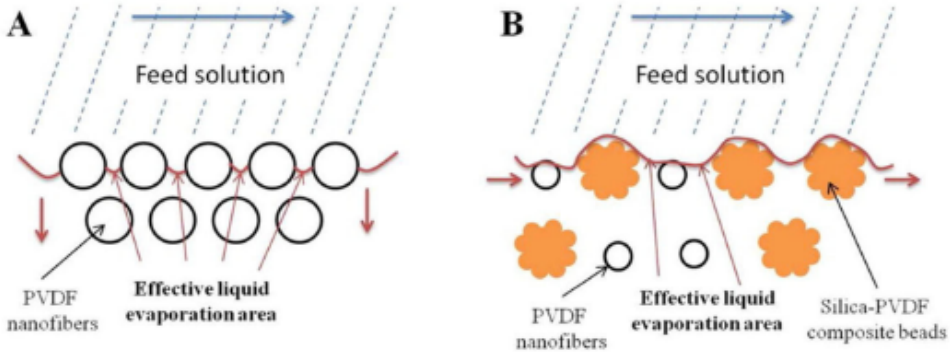

Figure 8. Schematic illustration depicting the enlargement of effective evaporation area for silica composite PVDF membranes (figure taken from Liao, Wang, et al. (2014)).

Theoretically, the overall resistance to mass transfer is given by the reciprocal of mass transfer coefficient (k), as follows:

$$\frac{1}{k} = \frac{1}{k^L} + \frac{1}{k^M} + \frac{1}{k^V} \tag{10}$$

where $1/k^L$ is the feed boundary layer resistance, $1/k^M$ is membrane resistance and $1/k^L$ is permeate boundary layer resistance (Vane et al., 2001). It is well-known that the feed boundary layer resistance depends on the feed flow rate and feed solution properties, while the permeate boundary layer resistance is recognized as negligible. The resistances to mass transfer through the membranes are coming from both collisions between vapor molecules and pore walls (i.e. Knudsen diffusion model), or the presence of air trapped in membrane pores and collisions between vapor and air molecules (i.e. molecular diffusion). The superhydrophobicity of the pore walls can reduce mass transfer resistance through mitigation of the negative effect of friction between the pore walls and vapor molecules. The mass transfer behavior within the superhydrophobic membrane can be considered as one having less pore wall collisions that facilitate the flow of vapor through the membrane. Additionally, improved vapor flux through, as called assisted diffusion or adsorption/desorption assisted diffusion, results as well form the reduction of the collisions between pore walls and vapor molecules. As shown in Figure 9, an unassisted transport is chaotic, and composed of many collisions that prolong the vapor molecule way from the feed to the permeate side. In the case of assisted diffusion, the adsorption/desorption capacity of pore walls may facilitate the vapor molecule transport.

A positive effect of increasing the water vapor flow was seen in membranes modified with CNTs. An et al. (2017) prepared electrospun nanofibres membranes with anchored functionalized CNTs. Due to the covalent modification and fluorination of CNTs, the well dispersibility within the

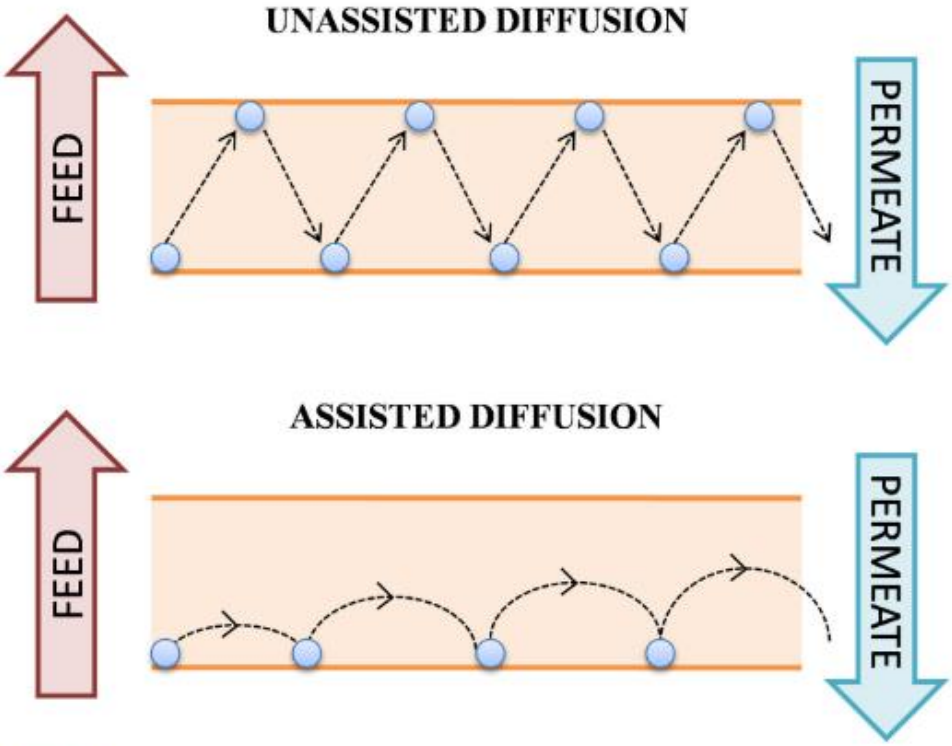

Figure 9. Schematic illustration showing the path of the vapor molecule through the membrane in the case of unassisted and assisted diffusion.

fibers was achieved together with good interfacial interaction between the filler and polymer matrix. Additionally, the authors suggested that the superior mass transfer was a result of the homogeneous embedding of the CNTs. This homogeneity resulted in membrane pore walls superhydrophobicity and effective water vapor molecules repelling, which lead to facilitated Knudsen and molecular diffusion transport and assisted surface diffusion. As a result, they observed around 35% higher average vapor flux value for the CNT modified membrane (~48.1 L/m^{2}h) than that without CNT modification (~33.6 L/m^{2}h). Tijing et al. (2016) prepared mixed matrix PcH with different concentrations of CNTs. This particular modification gave the possibility to obtain membranes with comparable pore size to the commercial PVDF membranes, however, much higher porosity (more than 85%) was reported. Due to the filler incorporation, the surface roughness increased leading to CA increase (of about 158°). The results indicate that CNT-incorporated nanofiber membranes presented 33% and 59% higher fluxes, for 35 and 70 g/L NaCl feed solution in DCMD process, respectively. Herein, the improved membrane performance was explained as an effect of CNTs incorporation. According to authors statement, the modification caused a surface hydrophobicity enhancement, hence, an

increase of pore wetting prevention. In general, such changes produced a bigger effective evaporation surface and higher water vapor flux. On the other hand, the presence of CNTs can promote the vapor transport due to its capacity to rapid adsorption/desorption of the vapor molecules (An et al., 2017).

According to Gethard et al. (2011), the rapid adsorption/desorption capacity of CNT allows the vapor molecules to follow a surface diffusion pattern, which increases overall vapor transport. The assisted diffusion may take place along the smooth surface of CNT as well as through their inner tube. They have found the mass transfer coefficient to be higher with the presence of CNTs in the membrane matrix. This increase was especially visible in the range of 60–80 °C, when the mass transfer coefficient was almost 6-fold higher than the unfilled membrane.

In a different approach, an activated diffusion via adsorption/desorption was also observed for electrospun PcH/graphene membranes (Woo, Tijing, et al., 2016). The addition of the graphene provoked a vapor flux increase, from 4.75 LMH (L/m^2h) for commercial membrane, up to 22.9 LMH for electrospun PcH/graphene membrane. Gontarek et al. (2019) have prepared PVDF/graphene composite membranes, and later tested them in DCMD set-up. The results showed a constant water vapor flux for over 18 h of operating time. Higher values of MD coefficient were observed in the membranes containing low graphene concentration when compared to pristine PVDF membrane. The flux enhancement was noted independently to the porosity decrease of the membranes. In such a study, the mechanism of assisted vapor transport was stated. This increase in water flux was correlated with interactions between graphene filler and water vapor, when the graphene at low concentration was well dispersed over the polymer matrix.

5.3. Permeate quality

The use of saline feed solution in MD may also lead to salt crystallization on the membrane surface and the rise of the partial wetting of the membrane. In theory, the solute molecules can be physically or chemically attached to the membrane surface through interactions with membrane functional groups (Meng et al., 2014). Once the deposition is formed on the membrane surface, the pores can be filled with the feed liquid and consequently, the type of transport is changing (Gryta, 2007). The use of appropriate membrane material may enable the control of partial wetting, thus increasing the permeate quality. According to the literature, a highly hydrophobic membrane can effectively reduce the salt deposition, improve fouling resistance and decrease the possibility of membrane wetting (Razmjou et al., 2012; Wei et al., 2012). Meng et al. (2014) explored the fouling and crystallization

behavior of nanocomposite PVDF membranes. They have prepared superhydrophobic surface through TiO_2 and fluorosilane coating, in which the water contact angle increased from 134° ± 0.4 up to 160° ± 1.4. These modified membranes showed higher resistance to concentrated salt solutions comparing to pristine membranes. In case of pristine PVDF and PTFE, a fast wetting has occurred due to the close contact with salt crystals that move across the surface, causing local pore enhancement, salt deposition and partial wetting. Due to the superhydrophobic surface modification, the contact between solutes and the membrane decreased as a result of water repulsion. However, not only superhydrophobicity, but also surface structure affects the probability of salt deposition. It was stated that the higher surface roughness decreases the chances of partial membrane wetting and reduces the capability of salt rejection.

Wang et al. (2018) prepared novel ZnO nanorods modified PVDF membrane with a micro/nanoscale hierarchical structure to solve the membrane fouling and wetting problems. Superhydrophobic surface has been applied to the VMD process for desalination of highly salty water. Modified membrane showed a stable superhydrophobic surface with a contact angle of 152°, easy cleaning property, and unique antifouling and antiwetting properties. After 8 h VMD, the modified membrane showed a similar permeate flux compared to the pristine PVDF membrane but a much higher quality of permeate. The ionic conductivities of the permeate from the pristine PVDF membrane reach 190.88 µS/cm after 8 h, while from the ZnO modified membranes only 10.19 µS/cm. Woo, Tijing, et al. (2016) achieved a complete salt rejection (100%) for long-term AGMD by using graphene/PcH membrane, while the commercial membrane displayed around 99.2%. Such results have been attributed to enhanced LEP (>186 kPa), contact angle (>162°) and porosity (>88%) values due to the incorporation of graphene and the formation of a multilevel roughness. Shao et al. (2019) modified PP membrane through SiO_2 nanoparticles coating and fluorination for simultaneously enhancement the interface roughness and superhydrophobicity. The membrane was used for highly concentrated saline solution treatment in VMD process. In the case of non-modified PP membranes, the serious membrane fouling in the form of salt crystallization in pores as the water evaporates was observed along with the progressive concentration polarization phenomena. In the contrary, modified membrane presented excellent wetting and fouling resistance during long-term concentration of NaCl and $MgCl_2$ solution. Additionally, no visible crystal embedding in the cross-section was observed. The fouling rate of non-modified membrane increased up to 5.20% for the highest tested feed concentration (15 wt% NaCl, 9 wt% $MgCl_2$) and was four times higher than that of the modified membrane.

In some cases, additional layer of nanomaterials reduces the vapor flux. Nthunya et al. (2020) prepared the superhydrophobic SiO_2-embedded PVDF nanofiber membranes, impregnated with carboxylated multiwalled CNTs and silver nanoparticles to enhance membrane fouling resistance. Although this modification caused a decrease in the initial vapor flux (from 42 LMH to 16 LMH), it also became an effective method for maintaining high salt rejection (recorded rejection decay was from 0.1–1.0%) and stable performance within 50 h of operation. It was observed that, membrane modification reduced the surface cake formation induced by the alginate and biofouling and inhibited the growth of microorganisms.

6. Conclusions and future trends in the field

In this review, an overview of superhydrophobic membranes for MD application is presented, highlighting the mechanisms leading to improved MD performance. This paper also demonstrates that the MMMs and nanoparticles modified membranes attract a lot of attention in superhydrophobic membranes preparation. In general, the recent findings imply the preparation of antiwetting membranes with strong water repellency to improve the membrane stability in long-term MD operation, enhance the vapor flux and improve the permeate quality. Using specific filling materials (such as CNTs, graphene and its derivatives, TiO_2, silica, ZIFs, among others), meaningful desalination performances have been obtained at lab scale. Herein, it is important mentioning that the right selection of the additive may bring multiple benefits and may be the key to obtain membranes for a large-scale processes. However, the emphasis has so far been placed on laboratory-scale experiments. This may be due to the cost of emerging nanofillers, such as graphene and CNTs. At this point, for the new researchers in the field, it is recommended to focus their research interest on cheaper substitutes of these materials but with the same effect on the membrane. Moreover, according to the main drawbacks of MD membranes (e.g. fouling, wetting, stability, heat and mass transfer, resistances), the research should focus their attention on producing next-generation membranes that will be able to meet all of the requirements for real seawater desalination. The formation of hierarchical micro/nano-scale surface morphology (reentrant structure) with air pockets gives the possibility to implement MD for real seawater desalination or industrial wastewater reclamation with the low-surface-tension contaminants (Lu et al., 2019). In addition to high hydrophobicity and low solid/liquid interface energy, reentrant structure plays an important role in creating omniphobic properties in a membrane, and allows achieving strong repellence toward liquids with

a wide range of surface tensions. Thus, omniphobic membranes appear to have promising properties for a real seawater desalination.

Disclosure statement

No potential conflict of interest was reported by the authors.

ORCID

Emilia Gontarek-Castro http://orcid.org/0000-0002-8493-1851
Roberto Castro-Muñoz http://orcid.org/0000-0002-7657-3302
Marek Lieder http://orcid.org/0000-0001-7410-5161

References

Abd Aziz, M. H., Dzarfan Othman, M. H., Alias, N. H., Nakayama, T., Shingaya, Y., Hashim, N. A., Kurniawan, T. A., Matsuura, T., Rahman, M. A., & Jaafar, J. (2020). Enhanced omniphobicity of mullite hollow fiber membrane with organosilane-functionalized TiO2 micro-flowers and nanorods layer deposition for desalination using direct contact membrane distillation. *Journal of Membrane Science*, *607*, 118137. https://doi.org/10.1016/j.memsci.2020.118137

Abraham, J., Vasu, K. S., Williams, C. D., Gopinadhan, K., Su, Y., Cherian, C. T., Dix, J., Prestat, E., Haigh, S. J., Grigorieva, I. V., Carbone, P., Geim, A. K., & Nair, R. R. (2017). Tunable sieving of ions using graphene oxide membranes. *Nature Nanotechnology*, *12*(6), 546–550. https://doi.org/10.1038/nnano.2017.21

Adams, L. K., Lyon, D. Y., & Alvarez, P. J. J. (2006). Comparative eco-toxicity of nanoscale TiO2, SiO2, and ZnO water suspensions. *Water Research*, *40*(19), 3527–3532. https://doi.org/10.1016/j.watres.2006.08.004

Alkhudhiri, A., Darwish, N., & Hilal, N. (2012). Membrane distillation: A comprehensive review. *Desalination*, *287*, 2–18. https://doi.org/10.1016/j.desal.2011.08.027

An, A. K., Lee, E. J., Guo, J., Jeong, S., Lee, J. G., & Ghaffour, N. (2017). Enhanced vapor transport in membrane distillation via functionalized carbon nanotubes anchored into electrospun nanofibres. *Scientific Reports*, *7*, 1–11. https://doi.org/10.1038/srep41562

Anitha, S., Brabu, B., John Thiruvadigal, D., Gopalakrishnan, C., & Natarajan, T. S. (2013). Optical, bactericidal and water repellent properties of electrospun nano-composite membranes of cellulose acetate and ZnO. *Carbohydrate Polymers*, *97*(2), 856–863. https://doi.org/10.1016/j.carbpol.2013.05.003

Attia, H., Alexander, S., Wright, C. J., & Hilal, N. (2017). Superhydrophobic electrospun membrane for heavy metals removal by air gap membrane distillation (AGMD). *Desalination*, *420*, 318–329. https://doi.org/10.1016/j.desal.2017.07.022

Bodell, B. R. (1963). Silicon rubber vapour diffusion in saline water distillation (United States Patent Serial No. 285,032).

Bhadra, M., Roy, S., & Mitra, S. (2014). Nanodiamond immobilized membranes for enhanced desalination via membrane distillation. *Desalination*, *341*(1), 115–119. https://doi.org/10.1016/j.desal.2014.02.036

Bhadra, M., Roy, S., & Mitra, S. (2016). Desalination across a graphene oxide membrane via direct contact membrane distillation. *Desalination*, *378*, 37–43. https://doi.org/10.1016/j.desal.2015.09.026

Bhattarai, S. R., Bhattarai, N., Yi, H. K., Hwang, P. H., Cha, D., & Kim, H. Y. (2004). Novel biodegradable electrospun membrane: Scaffold for tissue engineering. *Biomaterials*, *25*(13), 2595–2602. https://doi.org/10.1016/j.biomaterials.2003.09.043

Bonyadi, S., & Chung, T. S. (2007). Flux enhancement in membrane distillation by fabrication of dual layer hydrophilic-hydrophobic hollow fiber membranes. *Journal of Membrane Science*, *306*(1–2), 134–146. https://doi.org/10.1016/j.memsci.2007.08.034

Boo, C., Lee, J., & Elimelech, M. (2016). Engineering surface energy and nanostructure of microporous films for expanded membrane distillation applications. *Environmental Science & Technology*, *50*(15), 8112–8119. https://doi.org/10.1021/acs.est.6b02316

Cassie, A. B. D., & Baxter, S. (1944). Wettability of porous surfaces. *Transactions of the Faraday Society*, *40*(5), 546–551. https://doi.org/10.1039/tf9444000546

Castro-Muñoz, R., Ahmad, M. Z., & Fíla, V. (2019). Tuning of nano-based materials for embedding into low-permeability polyimides for a featured gas separation. *Frontiers in Chemistry*, *7*, 897–814. https://doi.org/10.3389/fchem.2019.00897

Castro-Muñoz, R., Buera-González, J., Iglesia, Ó. D. L., Galiano, F., Fíla, V., Malankowska, M., Rubio, C., Figoli, A., Téllez, C., & Coronas, J. (2019). Towards the dehydration of ethanol using pervaporation cross-linked poly(vinyl alcohol)/graphene oxide membranes. *Journal of Membrane Science*, *582*, 423–434. https://doi.org/10.1016/j.memsci.2019.03.076

Cerneaux, S., Strużyńska, I., Kujawski, W. M., Persin, M., & Larbot, A. (2009). Comparison of various membrane distillation methods for desalination using hydrophobic ceramic membranes. *Journal of Membrane Science*, *337*(1–2), 55–60. https://doi.org/10.1016/j.memsci.2009.03.025

Chen, B., Yang, Z., Zhu, Y., & Xia, Y. (2014). Zeolitic imidazolate framework materials: Recent progress in synthesis and applications. *Journal of Materials Chemistry A*, *2*(40), 16811–16831. https://doi.org/10.1039/C4TA02984D

Chen, L., Guo, Z., & Liu, W. (2016). Biomimetic multi-functional superamphiphobic FOTS-TiO2 particles beyond lotus leaf. *ACS Applied Materials & Interfaces*, *8*(40), 27188–27198. https://doi.org/10.1021/acsami.6b06772

Chen, L. H., Huang, A., Chen, Y. R., Chen, C. H., Hsu, C. C., Tsai, F. Y., & Tung, K. L. (2018). Omniphobic membranes for direct contact membrane distillation: Effective deposition of zinc oxide nanoparticles. *Desalination*, *428*, 255–263. https://doi.org/10.1016/j.desal.2017.11.029

Chen, M., Qin, X., & Zeng, G. (2016). Single-walled carbon nanotube release affects the microbial enzyme-catalyzed oxidation processes of organic pollutants and lignin model compounds in nature. *Chemosphere*, *163*, 217–226. https://doi.org/10.1016/j.chemosphere.2016.08.031

Cohen-Tanugi, D., & Grossman, J. C. (2012). Water desalination across nanoporous graphene. *Nano Letters*, *12*(7), 3602–3608. https://doi.org/10.1021/nl3012853

Curcio, E., & Drioli, E. (2005). Membrane distillation and related operations - A review. *Separation & Purification Reviews*, *34*(1), 35–86. https://doi.org/10.1081/SPM-200054951

Deka, B. J., Guo, J., Khanzada, N. K., & An, A. K. (2019). Omniphobic re-entrant PVDF membrane with ZnO nanoparticles composite for desalination of low surface tension oily seawater. *Water Research*, *165*, 114982. https://doi.org/10.1016/j.watres.2019.114982

Deshmukh, A., Boo, C., Karanikola, V., Lin, S., Straub, A. P., Tong, T., Warsinger, D. M., & Elimelech, M. (2018). Membrane distillation at the water-energy nexus: Limits, opportunities, and challenges. *Energy & Environmental Science*, *11*(5), 1177–1196. https://doi.org/10.1039/C8EE00291F

Devi, S., Ray, P., Singh, K., & Singh, P. S. (2014). Preparation and characterization of highly micro-porous PVDF membranes for desalination of saline water through vacuum membrane distillation. *Desalination*, *346*, 9–18. https://doi.org/10.1016/j.desal.2014.05.004

Dumée, L., Campbell, J. L., Sears, K., Schütz, J., Finn, N., Duke, M., & Gray, S. (2011). The impact of hydrophobic coating on the performance of carbon nanotube bucky-paper membranes in membrane distillation. *Desalination*, *283*, 64–67. https://doi.org/10.1016/j.desal.2011.02.046

Dumée, L., Germain, V., Sears, K., Schütz, J., Finn, N., Duke, M., Cerneaux, S., Cornu, D., & Gray, S. (2011). Enhanced durability and hydrophobicity of carbon nanotube bucky paper membranes in membrane distillation. *Journal of Membrane Science*, *376*(1–2), 241–246. https://doi.org/10.1016/j.memsci.2011.04.024

Duong, H. C., Chuai, D., Woo, Y. C., Shon, H. K., Nghiem, L. D., & Sencadas, V. (2018). A novel electrospun, hydrophobic, and elastomeric styrene-butadiene-styrene membrane for membrane distillation applications. *Journal of Membrane Science*, *549*, 420–427. https://doi.org/10.1016/j.memsci.2017.12.024

El-Bourawi, M. S., Ding, Z., Ma, R., & Khayet, M. (2006). A framework for better understanding membrane distillation separation process. *Journal of Membrane Science*, *285*(1–2), 4–29. https://doi.org/10.1016/j.memsci.2006.08.002

Eykens, L., De Sitter, K., Dotremont, C., Pinoy, L., & Van der Bruggen, B. (2017). Membrane synthesis for membrane distillation: A review. *Separation and Purification Technology*, *182*, 36–51. https://doi.org/10.1016/j.seppur.2017.03.035

Eykens, L., Hitsov, I., De Sitter, K., Dotremont, C., Pinoy, L., & Van der Bruggen, B. (2017). Direct contact and air gap membrane distillation: Differences and similarities between lab and pilot scale. *Desalination*, *422*, 91–100. https://doi.org/10.1016/j.desal.2017.08.018

Fang, H., Gao, J. F., Wang, H. T., & Chen, C. S. (2012). Hydrophobic porous alumina hollow fiber for water desalination via membrane distillation process. *Journal of Membrane Science*, *403–404*, 41–46. https://doi.org/10.1016/j.memsci.2012.02.011

Findley, M. E. (1967). Vaporization through porous membranes. *Industrial & Engineering Chemistry Process Design and Development*, *6*(2), 226–230. https://doi.org/10.1021/i260022a013

Francis, L., Maab, H., Alsaadi, A., Nunes, S., Ghaffour, N., & Amy, G. L. (2013). Fabrication of electrospun nanofibrous membranes for membrane distillation application. *Desalination and Water Treatment*, *51*(7–9), 1337–1343. https://doi.org/10.1080/19443994.2012.700037

Franken, A. C. M., Nolten, J. A. M., Mulder, M. H. V., Bargeman, D., & Smolders, C. A. (1987). Wetting criteria for the applicability of membrane distillation. *Journal of Membrane Science*, *33*(3), 315–328. https://doi.org/10.1016/S0376-7388(00)80288-4

García-Fernández, L., Wang, B., García-Payo, M. C., Li, K., & Khayet, M. (2017). Morphological design of alumina hollow fiber membranes for desalination by air gap membrane distillation. *Desalination*, *420*, 226–240. https://doi.org/10.1016/j.desal.2017.07.021

Gethard, K., Sae-Khow, O., & Mitra, S. (2011). Water desalination using carbon-nanotube-enhanced membrane distillation. *ACS Applied Materials & Interfaces*, *3*(2), 110–114. https://doi.org/10.1021/am100981s

Giacomello, A., Meloni, S., Chinappi, M., & Casciola, C. M. (2012). Cassie-Baxter and Wenzel states on a nanostructured surface: Phase diagram, metastabilities, and transition mechanism by atomistic free energy calculations. *Langmuir: The ACS Journal of Surfaces and Colloids*, *28*(29), 10764–10772. https://doi.org/10.1021/la3018453

Goh, S., Zhang, J., Liu, Y., & Fane, A. G. (2013). Fouling and wetting in membrane distillation (MD) and MD-bioreactor (MDBR) for wastewater reclamation. *Desalination*, *323*, 39–47. https://doi.org/10.1016/j.desal.2012.12.001

Gontarek, E., Macedonio, F., Militano, F., Giorno, L., Lieder, M., Politano, A., Drioli, E., & Gugliuzza, A. (2019). Adsorption-assisted transport of water vapour in super-hydrophobic membranes filled with multilayer graphene platelets. *Nanoscale*, *11*(24), 11521–11529. https://doi.org/10.1039/c9nr02581b

Gryta, M. (2007). Influence of polypropylene membrane surface porosity on the performance of membrane distillation process. *Journal of Membrane Science*, *287*(1), 67–78. https://doi.org/10.1016/j.memsci.2006.10.011

Gryta, M. (2018). Capillary polypropylene membranes for membrane distillation. *Fibers*, *7*(1), 1–11. https://doi.org/10.3390/fib7010001

Gu, Q., Ng, T. C. A., Zhang, L., Lyu, Z., Zhang, Z., Ng, H. Y., & Wang, J. (2020). Interfacial diffusion assisted chemical deposition (ID-CD) for confined surface modification of alumina microfiltration membranes toward high-flux and anti-fouling. *Separation and Purification Technology*, *23*, 116177. https://doi.org/10.1016/j.seppur.2019.116177

Gugliuzza, A., Ricca, F., & Drioli, E. (2006). Controlled pore size, thickness and surface free energy of super-hydrophobic PVDF® and Hyflon®AD membranes. *Desalination*, *200*(1–3), 26–28. https://doi.org/10.1016/j.desal.2006.03.229

Guo, J., Deka, B. J., Kim, K. J., & An, A. K. (2019). Regeneration of superhydrophobic TiO2 electrospun membranes in seawater desalination by water flushing in membrane distillation. *Desalination*, *468*, 114054. https://doi.org/10.1016/j.desal.2019.06.020

Guo, X., & Mei, N. (2014). Assessment of the toxic potential of graphene family nanomaterials. *Journal of Food and Drug Analysis*, *22*(1), 105–115. https://doi.org/10.1016/j.jfda.2014.01.009

Han, Y., Xu, Z., & Gao, C. (2013). Ultrathin graphene nanofiltration membrane for water purification. *Advanced Functional Materials*, *23*(29), 3693–3700. https://doi.org/10.1002/adfm.201202601

Hausmann, A., Sanciolo, P., Vasiljevic, T., Weeks, M., Schroën, K., Gray, S., & Duke, M. (2013). Fouling mechanisms of dairy streams during membrane distillation. *Journal of Membrane Science*, *441*, 102–111. https://doi.org/10.1016/j.memsci.2013.03.043

He, F., Gilron, J., Lee, H., Song, L., & Sirkar, K. K. (2008). Potential for scaling by sparingly soluble salts in crossflow DCMD. *Journal of Membrane Science*, *311*(1–2), 68–80. https://doi.org/10.1016/j.memsci.2007.11.056

Himma, N. F., Prasetya, N., Anisah, S., & Wenten, I. G. (2019). Superhydrophobic membrane: Progress in preparation and its separation properties. *Reviews in Chemical Engineering*, *35*(2), 211–238. https://doi.org/10.1515/revce-2017-0030

Hinds, B. J., Chopra, N., Rantell, T., Andrews, R., Gavalas, V., & Bachas, L. G. (2004). Aligned multiwalled carbon nanotube membranes. *Science (New York, N.Y.)*, *303*(5654), 62–65. https://doi.org/10.1126/science.1092048

Horseman, T., Yin, Y., Christie, K. S., Wang, Z., Tong, T., & Lin, S. (2021). Wetting, scaling, and fouling in membrane distillation: State-of-the-art insights on fundamental mechanisms and mitigation strategies. *ACS ES&T Engineering*, *1*(1), 117–140. https://doi.org/10.1021/acsestengg.0c00025

Jafari, A., Kebria, M. R. S., Rahimpour, A., & Bakeri, G. (2018). Graphene quantum dots modified polyvinylidenefluride (PVDF) nanofibrous membranes with enhanced performance for air Gap membrane distillation. *Chemical Engineering and Processing - Process Intensification*, *126*(2010), 222–231. https://doi.org/10.1016/j.cep.2018.03.010

Jamed, M. J., Alhathal Alanezi, A., & Alsalhy, Q. F. (2019). Effects of embedding functionalized multi-walled carbon nanotubes and alumina on the direct contact poly(vinylidene fluoride-co-hexafluoropropylene) membrane distillation performance. *Chemical Engineering Communications*, *206*(8), 1035–1057. https://doi.org/10.1080/00986445.2018.1542302

Jeong, S., Shin, B., Jo, W., Kim, H. Y., Moon, M. W., & Lee, S. (2016). Nanostructured PVDF membrane for MD application by an O2and CF4plasma treatment. *Desalination*, *399*, 178–184. https://doi.org/10.1016/j.desal.2016.09.001

Jia, Y., Yue, R., Liu, G., Yang, J., Ni, Y., Wu, X., & Chen, Y. (2013). Facile fabrication of nano-structured silica hybrid film with superhydrophobicity by one-step VAFS approach. *Applied Surface Science*, *265*, 405–411. https://doi.org/10.1016/j.apsusc.2012.11.020

Joshi, R. K., Carbone, P., Wang, F. C., Kravets, V. G., Su, Y., Grigorieva, I. V., Wu, H. A., Geim, A. K., & Nair, R. R. (2014). Precise and ultrafast molecular sieving through graphene oxide membranes. *Science (New York, N.Y.)*, *343*(6172), 752–754. https://doi.org/10.1126/science.1245711

Karanikola, V., Boo, C., Rolf, J., & Elimelech, M. (2018). Engineered slippery surface to mitigate gypsum scaling in membrane distillation for treatment of hypersaline industrial wastewaters. *Environmental Science & Technology*, *52*(24), 14362–14370. https://doi.org/10.1021/acs.est.8b04836

Ke, H., Feldman, E., Guzman, P., Cole, J., Wei, Q., Chu, B., Alkhudhiri, A., Alrasheed, R., & Hsiao, B. S. (2016). Electrospun polystyrene nanofibrous membranes for direct contact membrane distillation. *Journal of Membrane Science*, *515*, 86–97. https://doi.org/10.1016/j.memsci.2016.05.052

Kebria, M. R. S., Rahimpour, A., Bakeri, G., & Abedini, R. (2019). Experimental and theoretical investigation of thin ZIF-8/chitosan coated layer on air gap membrane distillation performance of PVDF membrane. *Desalination*, *450*, 21–32. https://doi.org/10.1016/j.desal.2018.10.023

Khayet, M., Mengual, J. I., & Matsuura, T. (2005). Porous hydrophobic/hydrophilic composite membranes: Application in desalination using direct contact membrane distillation. *Journal of Membrane Science*, *252*(1–2), 101–113. https://doi.org/10.1016/j.memsci.2004.11.022

Khayet, M., Velázquez, A., & Mengual, J. I. (2004). Modelling mass transport through a porous partition: Effect of pore size distribution. *Journal of Non-Equilibrium Thermodynamics*, *29*(3), 279–299. https://doi.org/10.1515/JNETDY.2004.055

Kołodziejczak-Radzimska, A., & Jesionowski, T. (2014). Zinc oxide-from synthesis to application: A review. *Materials (Basel, Switzerland)*, *7*(4), 2833–2881. https://doi.org/10.3390/ma7042833

Kullab, A., & Martin, A. (2011). Membrane distillation and applications for water purification in thermal cogeneration plants. *Separation and Purification Technology*, *76*(3), 231–237. https://doi.org/10.1016/j.seppur.2010.09.028

Kumar, R., Ahmed, M., Bhadrachari, G., Al-Mesri, A., & Thomas, J. P. (2020). A facile approach of thin film coating consisted of hydrophobic titanium dioxide over polypropylene membrane for membrane distillation graphical abstract keywords. *Journal of Membrane Science and Research*, *6*(2), 196–202. https://doi.org/10.22079/JMSR.2019.110904.1273

Laganà, F., Barbieri, G., & Drioli, E. (2000). Direct contact membrane distillation: Modelling and concentration experiments. *Journal of Membrane Science*, *166*(1), 1–11. https://doi.org/10.1016/S0376-7388(99)00234-3

Lai, Z. (2018). Development of ZIF-8 membranes: Opportunities and challenges for commercial applications. *Current Opinion in Chemical Engineering*, *20*, 78–85. https://doi.org/10.1016/j.coche.2018.03.002

Larbot, A., Gazagnes, L., Krajewski, S., Bukowska, M., & Kujawski, W. (2004). Water desalination using ceramic membrane distillation. *Desalination*, *168*, 367–372.

Lawson, K. W., & Lloyd, D. R. (1997). Membrane distillation. *Journal of Membrane Science*, *124*(1), 1–25. https://doi.org/10.1007/s00216-011-4733-9

Leaper, S., Abdel-Karim, A., Faki, B., Luque-Alled, J. M., Alberto, M., Vijayaraghavan, A., Holmes, S. M., Szekely, G., Badawy, M. I., Shokri, N., & Gorgojo, P. (2018). Flux-enhanced PVDF mixed matrix membranes incorporating APTS-functionalized graphene oxide for membrane distillation. *Journal of Membrane Science*, *554*, 309–323. https://doi.org/10.1016/j.memsci.2018.03.013

Lee, H. D., Kim, H. W., Cho, Y. H., & Park, H. B. (2014). Experimental evidence of rapid water transport through carbon nanotubes embedded in polymeric desalination membranes. *Small (Weinheim an Der Bergstrasse, Germany)*, *10*(13), 2653–2660. https://doi.org/10.1002/smll.201303945

Lee, J., Boo, C., Ryu, W. H., Taylor, A. D., & Elimelech, M. (2016). Development of omniphobic desalination membranes using a charged electrospun nanofiber scaffold. *ACS Applied Materials & Interfaces*, *8*(17), 11154–11161. https://doi.org/10.1021/acsami.6b02419

Lee, J.-G., Lee, E.-J., Jeong, S., Guo, J., An, A. K., Guo, H., Kim, J., Leiknes, T., & Ghaffour, N. (2017). Theoretical modeling and experimental validation of transport and separation properties of carbon nanotube electrospun membrane distillation. *Journal of Membrane Science*, *526*, 395–408. https://doi.org/10.1016/j.memsci.2016.12.045

Li, H., Liu, H., Shi, W., Zhang, H., Zhou, R., & Qin, X. (2020). Preparation of hydrophobic zeolitic imidazolate framework-71 (ZIF-71)/PVDF hollow fiber composite membrane for membrane distillation through dilute solution coating. *Separation and Purification Technology*, *251*, 117348. https://doi.org/10.1016/j.seppur.2020.117348

Li, X., Cao, Z., Zhang, Z., & Dang, H. (2006). Surface-modification in situ of nano-SiO 2 and its structure and tribological properties. *Applied Surface Science*, *252*(22), 7856–7861. https://doi.org/10.1016/j.apsusc.2005.09.068

Li, X., Yu, X., Cheng, C., Deng, L., Wang, M., & Wang, X. (2015). Electrospun superhydrophobic organic/inorganic composite nanofibrous membranes for membrane distillation. *ACS Applied Materials & Interfaces*, *7*(39), 21919–21930. https://doi.org/10.1021/acsami.5b06509

Li, X. M., Reinhoudt, D., & Crego-Calama, M. (2007). What do we need for a superhydrophobic surface? A review on the recent progress in the preparation of superhydrophobic surfaces. *Chemical Society Reviews*, *36*(8), 1350–1368. https://doi.org/10.1039/b602486f

Liang, S., Xiao, K., Mo, Y., & Huang, X. (2012). A novel ZnO nanoparticle blended polyvinylidene fluoride membrane for anti-irreversible fouling. *Journal of Membrane Science*, *394–395*, 184–192. https://doi.org/10.1016/j.memsci.2011.12.040

Liao, Y., Loh, C. H., Wang, R., & Fane, A. G. (2014). Electrospun superhydrophobic membranes with unique structures for membrane distillation. *ACS Applied Materials & Interfaces*, *6*(18), 16035–16048. https://doi.org/10.1021/am503968n

Liao, Y., Wang, R., & Fane, A. G. (2013). Engineering superhydrophobic surface on poly(-vinylidene fluoride) nanofiber membranes for direct contact membrane distillation. *Journal of Membrane Science*, *440*, 77–87. https://doi.org/10.1016/j.memsci.2013.04.006

Liao, Y., Wang, R., & Fane, A. G. (2014). Fabrication of bioinspired composite nanofiber membranes with robust superhydrophobicity for direct contact membrane distillation. *Environmental Science & Technology*, *48*(11), 6335–6341. https://doi.org/10.1021/es405795s

Liao, Y., Wang, R., Tian, M., Qiu, C., & Fane, A. G. (2013). Fabrication of polyvinylidene fluoride (PVDF) nanofiber membranes by electro-spinning for direct contact membrane distillation. *Journal of Membrane Science*, *425–426*, 30–39. https://doi.org/10.1016/j.memsci.2012.09.023

Liao, Y., Zheng, G., Huang, J. J., Tian, M., & Wang, R. (2020). Development of robust and superhydrophobic membranes to mitigate membrane scaling and fouling in membrane distillation. *Journal of Membrane Science*, *601*, 117962. https://doi.org/10.1016/j.memsci.2020.117962

Lu, K. J., Chen, Y., & Chung, T. S. (2019). Design of omniphobic interfaces for membrane distillation - A review. *Water Research*, *162*, 64–77. https://doi.org/10.1016/j.watres.2019.06.056

Ma, M., Hill, R. M., Lowery, J. L., Fridrikh, S. V., & Rutledge, G. C. (2005). Electrospun poly(styrene-block-dimethylsiloxane) block copolymer fibers exhibiting superhydrophobicity. *Langmuir: The ACS Journal of Surfaces and Colloids*, *21*(12), 5549–5554. https://doi.org/10.1021/la047064y

Ma, P. C., Siddiqui, N. A., Marom, G., & Kim, J. K. (2010). Dispersion and functionalization of carbon nanotubes for polymer-based nanocomposites: A review. *Composites Part A: Applied Science and Manufacturing*, *41*(10), 1345–1367. https://doi.org/10.1016/j.compositesa.2010.07.003

Macedonio, F., & Drioli, E. (2008). Pressure-driven membrane operations and membrane distillation technology integration for water purification. *Desalination*, *223*(1–3), 396–409. https://doi.org/10.1016/j.desal.2007.01.200

Mackie, J. S., & Meares, P. (1955). The diffusion of electrolytes in a cation-exchange resin membrane. *Proceedings of Royal Society*, *A232*, 498–509. https://doi.org/10.1246/nikkashi1921.58.819

Mali, S. S., Betty, C. A., Bhosale, P. N., & Patil, P. S. (2011). Hydrothermal synthesis of rutile TiO2 with hierarchical microspheres and their characterization. *CrystEngComm*, *13*(21), 6349–6351. https://doi.org/10.1039/c1ce05928a

Martínez, L., Florido-Díaz, F. J., Hernández, A., &., & Prádanos, P., (2003). Estimation of vapor transfer coefficient of hydrophobic porous membranes for applications in membrane distillation. *Separation and Purification Technology*, *33*(1), 45–55. https://doi.org/10.1016/S1383-5866(02)00218-6

McHale, G., Shirtcliffe, N. J., & Newton, M. I. (2004). Super-hydrophobic and super-wetting surfaces: Analytical potential? *The Analyst*, *129*(4), 284–287. https://doi.org/10.1039/b400567h

Meng, S., Ye, Y., Mansouri, J., & Chen, V. (2014). Fouling and crystallisation behaviour of superhydrophobic nano-composite PVDF membranes in direct contact membrane distillation. *Journal of Membrane Science*, *463*, 102–112. https://doi.org/10.1016/j.memsci.2014.03.027

Movafeghi, A., Khataee, A., Abedi, M., Tarrahi, R., Dadpour, M., & Vafaei, F. (2018). Effects of TiO2 nanoparticles on the aquatic plant Spirodela polyrrhiza: Evaluation of growth parameters, pigment contents and antioxidant enzyme activities. *Journal of Environmental Sciences*, *64*, 130–139. https://doi.org/10.1016/j.jes.2016.12.020

Naderi-Samani, H., Loghman-Estarki, M. R., Razavi, R. S., & Ramazani, M. (2017). The effects of organoclay on the morphology, thermal stability, transparence and hydrophobicity properties of polyamide – imide/nanoclay nanocomposite coatings. *Progress in Organic Coatings*, *112*, 162–168. https://doi.org/10.1016/j.porgcoat.2017.07.012

Nair, R. R., Wu, H. A., Jayaram, P. N., Grigorieva, I. V., & Geim, A. K. (2012). Unimpeded permeation of water through helium-leak-tight graphene-based membranes. *Science (New York, N.Y.)*, *335*(6067), 442–444. https://doi.org/10.1126/science.1211694

Nthunya, L. N., Gutierrez, L., Derese, S., Nxumalo, E. N., Verliefde, A. R., Mamba, B. B., & Mhlanga, S. D. (2019). A review of nanoparticle-enhanced membrane distillation membranes: Membrane synthesis and applications in water treatment. *Journal of Chemical Technology & Biotechnology*, *94*(9), 2757–2771. https://doi.org/10.1002/jctb.5977

Nthunya, L. N., Gutierrez, L., Nxumalo, E. N., Verliefde, A. R., Mhlanga, S. D., & Onyango, M. S. (2020). f-MWCNTs/AgNPs-coated superhydrophobic PVDF nanofibre membrane for organic, colloidal, and biofouling mitigation in direct contact membrane distillation. *Journal of Environmental Chemical Engineering*, *8*(2), 103654. https://doi.org/10.1016/j.jece.2020.103654

Nthunya, L. N., Gutierrez, L., Verliefde, A. R., & Mhlanga, S. D. (2019). Enhanced flux in direct contact membrane distillation using superhydrophobic PVDF nanofibre membranes embedded with organically modified SiO2 nanoparticles. *Journal of Chemical Technology & Biotechnology*, *94*(9), 2826–2837. https://doi.org/10.1002/jctb.6104

Ogawa, T., Ding, B., Sone, Y., & Shiratori, S. (2007). Super-hydrophobic surfaces of layer-by-layer structured film-coated electrospun nanofibrous membranes. *Nanotechnology*, *18*(16), 165607–165608. https://doi.org/10.1088/0957-4484/18/16/165607

Ollivier, H. (1907). Annales de Chimie et de Physique. *Annales de Chimie et de Physique*, *10*, 229.

Onda, T., Shibuichi, S., Satoh, N., & Tsujii, K. (1996). Super-water-repellent fractal surfaces. *Langmuir*, *12*(9), 5–7.

Orfi, J., Loussif, N., & Davies, P. A. (2016). Heat and mass transfer in membrane distillation used for desalination with slip flow. *Desalination*, *381*, 135–142. https://doi.org/10.1016/j.desal.2015.12.009

Pan, C.-Y., Xu, G.-R., Xu, K., Zhao, H.-L., Wu, Y.-Q., Su, H.-C., Xu, J.-M., & Das, R. (2019). Electrospun nanofibrous membranes in membrane distillation: Recent developments and future perspectives. *Separation and Purification Technology*, *221*, 44–63. https://doi.org/10.1016/j.seppur.2019.03.080

Peng, Y., Dong, Y., Fan, H., Chen, P., Li, Z., & Jiang, Q. (2013). Preparation of polysulfone membranes via vapor-induced phase separation and simulation of direct-contact membrane distillation by measuring hydrophobic layer thickness. *Desalination*, *316*, 53–66. https://doi.org/10.1016/j.desal.2013.01.021

Petcu, C., Purcar, V., Spătaru, C.-I., Alexandrescu, E., Şomoghi, R., Trică, B., Niţu, S., Panaitescu, D., Donescu, D., & Jecu, M.-L. (2017). The influence of new hydrophobic silica nanoparticles on the surface properties of the films obtained from bilayer hybrids. *Nanomaterials*, *7*(2), 47–10. https://doi.org/10.3390/nano7020047

Prince, J. A., Singh, G., Rana, D., Matsuura, T., Anbharasi, V., & Shanmugasundaram, T. S. (2012). Preparation and characterization of highly hydrophobic poly(vinylidene fluoride) - Clay nanocomposite nanofiber membranes (PVDF-clay NNMs) for desalination using direct contact membrane distillation. *Journal of Membrane Science*, *397–398*, 80–86. https://doi.org/10.1016/j.memsci.2012.01.012

Razmjou, A., Arifin, E., Dong, G., Mansouri, J., & Chen, V. (2012). Superhydrophobic modification of TiO 2 nanocomposite PVDF membranes for applications in membrane distillation. *Journal of Membrane Science*, *415–416*, 850–863. https://doi.org/10.1016/j.memsci.2012.06.004

Ren, L. F., Xia, F., Chen, V., Shao, J., Chen, R., & He, Y. (2017). TiO2-FTCS modified superhydrophobic PVDF electrospun nanofibrous membrane for desalination by direct

contact membrane distillation. *Desalination*, *423*, 1–11. https://doi.org/10.1016/j.desal.2017.09.004

Reneker, D. H., & Yarin, A. L. (2008). Electrospinning jets and polymer nanofibers. *Polymer*, *49*(10), 2387–2425. https://doi.org/10.1016/j.polymer.2008.02.002

Roy, K., Mukherjee, A., Maddela, N. R., Chakraborty, S., Shen, B., Li, M., Du, D., Peng, Y., Lu, F., & García Cruzatty, L. C. (2020). Outlook on the bottleneck of carbon nanotube in desalination and membrane-based water treatment-A review. *Journal of Environmental Chemical Engineering*, *8*(1), 103572. https://doi.org/10.1016/j.jece.2019.103572

Sae-Khow, O., & Mitra, S. (2010a). Carbon nanotube immobilized composite hollow fiber membranes for pervaporative removal of volatile organics from water. *The Journal of Physical Chemistry C*, *114*(39), 16351–16356. https://doi.org/10.1021/jp1064402

Sae-Khow, O., & Mitra, S. (2010b). Simultaneous extraction and concentration in carbon nanotube immobilized hollow fiber membranes. *Analytical Chemistry*, *82*(13), 5561–5567. https://doi.org/10.1021/ac100426y

Salehi, S., Jahanshahi, M., & Peyravi, M. (2018). Poly(vinylidene difluoride) membrane assisted by modified ZnO/ZIF nanoparticles for membrane distillation. *Chemical Engineering & Technology*, *41*(10), 1994–2004. https://doi.org/10.1002/ceat.201700496

Schneider, K., Hölz, W., Wollbeck, R., & Ripperger, S. (1988). Membranes and modules for transmembrane distillation. *Journal of Membrane Science*, *39*(1), 25–42. https://doi.org/10.1016/S0376-7388(00)80992-8

Seyed Shahabadi, S. M., Rabiee, H., Seyedi, S. M., Mokhtare, A., & Brant, J. A. (2017). Superhydrophobic dual layer functionalized titanium dioxide/polyvinylidene fluoride-co-hexafluoropropylene (TiO2/PH) nanofibrous membrane for high flux membrane distillation. *Journal of Membrane Science*, *537*, 140–150. https://doi.org/10.1016/j.memsci.2017.05.039

Shao, Y., Han, M., Wang, Y., Li, G., Xiao, W., Li, X., Wu, X., Ruan, X., Yan, X., He, G., & Jiang, X. (2019). Superhydrophobic polypropylene membrane with fabricated antifouling interface for vacuum membrane distillation treating high concentration sodium/magnesium saline water. *Journal of Membrane Science*, *579*, 240–252. https://doi.org/10.1016/j.memsci.2019.03.007

Shirtcliffe, N. J., McHale, G., Atherton, S., & Newton, M. I. (2010). An introduction to superhydrophobicity. *Advances in Colloid and Interface Science*, *161*(1–2), 124–138. https://doi.org/10.1016/j.cis.2009.11.001

Singh, A., Prasad, S. M., & Singh, S. (2018). Environmental nanotechnology, monitoring & management impact of nano ZnO on metabolic attributes and fl uorescence kinetics of rice seedlings. *Environmental Nanotechnology, Monitoring & Management*, *9*, 42–49. https://doi.org/10.1016/j.enmm.2017.11.006

Smolders, K., & Franken, A. C. M. (1989). Terminology for membrane distillation. *Desalination*, *72*(3), 249–262. https://doi.org/10.1016/0011-9164(89)80010-4

Srisurichan, S., Jiraratananon, R., & Fane, A. G. (2006). Mass transfer mechanisms and transport resistances in direct contact membrane distillation process. *Journal of Membrane Science*, *277*(1–2), 186–194. https://doi.org/10.1016/j.memsci.2005.10.028

Su, C., Horseman, T., Cao, H., Christie, K. S. S., Li, Y., & Lin, S. (2019). Robust superhydrophobic membrane for membrane distillation with excellent scaling resistance. *Environmental Science and Technology*, *53*, 11801−11809. https://doi.org/10.1021/acs.est.9b04362

Su, Y., Kravets, V. G., Wong, S. L., Waters, J., Geim, A. K., & Nair, R. R. (2014). Impermeable barrier films and protective coatings based on reduced graphene oxide. *Nature Communications*, *5*(1), 1–5. https://doi.org/10.1038/ncomms5843

Subramanian, N., Qamar, A., Alsaadi, A., Gallo, A., Ridwan, M. G., Lee, J.-G., Pillai, S., Arunachalam, S., Anjum, D., Sharipov, F., Ghaffour, N., & Mishra, H. (2019). Evaluating the potential of superhydrophobic nanoporous alumina membranes for direct contact membrane distillation. *Journal of Colloid and Interface Science*, *533*, 723–732. https://doi.org/10.1016/j.jcis.2018.08.054

Sun, P., Zhu, M., Wang, K., Zhong, M., Wei, J., Wu, D., Xu, Z., & Zhu, H. (2013). Selective ion penetration of graphene oxide membranes. *ACS Nano*, *7*(1), 428–437. https://doi.org/10.1021/nn304471w

Suresh, J., Pradheesh, G., Alexramani, V., Sundrarajan, M., & Hong, S. I. (2018). Green synthesis and characterization of zinc oxide nanoparticle using insulin plant (Costus pictus D. Don) and investigation of its antimicrobial as well as anticancer activities. *Advances in Natural Sciences: Nanoscience and Nanotechnology*, *9*(1), 015008. https://doi.org/10.1088/2043-6254/aaa6f1

Takashi, N., Masashi, M., Katsuhiko, N., Motonori, M., & Yasukiyo, U. (1999). The lowest surface free energy based on – CF3 alignment. *Langmuir*, *15*(13), 4321–4323. https://doi.org/10.1021/la981727s

Tamura, T., & Kawakami, H. (2010). Aligned electrospun nanofiber composite membranes for fuel cell electrolytes. *Nano Letters*, *10*(4), 1324–1328. https://doi.org/10.1021/nl1007079

Tang, L., Iddya, A., Zhu, X., Dudchenko, A. V., Duan, W., Turchi, C., Vanneste, J., Cath, T. Y., & Jassby, D. (2017). Enhanced flux and electrochemical cleaning of silicate scaling on carbon nanotube-coated membrane distillation membranes treating geothermal brines. *ACS Applied Materials & Interfaces*, *9*(44), 38594–38605. https://doi.org/10.1021/acsami.7b12615

Tang, N., Jia, Q., Zhang, H., Li, J., & Cao, S. (2010). Preparation and morphological characterization of narrow pore size distributed polypropylene hydrophobic membranes for vacuum membrane distillation via thermally induced phase separation. *Desalination*, *256*(1–3), 27–36. https://doi.org/10.1016/j.desal.2010.02.024

Termpiyakul, P., Jiraratananon, R., & Srisurichan, S. (2005). Heat and mass transfer characteristics of a direct contact membrane distillation process for desalination. *Desalination*, *177*(1–3), 133–141. https://doi.org/10.1016/j.desal.2004.11.019

Tian, M., Yin, Y., Yang, C., Zhao, B., Song, J., Liu, J., Li, X.-M., & He, T. (2015). CF4 plasma modified highly interconnective porous polysulfone membranes for direct contact membrane distillation (DCMD). *Desalination*, *369*, 105–114. https://doi.org/10.1016/j.desal.2015.05.002

Tijing, L. D., Woo, Y. C., Shim, W. G., He, T., Choi, J. S., Kim, S. H., & Shon, H. K. (2016). Superhydrophobic nanofiber membrane containing carbon nanotubes for high-performance direct contact membrane distillation. *Journal of Membrane Science*, *502*, 158–170. https://doi.org/10.1016/j.memsci.2015.12.014

Vane, L. M., Alvarez, F. R., & Mullins, B. (2001). Removal of methyl tert-butyl ether from water by pervaporation: Bench- and pilot-scale evaluations. *Environmental Science & Technology*, *35*(2), 391–397. https://doi.org/10.1021/es001362 +

Villaluenga, J. P. G., Khayet, M., López-Manchado, M. A., Valentin, J. L., Seoane, B., & Mengual, J. I. (2007). Gas transport properties of polypropylene/clay composite membranes. *European Polymer Journal*, *43*(4), 1132–1143. https://doi.org/10.1016/j.eurpolymj.2007.01.018

Wang, J. W., Li, L., Zhang, J. W., Xu, X., & Chen, C. S. (2016). β-Sialon ceramic hollow fiber membranes with high strength and low thermal conductivity for membrane distillation. *Journal of the European Ceramic Society*, *36*(1), 59–65. https://doi.org/10.1016/j.jeurceramsoc.2015.09.027

Wang, M., Liu, G., Yu, H., Lee, S.-H., Wang, L., Zheng, J., Wang, T., Yun, Y., & Lee, J. K. (2018). ZnO nanorod array modified PVDF membrane with superhydrophobic surface for vacuum membrane distillation application. *ACS Applied Materials & Interfaces*, *10*(16), 13452–13461. https://doi.org/10.1021/acsami.8b00271

Wang, R., Liu, Y., Li, B., Hsiao, B. S., & Chu, B. (2012). Electrospun nanofibrous membranes for high flux microfiltration. *Journal of Membrane Science*, *392–393*, 167–174. https://doi.org/10.1016/j.memsci.2011.12.019

Wang, Y., Han, M., Liu, L., Yao, J., & Han, L. (2020). Beneficial CNT intermediate layer for membrane fluorination toward robust superhydrophobicity and wetting resistance in membrane distillation. *ACS Applied Materials & Interfaces*, *12*(18), 20942–20954. https://doi.org/10.1021/acsami.0c03577

Wang, Z. L. (2004). Zinc oxide nanostructures: Growth, properties and applications. *Journal of Physics Condensed Matter*, *16*(25), 829–858. https://doi.org/10.1088/0953-8984/16/25/R01

Wei, X., Zhao, B., Li, X. M., Wang, Z., He, B. Q., He, T., & Jiang, B. (2012). CF 4 plasma surface modification of asymmetric hydrophilic polyethersulfone membranes for direct contact membrane distillation. *Journal of Membrane Science*, *407–408*, 164–175. https://doi.org/10.1016/j.memsci.2012.03.031

Wenzel, R. N. (1936). Resistance of solid surfaces to wetting by water. *Industrial & Engineering Chemistry*, *28*(8), 988–994. https://doi.org/10.1021/ie50320a024

Woo, Y. C., Kim, Y., Shim, W. G., Tijing, L. D., Yao, M., Nghiem, L. D., Choi, J. S., Kim, S. H., & Shon, H. K. (2016). Graphene/PVDF flat-sheet membrane for the treatment of RO brine from coal seam gas produced water by air gap membrane distillation. *Journal of Membrane Science*, *513*, 74–84. https://doi.org/10.1016/j.memsci.2016.04.014

Woo, Y. C., Tijing, L. D., Shim, W.-G., Choi, J.-S., Kim, S.-H., He, T., Drioli, E., & Shon, H. K. (2016). Water desalination using graphene-enhanced electrospun nanofiber membrane via air gap membrane distillation. *Journal of Membrane Science*, *520*, 99–110. https://doi.org/10.1016/j.memsci.2016.07.049

Xiao, Z., Zheng, R., Liu, Y., He, H., Yuan, X., Ji, Y., Li, D., Yin, H., Zhang, Y., Li, X.-M., & He, T. (2019). Slippery for scaling resistance in membrane distillation: A novel porous micropillared superhydrophobic surface. *Water Research*, *155*, 152–161. https://doi.org/10.1016/j.watres.2019.01.036

Xu, B., Zheng, Q., Song, Y., & Shangguan, Y. (2006). Calculating barrier properties of polymer/clay nanocomposites: Effects of clay layers. *Polymer*, *47*(8), 2904–2910. https://doi.org/10.1016/j.polymer.2006.02.069

Yan, L., Li, Y. S., Xiang, C. B., & Xianda, S. (2006). Effect of nano-sized Al2O3-particle addition on PVDF ultrafiltration membrane performance. *Journal of Membrane Science*, *276*(1–2), 162–167. https://doi.org/10.1016/j.memsci.2005.09.044

Yang, C., Li, X.-M., Gilron, J., Kong, D-f., Yin, Y., Oren, Y., Linder, C., & He, T. (2014). CF4 plasma-modified superhydrophobic PVDF membranes for direct contact membrane distillation. *Journal of Membrane Science*, *456*, 155–161. https://doi.org/10.1016/j.memsci.2014.01.013

Yang, C., Tian, M., Xie, Y., Li, X. M., Zhao, B., He, T., & Liu, J. (2015). Effective evaporation of CF4 plasma modified PVDF membranes in direct contact membrane distillation. *Journal of Membrane Science*, *482*, 25–32. https://doi.org/10.1016/j.memsci.2015.01.059

Yang, X., Wang, R., Shi, L., Fane, A. G., & Debowski, M. (2011). Performance improvement of PVDF hollow fiber-based membrane distillation process. *Journal of Membrane Science*, *369*(1–2), 437–447. https://doi.org/10.1016/j.memsci.2010.12.020

Yao, M., Tijing, L. D., Naidu, G., Kim, S. H., Matsuyama, H., Fane, A. G., & Shon, H. K. (2020). A review of membrane wettability for the treatment of saline water deploying membrane distillation. *Desalination*, *479*, 114312. https://doi.org/10.1016/j.desal.2020.114312

Yin, J., & Deng, B. (2015). Polymer-matrix nanocomposite membranes for water treatment. *Journal of Membrane Science*, *479*, 256–275. https://doi.org/10.1016/j.memsci.2014.11.019

Yin, Y., Jeong, N.-Y., & Tong, T. (2020). The effects of membrane surface wettability on pore wetting and scaling reversibility associated with mineral scaling in membrane distillation. *Journal of Membrane Science*, *614*, 118503. https://doi.org/10.1016/j.memsci.2020.118503

Yue, R., Meng, D., Ni, Y., Jia, Y., Liu, G., Yang, J., Liu, H., Wu, X., & Chen, Y. (2013). One-step flame synthesis of hydrophobic silica nanoparticles. *Powder Technology*, *235*, 909–913. https://doi.org/10.1016/j.powtec.2012.10.021

Zeyu, M., Hong, Y., Liyuan, M., & Su, M. (2009). Superhydrophobic membranes with ordered arrays of nanospiked microchannels for water desalination. *Langmuir: The ACS Journal of Surfaces and Colloids*, *25*(10), 5446–5450. https://doi.org/10.1021/la900494u

Zhang, J., Dow, N., Duke, M., Ostarcevic, E., Li, J. De., & Gray, S. (2010). Identification of material and physical features of membrane distillation membranes for high performance desalination. *Journal of Membrane Science*, *349*(1–2), 295–303. https://doi.org/10.1016/j.memsci.2009.11.056

Zhang, J., Song, Z., Li, B., Wang, Q., & Wang, S. (2013). Fabrication and characterization of superhydrophobic poly (vinylidene fluoride) membrane for direct contact membrane distillation. *Desalination*, *324*, 1–9. https://doi.org/10.1016/j.desal.2013.05.018

Zhang, Y., & Wang, R. (2013). Fabrication of novel polyetherimide-fluorinated silica organic-inorganic composite hollow fiber membranes intended for membrane contactor application. *Journal of Membrane Science*, *443*, 170–180. https://doi.org/10.1016/j.memsci.2013.04.062

Zhou, R., Rana, D., Matsuura, T., & Lan, C. Q. (2019). Effects of multi-walled carbon nanotubes (MWCNTs) and integrated MWCNTs/SiO2 nano-additives on PVDF polymeric membranes for vacuum membrane distillation. *Separation and Purification Technology*, *217*, 154–163. https://doi.org/10.1016/j.seppur.2019.02.013

Zhu, H., Wang, H., Wang, F., Guo, Y., Zhang, H., & Chen, J. (2013). Preparation and properties of PTFE hollow fiber membranes for desalination through vacuum membrane distillation. *Journal of Membrane Science*, *446*, 145–153. https://doi.org/10.1016/j.memsci.2013.06.037

Zhu, W., Liu, Y., Guan, K., Peng, C., Qiu, W., & Wu, J. (2019). Integrated preparation of alumina microfiltration membrane with super permeability and high selectivity. *Journal of the European Ceramic Society*, *39*(4), 1316–1323. https://doi.org/10.1016/j.jeurceram-soc.2018.10.022

Zhu, Y., Liu, X., Hu, Y., Wang, R., Chen, M., Wu, J., Wang, Y., Kang, S., Sun, Y., & Zhu, M. (2019). Behavior, remediation effect and toxicity of nanomaterials in water environments. *Environmental Research*, *174*, 54–60. https://doi.org/10.1016/j.envres.2019.04.014

Nanoscale

PAPER

Check for updates

Cite this: Nanoscale, 2019, 11, 11521

Adsorption-assisted transport of water vapour in super-hydrophobic membranes filled with multilayer graphene platelets†

E. Gontarek,[a,b] F. Macedonio,[a] F. Militano,[a] L. Giorno,[a] M. Lieder,[b] A. Politano,[c] E. Drioli[a,d,e] and A. Gugliuzza*[a]

Received 25th March 2019,
Accepted 22nd April 2019

DOI: 10.1039/c9nr02581b

rsc.li/nanoscale

The effects of confinement of multilayer graphene platelets in hydrophobic microporous polymeric membranes are here examined. Intermolecular interactions between water vapour molecules and nanocomposite membranes are envisaged to originate assisted transport of water vapour in membrane distillation processes when a suitable filler-polymer ratio is reached. Mass transport coefficients are estimated under different working conditions, suggesting a strong dependence of the transport on molecular interactions. Remarkably, no thermal polarization is observed, although the filler exhibits ultrahigh thermal conductivity. In contrast, enhanced resistance to wetting as well as outstanding mechanical and chemical stability meets the basic requirements of water purification via membrane distillation. As a result, a significant improvement of the productivity–efficiency trade-off is achieved with respect to the pristine polymeric membrane when low amounts of platelets are confined in spherulitic-like PVDF networks.

Introduction

The exceptional mechanical, electronic and thermal conductivity properties of atomically thin layers of graphene have enabled novel applications in the fields of optoelectronics,[1–5] polymeric nanocomposites,[6–11] catalysis,[12–14] and energy storage[15–18] as well as biosensing.[19–23] In particular, several studies have demonstrated the capabilities of multilayer graphene and few-layer graphite in membrane technology,[24–32] mostly for gas separation[33] and water purification.[34] For the latter processes, it is crucial to identify the mechanisms of gas selectivity and ion filtration through nanopores, holes and/or interspaces.[24] Herein, we propose to use multilayer graphene platelets (GPs), with a distribution of the thickness of around 5 layers, as fillers of spherulitic-like PVDF membranes. These kinds of membranes enable assisted transport mechanisms when tested in direct contact membrane distillation (DCMD), which uses a temperature gradient between two sides of the membrane to produce a gradient of partial pressure and, hence, induce the passage of water vapour through the pores from the hot side (feed solution) to the cold side (permeate solution), in which condensation occurs. As a result, fresh water is produced from salt solutions. In this case, the membrane acts as a physical barrier between two aqueous phases preventing their mixing. Currently, the major concern is the limited availability of membranes designed for efficient membrane distillation (MD).[35–41] Composite membranes represent a promising field to explore, since they offer complementary functionalities in unique interfaces, generally not achievable in pristine materials.[36,42–48]

Specifically, layered materials are regarded as a potential source of innovative features, which can favour the implementation of new-concept membrane desalination.[49] Graphitic systems would be advised against usage in thermally driven membrane processes, due to their very high thermal conductivity (~5000 W m^{-1} K^{-1} in the in-plane direction at 300 K for graphene[50] and ~2000 W m^{-1} K^{-1} for graphite[51]), as they could originate significant polarization events with severe reduction and/or zeroing of the fluxes. Given that one of the possible real driving forces of DCMD processes is the temperature gradient, the use of GPs in thermally driven operations could be in principle unsuitable. Nevertheless, our results demonstrate the total absence of thermal polarization, which combined with outstanding anti-wetting behaviour and break-

[a]Research Institute on Membrane Technology, ITM-CNR, Via Pietro Bucci 17/C, I-87030 Rende, Italy. E-mail: a.gugliuzza@itm.cnr.it
[b]On leave from Gdansk University of Technology, Department of Chemical Technology ul., G. Narutowicza 11/1280-233 Gdańsk, Poland
[c]Department of Physical and Chemical Sciences, University of L'Aquila, via Vetoio, 67100 L'Aquila, AQ, Italy
[d]Department of Environmental and Chemical Engineering, University of Calabria, Via P. Bucci, 87036 Rende, CS, Italy
[e]Hanyang University, WCU Energy Engineering Department, Room 917 9th Floor FTC Bldg., 17 Haengdang-dong, Seongdong-gu, Seoul 133-791, South Korea
†Electronic supplementary information (ESI) available. See DOI: 10.1039/c9nr02581b

ing resistance make GPs suitable for filling a polymer matrix. Conversely, water–GP interactions are envisaged to preside over mass transfer, yielding diffusion locally dependent on GPs confined in the polymer network. This work provides insightful evidence about the role of adhesive interactions activated at the water/graphene interface when a low amount of filler is entrapped in the polymer matrix, thus resulting in a fruitful assisted vapour transport. A further increase in the concentration of the filler induces a competition between adhesive and cohesive forces, which causes the penetrant to prolong its permanence inside of the membrane with consequent reduction of the mass transfer. Based on the experimental evidence, chemisorption at the vacancy and edge sites of confined fillers can be exploited to activate novel mechanisms for water purification *via* membrane distillation technology.

Results and discussion

We have prepared composite membranes by dispersing commercial GPs in NMP under alternated cycles of sonication and mechanical stirring for 2 h at 30 °C. Then, powder of PVDF has been added to the mixtures and stirred for further 24 h at 30 °C. After degassing, the solutions have been cast on glass supports and, then, coagulated in IPA and washed with deionized water. As an effect of solid–liquid demixing,[52] flat membranes with particulate morphology, a mean pore size of 0.2–0.5 μm and overall porosity (ε) within the range of 60 to 80% have been obtained.

Commercial GPs used in this work are layered materials with a maximum peaked around 5 layers, as confirmed by Raman spectroscopy (see the ESI†). This feature appears to be preserved when the filler is confined in membranes at various loadings. No filler sedimentation or dominant phase separation is observed macroscopically, but rather a fair distribution of GPs along the entire section of the membranes is detectable (Fig. 1).

Discrete domains are well discernable inside the polymeric matrix whilst a large number of free gaps, in which water vapour can freely diffuse through, are preserved. Table 1 shows high values of the overall porosity, which is regarded as the free volume fraction of membranes. Just a slight decrease in the value is observed at the highest loading of the filler due to a local formation of clusters. However, water vapour transmission rate (WVTR) experiments yield a tangible indication about a good diffusion of water vapour through all composite membranes (Fig. 2). Despite that a better capability to permeate is estimated for membranes containing GPs up to 5%, membranes with 10% of filler continue to exhibit a mass transport comparable to that observed for the pristine PVDF membrane independently of the decreased porosity. Assisted transport mechanisms could be, hence, conceivable.

Mechanically, the addition of the filler takes a further advantage of making the membrane stiffer so that an increase in the Young's modulus up to 1400 N mm^{-2} is obtained. At lower concentration, an increase in the resistance to stretching is also detectable with values up to 85 ± 10% for 0.5% of GPs. A further increase in the GP content causes the membranes to be particularly brittle and unmanageable (Fig. 3a). This behaviour is fully consistent with the highest number of crystalline domains detected by DSC analyses (Fig. 3b). Indeed, it is not surprising that inorganic fillers play a key role in crystallization processes, because they can modify the properties of semi-crystalline polymers.[53,54]

Accordingly, the membranes with a GP loading of 0.5% can be envisaged to be much more durable and, therefore, suitable for long-term MD experiments.

It is further interesting to observe that the addition of fillers to the polymeric solution causes a general amplification of the waterproofness with contact angle values up to 151 ± 3° as the filler fraction is 0.5% (Fig. 4).

Undoubtedly, the topography and chemistry of these membranes are rather complex, considering the fact that graphene platelets are randomly dispersed in perfluorinated environments. So, different local factors would be considered at the nanoscale level in order to explain which events control the wetting for. However, this purpose is over the aim of this work, whereas the definitive result can be regarded as a further targeted accomplishment for MD implementation. Furthermore, values of resistance to liquid entry pressure (LEP) around 1 bar endorse the goodness of all membranes so that each membrane enables a large resistance to the passage of salt solution, resulting in NaCl rejection values of 99.97 to 99.99% after 6 running hours of the MD process.

Fig. 5 confirms the goodness of the membrane with time. It shows a constant run over 18 running hours of the MD coefficient (B), defined as the ratio between the flux and partial pressure gradient at the membrane surface, with an estimation of 99.86% for the final rejection factor.

It should be noted that neither scaling nor thermal polarization affected water vapour diffusion, yielding a clear indication about the stability of the composite matrixes and thermal inertness of GPs. Vibrational spectra collected on filtered residue from feed and permeate streams at the end of experiments indicate no leaking of materials from membranes.

Concerning thermal polarization events, the confined five layer graphene platelets do not form a thermal continuum inside the insulating polymeric matrix, but rather discrete units and/or small accumulation at the highest concentrations. This kind of restriction prevents the formation of networks in the hosting polymer matrix, resulting in an ultralow thermal conductivity. This finding matches well with the concept of thermal interfacial resistance induced by confinement of the fillers.[55]

Although structural and chemical features well fit with criteria of MD and the process is preserved from undesired wetting and thermal polarization, the open issue is about the involvement of GPs in water vapour diffusion.

In this regard, it is interesting to observe how GPs loaded in the matrix can affect the mass transfer through the membrane when increasing driving force is applied (Fig. 6).

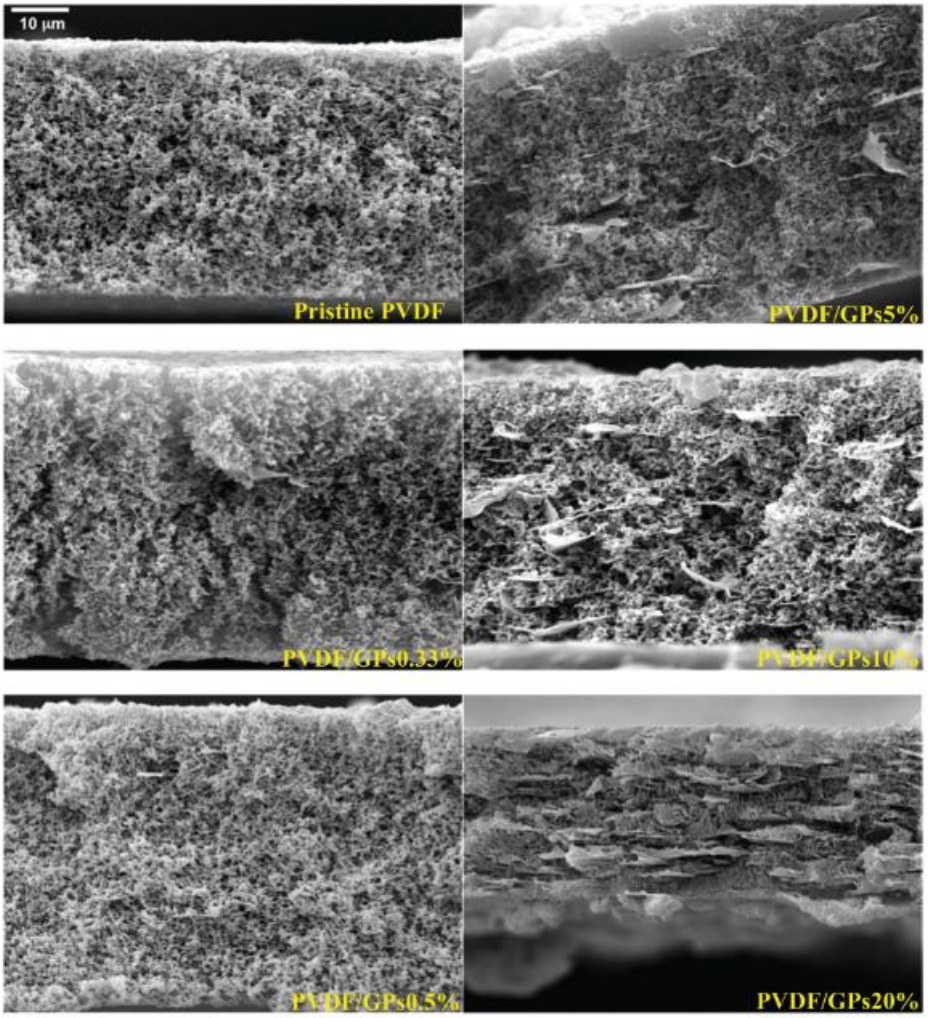

Fig. 1 SEM micrographs collected along the cross section of PVDF/GP composite membranes, including the pristine membrane and membranes with a loading of 0.33 to 20%. The scale bar denotes 10 μm.

Table 1 Overall porosity (ε) estimated for membranes uploading different amounts of multilayer graphene platelets

GP [%]	ε [%]
0	77 ± 2
0.33	77 ± 2
0.5	69 ± 2
5.0	65 ± 3
10	64 ± 6

Compared to pristine PVDF membranes, higher values of B can be estimated at 0.33 and 0.5% of GP loading, respectively. A further increase in the content of the filler causes instead additional resistance to mass transfer, resulting in a lower diffusion of water vapour. Also, an unusual diffusion for all samples is observed with respect to the pristine PVDF membrane. Specifically, the mass transport coefficient B estimated for composite membranes shows a singular and fluctuating behaviour as the driving force of the process is increased (Fig. 6).

This behaviour could be plausibly ascribed to the establishment of local interactions between water and the filler in the

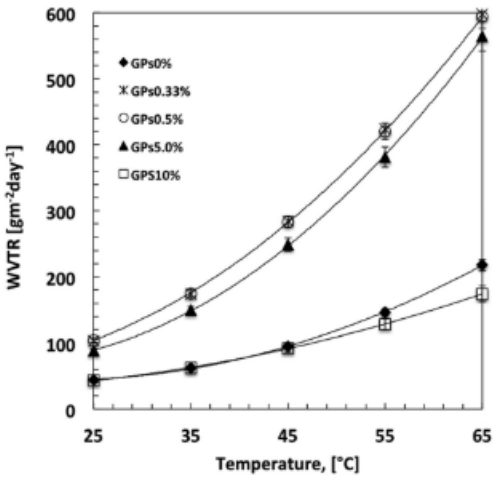

Fig. 2 WVTR estimated for PVDF pristine and composite membranes.

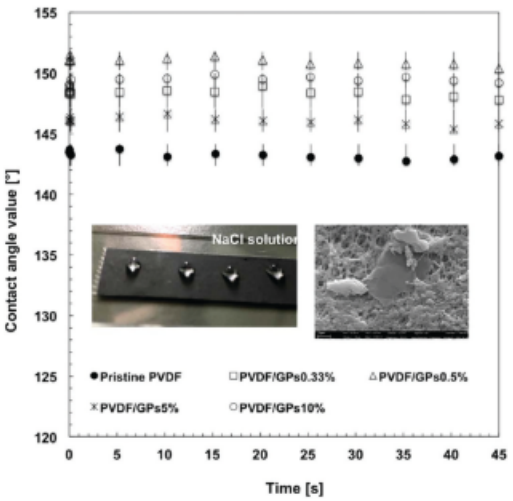

Fig. 4 Resistance to wetting of PVDF/GP membranes coming in contact to NaCl solution 0.6 M.

matrix.[56] This hypothesis is indeed corroborated by some experimental evidence provided by attenuated total reflection (ATR) analysis (Fig. 7). Spectra have been collected on samples, after water vapour passed through for 2 hours at 25 °C, according to the procedure used to estimate the WVTR. Notably, high-frequency extra absorption modes are observed around 3850 and 3750 cm^{-1} for composite membranes, while in spectra collected on pristine PVDF membranes these absorptions are not detectable. Previously, this feature has been revealed in pressurized water vapour[57] and its origin has been discussed in terms of stable and metastable dimers.[58–60]

These vibrational modes can be regarded as a fingerprint of water decomposition at GP defects and edges, as previously observed for epitaxial graphene on metals.[61] It is worth point-

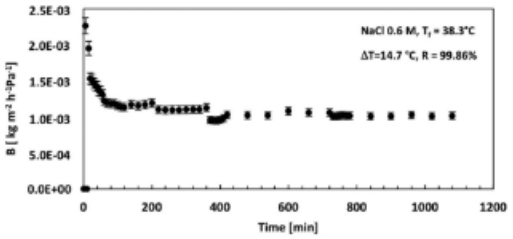

Fig. 5 MD coefficient (*B*) *vs.* working time estimated for membranes loaded with 0.5% of GPs.

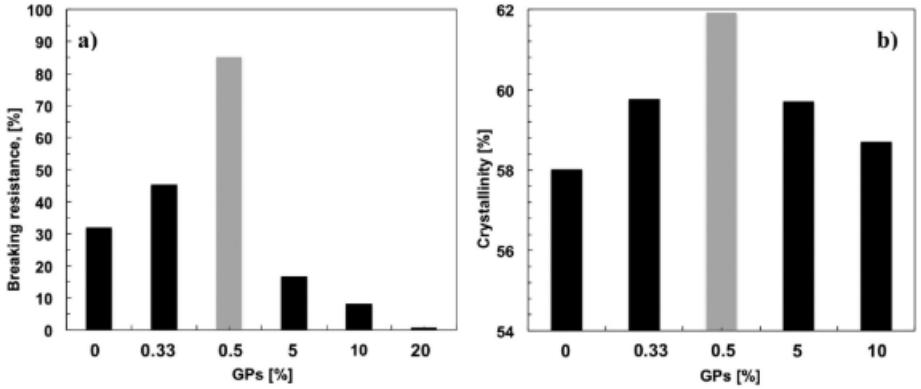

Fig. 3 (a) Breaking resistance evaluated for PVDF/GP membranes at different loadings of filler; (b) degree of crystallinity calculated from the ratio of the measured fusion heat ΔH_m to fusion heat ΔH_m° of 100% crystalline PVDF ($\Delta H_m^\circ = 104.7$ J g^{-1}).

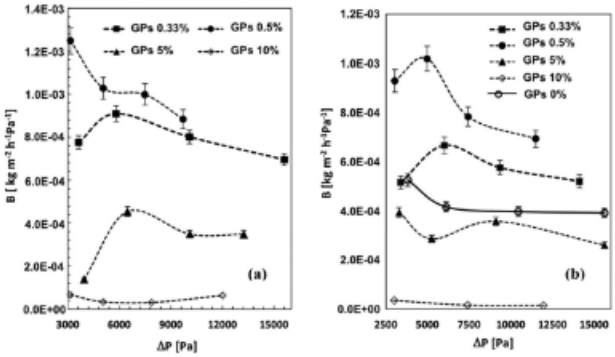

Fig. 6 Mass transfer coefficient of membrane distillation *vs.* partial pressure of water vapor: (a) pure water and (b) NaCl 0.6 M streams.

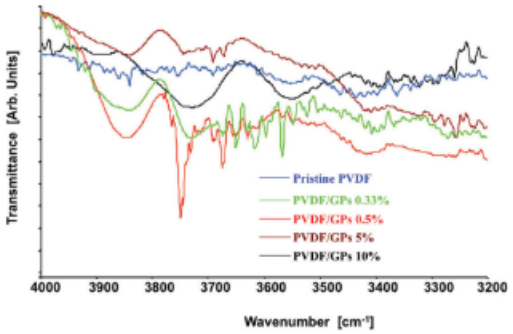

Fig. 7 ATR spectra collected on PVDF membranes at different loadings of GPs.

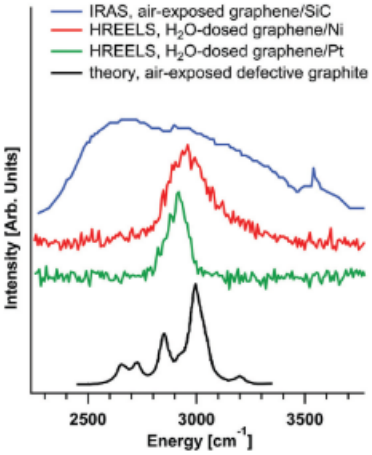

Fig. 8 Dissociative adsorption of atmospheric molecules at edges and vacancies on the surface of graphene. Red and green curves represent vibrational spectra acquired by HREELS for graphene/Ni(111) and graphene/Pt(111), respectively. The blue curve is the vibrational spectrum acquired by IRAS (infrared absorption spectroscopy) for epitaxial graphene on SiC exposed in ambient air humidity (data taken from ref. 62). Finally, theoretical data for air-exposed defective graphite in the black curve were taken from ref. 70.

ing out that the presence of a metal substrate is not an essential prerequisite for the dissociation of water molecules, as demonstrated by results for graphene grown on the semiconducting SiC[62] (blue curve in Fig. 8). Furthermore, the strength of the interaction with the substrate only plays a minor role, as indicated by the small energy shift in the C–H stretching recorded on strongly interacting graphene on Ni(111) (red curve in Fig. 8), for which the Dirac cone is washed out by the interaction with Ni d bands,[63–65] compared to the case of quasi-freestanding graphene on Pt(111) (green curve in Fig. 8); this means that the Dirac cone is preserved.[66] Actually, water decomposition has been predicted to occur also for defective graphite[67–69] (black curve in Fig. 8), suggesting that dissociative adsorption of water can also take place at graphitic materials, in proximity to defects and edges.

Concerning adsorption of O–H groups suggests however different scenarios. Much more intense absorptions shifted to higher wavenumbers are observed for membranes containing 0.5 and 0.33% of filler, whilst a shift towards lower wavenumbers is detected at a higher content of filler. This suggests that a much stronger interaction is established with water at the highest loading of the filler, thereby justifying a lower and irregular mass transfer.

Penetration and diffusion of water molecules through free gaps between GPs and polymers seem to take place *via* intermolecular interactions at defect sites of the filler, including edges and vacancies. At a low amount of the filler in the polymer matrix, adhesive interactions could be activated at the water/GP interface, resulting in assisted vapour transport. A further increase in the concentration of the filler can instead cause massive water uptake over the space between the GPs and polymer network, thus resulting in a potential compe-

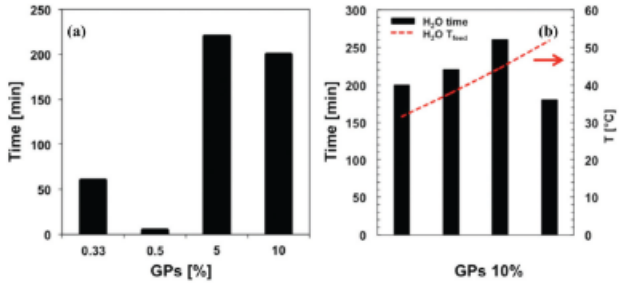

Fig. 9 Time necessary to water for diffusing through PVDF/GP membranes at 40 °C (a) and in all ranges of working temperature at the highest content of GPs (b).

tition between adhesive and cohesive forces, which causes the penetrant to prolong its permanence inside of the membrane. Likewise, local arrangements of platelets can affect nearby the interactions, thus causing locally increased or reduced vapour diffusion.

This hypothesis is further corroborated by the transient state of each experiment carried out with membranes at different loadings of GPs. When the concentration of GPs is significantly increased, a longer time is required for collecting water at the permeate side. Fig. 9a shows the time necessary to water molecules for moving from the feed to the permeate side through all membranes examined in this work when the T_{feed} is 30–40 °C. This event continues to be detectable, within all ranges of T_{feed}, for the membrane containing the highest amount of filler (GPs 10%, Fig. 9b).

In this case, even up to four running hours are required to observe the onset of permeation of water vapour through the membrane, thereby suggesting a longer permanence of the penetrant inside the matrix. Therefore, one can conclude that intermolecular water–platelets interactions may assist or inhibit diffusion of water molecules through membranes depending on the concentration of GPs. Based on experimental findings, a GP concentration of 0.5% can be regarded as a suitable compromise to promote well-balanced kinetics of sorption–desorption of the penetrant at GP edges and vacancies, thus leading to assisted transport. Differently, a massive concentration of GPs yields a considerable amount of stagnant and bonded water inside the membrane, resulting in slowed down transport.

In this context, GPs could bring benefits to water vapour transport through membranes, which equip the MD plant, if the amount and rearrangement into the matrix are well equilibrated.

Fig. 10 yields indication about a better substrate-filler ratio to obtain good PVDF/GP membrane performance for MD purposes, suggesting a GP loading of 0.5% to get enhanced productivity–efficiency trade-off as compared to pristine PVDF and other GPs/PVDF membranes.

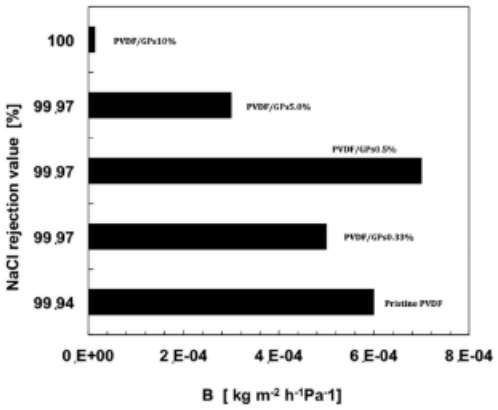

Fig. 10 Rejection-resistance to transport trade-off estimated for PVDF/GPs and pristine PVDF membranes at around ΔP = 9000 Pa.

Conclusions

We examined the effects of the confinement of GPs in superhydrophobic membranes concerning the possibility of assisted or hindered transport of water vapour when MD processes are implemented. The use of GPs in membrane distillation appears to be a practical route to replace the state-of-the-art membranes working as physical barriers with interactive interfaces through the exploitation of chemisorption at the vacancy and edge sites of confined fillers in order to activate novel mechanisms of water purification.

Experimental results indicate that composite membranes are able to take up water vapour *via* intermolecular interactions. The latter are demonstrated to play a key role in assisted transport mechanisms when low concentrations of filler are well rearranged inside of the matrix, whereas water fragments are expected to be stably adsorbed over free space between the polymer and graphene, thus leading to additional resistance to transport. Interestingly, this study provides a useful indication about the feasibility to use stacks of few layers of graphene in membranes to be tested in thermally

driven membrane operations such as membrane distillation. No thermal polarization is observed, contrary to common expectations on the basis of the ultrahigh thermal conductivity of graphene. Conversely, improved resistance to wetting together with mechanical and chemical stability over time can be obtained when the amount of the filler inside of the membrane is well calibrated and rearranged. As a result, significant improvement in terms of transport and salt rejection is achieved as compared to pristine PVDF. In this perspective, the use of GP-based membranes appears to be promising for boosting the implementation of new-concept fruitful purification processes in membrane technology.

Experimental section

Materials

PVDF (Solef®6020, Solvay Solexis: water adsorption <0.040% @23 °C after 24 h; d_p = 1.78 kg m^{-3}) was kindly supplied by Solavy Solexis. Graphene platelet (GP) powder (Sigma Aldrich: carbon, >95 wt%; oxygen, <2 wt%; area, 10 000 nm^2; morphology, irregular symmetry typical of flakes) was used. The Raman spectrum collected on GP powder strongly resembles the reference spectrum for five layers (see the ESI†), thereby yielding an indication about the distribution of the thicknesses peaking at around five layers. This feature is preserved when GPs are confined in the membrane at various concentrations. 1-Methyl-2-pyrrolidinone (NMP, Riedel de Haën: max 0.05% in water, d = 1.03 kg m^{-3}) and propan-2-olo (IPA, WWR PROLABO: d = 0.78 kg m^{-3}) were used as the solvent and non-solvent, respectively. Fluorinert (FCO, Novec) was used for gas–liquid displacement measurements. Ultra-pure water (filtered by using a USF ELGA plant) and NaCl solution 0.6 M were used as probe liquids to perform contact angle measurements. All materials were used as received.

Membrane preparation. The membranes were prepared by dry-wet phase inversion according to the procedure detailed in ref. 52. GPs were dispersed in NMP using an ultrasonic bath alternated with mechanical stirring for 2 hours at 30 °C. PVDF was, then, added to the mixture at a concentration of 12 wt% and the mixtures were left under mechanical stirring at 30 °C for 24 h, in the GP loading range from 0.33 to 20%. Herein, the content of the filler will be referred to as GPs0.33%, GPS0.5%, GPs5%, GPs10%, and GPs20%. After degassing, the dopes were uniformly cast on glass plates by using a casting knife regulated on 250 μm (Elcometer Instruments Inc.). The casting solutions were coagulated and left for 10 min in a bath containing IPA in order to promote solid–liquid demixing and then washed with ultra-pure water. The films were air-dried at room temperature overnight and, finally, annealed at 30 °C for 1 hour.

Methods

Structural and physicochemical properties. Structural features of the polymeric matrix were examined by SEM (Zeiss EVO MA10, Germany). The pore size and distribution were estimated according to the gas–liquid displacement technique (PM, Instruments). Samples with an effective area of 3.5 cm^2 were filled with FCO and the liquid was displaced from bigger to smaller pores with increasing pressure. The overall porosity was measured by filling them with FCO. The membrane weight was estimated before and after filling and the porosity was expressed in percentage as the ratio between the volume occupied by the fluorinert liquid and the volume of the membrane. Six specimens were tested for each kind of nanocomposite membrane. Changes in mechanical resistance were evaluated by using a tensile stress–strain meter (Roell/Zwick); an average of 4–5 specimens with an area of 10 cm^2 were tested at 20 °C. ATR spectra were directly collected and averaged from the sample surfaces after fluxing water vapour for 2 hours at 25 °C (UATR crystal Diamond/ZnSe-Spectrum One System by PerkinElmer Instruments). Raman spectroscopy measurements were carried out on the hybrid-membranes at room temperature using a Thermo Fisher DXR Raman microscope equipped with OMNICxi Raman imaging software 1.0. The 532.0 nm line was used at an incident power output of 3 mW.

High-resolution electron energy loss spectroscopy (HREELS) was performed with a Delta 0.5 spectrometer by Specs GmbH on a sample of monolayer graphene on Ni(111), successively exposed to water under ultrahigh vacuum up to saturation. The impinging energy was 3 eV, with an energy resolution of 4 meV. The resistance to liquid entry pressure of water (LEP_w) was measured in static mode by connecting the membrane in a container filled with distilled water. The container was pressurized with nitrogen and the pressure was read on a calibrated gauge. A slight pressure of nitrogen was applied to water for 15 min with an increasing pressure of 0.1 bar every 20 min. The pressure difference at which the liquid penetrates into the pore of the membrane is indicated as LEP_w. Three samples with a surface area of 12.56 cm^2 were tested for each kind of membrane. The resistance to wetting from pure water and salt solutions was investigated by measuring the contact angle value with time according to the sessile drop method (Cam 200 KSV instruments, Ltd).

Transport properties. The water vapor transmission rate (WVTR) was tested within a range of temperatures (25–65 °C) according to the cup-right method (ASTM E96B).[71] Thermally driven MD experiments were executed according to the Membrane Direct Contact (DC) configuration using NaCl solutions 0.6 M – flow rate = 100 mL min^{-1}; T_{feed} = 38 to 56 °C and T_{perm} = 15 °C. Retentate and distillate streams were converged, in a counter-current way, toward the membrane module containing the membrane, where the liquid water was evaporated. On the retentate side, a pump was taking and sending the heated feed to the membrane module. Also on the distillate side, a second pump ensured the counter-current recycle of the cold stream in order to remove from the solution the vapour diffusing through the membrane pores. The transmembrane fluxes were estimated by evaluating the weight variations in the distillate tanks. The thermal efficiency was calculated considering each single layer forming the tailor-made

membrane. The salt conductibility of the feed and permeate streams was measured by using a conductive meter (Eutech Instruments PC 2700).

Conflicts of interest

There are no conflicts of interest to declare.

Acknowledgements

We acknowledge financial support by 'a grant from the Italian Ministry of Foreign Affairs and International Cooperation' within the framework of the Great Relevance International Project Italy (MAECI)-China (NSFC) 2018–2020 – New Materials, with particular reference to Two-dimensional systems and Graphene.

References

1 F. H. L. Koppens, T. Mueller, P. Avouris, A. C. Ferrari, M. S. Vitiello and M. Polini, *Nat. Nanotechnol.*, 2014, **9**, 780–793.
2 J. Wu, Z. Yang, C. Qiu, Y. Zhang, Z. Wu, J. Yang, Y. Lu, J. Li, D. Yang, R. Hao, E. Li, G. Yu and S. Lin, *Nanoscale*, 2018, **10**, 8023–8030.
3 D. Paria, H. H. Jeong, V. Vadakkumbatt, P. Deshpande, P. Fischer, A. Ghosh and A. Ghosh, *Nanoscale*, 2018, **10**, 7685–7693.
4 M. Romagnoli, V. Sorianello, M. Midrio, F. H. L. Koppens, C. Huyghebaert, D. Neumaier, P. Galli, W. Templ, A. D'Errico and A. C. Ferrari, *Nat. Rev. Mater.*, 2018, **3**, 392–414.
5 T. Jiang, D. Huang, J. Cheng, X. Fan, Z. Zhang, Y. Shan, Y. Yi, Y. Dai, L. Shi, K. Liu, C. Zeng, J. Zi, J. E. Sipe, Y. R. Shen, W. T. Liu and S. Wu, *Nat. Photonics*, 2018, **12**, 430–436.
6 L.-Z. Guan, L. Zhao, Y.-J. Wan and L.-C. Tang, *Nanoscale*, 2018, **10**, 14788–14811.
7 M. Darder, P. Aranda, C. Ruiz-García, F. M. Fernandes and E. Ruiz-Hitzky, *Adv. Funct. Mater.*, 2018, **28**, 1704323.
8 L. Z. Guan, L. Zhao, Y. J. Wan and L. C. Tang, *Nanoscale*, 2018, **10**, 14788–14811.
9 D. Dutta, A. N. F. Ganda, J. K. Chih, C. C. Huang, C. J. Tseng and C. Y. Su, *Nanoscale*, 2018, **10**, 12612–12624.
10 J. H. Choe, J. Jeon, M. E. Lee, J. J. Wie, H. J. Jin and Y. S. Yun, *Nanoscale*, 2018, **10**, 2025–2033.
11 Z. Zeng, S. I. Seyed Shahabadi, B. Che, Y. Zhang, C. Zhao and X. Lu, *Nanoscale*, 2017, **9**, 17396–17404.
12 X. Cui, W. An, X. Liu, H. Wang, Y. Men and J. Wang, *Nanoscale*, 2018, **10**, 15262–15272.
13 S. Seo, K. Lee, M. Min, Y. Cho, M. Kim and H. Lee, *Nanoscale*, 2017, **9**, 3969–3979.
14 Y. Niu, X. Huang, X. Wu, L. Zhao, W. Hu and C. Ming Li, *Nanoscale*, 2017, **9**, 10233–10239.
15 X. Li and L. Zhi, *Chem. Soc. Rev.*, 2018, **47**, 3189–3216.
16 M. Zhao, X. Cui, Y. Xu, L. Chen, Z. He, S. Yang and Y. Wang, *Nanoscale*, 2018, **10**, 15379–15386.
17 A. Wu, S. Shen, X. Yan, G. Xia, Y. Zhang, F. Zhu and J. Zhang, *Nanoscale*, 2018, **10**, 12763–12770.
18 T. Liang, H. Wang, D. Xu, K. Liao, R. Wang, B. He, Y. Gong and C. Yan, *Nanoscale*, 2018, **10**, 17814–17823.
19 Z. Gao, H. Xia, J. Zauberman, M. Tomaiuolo, J. Ping, Q. Zhang, P. Ducos, H. Ye, S. Wang, X. Yang, F. Lubna, Z. Luo, L. Ren and A. T. C. Johnson, *Nano Lett.*, 2018, **18**, 3509–3515.
20 L. Sun, Y. Zhang, Y. Wang, Y. Yang, C. Zhang, X. Weng, S. Zhu and X. Yuan, *Nanoscale*, 2018, **10**, 1759–1765.
21 S. Afsahi, M. B. Lerner, J. M. Goldstein, J. Lee, X. Tang, D. A. Bagarozzi, D. Pan, L. Locascio, A. Walker, F. Barron and B. R. Goldsmith, *Bionsens. Bioelectron.*, 2018, **100**, 85–88.
22 Z. Wang, M. Gui, M. Asif, Y. Yu, S. Dong, H. Wang, W. Wang, F. Wang, F. Xiao and H. Liu, *Nanoscale*, 2018, **10**, 6629–6638.
23 B. Peng, J. Cui, Y. Wang, J. Liu, H. Zheng, L. Jin, X. Zhang, Y. Zhang and Y. Wu, *Nanoscale*, 2018, **10**, 1939–1945.
24 A. Gugliuzza, A. Politano and E. Drioli, *Curr. Opin. Chem. Eng.*, 2017, **16**, 78–85.
25 K. G. Zhou, K. S. Vasu, C. T. Cherian, M. Neek-Amal, J. C. Zhang, H. Ghorbanfekr-Kalashami, K. Huang, O. P. Marshall, V. G. Kravets, J. Abraham, Y. Su, A. N. Grigorenko, A. Pratt, A. K. Geim, F. M. Peeters, K. S. Novoselov and R. R. Nair, *Nature*, 2018, **559**, 236–240.
26 D. H. Seo, S. Pineda, Y. C. Woo, M. Xie, A. T. Murdock, E. Y. M. Ang, Y. Jiao, M. J. Park, S. I. Lim, M. Lawn, F. F. Borghi, Z. J. Han, S. Gray, G. Millar, A. Du, H. K. Shon, T. Y. Ng and K. Ostrikov, *Nat. Commun.*, 2018, **9**, 683.
27 A. Gugliuzza, A. Politano and E. Drioli, in *Graphene-based Membranes for Mass Transport Applications*, The Royal Society of Chemistry, 2019, pp. 211–224, DOI: 10.1039/9781788013017-00211.
28 L. Madauß, J. Schumacher, M. Ghosh, O. Ochedowski, J. Meyer, H. Lebius, B. Ban-Detat, M. E. Toimil-Molares, C. Trautmann, R. G. H. Lammertink, M. Ulbricht and M. Schleberger, *Nanoscale*, 2017, **9**, 10487–10493.
29 H. Qi, Z. Li, Y. Tao, W. Zhao, K. Lin, Z. Ni, C. Jin, Y. Zhang, K. Bi and Y. Chen, *Nanoscale*, 2018, **10**, 5350–5357.
30 S. Sahu and M. Zwolak, *Nanoscale*, 2017, **9**, 11424–11428.
31 S. Wang, Z. Tian, S. Dai and D. E. Jiang, *Nanoscale*, 2018, **10**, 14660–14666.
32 Y. G. Yan, W. S. Wang, W. Li, K. P. Loh and J. Zhang, *Nanoscale*, 2017, **9**, 18951–18958.
33 S. Huang, M. Dakhchoune, W. Luo, E. Oveisi, G. He, M. Rezaei, J. Zhao, D. T. L. Alexander, A. Züttel, M. S. Strano and K. V. Agrawal, *Nat. Commun.*, 2018, **9**, 2632.
34 Y. Yang, R. Zhao, T. Zhang, K. Zhao, P. Xiao, Y. Ma, P. M. Ajayan, G. Shi and Y. Chen, *ACS Nano*, 2018, **12**, 829–835.
35 Z. Cui, X. Li, Y. Zhang, Z. Wang, A. Gugliuzza, F. Militano, E. Drioli and F. Macedonio, *Desalination*, 2018, **440**, 68–77.

36 V. Speranza, F. Trotta, E. Drioli and A. Gugliuzza, *ACS Appl. Mater. Interfaces*, 2010, **2**, 459–466.
37 L. Eykens, I. Hitsov, K. De Sitter, C. Dotremont, L. Pinoy and B. Van der Bruggen, *Desalination*, 2017, **422**, 91–100.
38 Y. Choi, G. Naidu, S. Jeong, S. Vigneswaran, S. Lee, R. Wang and A. G. Fane, *Desalination*, 2017, **420**, 54–62.
39 J. Zuo, S. Bonyadi and T.-S. Chung, *J. Membr. Sci.*, 2016, **497**, 239–247.
40 L. Eykens, K. De Sitter, C. Dotremont, L. Pinoy and B. Van der Bruggen, *Ind. Eng. Chem. Res.*, 2016, **55**, 9333–9343.
41 P. Wang and T.-S. Chung, *J. Membr. Sci.*, 2015, **474**, 39–56.
42 A. Gugliuzza, V. Pingitore, D. Miriello and E. Drioli, *Phys. Chem. Chem. Phys.*, 2015, **17**, 12919–12926.
43 V. Pingitore, D. Miriello, E. Drioli and A. Gugliuzza, *Soft Matter*, 2015, **11**, 4461–4468.
44 V. Pingitore and A. Gugliuzza, *J. Phys. Chem. C*, 2013, **117**, 26562–26572.
45 Y. Han, L. Giorno and A. Gugliuzza, *Membranes*, 2017, **7**, 66.
46 Z. Zhang, L. Zou, C. Aubry, M. Jouiad and Z. Hao, *J. Membr. Sci.*, 2016, **515**, 204–211.
47 Q. Liu and G.-R. Xu, *Desalination*, 2016, **394**, 162–175.
48 F. Macedonio, A. Politano, E. Drioli and A. Gugliuzza, *Mater. Horiz.*, 2018, **5**, 912–919.
49 M. Perrotta, G. Saielli, G. Casella, F. Macedonio, L. Giorno, E. Drioli and A. Gugliuzza, *Appl. Mater. Today*, 2017, **9**, 1–9.
50 A. A. Balandin, S. Ghosh, W. Bao, I. Calizo, D. Teweldebrhan, F. Miao and C. N. Lau, *Nano Lett.*, 2008, **8**, 902–907.
51 C. Y. Ho, R. W. Powell and P. E. Liley, *J. Phys. Chem. Ref. Data*, 1972, **1**, 279–421.
52 A. Gugliuzza and E. Drioli, *J. Membr. Sci.*, 2007, **300**, 51–62.
53 N. Ning, S. Fu, W. Zhang, F. Chen, K. Wang, H. Deng, *et al.*, *Prog. Polym. Sci.*, 2012, **37**, 1425–1455.
54 S. L. Gao and J. K. Kim, Part 1. Crystallinity and interface adhesion, *Composites, Part A*, 2000, **31**, 517–530.
55 Z. Han and A. Fina, *Prog. Polym. Sci.*, 2011, **36**, 914–944.
56 M. A. Henderson, *Surf. Sci. Rep.*, 2002, **46**, 1–308.
57 A. A. Vigasin, Y. Jin and S. Ikawa, *Mol. Phys.*, 2008, **106**, 1155–1159.
58 A. A. Vigasin, *Mol. Phys.*, 2010, **108**, 2309–2313.
59 M. Y. Tretyakov and D. Makarov, *J. Chem. Phys.*, 2011, **134**, 084306.
60 Y. Bouteiller, B. Tremblay and J. P. Perchard, *Chem. Phys.*, 2011, **386**, 29–40.
61 A. Politano, M. Cattelan, D. W. Boukhvalov, D. Campi, A. Cupolillo, S. Agnoli, N. G. Apostol, P. Lacovig, S. Lizzit, D. Farías, G. Chiarello, G. Granozzi and R. Larciprete, *ACS Nano*, 2016, **10**, 4543–4549.
62 H. Yan, F. Xia, W. Zhu, M. Freitag, C. Dimitrakopoulos, A. A. Bol, G. Tulevski and P. Avouris, *ACS Nano*, 2011, **5**, 9854–9860.
63 A. Cupolillo, N. Ligato and L. S. Caputi, *Carbon*, 2012, **50**, 2588–2591.
64 A. al Taleb, G. Anemone, D. Farías and R. Miranda, *Carbon*, 2016, **99**, 416–422.
65 J. Sánchez-Barriga, A. Varykhalov, M. R. Scholz, O. Rader, D. Marchenko, A. Rybkin, A. M. Shikin and E. Vescovo, *Diamond Relat. Mater.*, 2010, **19**, 734–741.
66 P. Sutter, J. T. Sadowski and E. Sutter, *Phys. Rev. B: Condens. Matter Mater. Phys.*, 2009, **80**, 245411.
67 S. C. Xu, S. Irle, D. G. Musaev and M. C. Lin, *J. Phys. Chem. C*, 2006, **111**, 1355–1365.
68 A. Allouche and Y. Ferro, *Carbon*, 2006, **44**, 3320–3327.
69 H. K. Jeong, H. J. Noh, J. Y. Kim, L. Colakerol, P. A. Glans, M. H. Jin, K. E. Smith and Y. H. Lee, *Phys. Rev. Lett.*, 2009, **102**, 099701.
70 A. Allouche and Y. Ferro, *J. Nucl. Mater.*, 2007, **363**, 117–121.
71 A. Gugliuzza and E. Drioli, *J. Membr. Sci.*, 2013, **446**, 350–375.

water

MDPI

Article

Characterization of PVDF/Graphene Nanocomposite Membranes for Water Desalination with Enhanced Antifungal Activity

Emilia Gontarek-Castro [1,*], Maria Krystyna Rybarczyk [2], Roberto Castro-Muñoz [1,3], Monica Morales-Jiménez [4], Blanca Barragán-Huerta [4] and Marek Lieder [1]

[1] Department of Process Engineering and Chemical Technology, Faculty of Chemistry, Gdansk University of Technology, 11/12 G. Narutowicza St., 80-233 Gdansk, Poland; food.biotechnology88@gmail.com (R.C.-M.); lieder@pg.edu.pl (M.L.)
[2] Department of Geotechnical Engineering, Faculty of Civil Engineering and Architecture, Lublin University of Technology, 40 Nadbystrzycka St., 20-618 Lublin, Poland; m.rybarczyk@pollub.pl
[3] Tecnologico de Monterrey, Campus Toluca, Avenida Eduardo Monroy Cárdenas 2000, San Antonio Buenavista, Toluca de Lerdo 50110, Mexico
[4] Escuela Nacional de Ciencias Biológicas, Instituto Politécnico Nacional, Avenida Wilfrido Massieu s/n, Unidad Profesional Adolfo López Mateos, Mexico City 07738, Mexico; mmoralesj1902@alumno.ipn.mx (M.M.-J.); bbarraganh@ipn.mx (B.B.-H.)
* Correspondence: emilia.gontarek@pg.edu.pl

check for updates

Citation: Gontarek-Castro, E.; Rybarczyk, M.K.; Castro-Muñoz, R.; Morales-Jiménez, M.; Barragán-Huerta, B.; Lieder, M. Characterization of PVDF/Graphene Nanocomposite Membranes for Water Desalination with Enhanced Antifungal Activity. *Water* **2021**, *13*, 1279. https://doi.org/10.3390/w13091279

Academic Editor: Muhammad Wakil Shahzad

Received: 26 March 2021
Accepted: 28 April 2021
Published: 30 April 2021

Abstract: Seawater desalination is a worldwide concern for the sustainable production of drinking water. In this regard, membrane distillation (MD) has shown the potential for effective brine treatment. However, the lack of appropriate MD membranes limits its industrial expansion since they experience fouling and wetting issues. Therefore, hydrophobic membranes are promising candidates to successfully deal with such phenomena that are typical for commercially available membranes. Here, several graphene/polyvinylidene (PVDF_G) membranes with different graphene loading (0–10 wt%) were prepared through a phase inversion method. After full characterization of the resulting membranes, the surface revealed that the well-dispersed graphene in the polymer matrix (0.33 and 0.5 wt% graphene loading) led to excellent water repellence together with a rough structure, and a large effective surface area. Importantly, antifungal activity tests of films indicated an increase in the inhibition percentage for PVDF_G membranes against the *Curvularia* sp. fungal strain. However, the antifungal surface properties were found to be the synergistic result of graphene toxicity and surface topography.

Keywords: membrane distillation; graphene; membranes; anti-fungal activity

1. Introduction

Due to the current lack of drinking water, there is an urgent need to develop advanced processes for its production from natural sources. State-of-the-art technologies enable the treatment of sea water using selective membrane processes, such as reverse osmosis (RO) [1], pervaporation (PV) [2], and membrane distillation (MD) [3]. The latter is more affordable and economical due to the lower temperatures and process pressures, along with a higher salt rejection rate and lower susceptibility to concentration polarization. Unfortunately, the drawbacks of existing membrane materials, mainly fouling and wetting susceptibility, significantly limit their use in MD as a method of water desalination. Therefore, it is necessary to design novel structural materials to exploit the full potential of this membrane process.

Membrane fouling mitigation has been one of the main research challenges over the last years [4]. The fouling in MD depends on the physicochemical composition of the feed solution provoking organic, inorganic, and biological fouling, whereas the operating

parameters in MD also influence the fouling generation. In principle, the biological fouling (called biofouling) is initiated by the adhesion, growth, and replication of either bacterial or fungal species on the membrane surface [5]. The biofouling affects the membrane hydraulic permeability, which causes an increase in maintenance costs and the deterioration of the power density [6–8]. To date, a number of strategies, such as polymerization, chemical grafting, nanocomposite preparation, and surface coating, have been applied to obtain specific surface morphology and membrane properties [9,10]. When dealing with the use of any additive, the main disadvantage is weak interaction between the polymer and additives, which affects the long-term durability of the surface modification layer, further causing its release outside the membrane. Recent developments have shown that the modification of polymeric membranes with inorganic nanomaterials may improve the MD stability against different types of fouling [11], together with the upgrading of other important membrane properties (such as the mechanical and thermal properties of membranes) [12,13]. For instance, the hydrophobicity of graphene and its exceptional properties [14] make it a promising material for improving the performance of polymeric membranes toward MD. In our previous studies, we investigated the role of adhesive interactions activated at the water/graphene interface on the assisted vapor transport during MD tests, where the increase of the flux was observed in the membranes containing low graphene concentration when compared with pristine PVDF membrane [15]. In addition, graphene and graphene derivatives were reported to exhibit broad-spectrum antimicrobial and antifungal activity [16]. These properties of graphene-based nanostructures are based on their capacity to induce membrane and oxidative stress, which compromise bacterial and fungal proliferation and sporulation [17–19].

In this work, hydrophobic porous membranes were prepared based on polyvinylidene fluoride (PVDF) and different graphene nanoplatelets (GNP) loading. PVDF was chosen as a membrane component due to its low cost and good thermal, mechanical, and chemical stability. The role of the incorporated graphene in the polymeric membrane matrix was investigated in terms of membrane characterization (such as porosity, pore size, hydrophobicity, and roughness) and antifungal activity. To the best of our knowledge, we are the first to evaluate the antifungal activity of PVDF/GNP nanocomposite membranes. To evaluate the antifungal properties of the membranes, *Curvularia* sp. (closely related with the genus Cochliobolus) was chosen. This hyphomycete fungus causes severe crop losses worldwide and has been detected in drinking water distribution systems and in groundwater supply systems [20]. The membrane material used for water treatment should possess antifungal activity to mitigate membrane biofouling and to produce water free of microbial pathogens. Thus, for the antifungal test, we selected one of many examples of phytopathogenic fungus that can be found in water.

2. Materials and Methods

2.1. Materials

PVDF (Solef®6020, Solvay Specialty Polymers, Düsseldorf, Germany), graphene nanoplatelets (GNP), powder, hydrophobic (Sigma-Aldrich, Poznań, Poland), *N*-methyl-2-pyrrolidone (NMP, ACS reagent ≥99.0%, Sigma Aldrich, Poznań, Poland), and isopropanol (POCH, Gliwice, Poland) were used for membrane preparation. Fluorinert™ FC-40 (Sigma-Aldrich, Poznań, Poland) was used for overall porosity estimation.

2.2. Membrane Preparation

The polymeric solution was prepared by dissolving 11.7 wt% of PVDF powder in NMP under mechanical stirring for 24 h in 30 °C. After this, the solution was left for 3–4 h without stirring for the removal of bubbles. The membranes were later cast on a glass and spread with the micrometric film applicator (Elcometer) using a gap size of 250 µm, immersed sequentially for 10 min in isopropanol, and cleaned with deionized water. Then, the membranes were dried at room temperature overnight. For PVDF/graphene membrane preparation, GNP were first dispersed in NMP using an ultrasonic bath alternated with

mechanical stirring for 1.5 h. PVDF was then added to the mixture, and the membranes were prepared analogously to the PVDF ones. The GNP loading in PVDF membranes ranged from 0.33 to 10 wt%, and the membranes were named PVDF_0.33G, PVDF_0.5G, PVDF_5G, and PVDF_10G according to the GNP content.

2.3. Membrane Characterization

The morphology of the resulting membranes was analyzed using scanning electron microscopy (SEM, Zeiss-EVO MA10, Oberkochen, Germany) and an atomic force microscope. The atomic force microscopy was performed in a MultiMode 8, Nanoscope V (Veeco-Bruker, Plainview, NY, USA) using tapping mode and 5 × 5 μm of scan size. The average roughness (Ra) and the root mean square roughness (Rq) were calculated from the obtained images in NanoScope Analysis 1.4 software (Bruker Corporation, Billerica, MA, USA). The overall porosity is expressed as the total void inside the membrane. The pore size was estimated according to the gas–liquid displacement technique using a capillary flow porometer (PM, Instruments, CFP 1500, AXEL, Ithaca, NY, USA). The resistance to wetting with pure water was investigated by measuring the contact angle value (OCA 15 apparatus, Dataphysics, Filderstadt, Germany). Fourier transform infrared spectroscopy (FTIR) was used to collect spectra of the membranes in the scan range of 400–4000 cm^{-1} in ATR mode with a resolution of 16 cm^{-1} using a Nicolet iS10 FTIR spectrometer (Thermo Scientific Instrument Co., Boston, MA, USA). The X-ray diffraction patterns were recorded using an X-ray diffractometer (XRD, Rigaku MiniFlex 600, The Woodlands, TX, USA) in the range of 2θ = 5–80° with Cu-Kα radiation.

2.4. Antifungal Activity

The antifungal activity assay was performed on natural potato dextrose agar (PDA), prepared according to the procedure described in the literature [21]. Both 0.37 mg/mL of lincomycin and 0.37 mg/mL of chloramphenicol were used to minimize contamination with bacteria. The antifungal activity assay was tested on *Curvularia* sp. fungal species according to the method described previously [22]. All PVDF/GNP membranes were cut in square sized pieces (1 × 1) and assayed; pristine PVDF membrane was also evaluated and taken as a negative control and bioactive film from microalgae-based biopolymer as a positive control. The square-shaped membranes were placed on the center of PDA plates. After inoculation with a mycelial plug on the film surface, plates were incubated for three days at 28 °C in the dark. All trials were performed three times. The radial growth was measured and is expressed in cm, and the inhibition percentage was calculated using Equation (1), as follows:

$$Inhibition\ (\%) = \frac{negativecontrolarea - treatmentarea}{negativecontrolarea} \times 100\% \quad (1)$$

$$area = \pi \times r^2 \quad (2)$$

3. Results and Discussion

The characteristics and morphologies of the pristine and PVDF/GNP membranes are shown in Table 1. Although all the fabricated membranes showed highly porous structures between 64% and 77%, the composition of the membrane significantly influenced the membrane morphology and surface properties, such as roughness, pore size, and hydrophobicity. The surface of the pristine PVDF and PVDF/GNP membranes was analyzed by SEM, as shown in Figure 1. The analysis confirmed a successful incorporation of graphene nanoplatelets into the PVDF matrix. The pristine PVDF showed a sponge-like structure and relatively smooth surface, which is typical for porous polymeric membranes [23]. With the addition of graphene, this structure became more compact. This was confirmed by slightly reduced overall porosity values and a significant reduction in pore size, (especially for PVDF_5G and PVDF_10G), for which a smaller value was detected (from 0.5 μm to 0.27 and 0.24 μm, respectively). In the graphene-incorporated PVDF membranes, where GNP

were uniformly distributed in the membrane matrix (PVDF_0.33G and PVDF_0.5G), an enhancement in surface roughness was observed (Figure 1D,F). Nevertheless, with excess addition of GNP, they aggregated in the membrane matrix, as exhibited by PVDF_5G and PVDF_10G (Figure 1G,I). This led to porosity and pore size reduction, while the surface morphology tuned by the graphene incorporation was expected to affect the surface hydrophobicity. Similar results were observed previously when the aggregation of the graphene nanoparticles in the membrane matrix led to a smaller pore size, lower porosity, and increased thickness of the fabricated membranes [24].

In practice, the hydrophobicity of the surface depends on the high surface roughness and low surface energy of materials [25]. Moreover, the hydrophobicity in MD membranes is of particular importance, since it maintains the gas phase in the pores, which is required for MD. Thus, the surface roughness of the membranes has a strong influence on their wetting performance. For instance, the AFM images of all the membranes are shown in Figure 1B,D,F,H,J), while the Rq and Ra values of the membranes and their surface area are reported in Table 1. The pristine PVDF membrane, according to the SEM and AFM images, possessed a smooth and microporous surface, and the measured value of the Rq was about 289 nm. After incorporation of GNPs, the Rq parameter increased up to 524 and 375 nm for PVDF_0.33G and PVDF_0.5G, respectively. This confirms that graphene intercalation provides PVDF a rougher membrane surface. In general, the incorporation of nanomaterial in the polymeric membrane enhances its roughness, which is caused by the introduction of nano-scaled protrusions [26–28]. However, GNP aggregation, as observed for PVDF_5G and PVDF_10G, led to an Rq reduction of 292 and 183 nm, respectively. Thus, the highly rough surface of the PVDF_0.33G and PVDF_0.5G membranes can be attributed to the well-dispersed graphene nanoplatelets in the membrane matrix [12]. In general, rough surfaces are able to form an air gap between the surface protrusions, creating a gas–liquid interface between the liquid and the membrane surface, which is beneficial to enhancing the anti-wettability and anti-fouling properties of the membranes in MD [29].

Table 1. Properties of the pristine PVDF membrane and its graphene-based composites. Porosity and mean pore size analyses were performed 3 times for every sample and the values are reported as mean ± standard deviation.

Membrane	Porosity (%)	Mean Pore Size (μm)	Rq (nm)	Ra (nm)	Surface Area (μm^2)
PVDF	77 ± 2	0.48 (±0.09)	289	222	44.3
PVDF_0.33G	77 ± 2	0.53 (±0.02)	524	430	58.2
PVDF_0.5G	69 ± 2	0.56 (±0.06)	375	310	50.4
PVDF_5G	65 ± 3	0.27 (±0.01)	292	226	46.1
PVDF_10G	64 ± 6	0.24 (±0.01)	183	152	36.6

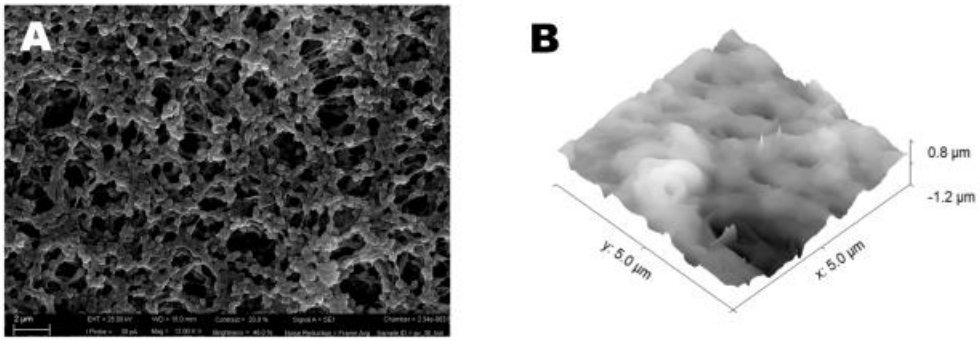

Figure 1. *Cont.*

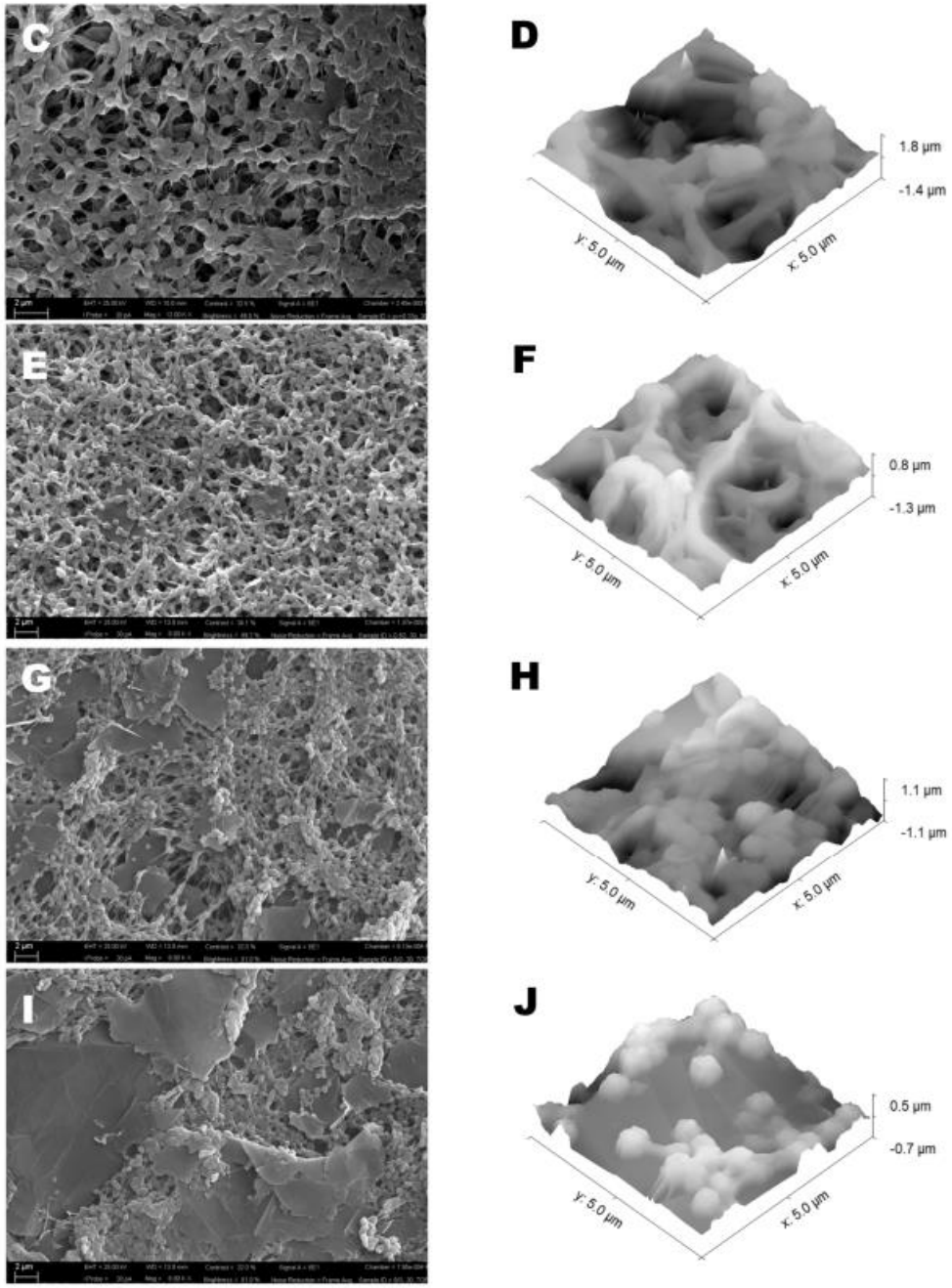

Figure 1. Top view SEM images (the scale bars in the images are 2 µm) and AFM 3D images (5 × 5 µm) of all the membranes: (**A**,**B**) pristine PVDF, (**C**,**D**) PVDF_0.33G, (**E**,**F**) PVDF_0.5G, (**G**,**H**) PVDF_5G, and (**I**,**J**) PVDF_10G.

The wetting property of membranes is a crucial characteristic for MD membranes since it reduces the performance by blocking the passages of vapor [30]. Thus, the contact angle (CA) is an efficient indicator used to measure the wettability of a membrane surface; therefore, the CA values of the resulting membranes surface toward water were measured and are illustrated in Figure 2. In principle, the initial water CA values were 110.9° ± 0.7°, 130.7° ± 0.9°, 139.5° ± 1.6°, 129.9° ± 2.2°, and 119.6° ± 2.2° for pristine PVDF, PVDF_0.33G, PVDF_0.5G, PVDF_5G, and PVDF_10G, respectively. These results indicate that well-dispersed GNP in a polymeric matrix improved the hydrophobicity of the fabricated membrane. However, the presence of GNP is not enough to impart suitable hydrophobic properties. For instance, PVDF_0.5G exhibited remarkable enhancement in hydrophobicity due to the highly enhanced surface roughness, as confirmed by AFM and SEM, whereas for PVDF_10G, only a slight increase was observed. In general, the CA values followed a similar trend as the surface roughness values described in the previous section. Importantly, the change in water CA value over time was determined. As shown in Figure 2, all of the samples showed a tendency of water droplets spreading on their surface over 30 min of observation. In the case of PVDF_0.5Gparticularly, the anti-wetting properties tended to be more stable over time, as it exhibited a decrease in the water CA value by only 8% (final water CA value equal 128.3° ± 2.3°). For other samples, a reduction in the water CA value by 15%, 13%, 15%, and 14% was noted for pristine PVDF (94.5° ± 1.1°), PVDF_0.33G (113.7° ± 1.7°), PVDF_5G (110.1° ± 1.8°), and PVDF_10G (102.6° ± 2.9°), respectively. Therefore, it is likely that the PVDF_0.5G membrane was sufficient to create a water-resistant surface.

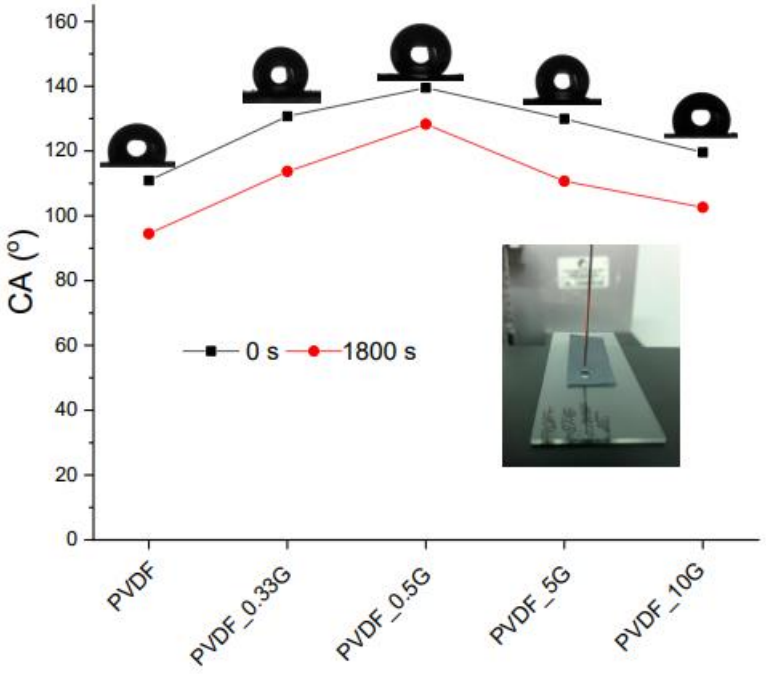

Figure 2. Water contact angle values for pristine PVDF membrane and its graphene-based composites.

Figure 3 presents the FTIR spectra of all fabricated membranes. In general, pristine PVDF and graphene nanocomposite membranes revealed the same typical absorption bands and basic structural characteristics of PVDF. The strong peaks at 839, 875, 1074, 1175, 1270, and 1400 cm^{-1} correspond to CH_2 rocking and CF_2 asymmetric stretching, C—C asymmetric stretching, C—C asymmetric stretching, CF_2 symmetric stretching, CF out-of-plane deformation, and CH_2 wagging vibration, respectively [31,32]. This means that the addition of graphene did not produce any change in the membrane characteristics in terms of the crystalline phase. Particularly, an additional weak signal was observed for composites at 1730 cm^{-1}.This represents the C=O stretching of the carbonyl and carboxylic groups present on the graphene sheets [33]. Thus, this confirms the successful incorporation of nanofiller inside the PVDF matrix.

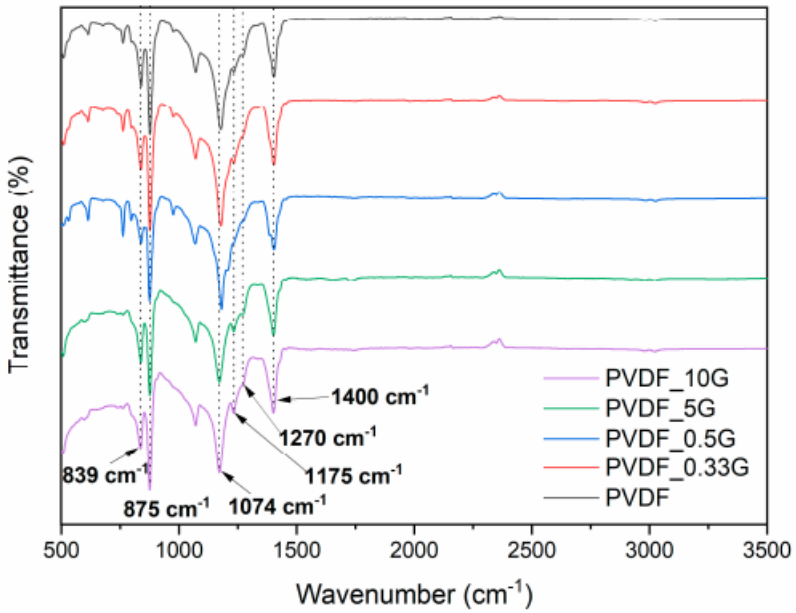

Figure 3. FTIR spectra comparison for pristine PVDF membrane and its graphene-based composites.

XRD analyses revealed the presence of the filler inside the membranes (Figure 4). The (002) and (004) peaks at 26.5° and 54.6°, respectively, represent the perpendicular direction (c-axis) to the hexagonal planes of graphite [34]. They were detected in GNP material as well as in PVDF/GNP membrane patterns, and their intensity increased with raising concentration as an effect of GNP confinement in the polymer matrix. The rest of the signals in nanocomposite membranes were from the PVDF crystalline phase. For example, medium reflections at 18.4° and 20°, and a weaker one at 35.9°, correspond to the reflections of 020, 110, and 200 of monoclinic α-phase crystal, respectively, while the peak at 39.1° refers to diffraction peak on the(211) planes of monoclinic γ-phase crystal [35].

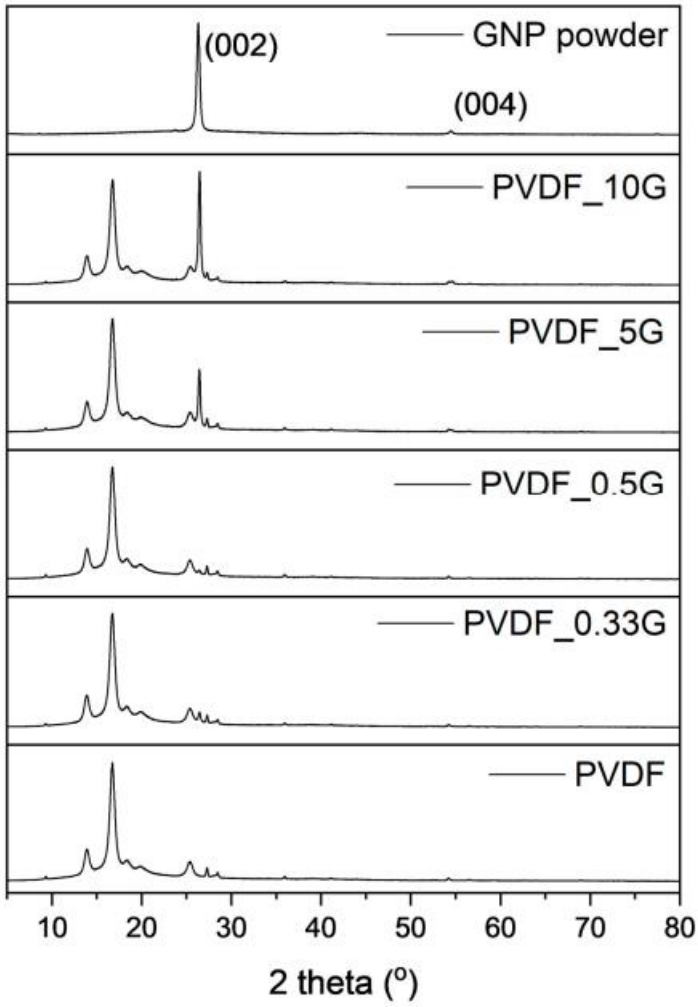

Figure 4. XRD patterns of pristine PVDF membrane and its graphene-based composites.

Figure 5 shows the inhibition percentage against *Curvularia* sp. fungal strain after 72 h. The best growth inhibition was achieved by PVDF_0.33G and PVDF_0.5G membranes, with an inhibition percentage of 74.9% and 75.7%, respectively. PVDF_5G exhibited a slightly lower inhibition percentage, reaching 61.7%. Such obtained values are in the range of studies evaluating the antibacterial properties of graphene-based materials against *E. coli*, *S. aureus* [36], and *B. subtilis* [37], with values between 60% and 99%. Pristine PVDF and PVDF_10G presented very weak antifungal activity in comparison with other samples. In general, there is a clear antimicrobial effect of the graphene when incorporated into PVDF membranes, as illustrated in Figure 6.

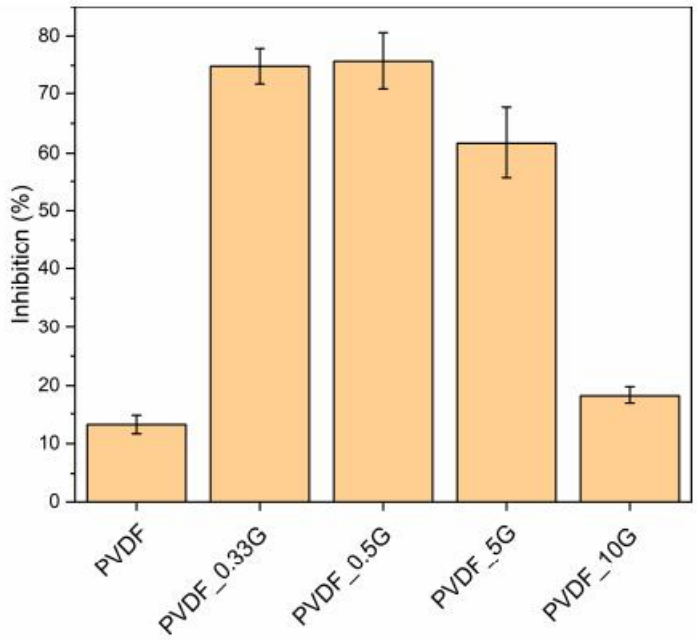

Figure 5. Antifungal inhibitions (%) of all fabricated membranes against *Curvularia* sp. fungal strain.

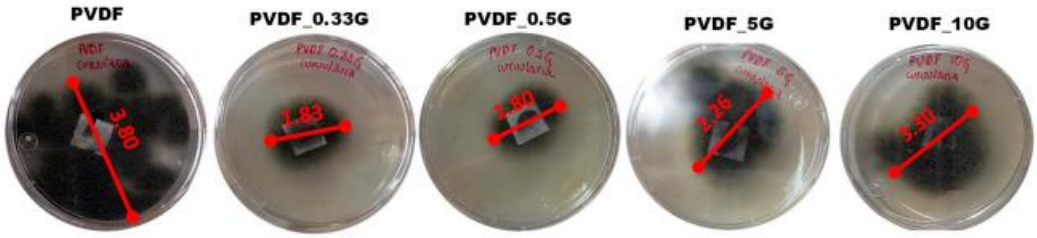

Figure 6. Photographs of antifungal inhibition of all fabricated membranes against *Curvularia* sp. fungal strain after 72 h.

Notably, the antibacterial and antifungal mechanism of graphene materials was previously reported [38]. To date, graphene materials were also combined with other inorganic nanoparticles (such as Ag, Ti, and Co) to attain 100% antimicrobial inhibition [39]. Different studies revealed that direct contact with graphene nanowalls can damage bacterial cell membranes, inhibiting the growth of the microorganism due to their extremely sharp edges [19,40]. Nevertheless, it is the oxidative stress that is the major mechanism of graphene toxicity [41]. Moreover, its antimicrobial activity was also explained with electron transfer, as graphene acts as an electron acceptor and abstracts electrons from the bacterial membrane, which may adversely affect the integrity of the membrane [42]. Notably, the presence of graphene in the membranes does not appear to be sufficient to provide total fungal growth inhibition. According to our results, the antifungal properties of membranes depend on the graphene content in the sample. This observation may be explained by the larger surface area of PVDF_0.33G and PVDF_0.5G compared with other samples, which could have promoted further interactions with the fungal cells. In general, antimicrobial properties of graphene-based materials increase with the graphene concentration [43].

Nevertheless, the antimicrobial surface properties should be considered as the synergistic results of the surface chemical composition and surface topography [44]. For example, some studies have reported the potential use of superhydrophobic surfaces in preventing biofilm formation [45,46]. Other studies revealed that an increase in surface roughness did not influence or even inhibit the adhesion of bacteria [47,48]. Perera-Costa et al. [49] created various surface patterns on polydimethylsiloxane (PDMS). The results indicated that all patterned surfaces were distinguished by a significant reduction in bacterial adhesion in contrast to the flat surfaces. In our studies, the addition of GNP to the polymeric matrix significantly influenced the topographic features of the membrane surface, as described in detail in the previous paragraphs. Thus, the weaker antifungal activity of PVDF_5G and PVDF_10G may be a direct result of their inferior water-repellent properties and less-rough surface compared with PVDF_0.33G and PVDF_0.5G samples. However, further studies are needed for a deeper analysis of cell–surface interactions in the case of graphene-based membranes and evaluation of the importance of different surface topography. Nevertheless, it can be stated that the inhibition of fungal growth showed by PVDF_0.33G and PVDF_0.5G is a promising result for the development of an antibiofouling membrane. Surface properties, such as hydrophobicity and topography, prevent biofilm formation through the inhibition of microorganism adhesion, whereas graphene addition provides the toxicity effect of oxidative stress against them.

4. Conclusions

In this work, PVDF/graphene composite membranes were successfully fabricated by a phase inversion method. GNPs were well-dispersed in the PVDF membrane matrix when low nanofiller loading was used (0.33 and 0.5 wt%), which was confirmed by SEM images. Among all the PVDF/GNP fabricated membranes, thePVDF_0.5G membrane (i.e., 0.5 wt% graphene loading) exhibited the most suitable properties in terms of pore size (~0.56 µm), porosity (~69%,) and hydrophobicity (~139.5°) for application to water desalination in the MD process. When GNP concentration was increased to over 0.5 wt%, the prepared membranes tended to have smaller pore size, lower overall porosity, and lower water CA values than that of the PVDF_0.5G membrane, which could be due to the nanofiller agglomeration. Notably, the highest antifungal inhibition against *Curvularia* sp. fungal strain was observed in the PVDF_0.5G membrane. The results found in this work indicate that well-dispersed graphene nanoplatelets in aPVDF membrane matrix can be potentially useful in real seawater desalination and disinfection using MD approaches.

Author Contributions: E.G.-C., membrane preparation and characterization, and writing—original draft; M.K.R., funding acquisition and editing; R.C.-M., writing—review and editing; M.M.-J., antifungal activity investigations; B.B.-H., supervision of antifungal activity investigations; M.L., supervision, review, and editing. All authors have read and agreed to the published version of the manuscript.

Funding: This research received no external funding.

Institutional Review Board Statement: Not applicable.

Informed Consent Statement: Not applicable.

Data Availability Statement: The data presented in this study is available on request from the corresponding author.

Acknowledgments: R. Castro-Muñoz acknowledges the School of Science and Engineering and the FEMSA-Biotechnology Center at Tecnológico de Monterrey for their support through the Bioprocess (0020209I13) Focus Group. Financial support from the Polish National Agency for Academic Exchange (NAWA) under Ulam Programme (agreement no. PPN/ULM/2020/1/00005/U/00001) is also gratefully acknowledged. M.K. Rybarczyk would like to acknowledge the COST Action CA15107 Multicomp, supported by the COST Association (European Cooperation in Science and Technology).

Conflicts of Interest: The authors declare no conflict of interest.

References

1. Greenlee, L.F.; Lawler, D.F.; Freeman, B.D.; Marrot, B.; Moulin, P. Reverse Osmosis Desalination: Water Sources, Technology, and Today's Challenges. *Water Res.* **2009**, *43*, 2317–2348. [CrossRef]
2. Castro-Muñoz, R. Breakthroughs on Tailoring Pervaporation Membranes for Water Desalination: A Review. *Water Res.* **2020**, *187*, 116428. [CrossRef] [PubMed]
3. Figoli, A.; Simone, S.; Criscuoli, A.; Al-Jlil, S.A.; Al Shabouna, F.S.; Al-Romaih, H.S.; Di Nicolò, E.; Al-Harbi, O.A.; Drioli, E. Hollow Fibers for Seawater Desalination from Blends of PVDF with Different Molecular Weights: Morphology, Properties and VMD Performance. *Polymer* **2014**, *55*, 1296–1306. [CrossRef]
4. Pichardo-Romero, D.; Garcia-Arce, Z.P.; Zavala-Ramírez, A.; Castro-Muñoz, R. Current Advances in Biofouling Mitigation in Membranes for Water Treatment: An Overview. *Processes* **2020**, *8*, 182. [CrossRef]
5. Rybarczyk, M.K.; Gontarek-Castro, E.; Ollik, K.; Lieder, M. Biomass-Derived Nitrogen Functionalized Carbon Nanodots and Their Anti-Biofouling Properties. *Processes* **2021**, *9*, 61. [CrossRef]
6. Hwang, B.K.; Lee, W.N.; Park, P.K.; Lee, C.H.; Chang, I.S. Effect of Membrane Fouling Reducer on Cake Structure and Membrane Permeability in Membrane Bioreactor. *J. Memb. Sci.* **2007**, *288*, 149–156. [CrossRef]
7. Charfi, A.; Ben Amar, N.; Harmand, J. Analysis of Fouling Mechanisms in Anaerobic Membrane Bioreactors. *Water Res.* **2012**, *46*, 2637–2650. [CrossRef] [PubMed]
8. Hliavitskaya, T.; Plisko, T.; Pratsenko, S.; Bildyukevich, A.; Lipnizki, F.; Rodrigues, G.; Sjölin, M. Development of Antifouling Ultrafiltration PES Membranes for Concentration of Hemicellulose. *J. Appl. Polym. Sci.* **2021**, *138*, 1–14. [CrossRef]
9. Ayyavoo, J.; Nguyen, T.P.N.; Jun, B.M.; Kim, I.C.; Kwon, Y.N. Protection of Polymeric Membranes with Antifouling Surfacing via Surface Modifications. *Colloids Surfaces A Physicochem. Eng. Asp.* **2016**, *506*, 190–201. [CrossRef]
10. Li, Q.; Imbrogno, J.; Belfort, G.; Wang, X.-L. Making Polymeric Membranes Antifouling via "Grafting from" Polymerization of Zwitterions. *J. Appl. Polym. Sci.* **2015**, *132*, 41781. [CrossRef]
11. Gontarek-Castro, E.; Castro-Muñoz, R.; Lieder, M. New Insights of Nanomaterials Usage toward Superhydrophobic Membranes for Water Desalination via Membrane Distillation: A Review. *Crit. Rev. Environ. Sci. Technol.* **2021**, 1–46. [CrossRef]
12. Papageorgiou, D.G.; Kinloch, I.A.; Young, R.J. Mechanical Properties of Graphene and Graphene-Based Nanocomposites. *Prog. Mater. Sci.* **2017**, *90*, 75–127. [CrossRef]
13. Castro-Muñoz, R.; Buera-González, J.; de la Iglesia, Ó.; Galiano, F.; Fíla, V.; Malankowska, M.; Rubio, C.; Figoli, A.; Téllez, C.; Coronas, J. Towards the Dehydration of Ethanol Using Pervaporation Cross-Linked Poly(Vinyl Alcohol)/Graphene Oxide Membranes. *J. Memb. Sci.* **2019**, *582*, 423–434. [CrossRef]
14. Sun, P.; Wang, K.; Zhu, H. Recent Developments in Graphene-Based Membranes: Structure, Mass-Transport Mechanism and Potential Applications. *Adv. Mater.* **2016**, *28*, 2287–2310. [CrossRef] [PubMed]
15. Gontarek, E.; Macedonio, F.; Militano, F.; Giorno, L.; Lieder, M.; Politano, A.; Drioli, E.; Gugliuzza, A. Adsorption-Assisted Transport of Water Vapour in Super-Hydrophobic Membranes Filled with Multilayer Graphene Platelets. *Nanoscale* **2019**, *11*, 11521–11529. [CrossRef] [PubMed]
16. De Carvalho, A.P.A.; Conte Junior, C.A. Green Strategies for Active Food Packagings: A Systematic Review on Active Properties of Graphene-Based Nanomaterials and Biodegradable Polymers. *Trends Food Sci. Technol.* **2020**, *103*, 130–143. [CrossRef]
17. Zou, X.; Zhang, L.; Wang, Z.; Luo, Y. Mechanisms of the Antimicrobial Activities of Graphene Materials. *J. Am. Chem. Soc.* **2016**, *138*, 2064–2077. [CrossRef]
18. Liu, S.; Zeng, T.H.; Hofmann, M.; Burcombe, E.; Wei, J.; Jiang, R.; Kong, J.; Chen, Y. Antibacterial Activity of Graphite, Graphite Oxide, Graphene Oxide, and Reduced Graphene Oxide: Membrane and Oxidative Stress. *ACS Nano* **2011**, *5*, 6971–6980. [CrossRef]
19. Sawangphruk, M.; Srimuk, P.; Chiochan, P.; Sangsri, T.; Siwayaprahm, P. Synthesis and Antifungal Activity of Reduced Graphene Oxide Nanosheets. *Carbon* **2012**, *50*, 5156–5161. [CrossRef]
20. Aguas, Y.; Hincapie, M.; Fernández-Ibáñez, P.; Polo-López, M.I. Solar photocatalytic disinfection of agricultural pathogenic fungi (Curvularia sp.) in real urban wastewater. *Sci. Total Environ* **2017**, *607–608*, 1213–1224. [CrossRef]
21. Sun, H.Y.; Wang, H.C.; Chen, Y.; Li, H.X.; Chen, C.J.; Zhou, M.G. Multiple Resistance of Botrytis Cinerea from Vegetable Crops to Carbendazim, Diethofencarb, Procymidone, and Pyrimethanil in China. *Plant Dis.* **2010**, *94*, 551–556. [CrossRef]
22. Mirón-Mérida, V.A.; Yáñez-Fernández, J.; Montañez-Barragán, B.; Barragán Huerta, B.E. Valorization of Coffee Parchment Waste (Coffea Arabica) as a Source of Caffeine and Phenolic Compounds in Antifungal Gellan Gum Films. *LWT* **2019**, *101*, 167–174. [CrossRef]
23. Athanasekou, C.; Sapalidis, A.; Katris, I.; Savopoulou, E.; Beltsios, K.; Tsoufis, T.; Kaltzoglou, A.; Falaras, P.; Bounos, G.; Antoniou, M.; et al. Mixed Matrix PVDF/Graphene and Composite-Skin PVDF/Graphene Oxide Membranes Applied in Membrane Distillation. *Polym. Eng. Sci.* **2019**, *59*, E262–E278. [CrossRef]
24. Woo, Y.C.; Kim, Y.; Shim, W.G.; Tijing, L.D.; Yao, M.; Nghiem, L.D.; Choi, J.S.; Kim, S.H.; Shon, H.K. Graphene/PVDF Flat-Sheet Membrane for the Treatment of RO Brine from Coal Seam Gas Produced Water by Air Gap Membrane Distillation. *J. Memb. Sci.* **2016**, *513*, 74–84. [CrossRef]
25. Li, X.; Shan, H.; Cao, M.; Li, B. Facile Fabrication of Omniphobic PVDF Composite Membrane via a Waterborne Coating for Anti-Wetting and Anti-Fouling Membrane Distillation. *J. Memb. Sci.* **2019**, *589*, 117262. [CrossRef]
26. An, A.K.; Lee, E.J.; Guo, J.; Jeong, S.; Lee, J.G.; Ghaffour, N. Enhanced Vapor Transport in Membrane Distillation via Functionalized Carbon Nanotubes Anchored into Electrospun Nanofibres. *Sci. Rep.* **2017**, *7*, 1–11.

27. Boo, C.; Lee, J.; Elimelech, M. Engineering Surface Energy and Nanostructure of Microporous Films for Expanded Membrane Distillation Applications. *Environ. Sci. Technol.* **2016**, *50*, 8112–8119. [CrossRef] [PubMed]
28. Deka, B.J.; Guo, J.; Khanzada, N.K.; An, A.K. Omniphobic Re-Entrant PVDF Membrane with ZnO Nanoparticles Composite for Desalination of Low Surface Tension Oily Seawater. *Water Res.* **2019**, *165*, 114982. [CrossRef] [PubMed]
29. Razmjou, A.; Arifin, E.; Dong, G.; Mansouri, J.; Chen, V. Superhydrophobic Modification of TiO2 Nanocomposite PVDF Membranes for Applications in Membrane Distillation. *J. Memb. Sci.* **2012**, *415–416*, 850–863. [CrossRef]
30. Ray, S.S.; Lee, H.K.; Kwon, Y.N. Review on Blueprint of Designing Anti-Wetting Polymeric Membrane Surfaces for Enhanced Membrane Distillation Performance. *Polymers* **2020**, *12*, 23. [CrossRef]
31. Nallasamy, P.; Mohan, S. Vibrational Spectroscopic Characterization of Form II Poly(Vinylidene Fluoride). *Indian J. Pure Appl. Phys.* **2005**, *43*, 821–827.
32. Woo, Y.C.; Lee, J.J.; Tijing, L.D.; Shon, H.K.; Yao, M.; Kim, H.S. Characteristics of Membrane Fouling by Consecutive Chemical Cleaning in Pressurized Ultrafiltration as Pre-Treatment of Seawater Desalination. *Desalination* **2015**, *369*, 51–61. [CrossRef]
33. Lai, Y.; Wan, L.; Wang, B. PVDF/Graphene Composite Nanoporous Membranes for Vanadium Flow Batteries. *Membranes* **2019**, *9*, 89. [CrossRef] [PubMed]
34. Sun, G.; Li, X.; Qu, Y.; Wang, X.; Yan, H.; Zhang, Y. Preparation and Characterization of Graphite Nanosheets from Detonation Technique. *Mater. Lett.* **2008**, *62*, 703–706. [CrossRef]
35. Cai, X.; Lei, T.; Sun, D.; Lin, L. A Critical Analysis of the α, β and γ Phases in Poly(Vinylidene Fluoride) Using FTIR. *RSC Adv.* **2017**, *7*, 15382–15389. [CrossRef]
36. Yang, Z.; Hao, X.; Chen, S.; Ma, Z.; Wang, W.; Wang, C.; Yue, L.; Sun, H.; Shao, Q.; Murugadoss, V.; et al. Long-Term Antibacterial Stable Reduced Graphene Oxide Nanocomposites Loaded with Cuprous Oxide Nanoparticles. *J. Colloid Interface Sci.* **2019**, *533*, 13–23. [CrossRef]
37. Duan, L.; Wang, Y.; Zhang, Y.; Liu, J. Graphene Immobilized Enzyme/Polyethersulfone Mixed Matrix Membrane: Enhanced Antibacterial, Permeable and Mechanical Properties. *Appl. Surf. Sci.* **2015**, *355*, 436–445. [CrossRef]
38. Castro-Muñoz, R. The Role of New Inorganic Materials in Composite Membranes for Water Disinfection. *Membranes* **2020**, *10*, 101. [CrossRef]
39. Kumar, P.; Huo, P.; Zhang, R.; Liu, B. Antibacterial Properties of Graphene-Based Nanomaterials. *Nanomaterials* **2019**, *9*, 737. [CrossRef] [PubMed]
40. Akhavan, O.; Ghaderi, E. Toxicity of Graphene and Graphene Oxide Nanowalls against Bacteria. *ACS Nano* **2010**, *4*, 5731–5736. [CrossRef]
41. Smith, S.C.; Rodrigues, D.F. Carbon-Based Nanomaterials for Removal of Chemical and Biological Contaminants from Water: A Review of Mechanisms and Applications. *Carbon* **2015**, *91*, 122–143. [CrossRef]
42. Chen, J.; Deng, F.; Hu, Y.; Sun, J.; Yang, Y. Antibacterial Activity of Graphene-Modified Anode on Shewanella Oneidensis MR-1 Biofilm in Microbial Fuel Cell. *J. Power Sources* **2015**, *290*, 80–86. [CrossRef]
43. Zhu, J.; Wang, J.; Hou, J.; Zhang, Y.; Liu, J.; Van der Bruggen, B. Graphene-Based Antimicrobial Polymeric Membranes: A Review. *J. Mater. Chem. A.* **2017**, *5*, 6776–6793. [CrossRef]
44. Wu, S.; Zhang, B.; Liu, Y.; Suo, X.; Li, H. Influence of Surface Topography on Bacterial Adhesion: A Review (Review). *Biointerphases* **2018**, *13*, 060801. [CrossRef]
45. Lin, C.; Tang, P.; Zhang, W.; Wang, Y.; Zhang, B.; Wang, H.; Zhang, L. Effect of Superhydrophobic Surface of Titanium on Staphylococcus Aureus Adhesion. *J. Nanomater.* **2011**, *2011*, 1–8.
46. Crick, C.R.; Ismail, S.; Pratten, J.; Parkin, I.P. An Investigation into Bacterial Attachment to an Elastomeric Superhydrophobic Surface Prepared via Aerosol Assisted Deposition. *Thin Solid Films* **2011**, *519*, 3722–3727. [CrossRef]
47. Rizzello, L.; Sorce, B.; Sabella, S.; Vecchio, G.; Galeone, A.; Brunetti, V.; Cingolani, R.; Pompa, P.P. Impact of Nanoscale Topography on Genomics and Proteomics of Adherent Bacteria. *ACS Nano* **2011**, *5*, 1865–1876. [CrossRef]
48. Lüdecke, C.; Roth, M.; Yu, W.; Horn, U.; Bossert, J.; Jandt, K.D. Nanorough Titanium Surfaces Reduce Adhesion of Escherichia Coli and Staphylococcus Aureus via Nano Adhesion Points. *Colloids Surf. B* **2016**, *145*, 617–625. [CrossRef]
49. Perera-Costa, D.; Bruque, J.M.; González-Martín, M.L.; Gómez-García, A.C.; Vadillo-Rodríguez, V. Studying the Influence of Surface Topography on Bacterial Adhesion Using Spatially Organized Microtopographic Surface Patterns. *Langmuir* **2014**, *30*, 4633–4641. [CrossRef] [PubMed]

membranes

MDPI

Article

Graphene-Coated PVDF Membranes: Effects of Multi-Scale Rough Structure on Membrane Distillation Performance

Emilia Gontarek-Castro [1,*], Giuseppe Di Luca [2], Marek Lieder [1] and Annarosa Gugliuzza [2,*]

[1] Department of Process Engineering and Chemical Technology, Faculty of Chemistry, Gdansk University of Technology, 11/12 G. Narutowicza St., 80-233 Gdansk, Poland; lieder@pg.edu.pl
[2] Research Institute on Membrane Technology, CNR-ITM, Via Pietro Bucci 17/C, 87036 Rende, Italy; g.diluca@itm.cnr.it
* Correspondence: emilia.gontarek@pg.edu.pl (E.G.-C.); a.gugliuzza@itm.cnr.it (A.G.)

Abstract: Graphene-coated membranes for membrane distillation have been fabricated by using a wet-filtration approach. Graphene nanoplatelets have been deposited onto PVDF membrane surfaces. Morphology and physicochemical properties have been explored to evaluate the changes in the surface topography and related effects on the membrane performance in water desalination. The membranes have been tested in membrane distillation plants by using mixtures of sodium chloride and humic acid. The multi-scale rough structure of the surface has been envisaged to amplify the wetting and fouling resistance of the graphene-coated membranes so that a better flux and full salt rejection have been achieved in comparison with pristine PVDF. Total salt rejection and an increase of 77% in flux have been observed for coated membrane with optimized graphene content when worked with NaCl 0.6 M (DCMD, $\Delta T \approx 24$ °C) over a test period of 6 h. The experimental findings suggest these novel graphene-coated membranes as promising materials to develop functional membranes for high-performing water desalination.

Keywords: membrane distillation; graphene; multi-scale roughness; antiwetting and antifouling properties

check for updates

Citation: Gontarek-Castro, E.; Di Luca, G.; Lieder, M.; Gugliuzza, A. Graphene-Coated PVDF Membranes: Effects of Multi-Scale Rough Structure on Membrane Distillation Performance. *Membranes* **2022**, *12*, 511. https://doi.org/10.3390/membranes12050511

Academic Editor: Pei Sean Goh

Received: 24 April 2022
Accepted: 7 May 2022
Published: 10 May 2022

Publisher's Note: MDPI stays neutral with regard to jurisdictional claims in published maps and institutional affiliations.

1. Introduction

In the last century, population and industrial growth have increased producing worldwide demand for water. This request will become even more amplified due to the further demographic and economic expansion along with the persistent exploitation of water basins. The World Water Council estimates that a few billion people living on Earth will suffer from water scarcity or poor water quality by 2030 [1]. Therefore, there is an urgency to identify suitable and eco-sustainable strategies for the management of natural water resources and the production of freshwater. Membrane technology takes advantages over many other technologies due to its easier maintenance, compact modular construction, higher separation factor, no use of chemical additives, and regeneration of spent media [2]. Nowadays, a lot of research is focused on reliable approaches to improve separation performances through the fabrication of novel membranes and/or modification of the existing ones [3–5].

Membrane distillation (MD) is a promising and eco-sustainable alternative for seawater desalination [6]. It requires the use of hydrophobic micro-porous membranes that separate feed and permeate streams preventing their mixing. MD is driven by the vapor pressure difference across the membrane, which can be induced by a gradient of temperature or concentration. Numerous hydrophobic membranes have been developed and tested in laboratory on a model brine solution, proving the efficiency of MD in water desalination [7–9]. Among them, polypropylene (PP) [10], polytetrafluoroethylene (PTFE) [11] and poly (vinylidene fluoride) (PVDF) [12] are the most popular ones. Nevertheless, membrane fouling and wetting still remain open issues, especially for real seawater processing [13]. For instance, desalination of hypersaline solutions usually leads to scaling at the membrane

surface [14], while the treatment of solutions containing organic compounds, including acids and protein-type macromolecules, causes frequently fouling with the subsequent decline of the flux [15]. Due to the interactions between components dissolved in the streams and membrane functional groups, additional layers formation on the membrane surface and pore plugging take place causing increased resistance to the transport [16–19]. Properly selected membrane materials may reduce the susceptibility to wetting and fouling phenomena [20,21]. Chemical and morphological features can be well addressed in controlling the final performance of membrane separations including membrane distillation [22,23].

It was observed that the creation of a superhydrophobic membrane could effectively deal with wetting and fouling phenomena [7]. There are two main criteria for enhancing membrane hydrophobicity. Membrane surface energy can be reduced and surface roughness can be manipulated [24]. The first criterion is usually achieved using fluoropolymers or low surface energy modifiers. In the context of surface roughness, it has been observed that the creation of micro- and nanostructured surfaces, also called hierarchical structures, can bring excellent antiwetting properties [25,26]. According to the Cassie–Baxter model [26], rough and complex topography prevent the surface from being penetrated and wetted by the liquid as the air trapped in the grooves between solid substrate protrusions forms an air/solid hydrophobic surface. Due to the increased number of sharp and narrow protrusions for multi-scale rough structures, there is an unusually strong water-repellency on the surfaces, as the contact area between liquid and solid is reduced. A favorable manner to achieve the hierarchical structure is by nanoparticle incorporation. Usually, nanoparticles are incorporated onto a membrane surface by dip-coating method or deposition. For instance, silver nanoparticles have been deposited on PVDF membrane and fabricated membranes showed an increase in the CA and roughness value from 126° up to 136° and from 99.1 to 157.6 nm, respectively [27]. In other studies, polystyrene (PS) microspheres with silica nanoparticles have been coated onto commercial membranes. As fabricated hierarchical membrane exhibited a significant increase in surface roughness value of 343 nm, while the pristine membrane had a roughness of 99 nm [28].

Based on this concept, in this study, a nanostructured coating of graphene nanoplatelets (GNPs) has been fabricated onto the surface of the flat sheet PVDF membrane by using a wet-filtration method. The complex surface topography generated after graphene deposition has been demonstrated to impart much-improved antiwetting and antifouling properties with respect to pristine surfaces. The effectiveness of graphene-coated PVDF membranes has been evaluated during desalination via the direct contact membrane distillation (DCMD) process by working mixtures of NaCl and humic acid (HA) with a degree of salinity of 35 gL^{-1}—typical content of salts in seawater. Effects on the flux and rejection as well as recovery of initial permeation properties have been investigated. Based on the results achieved, this kind of graphene-coated membrane exhibits structure-transport properties relationships suitable to enhance their efficiency during the MD process with respect to the non-modified PVDF membranes. The capability of these composite membranes to recover water flux after simple washing cycles with distilled water has been also investigated, resulting in an eco-sustainable cleaning procedure. Thus, the performance of these graphene-coated membranes is promising for the realization of new functional membrane materials to be worked in high-performing MD operations.

2. Materials and Methods

2.1. Materials

PVDF (Solef®6020, Solvay Solexis: water adsorption < 0.040% @23 °C after 24 h; d = 1.78 Kg/m^3) was donated by Solvay Solexis (Milan, Italy). Hydrophobic graphene nanoplatelets (GPNs) powder with a lateral size > 25 μm, (Sigma-Aldrich, Milan, Italy, Carbon > 95 wt.%; Oxygen < 2 wt.%) was used for membrane coating. N-methyl-2-pirrolidinone (NMP, Riedel de Haën, Milan, Italy) and 2-propanol (IPA, WWR PROLABO, Milan, Italy) were used for membrane preparation. POREWICK was used for pore size

investigation. Sodium chloride (NaCl, WVR PROLABO, Milan, Italy) and Humic acid (HA, Sigma-Aldrich, Milan, Italy) were used for preparing stream solutions.

2.2. Preparation of PVDF Membranes

Polymeric solutions were prepared by dissolving 12 wt.% of PVDF powder in NMP under mechanical stirring for 24 h at 30 °C. Then, the solutions were left for 4 h without stirring in order to remove air bubbles. The solutions were cast on a glass support by using a micrometric film applicator (Elcometer) with a gap size of 250 µm. The casting solutions were then coagulated in 2-propanol and washed with deionized water.

2.3. WET-Filtration Method

Graphene dispersion was prepared by adding graphene to water/2-propanol mixture (volume ratio 7/3) at concentrations of 0.05 $mgmL^{-1}$ and 0.005 $mgmL^{-1}$. Each solution underwent approximately 20 stirring/sonication cycles (20/20 min) to well-disperse the nanomaterials in the solvents. A dead-end filtration cell was used to deposit graphene on the skin layer of PVDF membranes with a diameter of 7 cm. For each dispersion, a volume of 20 mL was poured into the cell and left for 10 min in contact with a membrane surface. Then, a pressure of 1 bar was applied for 10 min in order to remove the mixture of solvents. Each membrane was dried in the air for 24 h. The flat sheet phase inversed PVDF membrane was denoted as pristine PVDF and used for comparison. The coated membranes underwent the leaching test in order to evaluate the stability of attachment of GNPs to the membrane surfaces. A vigorous stirring in distilled water for a period of 24 h was applied for pieces of both coated membranes. Then, the water was filtrated through PTFE filters with 0.2 µm pore size and the filters were subjected to XRD analysis. No graphene traces were found on the filter. A schematic diagram for the fabrication of the graphene-coated membrane is shown in Figure 1.

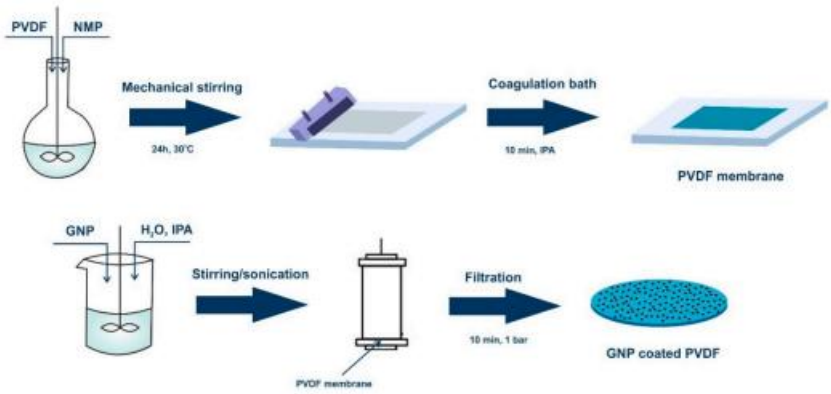

Figure 1. Schematic diagram for the fabrication of the graphene-coated membrane.

2.4. Membrane Characterization

The morphology of the membranes was analyzed based on the images taken by scanning electron microscope (SEM; Quanta 200, FEI Company, Oberkochen, Germany) and atomic force microscope (AFM, MultiMode 8, NanoScope V, Veeco-Bruker, Plainview, NY, USA). The overall porosity values corresponded to the total void inside the membranes. The pore size was estimated using capillary flow porometer (CFP 1500 AXEL, Porous Materials Inc., Ithaca, NY, USA) [5]. The wetting resistance with pure water and 0.6 M NaCl solution was examined by measuring the contact angle value (Cam 200 KSV instruments, LTD, Helsinki, Finland). Infrared spectra were collected on the top surface of membranes by using a Nicolet iS10 FTIR spectrometer (Thermo Scientific Instrument Co., Boston, MA,

USA). X-ray diffractometer ((XRD, Rigaku MiniFlex 600, The Woodlands, TX, USA)) was used to identify the crystalline structure in the range from 5° to 80°.

2.5. Membrane Distillation Tests

Thermally-driven MD experiments were performed by using a flat circular module with area of 2.27 cm^2. The DCMD configuration was chosen and 0.6 M NaCl solutions and related mixtures with HA (0.5 and 1.0 $mgmL^{-1}$) were tested. A flow rate of 2.68 Lh^{-1} at the feed side and 2.23 Lh^{-1} at the permeate side were used. The temperature of feed was kept around 40 °C and a difference of temperature (ΔT) of ~24 °C was applied across the membrane. Each experiment was run for 6 h continuously; retentate and distillate fractions were led in a counter-current flow, toward the membrane cell. The skin side of the membrane was facing the hyper-saline solutions, whereas the reverse side of the membrane was contacting the distillate stream. Two pumps were used to transport the heated feed and cooled permeate to and from the membrane module. The trans-membrane fluxes were estimated by taking into account the weight variations in the distillate with time and the effective surface area of membranes. The salt rejection (R) was determined by measuring the salt concentration on the feed side and permeate side by using a conductivity meter (HI 2300 bench meter supplied by Hanna Instruments, Woonsocket, RI, USA). After MD experiments, the membranes were washed with water at 50 °C for three consecutive cycles, each one of 30 min. Water permeation testing was repeated after working each saline stream.

3. Results and Discussion

3.1. Chemical and Morphological Features of Membranes

Graphene-coated membranes have been fabricated through a combined phase inversion and wet-filtration approach. Microporous PVDF substrate has been realized according to the immersion precipitation phase inversion and successively has been immobilized by filtration of graphene nanoplates dispersing solutions.

PVDF is a semi-crystalline material and related membranes exhibit a particulate-like morphology while graphene nanoplatelets are dispersed randomly through the membrane surface. XRD crystallographic analyses reveal that PVDF crystalline phase is dominated by both the α and γ phase, as indicated by medium reflections at 18.4 and 20° and weaker at 35.9 corresponding to the reflections of 020, 110, and 200 of monoclinic α-phase crystal as well as weak 39.1 peak corresponding to diffraction peak on planes (211) of monoclinic γ-phase crystal [29] (Figure 2a). The coexistence of two crystalline forms is further confirmed by infrared analysis (Figure 3), showing small peaks at 976 cm^{-1} typical of α-PVDF form, while the band at 833 cm^{-1} is exclusively assigned to the γ-PVDF phase [30]. Further, the crystalline phase of PVDF membranes is dominated by the α phase. XRD spectra collected on 0.05G/PVDF and 0.005G/PVDF membranes show additional peaks at 26.5 (002) and 54.6° (004), which are usually the strongest two in the XRD pattern of natural graphite (Figure 2b). They represent a perpendicular direction (c-axis) to the graphite hexagonal planes, which indicates the presence of graphene on the membranes [31]. FTIR spectra of graphene-coated membranes show additional broad adsorptions in the regions 1500–2000 cm^{-1} and 2500–3720 cm^{-1}, especially in the case of the membranes with the largest amount of graphene (0.05G/PVDF). The wide signal centered around 3750 cm^{-1} is associated with hydroxyl groups, whereas the broad region, 1500–2000 cm^{-1} arises from the overlapping of different bands usually falling in the region of 1635–1570 cm^{-1} and assigned to –C=C conjugated stretching and around 1720 cm^{-1} corresponding to C=O stretching vibrations [32]. This yields indication about oxidation and defects of graphene flakes deposited onto the surface.

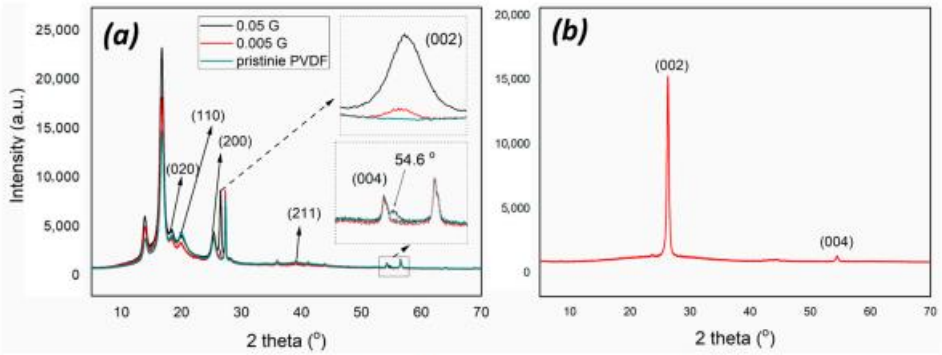

Figure 2. XRD patterns of PVDF and graphene-coated PVDF membranes (**a**), XRD of graphene nanoplatelets (**b**).

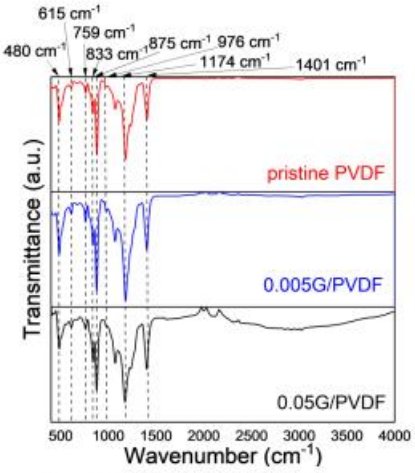

Figure 3. ATR spectra of PVDF and graphene-coated PVDF membranes.

The crystallization of PVDF polymer chains yields particulate-like morphology during the demixing process leading to the formation of symmetric structures wherein polymer particles are intercalated by voids uniformly distributed through the network (Figure 4a). These free gaps represent the pores of the membranes and determine the overall porosity of the structures, as summarized in Table 1.

PVDF and 0.005G/PVDF membranes show comparable mean and the largest pore size, whereas a reduction is tuned for 0.05G/PVDF. The overall porosity, as well as the thickness, are instead comparable for all membranes. This suggests that the bulk of each membrane is preserved, while graphene platelets are confined to the membrane surface exclusively. SEM micrographs collected across the membrane sections show the formation of a tiny layer onto the top surface of the membranes, especially at higher concentrations of graphene, and confirm that there is no inclusion of flakes inside the membrane structure (Figure 4). The deposition of a larger amount of graphene flakes gives rise to a major obstruction of the free gaps (pores) distributed through the surface, resulting in the formation of a cracked graphene layer mainly (Figure 4b). In the case of lower concentrated graphene dispersion, a random distribution of graphene nanoplatelets is instead observed so that the pores are not clogged, and a large number of free gaps are preserved (Figure 4c).

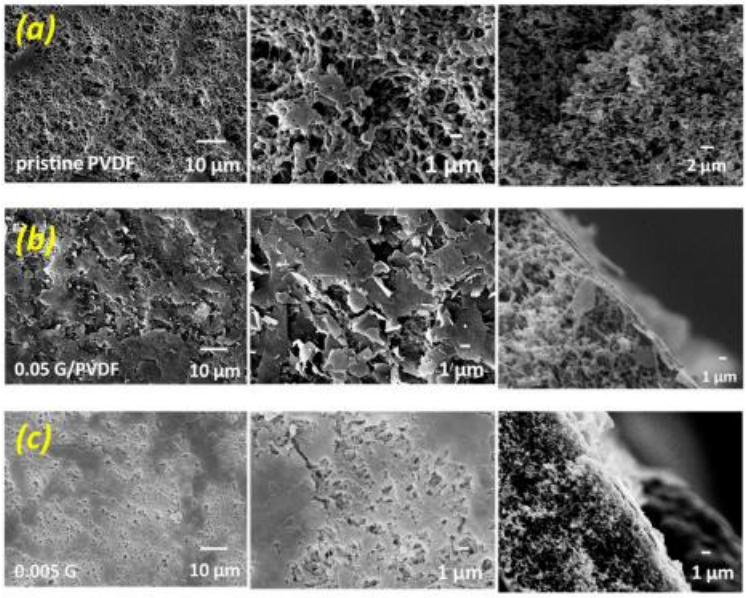

Figure 4. SEM micrographs collected onto membrane surface (first and second column) and across the section (third column) of pristine PVDF (**a**), 0.05G/PVDF (**b**) and 0.005G/PVDF (**c**) membranes.

Table 1. Structural properties estimated for all membranes.

Sample	Thickness (µm)	Porosity (%)	Largest Pore Size (µm)	Mean Pore Size (µm)
PVDF	50 ± 1	65 ± 4	0.7 ± 0.1	0.48 ± 0.09
0.05G/PVDF	50 ± 1	62 ± 2	0.43 ± 0.09	0.24 ± 0.01
0.005G/PVDF	50 ± 4	63 ± 2	0.80 ± 0.06	0.49 ± 0.01

3.2. Wetting Properties of Membranes

Chemical and morphological changes in the surface bring inevitably variations in the wetting behavior (Figure 5). A water contact angle value of 124 ± 4° is detected on an unmodified PVDF membrane surface, whereas the deposition of low content of graphene gives rise to the enhanced waterproofness reaching values up to 136 ± 4°. On the contrary, the deposition of a higher concentrated graphene layer causes a significant reduction of hydrophobicity of the surface with contact angle values down to 97 ± 2°. In general, the degree of hydrophobicity of graphene cannot be unequivocally defined, since it is strongly dependent on numerous features such as graphene type, number of layers, defects in the structure, supporting substrate, and impurities, including polymer residues [33,34]. For instance, the study of Wang et al. [35] shows that the water contact angle on a stack of a few graphene layers reached values of 98° while it increases significantly to 127° on a graphene monolayer. On the other hand, Taherian et al. [36], proved that the value of 127° is an unrealistic estimate. They stated that the expected value would be in the range between 95° and 100°. Therefore, the CA estimated for 0.05G/PVDF represents the typical value for the graphene layer. Further, the function of intermolecular interactions established at the graphene and droplet interface and the role of the morphological component of the surface cannot be neglected. In the case of 0.005G/PVDF membranes, the deposition of graphene leads to a non-uniform graphene distribution on the membrane surface with stacked layers that reach thicknesses of 19 ± 5 nm, whilst the surface of 0.05G/PVDF membrane appears to

be covered almost entirely with an extent of assembled layers up to 190 ± 24 nm (Figure 2). Consequently, for 0.005G/PVDF membranes effects of both liquid–graphene and liquid–substrate interactions as well as chemical affinity, surface heterogeneities, and surface roughness play a key role in the waterproofness enhancement [37]. The time-dependent images of water droplets within the first 30 min of contact with membrane surfaces confirm improved wetting resistance properties. In this study, it is interesting to observe how water droplet spreads more quickly in the first 30 min when in contact with pristine PVDF and 0.05G/PVDF. A reduction of 10 and 12% can be estimated for the respective contact angle values. Instead, the 0.005G/PVDF membrane continues to exhibit a relatively stable wetting resistance over time with a slight decrease of 4% in the contact angle value.

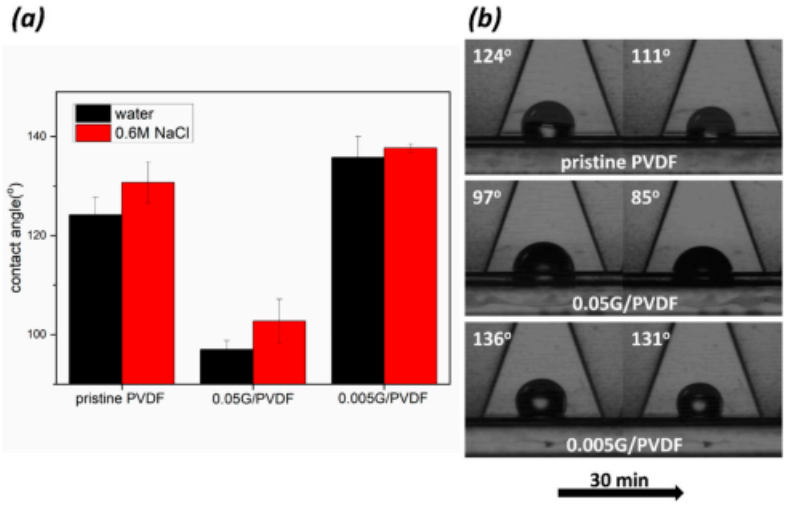

Figure 5. Resistance to wetting of membranes: (**a**) water contact angle of water and 0.6 M NaCl solution at zero time; (**b**) time-dependent images of water droplets within the first 30 min of contact with membrane surfaces.

With this regard, it is helpful to consider the slight linear decrease of the droplet size and CA value with time as a consequence of liquid evaporation as well. As known, there are three different evaporation mechanisms that occur in water droplet evaporation on a solid surface [38]. They include a constant contact radius (CCR) configuration with a continuous decrement of the CA values, a constant contact angle (CCA) configuration with a gradual decrease of the solid–liquid interface area (contact radius), and a mixed mode where mixed behavior is observed. The trend of the evaporation rate of water droplets placed over the smooth surfaces depends on the absolute value of CA values; in other words, CCR mode takes place when the CA value is lower than 90° while CCA mode occurs when the CA value tends to be greater than 90°, without considering any effect of surface morphology, as well as the surfaces' composition [39]. As CCR mode originates from the three-phase contact line pinned to the surface, it is more likely that drop evaporation mode depends strongly on the CA hysteresis than on the absolute CA value [40]. Shin et al. [41] stated that the surface features substantially influence the evaporation rate, and the overall evaporation time takes longer as the membrane surface presents a more hydrophobic nature. In our study, the decrement in the CA value of the tested samples can be observed as the evaporation proceeds. In the case of a 0.05G/PVDF membrane, no contact radius reduction is observed, thus the droplet follows CCR evaporation mode with time, indicating a competitive hydrophilic nature of the surface (Figure 6). Instead, the contact area line of water on pristine PVDF and

0.005G/PVDF recedes, and no pinning is observed. According to Shin et al. [41], there is no pinning (CCR mode) during droplet evaporation on a superhydrophobic surface and the water droplet maintains the spherical shape until the end of evaporation. Our observations prove that 0.005G/PVDF membrane surface shows hydrophobic behavior decisively since the droplet remains in spherical shape—only a slight drop of contact angle is noted—throughout the time of droplet evaporation.

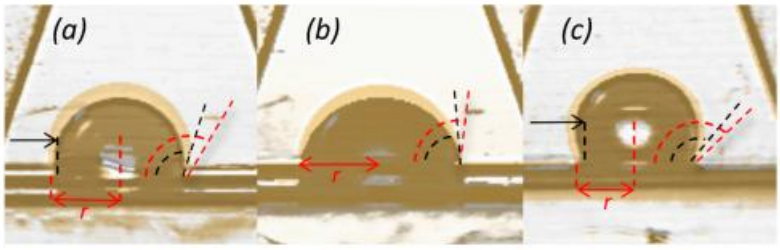

Figure 6. The time-dependent changes in contact radius and contact angle of evaporating droplet on (**a**) pristine PVDF, (**b**) 0.05G/PVDF and (**c**) 0.005G/PVDF surface.

In the case of 0.05G/PVDF, the slight degree of oxidation could facilitate local graphene–water interactions; however, the dependence of wetting behavior on the nanoscale structure needs to be examined. AFM micrographs reveal that the presence of a low amount of graphene introduces additional nanoscale structures in the surfaces (Figure 7). The significance of multi-scale rough structure on surface hydrophobicity enhancement has been inspired by nature and is already well understood [42]. For instance, the structure of lotus leaves—one of the most famous examples of naturally occurring superhydrophobic surfaces—consists of a combination of micro-roughness (around 10 μm) and nano-roughness (around 100 nm) [43]. The coexistence of these two morphological effects has been demonstrated to enhance antiwetting properties in a membrane coated with fluorinated TiO_2 or SiO_2 nanoparticles [44,45]. In our study, AFM analysis indicates an additional fine-structure mainly in graphene-coated membranes obtained from 0.005 $mgmL^{-1}$ graphene liquid dispersions (Figure 7b).

This second topography scale is expected to induce a series of mixed states between Wenzel and Cassie–Baxter with an important contribution to the last one wherein the graphene groove scale is predominant. Values of *Ra* 272 ± 10 nm, *Rq* 327 ± 6 nm, and *Rz* 767 ± 73 have been calculated throughout the 0.005G/PVDF. In a more targeted manner, *Rz* value is the average of the highest peaks and deepest valleys, the PVDF (Table 2). So, the strongest anti-wetting property of 0.005G/PVDF can be plausibly attributed to the multi-scale rough structure.

A larger deposition of graphene flakes produces a new one-scale situation predominantly (Figure 7c), which leads to a more flattened surface with values of *Ra* 97 ± 7 nm, *Rq* 133 ± 15 nm, and *Rz* 180 ± 16 nm. The lowest surface roughness associated with local graphene oxidation is hence expected to produce a lower resistance to the liquid spreading for 0.05G/PVDF membrane surface. Differently from two graphene-coated membranes, the pristine PVDF surface exhibits surface roughness values of *Ra* 214 ± 19 nm, *Rq* 272 ± 10 nm, and *Rz* 499 ± 21 nm, respectively. In this case, Figure 7a shows the presence of pores and other surface deformities due to spherulitic-like polymer particles, which cause a reasonable predominant Wenzel regime with contact angle values of 124 ± 4° and a quicker receding of the contact area line of water (Figures 5 and 6).

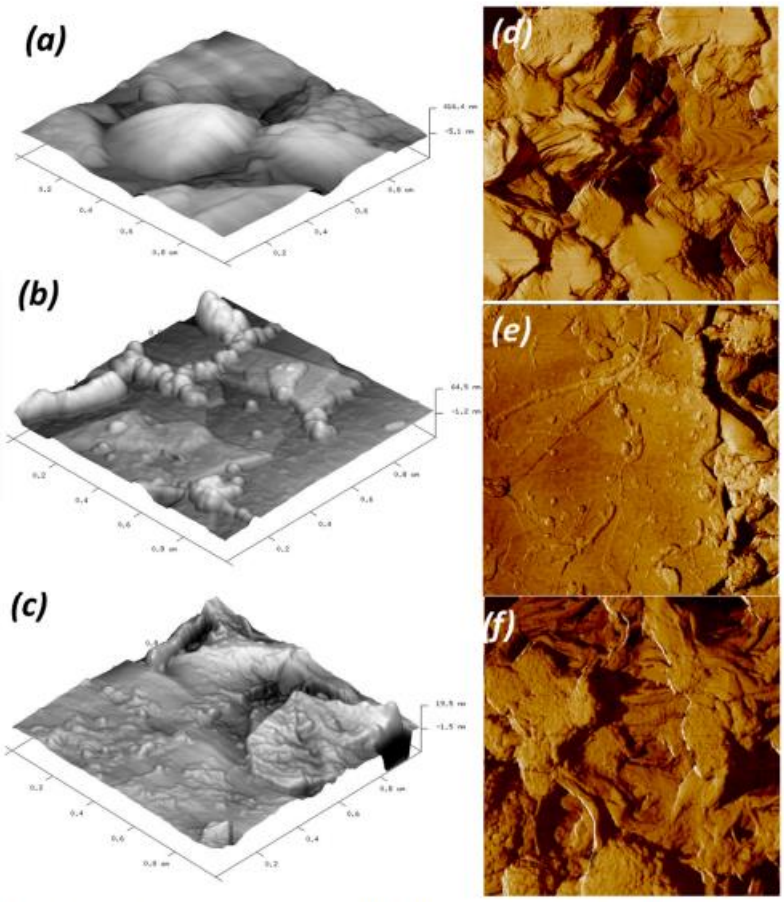

Figure 7. 3D AFM images of (**a**) pristine PVDF, (**b**) 0.005G/PVDF, (**c**) 0.05G/PVDF membranes (projected surface 1 µm × 1 µm) and 2D AFM images of (**d**) pristine PVDF, (**e**) 0.005G/PVDF, (**f**) 0.05G/PVDF membranes (projected surface 5 µm × 5 µm).

Table 2. Surface roughness estimated for all membranes.

Sample	*Ra* (nm)	*Rq* (nm)	*Rz* (nm)
PVDF	214 ± 19	272 ± 10	499 ± 21
0.05G/PVDF	97 ± 7	133 ± 15	180 ± 16
0.005G/PVDF	272 ± 10	327 ± 6	767 ± 73

It is quite important to observe as NaCl solution spreads less than pure water (Figure 5a). This indicates no interaction between salt, polymer, and graphene in full agreement with the literature. Palacio et al. [46] demonstrated that in NaCl/graphene interface NaCl films adapt to the graphene without disrupting its morphology; no chemical interactions or intercalation takes place with graphene, confirming the total inertness of materials.

3.3. Membrane Distillation Experiments

DCMD tests have been carried out on pristine PVDF, 0.05G/PVDF, and 0.005G/PVDF membranes. After six running hours, better performance has been tuned for the graphene-coated membranes with an incremental ratio of the flux decisively higher for 0.005G/PVDF as compared to the pristine PVDF membrane (Figure 8a).

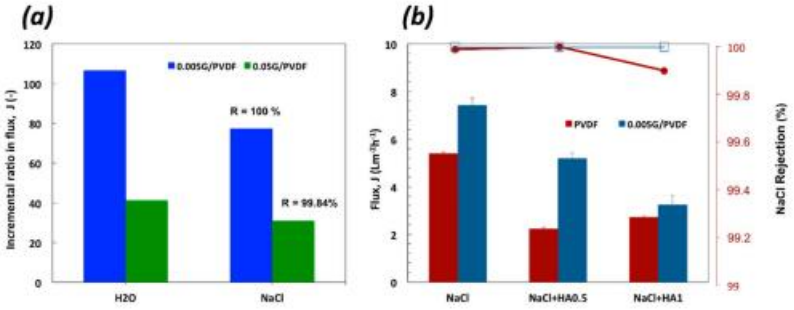

Figure 8. Transport measured through all membranes coming in contact with pure water, NaCl 0.6 M and mixtures of NaCl and HA (0.6 M/0.5 mg mL^{-1} and 0.6 M/1.0 mg mL^{-1}): (**a**) Incremental ratio in the flux for 0.005G/PVDF and 0.05G/PVDF membranes with respect to pristine PVDF membrane at T_{feed} = 33 °C; (**b**) Flux (J) and salt rejection (R) estimated at T_{feed} = 40 °C for pristine and 0.005G/PVDF membranes.

An increase of 106 and 77% in flux is measured through 0.005G/PVDF when worked with pure water and NaCl 0.6 M, respectively. Under similar conditions, for 0.05G/PVDF membrane the incremental ratio is of 41% with pure water and 31% with NaCl 0.6 M. A total salt rejection (100%) is obtained with 0.005G/PVDF against a value of 99.84% for 0.05G/PVDF (Figure 8a). The under-performance of 0.05G/PVDF is basically due to smaller pore size (Table 1) and lower resistance to wetting (Figure 5). Subsequently, additional resistance to transport opposes water vapor diffusion while liquid spreading let small saline droplets pass through the membrane pores, reducing slightly the efficiency of the separation. In this context, further experiments have been continued on pristine PVDF and 0.005G/PVDF membranes in order to investigate the antifouling properties and reliability of uncoated and coated membranes. Since humic acid (HA) is considered one of the most significant sources in feed water causing organic fouling, mixtures of NaCl (0.6 M) and HA (0.5 and 1.0 mg mL^{-1}) have been processed for 6 h at T_{feed} of 40 °C and under a difference of temperature (ΔT) of ~24 °C across the membranes. Figure 8b shows that already small amounts of HA affect visibly the performance of the pristine PVDF membrane with a reduction of 59% of the flux. A lowering of 30% is instead valued for 0.005G/PVDF at a lower HA concentration (0.5 mg mL^{-1}) in the feed. At higher content of HA, an important reduction of the flux is detected for both the membranes, although 0.005G/PVDF continues to exhibit a better performance whatever the operative context examined.

As is well known, there are two possible ways to increase the vapor flux through the membrane during the MD process: (a) to increase the driving force; (b) to reduce the mass transport resistance [7]. The driving force of the process can be increased by enhancing the vapor pressure difference across the membrane. A common approach is to increase the temperature difference between feed and permeate or to increase the effective evaporation area on the feed side. In this study, multi-scale roughness amplifies the mass transfer through the graphene-coated membrane, preventing pore wetting concurrently. The results are higher fluxes along with a total salt rejection (Figure 8b). Indeed, the numerous holes and slots distributed through the graphene-coated surface reduce the contact area between solid and liquid increasing the contact area between membrane and water vapor. As mentioned, 0.005G/PVDF exhibits the highest surface roughness values with the highest

standard deviation of the height distribution (Rq) and the uppermost average (Rz) of the five highest peaks and the deepest valleys along the sampling length (Table 2). Considering that Rq is much more sensitive than Ra and provides an indication about the nanoscale texture of surface roughness and Rz yields indication about skews and kurtosis resulting from the surface roughness profile irregularities, we can assume that the protuberances distributed through 0.005G/PVDF surface cause entrapment of air bubbles. In this way, liquid spreading and intrusion are prevented according to the Cassie–Baxter rules, thereby resulting in a major ability of the membrane to contrast wetting and flooding events. On the other hand, water in a vapor state finds a larger number of free gaps through which it can diffuse. Moreover, considering the defective structure of graphene nanoplatelets, effective sorption sites are available for water vapor molecules, which are, unlike water molecules, devoid of hydrogen bonds. The result is a major interfacial area associated with mass transfer assistance. In our previous study [8], the involvement of graphene nanoplatelets in mass transport during membrane distillation experiments has been demonstrated; the dependence of the mass transport coefficient of water on the amount of graphene confined inside the membranes has been found, thus confirming the occurrence of assisted diffusion of water vapor through the membranes. Therefore, it is not surprising to observe an increase in fluxes when working membrane with graphene flakes onto the surface. The schematic summarization of enhanced water vapor flux is depicted in Figure 9.

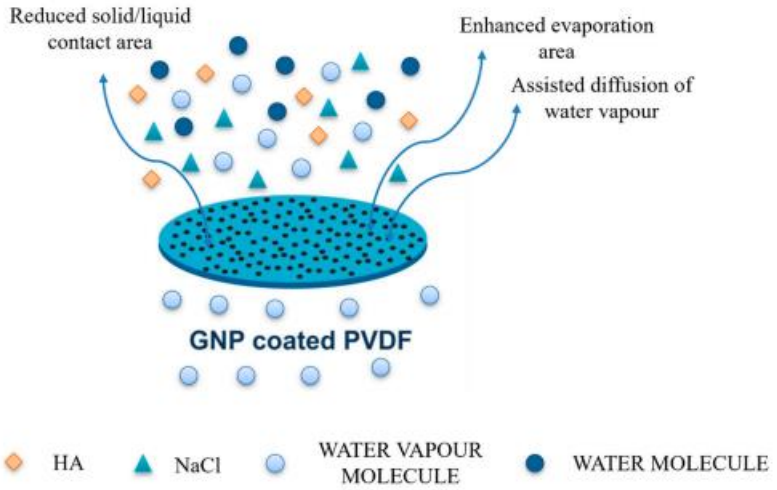

Figure 9. The schematic summarization of enhanced water vapor flux through GNP coated PVDF membranes.

It is also relevant to observe how graphene is actively involved in the mitigation of fouling (Figure 10). The normalized flux is regarded as a good indicator of the capability of membranes to counteract the adhesion of foulants onto the surface. After two running hours, pristine PVDF membranes show a gradual decline in the flux that becomes more pronounced when salt solution is added with HA. On the contrary, the normalized fluxes estimated for the 0.005G/PVDF membrane increase with time, yielding a clear indication of the ability of the graphene nanoplatelets to assist water vapor diffusion through the membranes while aggregations of salts and humic acid onto the surface are contrasted.

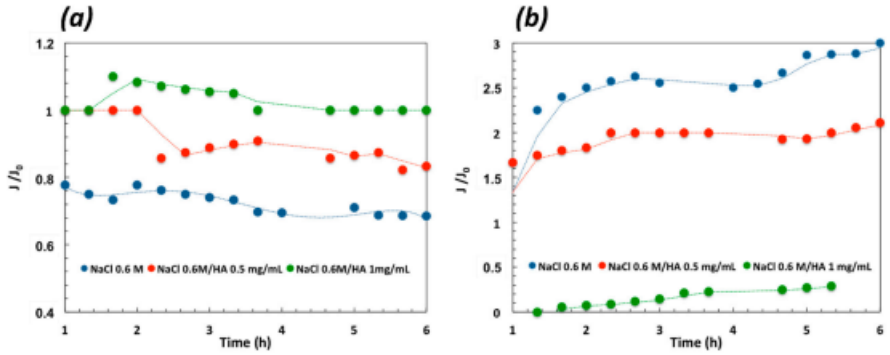

Figure 10. Normalized flux estimated for pristine PVDF (**a**) and 0.005G/PVDF (**b**) when working different NaCl/HA mixtures at T_{feed} 40 °C.

Despite that the antifouling properties of graphene are known, nano and micro-scale structures responsible for a multi-level roughness can be further envisaged to prevent wetting inside the membrane pores according to the Cassie–Baxter model. Again, the contact area of water and membrane is reduced as water is supported by a rough surface comprising the protrusions of the membrane and the air pockets between these protrusions. Subsequently, the susceptibility to foulants deposition is expected to decrease differently from what occurs on pristine PVDF membrane surface that is in a predominant Wenzel state [16,47]. In this case, the foulant adsorption takes place more easily leading to an additional resistance to water diffusion.

The fouling is totally reversible for the graphene-coated membrane after three cycles of washing with water at 50 °C (Figure 11). A loss of 9% is instead estimated for pristine PVDF membranes. To sum up, 0.005G/PVDF provides the appropriate roughness without affecting the pore size and porosity of pristine PVDF. Graphene addition generates multi-level roughness on the membrane surface, which leads to waterproofness and enhanced mass transfer and protects against undesired phenomena such as fouling and wetting. As a result, an improved productivity–efficiency trade-off is obtained along with higher durability and chemical resistance.

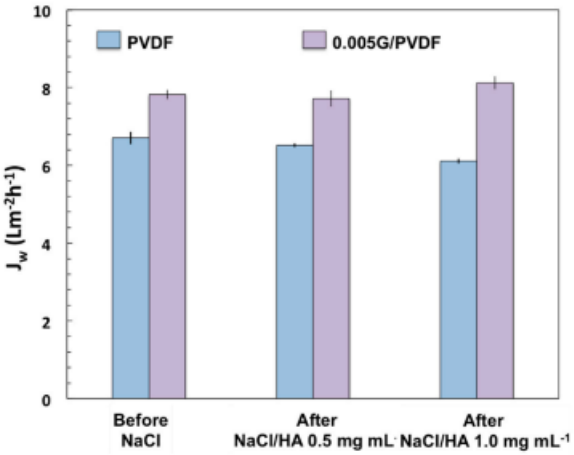

Figure 11. Water flux (J_w) measured before testing NaCl 0.6 M and after testing NaCl/HA (0.5 and 1.0 $mgmL^{-1}$) solutions at 40 °C (T_{feed}).

A comparative analysis reveals as a few graphene nanoplatelets deposited throughout the surface yield the best performance from productivity, selectivity, and economic points of view (Table 3). Although, the examined membranes exhibit a wide range of vapor fluxes (from 3 up to 18 L/m^2 h), the one produced in this work (0.005G/PVDF) can be considered competitive for the following reasons:

Table 3. Structural properties estimated for all membranes.

Membrane	MD Configuration	Process Parameters	Flux (L/m^2 h)	Rejection	Reference
PVDF + GNP (0.5 wt%)	DCMD	0.6 M NaCl Tf: 56 °C Tp: 15 °C	~9	99.9%	[8]
PVDF-f-G	DCMD	0.5 M NaCl Tf: 70 °C Tp: 20 °C	~3	99.9%	[48]
PVDF + GQDs (0.3) wt%	AGMD	0.6 M NaCl Tf: 60 °C Tp: 20 °C	18	99.8%	[49]
PVDF + GO- APTS 0.3%	AGMD	0.6 M NaCl Tf: 85 °C Tp: 23 °C	5.4	99.6%	[50]
PVDF + GO- APTS 0.3%	AGMD	0.6 M NaCl Tf: 85 °C Tp: 25 °C	6.25	99.9%	[50]
Coated 0.005G/PVDF	DCMD	0.6 M NaCl Tf: 40 °C Tp: 16 °C	7.5	100%	This work

(a) Large flux is obtained at lower feed temperature and using small temperature differences across the membranes, resulting in a cheaper process.
(b) A simpler and inexpensive DCMD configuration can be used to get the best-performing processes for productivity and selectivity under softer working conditions without the necessity to increase electric energy inputs like the VMD configuration.

Most of the works found in the literature report PVDF membranes modified with graphene oxide (GO) or graphene quantum dots (GQDs), while graphene nanoplatelets are not usually employed as additives for surface modification by the wet-filtration approach.

4. Conclusions

A new kind of PVDF surface modification by the wet-filtration method has been proposed. Complex topographies due to additional nanoscale structure have been detected on the graphene-coated membranes, especially when low graphene content dispersing solutions have been used. The multilevel surface roughness has been regarded as responsible for a better antiwetting and anti-flooding behavior and an effective evaporation area. MD experiments have been performed using complex mixtures of NaCl and humic acid. Graphene-coated membranes have been demonstrated to have a performance higher than non-modified PVDF and other graphene-functionalized membranes, with a better productivity–rejection trade-off under softer working conditions. After six running hours, the membranes exhibit good stability, mitigated fouling, and total recovery of the initial water permeation. These findings suggest great potential of graphene-coated membranes for highly performing MD processes.

Author Contributions: Conceptualization, E.G.-C. and A.G.; Investigation, E.G.-C. and G.D.L.; Data Analysis, E.G.-C. and A.G.; Writing draft, E.G.-C. and A.G.; Review & Editing, A.G. and M.L.; Funding Acquisition, A.G. All authors have read and agreed to the published version of the manuscript.

Funding: This research was funded by the grant from 'the Italian Ministry of Foreign Affairs and International Cooperation' within the framework of the Great Relevance International Project Italy (MAECI)-China (NSFC) 2018–2020—New Materials, with particular reference to Two-dimensional systems and Graphene (2DMEMPUR), MAE0088962, 21 May 2018.

Data Availability Statement: Data is contained within the article.

Acknowledgments: We acknowledge financial grant from 'the Italian Ministry of Foreign Affairs and International Cooperation' within the framework of the Great Relevance International Project Italy (MAECI)-China (NSFC) 2018–2020—New Materials, with particular reference to Two-dimensional systems and Graphene (2DMEMPUR), MAE0088962, 21 May 2018. E.G.C. would like to highly acknowledge Institute on Membrane Technology (ITM), Italy, for the possibility of carrying out an internship in their unit. This work was supported by Gdansk University of Technology by InterPhD II (POWER) project (No. POWR.03.02.00-IP.08-00-DOK/16).

Conflicts of Interest: The authors declare no conflict of interest.

References

1. Pendergast, M.M.; Hoek, E.M.V. A Review of Water Treatment Membrane Nanotechnologies. *Energy Environ. Sci.* **2011**, *4*, 1946. [CrossRef]
2. Lee, A.; Darling, S.B.; Elam, J.W. Membrane Materials for Water Purification: Design, Development, and Application. *Environ. Sci. Water Res. Technol.* **2016**, *2*, 17–42. [CrossRef]
3. Speranza, V.; Trotta, F.; Drioli, E.; Gugliuzza, A. High-Definition Polymeric Membranes: Construction of 3D Lithographed Channel Arrays through Control of Natural Building Blocks Dynamics. *ACS Appl. Mater. Interfaces* **2010**, *2*, 459–466. [CrossRef] [PubMed]
4. Perrotta, M.L.; Saielli, G.; Casella, G.; Macedonio, F.; Giorno, L.; Drioli, E.; Gugliuzza, A. An Ultrathin Suspended Hydrophobic Porous Membrane for High-Efficiency Water Desalination. *Appl. Mater. Today* **2017**, *9*, 1–9. [CrossRef]
5. Frappa, M.; Del Rio Castillo, A.E.; Macedonio, F.; Politano, A.; Drioli, E.; Bonaccorso, F.; Pellegrini, V.; Gugliuzza, A. A Few-Layer Graphene for Advanced Composite PVDF Membranes Dedicated to Water Desalination: A Comparative Study. *Nanoscale Adv.* **2020**, *2*, 4728–4739. [CrossRef]
6. Gugliuzza, A.; Basile, A. Membrane Contactors: Fundamentals, Membrane Materials and Key Operations. In *Handbook of Membrane Reactors*; Elsevier: Amsterdam, The Netherlands, 2013; pp. 54–106.
7. Gontarek-Castro, E.; Castro-Muñoz, R.; Lieder, M. New Insights of Nanomaterials Usage toward Superhydrophobic Membranes for Water Desalination via Membrane Distillation: A Review. *Crit. Rev. Environ. Sci. Technol.* **2021**, *52*, 2104–2149. [CrossRef]
8. Gontarek, E.; Macedonio, F.; Militano, F.; Giorno, L.; Lieder, M.; Politano, A.; Drioli, E.; Gugliuzza, A. Adsorption-Assisted Transport of Water Vapour in Super-Hydrophobic Membranes Filled with Multilayer Graphene Platelets. *Nanoscale* **2019**, *11*, 11521–11529. [CrossRef]
9. Mao, Y.; Huang, Q.; Meng, B.; Zhou, K.; Liu, G.; Gugliuzza, A.; Drioli, E.; Jin, W. Roughness-Enhanced Hydrophobic Graphene Oxide Membrane for Water Desalination via Membrane Distillation. *J. Memb. Sci.* **2020**, *611*, 118364. [CrossRef]
10. Tang, N.; Jia, Q.; Zhang, H.; Li, J.; Cao, S. Preparation and Morphological Characterization of Narrow Pore Size Distributed Polypropylene Hydrophobic Membranes for Vacuum Membrane Distillation via Thermally Induced Phase Separation. *Desalination* **2010**, *256*, 27–36. [CrossRef]
11. Zhu, H.; Wang, H.; Wang, F.; Guo, Y.; Zhang, H.; Chen, J. Preparation and Properties of PTFE Hollow Fiber Membranes for Desalination through Vacuum Membrane Distillation. *J. Memb. Sci.* **2013**, *446*, 145–153. [CrossRef]
12. Devi, S.; Ray, P.; Singh, K.; Singh, P.S. Preparation and Characterization of Highly Micro-Porous PVDF Membranes for Desalination of Saline Water through Vacuum Membrane Distillation. *Desalination* **2014**, *346*, 9–18. [CrossRef]
13. Tijing, L.D.; Woo, Y.C.; Choi, J.S.; Lee, S.; Kim, S.H.; Shon, H.K. Fouling and Its Control in Membrane Distillation-A Review. *J. Memb. Sci.* **2015**, *475*, 215–244. [CrossRef]
14. Kullab, A.; Martin, A. Membrane Distillation and Applications for Water Purification in Thermal Cogeneration Plants. *Sep. Purif. Technol.* **2011**, *76*, 231–237. [CrossRef]
15. Hausmann, A.; Sanciolo, P.; Vasiljevic, T.; Weeks, M.; Schroën, K.; Gray, S.; Duke, M. Fouling of Dairy Components on Hydrophobic Polytetrafluoroethylene (PTFE) Membranes for Membrane Distillation. *J. Memb. Sci.* **2013**, *442*, 149–159. [CrossRef]
16. Meng, S.; Ye, Y.; Mansouri, J.; Chen, V. Fouling and Crystallisation Behaviour of Superhydrophobic Nano-Composite PVDF Membranes in Direct Contact Membrane Distillation. *J. Memb. Sci.* **2014**, *463*, 102–112. [CrossRef]
17. Perrotta, M.L.; Macedonio, F.; Tocci, E.; Giorno, L.; Drioli, E.; Gugliuzza, A. Graphene Stimulates the Nucleation and Growth Rate of NaCl Crystals from Hypersaline Solution via Membrane Crystallization. *Environ. Sci. Water Res. Technol.* **2020**, *6*, 1723–1736. [CrossRef]
18. Gugliuzza, A.; Aceto, M.C.; Drioli, E. Interactive Functional Poly(Vinylidene Fluoride) Membranes with Modulated Lysozyme Affinity: A Promising Class of New Interfaces for Contactor Crystallizers. *Polym. Int.* **2009**, *58*, 1452–1464. [CrossRef]

19. Frappa, M.; Castillo, A.E.D.R.; Macedonio, F.; Di Luca, G.; Drioli, E.; Gugliuzza, A. Exfoliated Bi2Te3-Enabled Membranes for New Concept Water Desalination: Freshwater Production Meets New Routes. *Water Res.* **2021**, *203*, 117503. [CrossRef]
20. Han, Y.; Giorno, L.; Gugliuzza, A. Photoactive Gel for Assisted Cleaning during Olive Mill Wastewater Membrane Microfiltration. *Membranes* **2017**, *7*, 66. [CrossRef]
21. Gugliuzza, A.; Fabiano, R.; Garavaglia, M.G.; Spisso, A.; Drioli, E. Study of the Surface Character as Responsible for Controlling Interfacial Forces at Membrane-Feed Interface. *J. Colloid Interface Sci.* **2006**, *303*, 388–403. [CrossRef]
22. Bhadra, M.; Roy, S.; Mitra, S. Desalination across a Graphene Oxide Membrane via Direct Contact Membrane Distillation. *Desalination* **2016**, *378*, 37–43. [CrossRef]
23. Shirtcliffe, N.J.; McHale, G.; Atherton, S.; Newton, M.I. An Introduction to Superhydrophobicity. *Adv. Colloid Interface Sci.* **2010**, *161*, 124–138. [CrossRef]
24. De Luca, G.; Gugliuzza, A.; Drioli, E. Competitive hydrogen-bonding interactions in modified polymer membranes: A density functional theory investigation. *J. Phys. Chem. B.* **2009**, *113*, 5473–5477. [CrossRef]
25. Wang, M.; Liu, G.; Yu, H.; Lee, S.H.; Wang, L.; Zheng, J.; Wang, T.; Yun, Y.; Lee, J.K. ZnO Nanorod Array Modified PVDF Membrane with Superhydrophobic Surface for Vacuum Membrane Distillation Application. *ACS Appl. Mater. Interfaces* **2018**, *10*, 13452–13461. [CrossRef] [PubMed]
26. Cassie, A.B.D.; Baxter, S. Wettability of Porous Surfaces. *Trans. Faraday Soc.* **1944**, *40*, 546. [CrossRef]
27. Shan, H.; Liu, J.; Li, X.; Li, Y.; Tezel, F.H.; Li, B.; Wang, S. Nanocoated Amphiphobic Membrane for Flux Enhancement and Comprehensive Anti-Fouling Performance in Direct Contact Membrane Distillation. *J. Memb. Sci.* **2018**, *567*, 166–180. [CrossRef]
28. Zheng, R.; Chen, Y.; Wang, J.; Song, J.; Li, X.M.; He, T. Preparation of Omniphobic PVDF Membrane with Hierarchical Structure for Treating Saline Oily Wastewater Using Direct Contact Membrane Distillation. *J. Memb. Sci.* **2018**, *555*, 197–205. [CrossRef]
29. Cai, X.; Lei, T.; Sun, D.; Lin, L. A Critical Analysis of the α, β and γ Phases in Poly(Vinylidene Fluoride) Using FTIR. *RSC Adv.* **2017**, *7*, 15382–15389. [CrossRef]
30. Kabir, E.; Khatun, M.; Nasrin, L.; Raihan, M.J.; Rahman, M. Pure β-Phase Formation in Polyvinylidene Fluoride (PVDF)-Carbon Nanotube Composites. *J. Phys. D Appl. Phys.* **2017**, *50*, 163002. [CrossRef]
31. Sun, G.; Li, X.; Qu, Y.; Wang, X.; Yan, H.; Zhang, Y. Preparation and Characterization of Graphite Nanosheets from Detonation Technique. *Mater. Lett.* **2008**, *62*, 703–706. [CrossRef]
32. Bello, R.H.; Coelho, L.A.; Becker, D. Role of Chemical Funcionalization of Carbon Nanoparticles in Epoxy Matrices. *J. Compos. Mater.* **2018**, *52*, 449–464. [CrossRef]
33. Hong, G.; Han, Y.; Schutzius, T.M.; Wang, Y.; Pan, Y.; Hu, M.; Jie, J.; Sharma, C.S.; Müller, U.; Poulikakos, D. On the Mechanism of Hydrophilicity of Graphene. *Nano Lett.* **2016**, *16*, 4447–4453. [CrossRef] [PubMed]
34. Belyaeva, L.A.; van Deursen, P.M.G.; Barbetsea, K.I.; Schneider, G.F. Hydrophilicity of Graphene in Water through Transparency to Polar and Dispersive Interactions. *Adv. Mater.* **2018**, *30*, 1703274. [CrossRef] [PubMed]
35. Wang, S.; Zhang, Y.; Abidi, N.; Cabrales, L. Wettability and Surface Free Energy of Graphene Films. *Langmuir* **2009**, *25*, 11078–11081. [CrossRef] [PubMed]
36. Taherian, F.; Marcon, V.; Van Der Vegt, N.F.A.; Leroy, F. What Is the Contact Angle of Water on Graphene? *Langmuir* **2013**, *29*, 1457–1465. [CrossRef]
37. Yu, Y.S.; Wang, Z.; Zhao, Y.P. Experimental and Theoretical Investigations of Evaporation of Sessile Water Droplet on Hydrophobic Surfaces. *J. Colloid Interface Sci.* **2012**, *365*, 254–259. [CrossRef]
38. Xu, W.; Leeladhar, R.; Kang, Y.T.; Choi, C.H. Evaporation Kinetics of Sessile Water Droplets on Micropillared Superhydrophobic Surfaces. *Langmuir* **2013**, *29*, 6032–6041. [CrossRef]
39. Birdi, K.S.; Vu, D.T. Wettability and the evaporation rates of fluids from solid surfaces. *J. Adhes. Sci. Technol.* **1993**, *7*, 485–493. [CrossRef]
40. Extrand, C.W. Contact Angles and Hysteresis on Surfaces with Chemically Heterogeneous Islands. *Langmuir* **2003**, *19*, 3793–3796. [CrossRef]
41. Shin, D.H.; Lee, S.H.; Jung, J.Y.; Yoo, J.Y. Evaporating Characteristics of Sessile Droplet on Hydrophobic and Hydrophilic Surfaces. *Microelectron. Eng.* **2009**, *86*, 1350–1353. [CrossRef]
42. Liu, T.; Kim, C.-J. Turning a Surface Superrepellent Even to Completely Wetting Liquids. *Science* **2014**, *346*, 1096–1100. [CrossRef] [PubMed]
43. Li, X.M.; Reinhoudt, D.; Crego-Calama, M. What Do We Need for a Superhydrophobic Surface? A Review on the Recent Progress in the Preparation of Superhydrophobic Surfaces. *Chem. Soc. Rev.* **2007**, *36*, 1350–1368. [CrossRef] [PubMed]
44. Liao, Y.; Wang, R.; Fane, A.G. Fabrication of Bioinspired Composite Nanofiber Membranes with Robust Superhydrophobicity for Direct Contact Membrane Distillation. *Environ. Sci. Technol.* **2014**, *48*, 6335–6341. [CrossRef] [PubMed]
45. Razmjou, A.; Arifin, E.; Dong, G.; Mansouri, J.; Chen, V. Superhydrophobic Modification of TiO2 Nanocomposite PVDF Membranes for Applications in Membrane Distillation. *J. Memb. Sci.* **2012**, *415–416*, 850–863. [CrossRef]
46. Palacio, I.; Lauwaet, K.; Vázquez, L.; Palomares, F.J.; González-Herrero, H.; Martínez, J.I.; Aballe, L.; Foerster, M.; García-Hernández, M.; Martín-Gago, J.Á. Ultra-Thin NaCl Films as Protective Layers for Graphene. *Nanoscale* **2019**, *11*, 16767–16772. [CrossRef]
47. An, A.K.; Lee, E.J.; Guo, J.; Jeong, S.; Lee, J.G.; Ghaffour, N. Enhanced Vapor Transport in Membrane Distillation via Functionalized Carbon Nanotubes Anchored into Electrospun Nanofibres. *Sci. Rep.* **2017**, *7*, 41562. [CrossRef]

48. Grasso, G.; Galiano, F.; Yoo, M.J.; Mancuso, R.; Park, H.B.; Gabriele, B.; Figoli, A.; Drioli, E. Development of Graphene-PVDF Composite Membranes for Membrane Distillation. *J. Memb. Sci.* **2020**, *604*, 118017. [CrossRef]
49. Jafari, A.; Kebria, M.R.S.; Rahimpour, A.; Bakeri, G. Graphene Quantum Dots Modified Polyvinylidenefluride (PVDF) Nanofibrous Membranes with Enhanced Performance for Air Gap Membrane Distillation. *Chem. Eng. Process. Process Intensif.* **2018**, *126*, 222–231. [CrossRef]
50. Leaper, S.; Abdel-Karim, A.; Faki, B.; Luque-Alled, J.M.; Alberto, M.; Vijayaraghavan, A.; Holmes, S.M.; Szekely, G.; Badawy, M.I.; Shokri, N.; et al. Flux-Enhanced PVDF Mixed Matrix Membranes Incorporating APTS-Functionalized Graphene Oxide for Membrane Distillation. *J. Memb. Sci.* **2018**, *554*, 309–323. [CrossRef]